A FREQUENCY DOMAIN BASED INVERSE GROUND RESPONSE ANALYSIS FRAMEWORK FOR THE DETERMINATION OF DYNAMIC SOIL PROPERTIES

Submitted for the degree of

DOCTOR OF PHILOSOPHY

By

Joy Kumar Mondal

DEPARTMENT OF CIVIL ENGINEERING
INDIAN INSTITUTE OF TECHNOLOGY GUWAHATI
GUWAHATI – 781039
December 2022

DEDICATED TO MY BELOVED

PARENTS,

MY BEAUTIFUL WIFE

AND

MY TEACHER PRANAB KUMAR MAJUMDER

Statement

I do hereby declare that the matter contained in this thesis is the outcome of investigations carried out by me at the Department of Civil Engineering, Indian Institute of Technology Guwahati, Guwahati, Assam, India.

In keeping with the general practice of reporting scientific observations, due acknowledgements have been made whenever the work described is based on findings of other investigators.

Joy Kumar Mondal

Place: IIT Guwahati — Joy Kumar Mondal

Date: 1st December-2022

Certificate

This is to certify that the thesis entitled “A Frequency Domain based Inverse Ground Response Analysis Framework for the Determination of Dynamic Soil Properties” being submitted by Mr. Joy Kumar Mondal, (Enrollment number 176104112) to the Indian Institute of Technology Guwahati for the award of the degree of Doctor of Philosophy is a record of bonafide research work carried out by him. The thesis work in my opinion has reached the requisite standard for the degree of Doctor of Philosophy.

The results embodied in this thesis have not been submitted in any other University/ Institute for the award of any Degree or Diploma.

Date: 31/07/2023

Place: Guwahati

Dr. Abhishek Kumar
Associate Professor
Indian Institute of Technology Guwahati,
Assam, India-781039

Acknowledgement

My PhD research has been accomplished thanks to the kind and unrestrained assistance of many people. I would want to use this occasion to express my heartfelt appreciation to everyone for their unwavering support.

I want to start by expressing my gratitude to my mentor and supervisor, Dr. Abhishek Kumar for his unconditional support, priceless technical advice and patience. Working with him during my PhD studies has been a privilege and a wonderful joy that has improved me not only as a researcher but a better person too. He has been like a family member to me who has always inspired me to improve as a researcher, because of his enthusiasm and commitment to his work. I am incredibly appreciative of his personal kindness, compassion, and commitment to my welfare. For my PhD, I could not have asked for a better supervisor.

I would also like to thank the rest of my Doctoral committee: Dr. Anil Kumar Mishra, Dr. Rishikesh Bharti and Dr. Sachin S. Gautam for their guidance, constructive comments and creative suggestions at every stage of my PhD research.

I am very grateful to my lab mates and dear friends Dr. Harinarayan N.H, Mr. Niranjan Borah, Mr. Surender Singh, Mr. Prem Kumar, Mr. Rahul Raoniar for their delightful presence and personal support. Without them, the lab would have been a monotonous place.

I would like to thank the Indian Institute of Technology Guwahati (IITG) for providing me opportunity and financial support to carry out my PhD work.

I express my thanks to all my teachers who have laid the cornerstones for this journey in my life. Furthermore, I want to thank my parents immensely for their consistent support and encouragement of me in pursuing my dream.

Last but not the least, I want to convey my gratefulness to my wife Ranu for tolerating me and supporting me through the darkest hours of my life.

Joy Kumar Mondal

Joy Kumar Mondal

ABSTRACT: Effect of local soil in amplifying bedrock motion during earthquakes (EQs) is an important phenomenon, and is observed globally. As a result, the bedrock motion at times increases manifold while reaching the surface. Such amplification in ground motions due to local soil is termed as local site effect (LSE) and can numerically be quantified by performing ground response analysis (GRA). Understanding the effect of local soil requires information about subsoil type as well as shear strain dependent behavior of each subsoil layer (known as dynamic soil properties curves or DSPCs). While subsoil type can be determined based on in-situ borelogs, determination of DSPCs is a cumbersome process involving detailed instrumentation and expertise. Further, laboratory based DSPCs too have limitation as it is not entirely possible to replicate subsoil condition through laboratory tests. As a result, DSPCs of local soil are not readily available for regional and site-specific soils. Due to this reason, while attempting to estimate LSE, majority of site-specific studies consider DSPCs developed for other region soils. Another alternative towards determination of site-specific DSPCs are by analyzing EQ data from downhole seismic array records. Downhole seismic arrays are in-situ setup to record subsoil behavior during EQ ground shaking at different depths.

Present thesis consists of a total of 7 chapters. Chapter 1 provides background of the problem definition of present study, in the light of past EQs and the existing literature. A detailed overview of various attempts done globally in order to assess dynamic soil properties of in-situ soil based on recordings from downhole seismic arrays is provided in Chapter 2. Such studies can primarily be divided into frequency domain methods and time domain methods. Further,

other advanced methods have also been used by various researchers. Based on the review, it is found that most of the frequency domain studies target to determine change in shear modulus (G) with shear strain (γ) but no to very limited studies target to determine damping ratio (β) variation with γ (or β curve). Additionally, frequency domain methods which focused on determining variation of G with γ (modulus degradation curve or G/G_{max} curve) were limited to finding out soil properties for the surficial layer only. It has to be highlighted here that the 'surficial layer' in such studies was defined as the soil material present between top two accelerometers from the ground surface. In many such studies, the distance between these two top accelerometers was as long as 10m. Further, there may be different soil layers, composed of different soil materials, present between top two accelerometers. During an EQ excitation, each of such soil layers will behave distinctively. However, earlier studies considered such multiple soil layers as one and found out DSPCs which represented the behavior of multiple soil layers combined. Present thesis in Chapter 3 proposes frequency domain methodology employing seismic downhole arrays focuses on determining β curve for the surficial layer. In doing so, EQ data recorded at both shallow depth and great depth are utilized. Later, the methodology is extended in Chapter 4 to determine DSPCs (G/G_{max} curve and β curve) for both the surficial layer and the layer below it. In Chapter 5, a generalized methodology is developed that can be applied to multiple soil layer system to determine DSPCs of each layer involved. It has to be highlighted here that for India, no downhole array is available till date. In addition, global downhole array data are also not readily available in most of the cases. Thus, testing of proposed methodologies in Chapters 3, 4 and 5 are solely based on ground motion records from Lotung downhole array.

For major infrastructure development in India, accurate assessment of LSE is must. However, since site-specific DSPCs are not available for most of the sites to do so. Hence,

depending upon selected DSPC, different outcomes can be obtained from different set of DSPCs. Selection of DSPCs and input motion at times can be difficult for the user. mastandard DSPCs are mostly being used for LSE quantification. In such cases, if the component of LSE (due to soil nonlinearity) can be determined in advance, even linear GRA (LGRA) can provide comparable results to that of equivalent linear GRA (ELGRA), eliminating necessity for site-specific DSPCs for every site of interest. With this objective, in Chapter 6 attempts are made to develop four empirical correlations for Guwahati city, which when used with LGRA results, estimate results similar to ELGRA without selecting a particular DSPC and complete input motion. Chapter 7 presents major conclusions from the present work and goals for future work.

Contents

List of Figures

List of Tables

List of Abbreviations

EQ:	Earthquake
LSE:	Local site effects
GRA:	Ground response analysis
DSPC:	Dynamic soil property curve
LGRA:	Linear ground response analysis
ELGRA:	Equivalent linear ground response analysis
SPT:	Standard penetration test
MASW:	Multi channel analysis of surface waves
HVSR:	Horizontal to vertical spectral ratio
EPRI:	Electric and Power Research Institute
TPC:	Taiwan Power Company
LSST:	Large scale seismic testing
SSI:	Soil structure interaction
DHA:	Downhole array A
DHB:	Downhole array B
PI:	Port Island
ANN:	Artificial neural network
EKF:	Extended Kalman Filter
EBM:	Extended Bayesian Method
GA:	Genetic Algorithm
PGA:	Peak ground acceleration
PGV:	Peak ground velocity
SH:	Vertically propagating shear waves
NTU:	National Taiwan University
UCD:	University of California, Davis
UT:	University of Texas, Austin
EW:	East-west
NS:	North-south
UD:	Up-down
PHA:	Peak horizontal acceleration
NUPEC:	Nuclear Power Engineering Corporation
NRC:	Nuclear Regulatory Commission
CAO:	Central De Abasto Oficinas
FIR:	Finite duration impulse response
ARMA:	Auto regressive moving average
NLGRA:	Nonlinear ground response analysis
IGRA:	Inverse ground response analysis
ANOVA:	One way analysis of variance
FAS_4:	Fourier amplitude spectrum at 4m depth
PGA_diff1:	Percentage error in PGA for surficial layer
PGA_diff2:	Percentage error in PGA for second layer
LSE_{NL}:	LSE due to nonlinear soil behavior
AF:	Amplification factor
SC:	Seismic site class

PGA_{EL}: PGA obtained based on ELGRA
PGA_{LN}: PGA obtained based on LGRA
HFT: Himalayan Frontal Thrust
GWT: Ground water table
1D: One dimensional

List of symbols

γ:	Shear strain
G:	Shear modulus
β:	Damping ratio
G/G_{max}:	Shear modulus degradation
V_s:	Shear wave velocity
V_p:	P wave velocity
τ:	Shear stress
G_{sec}:	Secant shear modulus
T:	Predominant time period
H=	Thickness of soil layer
ρ:	Soil mass density
T_{min}:	Minimum value of T
γ_{avg}:	Average γ
f:	Resonant frequency
$H(\omega)$:	Transfer function
f_n:	Fundamental natural frequency of soil layer
M_L:	Richter Local Magnitude
V_s^{max}:	Maximum V_s value
M_w:	Moment magnitude
λ:	Wavelength
γ_{tl}:	Linear cyclic shear strain
γ_{tv}:	Volumetric shear strain
$H(\omega)_{RR}$:	Empirical transfer function
V_{ss}:	Shear wave velocity of soil layer
V_{sr}:	Shear wave velocity of rock layer
α_s^*:	Complex impedance ratio
V_s^*:	Complex shear wave velocity
$H(\omega)_{CR}$:	Theoretical transfer function
γ_{eff}:	Effective shear strain
$H(\omega)_{0\text{-}4}$:	Transfer function between the ground surface and 4m depth
t_p:	Starting point of P wave
T_c:	Fundamental natural period of first two layers
T_1:	Fundamental natural period of the surficial layer
T_2:	Fundamental natural period of the second layer
$H(\omega)_{CR,\ 6\text{-}11}$:	Theoretical transfer function between DHB6 and DHB11
$H(\omega)_{RR.\ 6\text{-}11}$:	Empirical transfer function between DHB6 and DHB11
γ_{ref}:	Reference shear strain
$H(\omega)_{CR,\ n\text{-}n+1}$:	Theoretical transfer function between accelerometer level n and n+1
$H(\omega)_{RR,\ n\text{-}n+1}$:	Empirical transfer function between accelerometer level n and n+1
a, c:	Regression coefficients

CHAPTER 1: BACKGROUND

1.1 Introduction

Ground motion at a particular site, during an earthquake (EQ), is a combined function of fault mechanism, regional seismicity, regional bedrock properties and local site effects. While the bedrock motion can be determined by a deterministic or probabilistic seismic hazard study, these can be further altered significantly when travel from various soil layers existing between the bedrock and the surface. This phenomenon is called as local site effect (LSE) and can numerically be determined by conducting a detailed GRA. The amplitude of motions between the bedrock and the surface either gets amplified or de-amplified. Numerous examples are present in the literature highlighting the importance of LSE in controlling damage scenario during an EQ. The most profound example where effect of LSE was well recognized was during the September 19, 1985 Michocan (M_s 8.1) EQ. During this EQ, only moderate level of shaking was felt near the source (Pacific coast of Mexico). However, Mexico City, which is located 350km away from the source, witnessed intense ground shaking. Similar observation was also made during the 1989 San Francisco Bay EQ (Ms=7.1). The shaking intensity felt at the epicenter (located near Mt Loma Prieta) was found as VII (MMI). On the other hand, an intensity of IX (MMI) was felt at San Francisco, located 100km north of the epicenter. Similar to above examples from other parts of the globe, there have been various cases even in India when LSE

played a crucial role in deciding the surface seismic hazard value during an EQ. Though the epicenter of the 1999 Chamoli EQ was located between the lower and higher Himalayas, this EQ jeopardized several structures in Delhi and Dehradun, located at around 200 km distance from the epicentre. The preceding discussion emphasizes on the need of estimating LSE in order to quantify surface seismic hazard values which subsequently control induced infrastructural damages and even loss of lives.

To estimate the LSE numerically, it is very important to have clear idea about subsoil types and their dynamic soil properties. Subsoil type can be determined based on in-situ borehole drilling. Dynamic soil properties, expressed in the form of Dynamic Soil Property Curves (DSPC), are the locus of normalized shear modulus versus shear strain (γ) and damping ratio versus γ of the subsoil. While performing GRA, DSPC of subsoil are prerequisite. Despite the fact that DSPCs of subsoil are a prerequisite, these are mostly not available on regional scale. As a result, it is a common practice to use standard DSPCs (including modulus degradation or G/G_{max} and damping ratio or β curves) which are developed for other regions.

Anbazhagan et al. (2007) performed equivalent linear GRA using SHAKE2000 for Bangalore city based on both Standard Penetration Test (SPT)–based N values and Multichannel Analysis of Surface Waves (MASW) test based shear wave velocity (V_s) profiles. The dynamic soil properties of sand and rock layers of Bangalore region were approximated with those developed by Seed and Idriss (1970) and Schnabel (1973) respectively. In another work by Ranjan (2005), GRA for Dehradun city was attempted. Necessary soil information (V_s profile)

was obtained by MASW tests at 31 locations across the city. Soil types and thicknesses were obtained from the available borelogs and earlier published literature. In the work by Ranjan (2005) however, clay, sand, gravel and rocky layers were modeled with DSPCs developed by Sun et al. (1988), Seed and Idriss (1970), Seed et al. (1986) and Gazetas et al. (1992) respectively. In another work, Kumar et al. (2016) attempted GRA for typical location in Delhi region. The analyses were based on 41 borehole data obtained for the location under study and using 30 globally recorded EQ data as input ground motions. In the absence of regional DSPCs for Delhi region, Kumar et al. (2016) adopted such curves developed by Sun et al. (1988), and Seed and Idriss (1970) for modeling clay and sand layers. Similarly, Phanikanth et al. (2011) performed GRA for 4 typical sites in Mumbai by modelling clay and sand layers with curves by Sun et al. (1988), and Seed and Idriss (1970) respectively.

Use of DSPCs, developed for other regions, for GRA is not only limited to studies in India but in other parts of globe as well. Besrat et al. (2018) performed equivalent linear GRA (ELGRA) for few sites located at Hawassa city in southern Ethiopia. In that work also, DSPCs were taken from Seed et al. (1986) to model cohesionless soil. In another work performed by Stanko et al. (2019), ELGRA was carried out using time series approach and random vibration theory approach. In that work, sand and gravel layers were modelled using material curves developed by Seed et al. (1986) and clay layers were modelled using curves developed by Vucetic and Dobry (1991). Stanko et al. (2017) performed ELGRA on the site of Trakoš˙c´an Castle of Croatia. In that work, Horizontal to vertical spectral ratio (HVSR) technique was followed to determine initial soil properties which were later used for ELGRA. Further, soil layers were modelled using material curves proposed by Seed et al. (1986), Vucetic and Dobry (1991) and Schnabel et al. (1972) for sand, clay and rock layers respectively. Uthayakumar and

Naesgaard (2004) performed ELGRA based on 4 soil profiles from Fraser River Delta, British Columbia. In the work, Uthayakumar and Naesgaard (2004) modeled sand layers by Seed et al. (1986). Similarly, clayey silt layers were modeled using Vucetic and Dobry (1991).

It must be highlighted here that the dynamic soil properties developed by Seed and Idriss (1970), Sun et al. (1988), Seed et al. (1986) and Gazetas et al. (1992), Vucetic and Dobry (1991), Schnabel (1972) were based on data from California, Canada, Japan, United States etc. Since such curves are not available on regional scale for earlier discussed regions, these were utilized in regional GRA. It has to be mentioned here that dynamic soil characteristics from different regions may be different due to the difference in terms of soil type, mineral composition, its relative age, soil structure, pore pressure conditions and possible overburden pressure, under which a soil layer exists. Thus, assessing local site effect on regional/ site-specific level by means of using soil properties for other region soil may have direct impact on the application of such GRA in arriving at surface seismic hazard scenario and subsequently in quantifying LSE. Earlier, Anbazhagan et al. (2017) highlighted that standard DSPCs are being employed for quantifying regional LSE without considering the applicability of such standard DSPCs for the site of interest. Anbazhagan et al. (2017) further carried out an extensive study where applicability of such standard DSPCs in carrying out GRA was discussed. For the purpose, recorded EQ data both at the ground surface and some depth below the ground surface were utilized. Based on the research, Anbazhagan et al. (2017) sorted out different standard DSPCs to be employed for GRA study for particular soil types. It was observed by Anbazhagan et al. (2017) that selection of standard DSPCs without proper guidelines could have significant effect on the outcome from GRA. This highlights the need for the development of DSPCs on regional/ local scale.

Development of the DSPCs in laboratory is a cumbersome exercise and requires rigorous laboratory testing methods to account for different γ levels. Further, disturbance induced during soil sampling also restricts determined soil properties to be used confidently while performing GRA. On the other hand, observations of subsoil systems which are subjected to various levels of shaking collectively during various EQ events, by means of continuous instrumentation, can provide useful information about the actual ground response (Archuleta et al. 2000a; b; Baise and Glaser 2000; Baro et al. 2018; Elgamal et al. 1995a; Kumar et al. 2017). Further, recordings from such systems can also be used to test existing GRA models (Zeghal et al. 1995). EQ events serve as naturally occurring experiments and the data in the form of EQ records provides the outcome of such experiment. Development of downhole arrays worldwide has provided an insight into the complex wave propagation mechanism through soil. Downhole arrays provide EQ records at different depths from the ground surface, during different EQs. These EQ records further can be utilized to estimate dynamic soil properties of *in-situ* soil layers. Detailed information on various downhole arrays and methodologies that utilize EQ data from downhole arrays to determine DSPCs is provided in subsequent chapters of this thesis.

CHAPTER 2: SYSTEMATIC REVIEW

2.1 Introduction

As highlighted earlier, in order to understand LSE during a probable seismic scenario, GRA should be performed. Further, while performing GRA, DSPC of regional subsoils are an important input. However, due to non-availability of regional DSPC, DSPC developed for other part of world are used extensively in GRAs. Even if regional DSPC based on laboratory investigations are available for a particular site, they do not represent the actual site condition in terms of in-situ stress condition (Elgamal et al. 2001). The actual field condition during an EQ may be different from the one created during laboratory testing due to sampling disturbances, specimen size, equipment compliance and loading conditions (Chang et al. 1991a). Worldwide development of downhole array recording systems has provided an insight to actual wave propagation problem. Downhole array recordings are frequently used to calibrate the existing tools for GRA (Elgamal et al. 2001). In works related to downhole arrays, researchers tried to extract dynamic soil properties by applying different inversion techniques. These inversion analyses can be performed either on frequency domain platform or on time domain platform. In addition, tools such as artificial neural network (ANN), genetic algorithms and different optimization schemes have also been adopted for the purpose (Baise and Glaser 2000; Glaser and Leeds 1996; Tsai and Hashash 2007). In this chapter, a detailed review on the works performed using frequency domain and time domain procedures, to arrive at dynamic soil properties of subsoil, based on downhole array recordings, following inverse analysis, is presented.

The frequency domain identification procedure deals with identification of transfer function between up-hole and downhole acceleration time histories. Transfer function can be

estimated from actual acceleration time histories by adopting auto-spectral analysis or cross-spectral analysis or Fourier spectral analysis (Chang et al. 1991a; Ghayamghamian and Kawakami 1996; Ghayamghamian and Matosaka 2001). The time domain identification procedure on the other hand is based on shear beam idealization of soil profile (Zeghal et al. 1995). Findings by (Koga and Matsuo 1990) for the determination of shear stress (τ) and γ time histories from acceleration time histories were applied in all of the time domain procedures.

Inverse analyses procedures first came to recognition in the late 80's and early 90's. Chang et al. (1989,1991a, 1991b) evaluated the variation of soil stiffness with γ using LSST downhole acceleration records at Lotung test site based on Fourier spectral analysis. In another work, Chang et al. (1996) utilized EQ data from the Lotung downhole array to estimate dynamic soil properties. Fourier spectral ratio technique was employed by Chang et al. (1996) for the purpose. Kokusho et al. (1996) performed inverse ground response analysis (IGRA) using 1995 Kobe EQ data, recorded at four different sites around the fault zone. Dynamic soil properties were then obtained using spectral ratio technique. Based on the work, Kokusho et al. (1996) found that the obtained dynamic soil property curves had a clear dependency on the level of γ. Later, Sato et al. (1996) back-calculated the V_s and β values at the same 4 sites which were used by Kokusho et al., (1996). Ghayamghamian and Kawakami (1996) adopted cross-spectral analysis technique to determine G/G_{max} curves for seven downhole array sites located in Japan. Further, the curves from 7 sites were combined and compared with the available standard curves in the literature. The degradation behavior of G, as a function of γ, was evident from the back-calculated values. Similarly, in another work, Ghayamghamian and Motosaka (2001) adopted cross-spectral analysis and determined the G/G_{max} curves for Chiba downhole array site. In addition, Ghayamghamian and Matosaka (2001) adopted time domain methodology and evaluated G and β

values for different γ values using Chiba test site downhole array recordings. Work, by Zeghal et al. (1995) back-calculated dynamic soil properties at Lotung downhole array by time domain methodology. Further, Zeghal et al. (1995) used finite difference technique to obtain γ and τ time histories directly from acceleration time histories. Obtained time histories were then used to evaluate secant shear modulus and β properties at different γ levels. It must be mentioned here that the work by Zeghal et al. (1995) was based on time domain methodology. Similarly, using pore water pressure records, up-hole and downhole acceleration records, gradual degradation in G during the 1987 Superstition hill's EQ at the California Wildlife refuge site was studied (Elgamal 1992; Gunturi et al. 1998; Zeghal and Elgamal 1994). The downhole and up-hole records along with pore pressure record were used to estimate τ-γ time histories. These τ-γ time histories were useful in understanding the site behavior during liquefaction. Further, at maximum value of γ, strain hardening behavior in soil was also observed at the site (Zeghal and Elgamal 1994). In works by Abdel-Ghaffar and Scott (1979), 2 EQ recordings (M_L 6.3 and 4.7) were used to determine G and β properties of an earthen dam (Santa Felicia dam located in Southern California). In the next sections, an overview of downhole arrays that have been selected frequently for the purpose of carrying out IGRA studies are discussed. Additionally, a systematic review on different IGRA methodologies is attempted.

2.2 Downhole arrays used for the inverse analysis

Earliest downhole arrays were installed in Japan and USA (Elgamal et al. 2001). According to Shima (1962), in Japan, a downhole array consisting of 2 surface and 2 downhole seismometers, was installed at the Tokyo station which recorded 7 EQs in 1950. On the other hand, the first

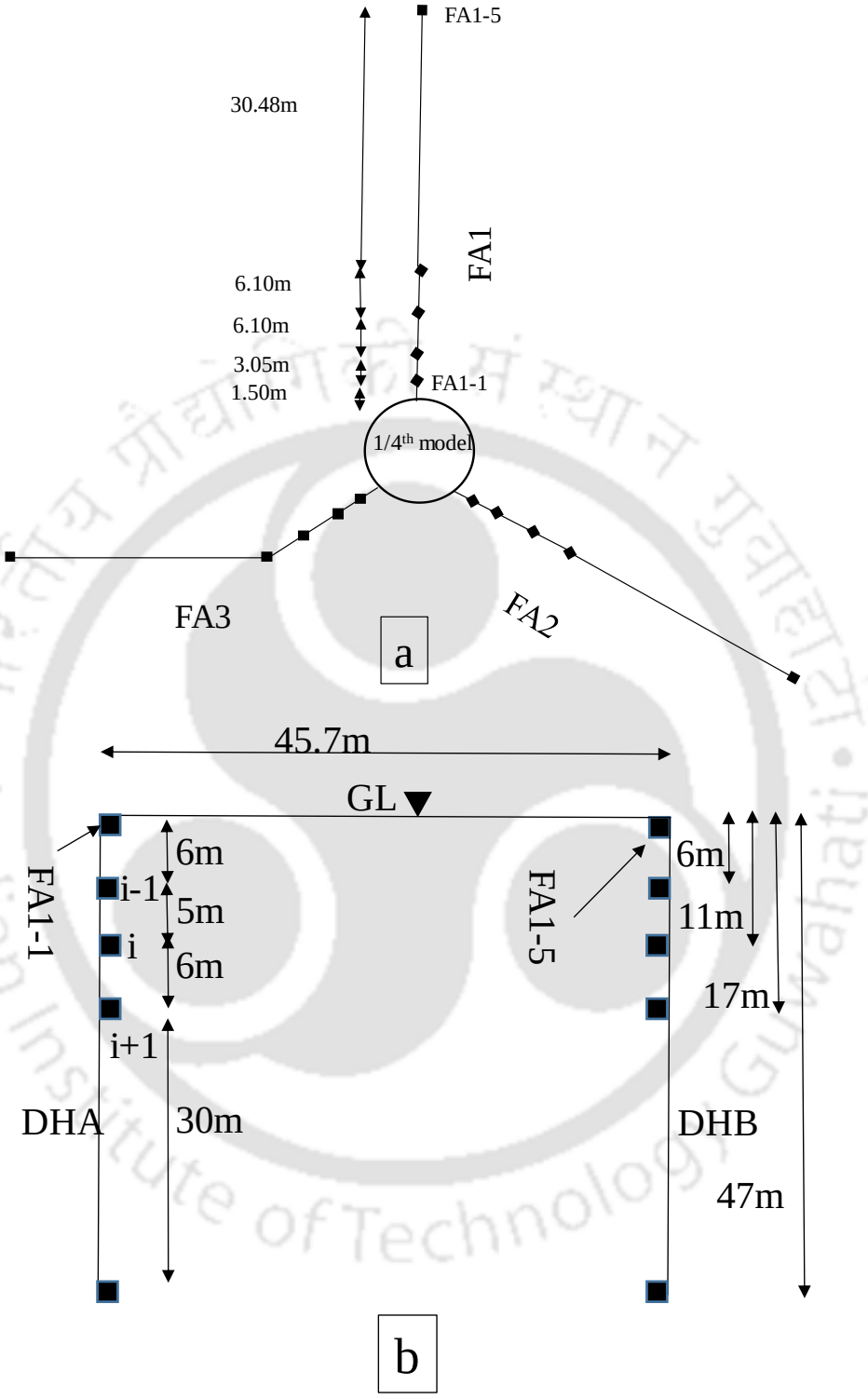

Figure 2.1, Lotung downhole array details for; a) for linear surface arrays FA1, FA2 and FA3 and b) downhole arrays DHA and DHB (modified after Elgamal et al. 1995)

downhole array that recorded a set of acceleration time histories in USA was located at Union Bay in Seattle, Washington (Seed and Idriss 1970b). After this, many downhole arrays were installed in US, Japan, Taiwan, Mexico, Greece and New Zealand (Elgamal et al. 2001). Most of the downhole arrays in USA are located in California (Elgamal et al. 2001), including arrays in Garner Valley, Wildlife Refuge, Borrego Valley, Treasure Island, Hollister Municipal Airport, San Francisco, McGee Creek, Los Angeles, Cholame Valley near Parkfield and Cajon Pass). Apart from these, Paducah in Kentucky (Street et al. 1997) and an array at Northeastern University in Boston, Massachusetts are notable mentions. In Japan also, a number of downhole array sites were established, such as: Port Island, Rokko Island, Chiba, Ashigara Valley, Kushiro, Hokkaido, Hiyoshi, TKS, KNK, SGK, Shuzenji, Chosi, Tateyama, Higashimatsuyama, Sunamachi, Etchujima, TTRL, Samukawa, Fujisawa, Shinfuji, Sandai, Tomioka, Fuchu, Westa, Shizuoka, Iwaki, Yokohama, Kanto etc. (Elgamal et al. 2001). Similarly, in Taiwan also, many downhole arrays are operating (Lotung, Hualien, Wuku, Dahanetc). Further, downhole arrays in Mexico, China, Greece and New Zealand are also existing (Elgamal et al. 2001). In this chapter, a detailed review about downhole arrays, records from which were used in arriving at dynamic soil properties following inverse analysis, is presented.

2.2.1 Lotung downhole array:

The Electric Power Research Institute (EPRI) of Palo Alto, California along with Taiwan Power Company (TPC) jointly conducted a model study (Large Scale Seismic Testing, or LSST) in 1984. The study was aimed at understanding the soil-structure interaction (SSI) problem and the response of a model nuclear power plant reactor containment structure under seismic loading. Two scaled-down ($1/4^{th}$ and $1/12^{th}$) models of the containment structure were constructed at a site located at Lotung in north-west Taiwan (24.6822051N, 121.7389236E). The Lotung site was

chosen for the construction of model structures because of a couple of reasons. Firstly, the soil profile here consists of soft alluvium with nearly horizontal stratification. Secondly, the site is located in a seismically active region (Chang et al. 1996; Tang et al. 1989). The instrumentation here consists of three linear surface arrays (FA1, FA2 and FA3 as shown on Figure 2-1a) and 2-downhole arrays (DHA and DHB as shown on Figure 2-1b). The arrangement of the accelerometers is shown in Figure 2-1 (a, b). The three surface arrays are located 120^{o} apart from each other, centering the 1/4th model structure. Each of these three surface arrays consists of five individual triaxial accelerometers. The first accelerometer is located outside the perimeter of the containment structure, and the subsequent accelerometers are located at ½, 1 ½, 2 and 4 ½ diameters (of the model containment structure) away from the wall of the containment structure (Tang et al. 1989). The downhole accelerometers are located below the first (FA1-1) and last (FA1-5) surface accelerometers along the FA1 (See Figure 2-1). They are embedded at 6m, 11m, 17m, and 47m depths, in addition to the surface accelerometer. It should be highlighted here that the downhole accelerometers are not located precisely below the surface accelerometer. Instead, these are located in different boreholes centering the surface accelerometers (FA1-1 for DHA and FA1-5 for DHB) (Tang et al. 1989).

The local geology consists of Holocene alluvium about 35m thick, underlain by Pleistocene materials of approximately 350m thickness that overlies Miocene bedrock. The Holocene layer consists of alternate layers of silty sand and sandy silt with some gravel fraction. The soil below the Holocene layer consists of clayey silt and silty clay (Tang et al. 1989). For the purpose of LSST experiment, eight boreholes were drilled at the test site. These borehole data were further used to generate soil profiles at the study location (Mar et al. 1991; Tang et al. 1989). For the present study, a borelog for the DHB site is generated (see Table 2-1) based on the soil profile

information available from Mar et al. (1991) and Tang et al. (1989). It can be observed from Table 2-1 that the lithology at the DHB site consists of alternate layers of gravel, silt, and sand up to a depth of 34m. Below this lies sandy silt and silty clay layers that extend till 60m depth. A typical SPT test result which is obtained from (Elgamal et al. 1995), is presented in Figure 2-2 here. From Figure 2-2, it can be clearly observed the SPT-N values in the top 20m layer are low (less than 10), suggesting the presence of soft soil. Beneath this depth (between 20-34m), the average SPT-N value increases to 11. Further, SPT-N values between 34m and 37m depth are comparatively higher (≈ 35) than the rest of the borehole. After this, the average SPT-N value drops to 12 for the remaining depth. In addition, low γ corresponding V_s profile based on geophysical methods is also available for the Lotung site (Anderson and Tang 1989), as shown in Figure 2-3. According to Anderson and Tang (1989), V_s values increase gradually from the ground surface to deeper layers. Values of V_s were observed to be 100m/s at the ground surface, 250m/s at a depth of 20m, and 280m/s at 60m depth. Similarly, V_s values in the depth range of 60

Table 2.1, Soil stratification details at DHB

Depth (m)	Soil type
2.28	Gravel
13.82	Silty sand and
25.23	Gravel
28.08	Sandy silt
34.2	Gravel
60	Sandy silt and silty clay

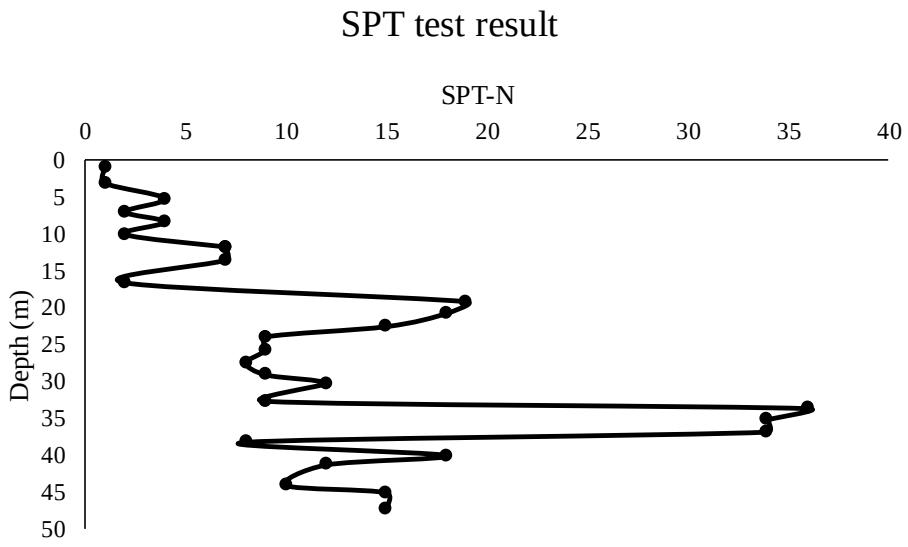

Figure 2.2, SPT-N profile at Lotung site considered for present work

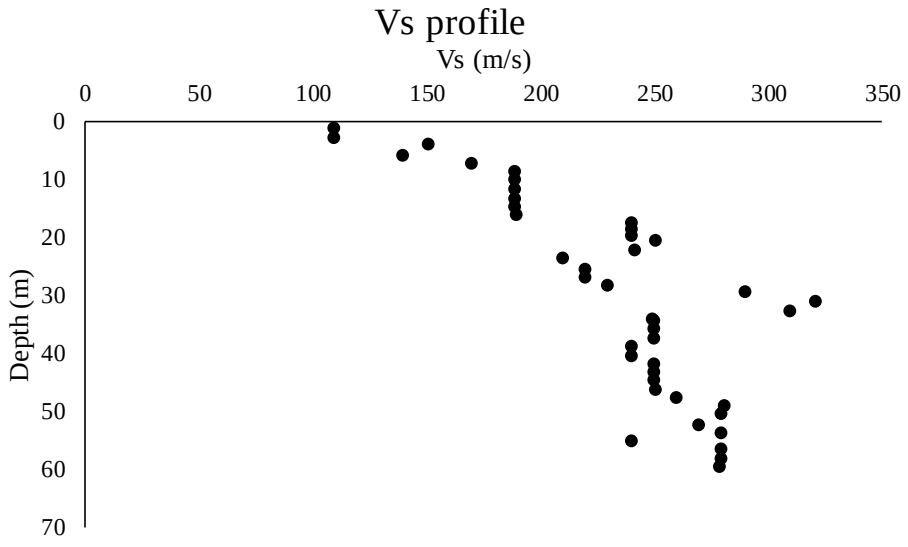

Figure 2.3, V_s profile at Lotung site

to 80m and 80 to 150m depths were found to be 320m/s and 480m/s, respectively. On the contrary, the V_s value in the depth range of 30 to 33m was observed to be 300-330m/s, which was higher than adjacent layers (Tang et al. 1989).

2.2.2 Port Island downhole array (Japan)

Port Island (PI) is a reclaimed island located southwest of Kobe, Japan. A downhole array system at PI was installed in August 1991 by the Development Division, Kobe City (Iwasaki

1995; Iwasaki and Tai 1996). The instrumentation at the site consists of four downhole accelerometers extending to a depth of 82m. The other 3 accelerometers are placed at 0, 16 and 32m depths below ground surface (Iwasaki and Tai 1996). The subsurface lithology at PI can be divided into five major strata. These include; i) The surface layer consisting of reclaimed loose sandy layer up to 19m depth; ii) An alluvial clay layer between 19m and 27m depth; iii) diluvial (formed by flood) sand and gravel strata interlayered with clay between 27-61m depth; iv) a diluvial clay layer between 61-82m depth; v) Sand and gravel layers interlayered with clay below 82m depth (Elgamal et al. 2001). The water table was located at 4.5m depth from the ground surface (Yangisawa and Kazama 1996). For the PI site, SPT-N, primary wave velocity (V_p) and V_s profile are also available (Iwasaki 1995). It was observed by Iwasaki (1995) that V_s values increase with the depth from the ground surface. V_s value at ground surface was about 170m/s, which increases to 210m/s at a depth of 19m. V_s value in the alluvial clay layer was comparatively lower (180m/s) than the adjacent layers. Further, V_s recorded at the top of the diluvial sand layer was 245m/s, which increased to a value of 350m/s at 61m depth. In contrast, V_s value observed at the diluvial clay layer was only 305m/s, which again increased to a value of 320m/s in the gravel layer located below 82m depth.

2.2.3 Chiba downhole array (Japan)

Chiba downhole array is located at the Chiba experiment station, at the University of Tokyo (Elgamal et al. 2001) about 30km east of Tokyo. The latitude and longitude of the array site are 35° 37’ 17’’N and 140° 6’37”E (Katayama et al. 1990). This array system was installed in 1982. Further, details about the arrays can be found in Katayama et al. (1990). At the downhole array locations, the accelerometers are placed at 1m depth from the surface and in the downhole (Katayama et al. 1990). While initial set-up had 11 downhole arrays, consisting of 36

accelerometers, later 4 boreholes with 8 accelerometers were added in 1985 (Katayama et al. 1990). Based on the borehole record obtained at the Chiba site, information on the site lithology was obtained. The top 5m layer consists of loam underlain by a sandy clay layer having thickness from 2m to 4m. Below the clay layer, a diluvial sand layer is present, interspersed with intermediate clay layers. SPT-N values obtained at the loam layer and clay layer were less than 10 (Katayama et al. 1990). However, SPT-N values in the diluvial sand layer were in the range 20-30, with low SPT-N values recorded for the intermediate clay layers. The ground water table was located at 5m depth from the ground surface (Katayama et al. 1990). V_S value increases gradually from surface to downhole. In the top 5 m, average V_S is around 140m/s after which it attains an average value of 320m/s for the next 19m thickness. Beneath this, average V_S is around 420m/s in depth range of 24m-40m.

2.3 Systematic review methodology

A systematic review is an approach that identifies existing researches, picks and assesses ideas, analyzes and synthesizes data, and publishes findings that provide relatively unambiguous judgments about existence and non-existence of research outcomes. A systematic review differs from a traditional literature review in that it investigates the responses to well-stated research questions. To do a systematic review, a step by step manner (see flowchart given in Figure 2-4), as suggested by Denyer and Tranfield (2009) has been followed here. The first step of a systematic review is to form research questions based on the current trends in the corresponding research area (Abdirad and Dossick 2016). Once research questions are formulated, related literature are searched for. Research papers are then chosen based on selection criteria. Finally, based on analyses and synthesis of the selected research papers, answers to the predefined research questions are found out.

Figure 2.4, Steps of systematic review adopted in this thesis work (based on Denyer and Tranfield 2009)

2.4 Research questions

A set of research questions are framed to explore the influence of various controlling parameters on inverse GRA and possible research gap, based on the present systematic review. Considering the importance of DSPCs of *in-situ* soil, answers to the following four research questions, related to inverse GRA using seismic array records, are searched.

Research question 1: What are the limitations of existing studies which have proposed inverse GRA frameworks for determining DSPCs?

Research question 2: How existing studies highlight the importance of Peak Ground Acceleration (PGA) of input motion in determining DSPCs?

Research question 3: How existing studies highlight the importance of frequency content of input motion in determining DSPCs?

Research question 4: Whether existing studies attempted the estimation of G or β or both, based on inverse GRA?

2.5 Selection of studies

Based on above research questions, a search criteria is formulated. The criteria include search strings such as 'Dynamic soil properties estimation from downhole array records' and 'Dynamic soil properties back-calculated from downhole array records'. A number of peer reviewed databases (ASCE, Elsevier, Science direct), textbooks, and other sources are searched for relevant studies. A number of keywords and Boolean operators are used in searching the relevant literature. Once the search is conducted on various databases, the titles are screened by the authors, the duplicate records are removed, and the abstracts of all the relevant papers are screened.

2.5.1 The inclusion and exclusion criteria

Earlier, Oskay and Zeghal (2011) conducted an extensive review on the methodologies developed for inverse analyses for geotechnical earthquake engineering problems. Oskay and Zeghal (2011) characterized the inverse methodologies based on the application of constitutive modeling (τ-γ relationships). A complete classification of such inverse techniques is provided in Figure 2-5. It can be observed from Figure 2-5 that the inverse analysis techniques are classified into two broad classes; A) techniques which do not utilize constitutive relations and, B) techniques which utilize constitutive relations. In this study, referring to Figure 2-5, works which did not adopt constitutive modelling, are considered for review. Studies which performed IGRA based on either frequency domain or time domain methodologies are included. Studies which are not based on methodologies mentioned above are excluded in the systematic review. Other constitutive model based methods [such Extended Kalman Filter, Extended Bayesian Method, Artificial Neural Network, Genetic Algorithm] are only mentioned and not discussed in detail in

this study. Further, works which belong to response characterization method are considered and works where time-series modeling was performed, are left out. It should be highlighted here that

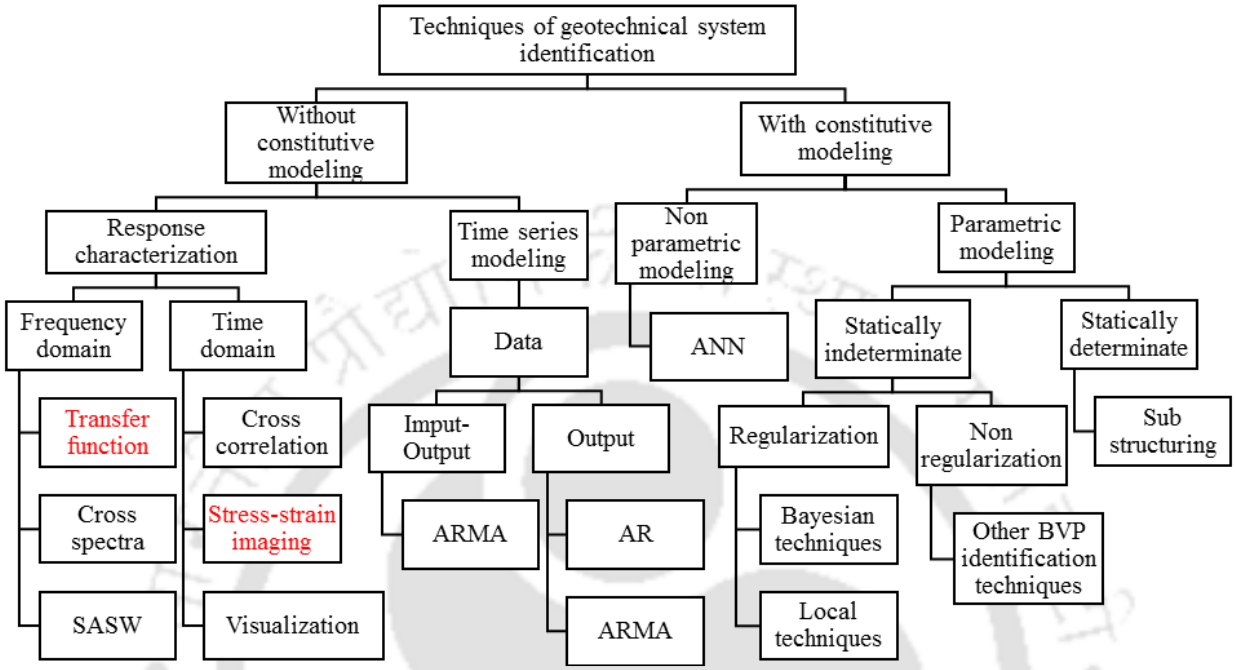

Figure 2.5, Methodologies developed (modified after Oskay and Zeghal 2011)

cross-spectrum and cross-correlation analyses are suitable for the estimation of low γ corresponding average V_s values for levelled site (Oskay and Zeghal 2011) and are excluded here. The categories of studies selected for the present review work are highlighted in red color in Figure 2-5.

Based on the above discussed criteria, the shortlisted studies are read in full text, and based on the inclusion and exclusion criteria, the relevant papers are selected and considered for review. Initially, only those papers which determines at least one of G/G_{max} or β curve from downhole array records, are considered. In doing so, papers which back-calculated V_s profile or low γ corresponding β values, are excluded. Remaining papers are categorized either into frequency domain or time domain methodology, based on earlier discussed criteria. In doing so, it is found that some of the works were based on same methodology adopted by same authors but

performed on different downhole array. In such cases, only one representative work from such studies are considered for the review. In addition, if same authors had published work in journal as well as conferences, work published in journal are referred while conference works are excluded in the current systematic review.

2.5.2 Results

Based on above discussed criteria, the search operation is carried out in peer review databases which initially yielded a total of 35 papers. Out of these, 4 were duplicate records and are removed. The titles of 31 papers are screened. After initial screening, the abstracts of 27 papers are read. Further, a total of 16 papers are read in full text out of which 11 papers are finally considered for the systematic review to find answers for earlier posed research questions.

2.5.3 Frequency domain method

2.5.3.1 *Tokimatsu and Midorikawa (1981)*

The earliest attempt to determine DSPC from EQ recordings was made by Tokimatsu and Midorikawa (1981). At the time of above work, downhole arrays, which could record acceleration time histories at different depths, were not available. Thus, G/G_{max} curves were developed based on surface recordings only. For the purpose, 4 recording stations (Hososhima, Hiroo, Kushiro J.M.A. and Kushiro harbor) located in Japan were considered. The soil condition and SPT-N values were also available for the sites (Tokimatsu et al. 1989). The soil profile at these four sites were composed of mainly clay, silt and sand layers. However, the presence of gravel layer was also identified at Hiroo site. The soil condition information at Hiroo, Kushiro J.M.A. and Kushiro harbor was available up to 20-25m depth. In contrast, soil information was available for 60m depth at the Hososhima site. At each of these stations, a surface accelerometer

was installed which recorded acceleration time histories during different EQs in both EW and NS direction. For the work, multiple EQ records consisting of Peak Ground Acceleration (PGA) varying from low to high range were considered, at each of the 4 stations. The maximum and minimum PGAs considered for the analyses at Hososhima, Hiroo, Kushiro J.M.A. and Kushiro harbor were 0.020g and 0.282g, 0.064g and 0.605g, 0.083g and 0.513g and 0.030g and 0.166g respectively. The methodology adopted considered spectrum analysis and multi-reflection theory of waves. The representative G/G_{max} values were determined by spectral analysis while γ was determined based on multi-reflection theory (Tokimatsu and Midorikawa 1981). According to Tokimatsu and Midorikawa (1981), the method used for the determination of G/G_{max} and γ was based on the following assumptions; i) The soil profile was considered to behave like one dimensional rod. In addition, it was assumed that the soil profile consisted of only two layers, i.e., surface layer with a finite thickness and bedrock with infinite thickness. ii) Ground surface motions were considered to be generated due to vertically propagating shear waves (SH) only. iii) Change in predominant frequency of ground motion between bedrock and surface was attributed to nonlinear soil properties. iv) The β values used for the computation of γ could not be back calculated. Thus, β values considered for the purpose were obtained through a correlation based on G/G_{max} values. The analyses procedure was based on the identification of predominant time period (T) from velocity response spectra of the corresponding surface motions.

According to Tokimatsu and Midorikawa (1981), T changed depending on the PGA value of the motion. As PGA increased, T also increased accordingly indicating nonlinear soil behavior. Thus, once the value of T was identified, it was correlated to obtain G value ($G=16\rho\frac{H^2}{T^2}$, H= thickness of surficial layer and ρ is its mas density). Further, G_{max} values were computed for

different sites, based on minimum value of T (T_{min}) obtained from velocity response spectra of weak motions. Therefore, G/G_{max} values were correlated to $(T_{min}/T)^2$ to obtain G/G_{max} curves at different sites. Corresponding γ time histories were computed based on an equation derived from one dimensional wave equation and multi reflection theory. The representative average γ value (γ_{avg}) was taken as 0.65 times of peak γ. According to Tokimatsu and Midorikawa (1981), parameters required for the computation of γ included V_s and β of the surficial layer along with velocity time history at the ground surface. Further, Tokimatsu and Midorikawa (1981) highlighted that the procedure can determine meaningful results when the impedance ratio (surface/bedrock) is less than 0.3. According to Tokimatsu and Midorikawa (1981), such low impedance ratio ensured nonlinear response in the bedrock (if any) which would have had negligible effect on the response at the ground surface. The method was first employed on EQ records obtained at Hososhima site. At this site, top 51m soil was composed of fine sand, silt and clay overlying tertiary bedrock in varying thicknesses. However, for the analyses purpose, all these different soil layers, (up to 51m depth) were considered as a single soil layer resting over the bedrock. Thus, G/G_{max} values obtained at this site represented dynamic soil properties for the entire 51m depth. The back calculated G/G_{max} values were compared with the results obtained by Iwasaki et al. (1979) for clay, conducted for confining stresses, representative of the site condition at Hososhima. Though much scatter was observed in the back-calculated G/G_{max} values, according to Tokimatsu and Midorikawa (1981), the values showed degradation trend with increasing γ. A similar procedure was applied to other 3 sites as well. G/G_{max} values furnished through the analyses, performed on these sites, when compared with G/G_{max} curves developed by Kokusho (1980) and Iwasaki et al. (1979) for clay soil (as shown in Figure 2-6), were found consistent with laboratory findings. In addition, Tokimatsu and Midorikawa (1981)

while attempting to correlate G/G_{max} with respective PGA and peak ground velocity (PGV) separately for all the sites, found the data to be much scattered in case of G/G_{max} vs PGA. However, G/G_{max} vs PGV plot showed reasonable dependency irrespective of site. In addition, correlation between PGV and γ were also established for all the sites. Further, from PGV vs γ plot (on log-log scale), a slope of 1 was observed up to a γ of 10^{-4} (indicating linear behavior). Beyond this value of γ, the slope was no longer unity, indicating nonlinear soil behavior (Tokimatsu and Midorikawa 1981). Another important observation made by Tokimatsu and Midorikawa (1981) was that both G/G_{max} and γ values were better correlated with PGV rather than with PGA.

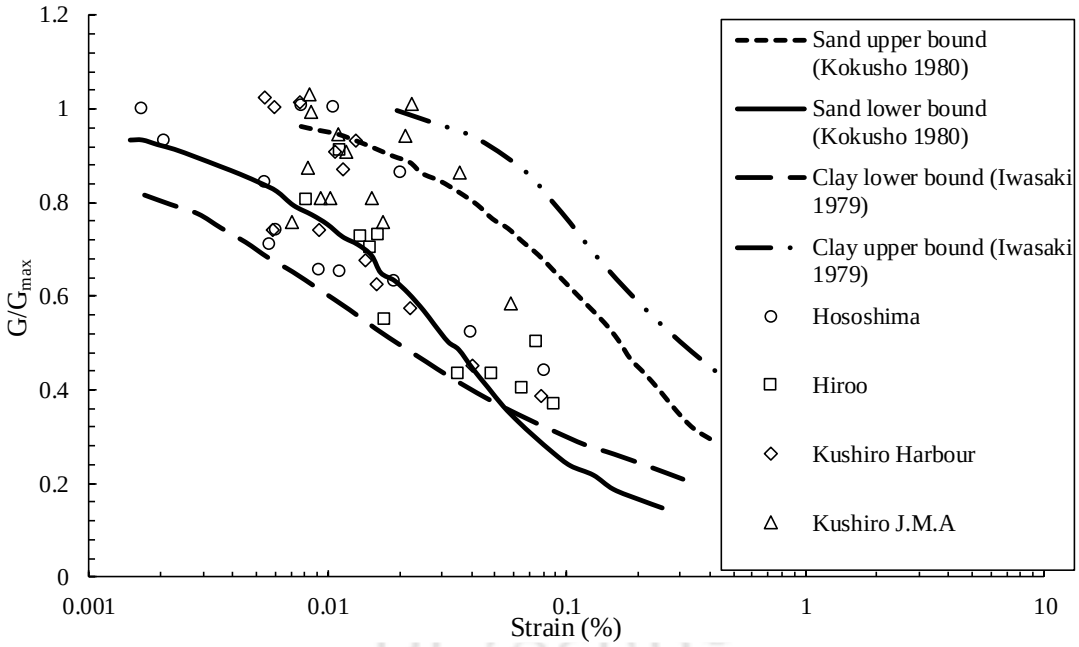

Figure 2.6, Comparison of back computed G/G_{max} by Tokimatsu and Midorikawa (1981) with other data

In another work, above methodology of Tokimatsu and Midorikawa (1981) was used by Tokimatsu et al. (1989) to obtain G/G_{max} values for Shiogama, Hososhima, Hiroo and Kushiro J.M.A. sites. In other work, Tokimatsu et al. (2006) adopted the same methodology to estimate G/G_{max} curves at K-Net Ojiya and J.M.A. Ojiya site. Similarly, Midorikawa and Miura (2008)

adopted above methodology to estimate G/G_{max} curves for K-Net Ojiya, K-Net Anamizu, J.M.A. Wajima and K-Net Kashiwazaki site.

2.5.3.2 *Chang et al. (1991a)*

Pioneering work in frequency domain was done by Chang et al. (1989, 1990, 1991a, b). Chang et al. (1991a) work was based on EQ records from the Lotung site. In the work by Chang et al. (1991a), 7 different EQ motions, recorded at DHB site, were used. Selected motions had PGA ranging from 0.03-0.21g, which could provide insight into both linear and nonlinear soil response. Acceleration records were available at ground surface and at 6m, 11m, 17m and 47m depths from the ground surface at DHB site. Further, both East-West (EW) component and North-South (NS) components of all the ground motion records were considered. The analysis was based on the fact that resonant frequency (f) of the transfer function (ratio of smoothen Fourier spectra between any two depths) [$H(\omega)$] itself is a function of the G and β. Further, it was pointed out that the change in f of the $H(\omega)$ can be used to back-calculate G value of the soil layer under consideration. The work assumed that all the ground motions considered for the analyses were the results of vertically propagating shear waves. Selection of vertically propagating shear waves for the analyses was justified by the fact that the transfer function is insensitive to incident wave having incident angle less than 30˚ (Wolf and Obernhuber 1982). Further, it was assumed that the entire ground motion record composed of shear wave component only, as the peak energy portion of the records belonged to shear wave arrival time. The entire analyses were divided into six phases. In 1st phase, the Fourier spectra were computed for all the motions, at each of the earlier mentioned depths. In computing Fourier spectra, the total durations of the ground motions were used. In 2nd phase, the Fourier spectra were smoothened using a 1Hz moving triangular averaging operator. In 3rd phase, the $H(\omega)$ of the

smoothened Fourier spectra between the surface and considered accelerometer-corresponding depth were estimated. Subsequently, the f of the transfer functions was estimated. In 4th phase, fundamental frequency (f_n) of each layer was computed with the help of the f determined in advance and the solution developed for two layers problem by Madera (1970). The procedure developed by Madera (1970) utilizes f of $H(\omega)$ between surface and a particular accelerometer level in iterative manner to find out f_n of the layer immediately below the depth. Once the value of f_n for each soil layers was known, V_s was determined by multiplying f_n with four times the layer thickness ($V_s = 4f_nH$). In 5th phase, γ at different depths were calculated by the computer code SHAKE (Schnabel et al. 1972). β curves, determined in the laboratory, were used for computing γ at various depths. In the final phase, estimated V_s values in step 4 were normalized with respect to the low γ (< 10^{-4} %) corresponding V_s values which were reported based on field testing. From the steps followed, it was also found that f decreases as PGA increases. Proposed G/G_{max} curve was consistent with respect to the shape of the curve. In addition, values of G/G_{max} were in good agreement with those obtained from resonant column test data for γ < 2X10^{-3}%. Further, for γ range of 5X10^{-3}% to 2X10^{-2} %, estimated G/G_{max} values were 10% lower than the laboratory outcomes. In addition, G/G_{max} values obtained were found matching with cyclic triaxial

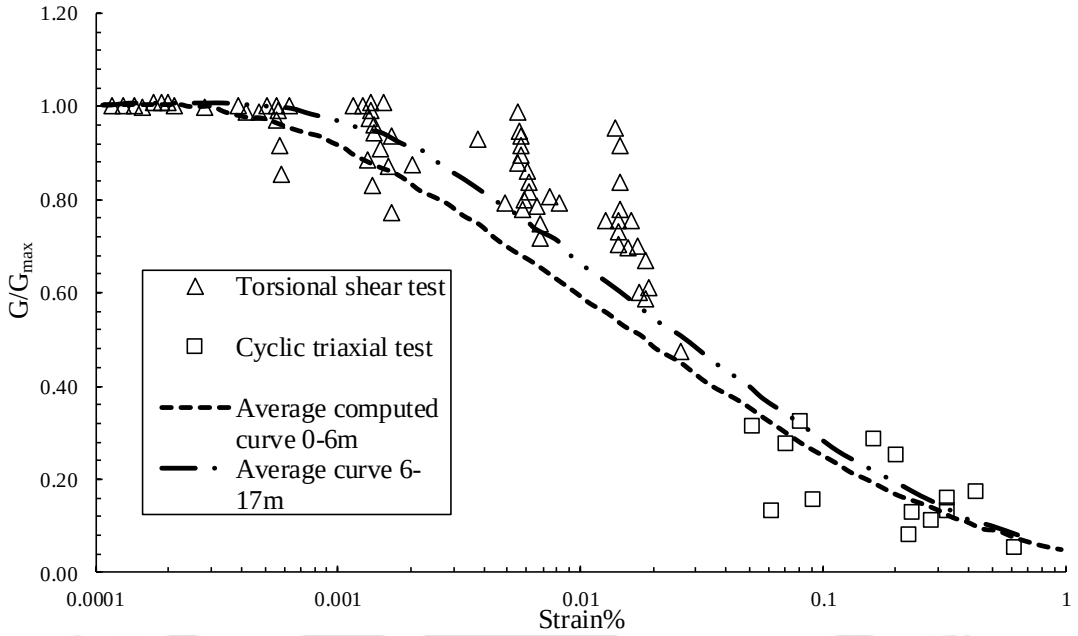

Figure 2.7, Comparison of back calculated G/G_{max} by Chang et al. (1991a) with other data

findings for γ range of $3X10^{-2}$% to $2X10^{-1}$ % (Figure 2.7). It has to be mentioned here that the work by Chang et al. (1991a) did not attempt to estimate β values rather used β obtained from laboratory investigation to determine γ values.

2.5.3.3 *Chang et al. (1996)*

In another work performed by Chang et al. (1996), again EQ data from Lotung site (DHB) were considered. The objectives of this work were; i) to gather field evidence of nonlinear soil behavior during an EQ, ii) to check the usefulness of the V_s profile determined by geophysical methods iii) to check the usefulness of the G/G_{max} curves determined from laboratory experiments. In order to accomplish the preceding objectives, 7 EQ records (LSST 6, 7, 9, 10, 11, 12, 16) at Lotung site with PGA ranging from 0.03g to 0.21g were considered. Chang et al. (1996) further highlighted that the epicentral distance and magnitude (M_L) of the selected EQs ranged as 5.0 to 77.9km and 4.5 to 7 respectively. In addition, it was mentioned that the azimuths of the EQs turn the orientation of the accelerometers as either radial (parallel to the azimuth of

EQ) or transverse (perpendicular to the azimuth direction) to the EQ source. In case of EQs which were considered for the analyses, it was found out all the accelerometers at the DHB site were oriented either radial or transverse with respect to the azimuths of the EQs except for LSST 9, 10 and 12. For these 3 EQs, the NS and EW components recorded at the site were thus decomposed and added to obtain radial and transverse components (Chang et al. 1996). In the work, Fourier spectral ratio (Fourier spectral analysis) technique was applied to accomplish above mentioned objectives. Chang et al. (1996) highlighted, Fourier spectral ratio technique could produce better result compared to other methods (procedures used in auto spectral ratio, cross spectral ratio, time domain method) as it is supported by wave propagation theory and can take into account both upward and downward travelling waves. In addition, formulation of error optimization schemes was also not required for the used methodology (Chang et al. 1996). The method was based on the identification of fundamental resonant frequency of a soil column between the surface and a particular depth. In order to achieve this, the Fourier spectra of the EQ records were computed at different depths. While computing Fourier spectra, either entire time history or segment of a time history can be used as highlighted by Chang et al. (1996). These spectra were then smoothened with a moving triangular averaging operator having a bandwidth of 1Hz. Further, the ratios of these spectra (transfer function) between surface and different accelerometer level were computed for all frequency ranges. According to Chang et al. (1996), two important characteristic of the $H(\omega)$, which can be used to identify f are the lowest frequency at which the $H(\omega)$ reaches peak and (alternatively) the frequency at which phase angle becomes 90˚. Once the f between surface and different acceleration levels were determined, these were further utilized to find out f_n of different soil layers. In order to determine the f_n, the solution developed for two layer problem by (Madera 1970) was applied. Computed f_n values of

different soil deposits were then used to find out V_s ($V_s = 4f_nH$, H= thickness of soil layer) values for different layers. The γ time histories were computed through deconvolution analysis incorporated in SHAKE (Schnabel et al. 1972). Computation of γ time histories requires surface time history and representative equivalent linear G and β values for each of the layers at a particular γ level. G values (determined from back-calculated V_s values) provided in SHAKE (Schnabel 1972) were determined by the earlier mentioned procedure. However, the β values were obtained based on laboratory based β curves, on samples from Lotung site by National Taiwan University (NTU). These data were based on resonant column test for low to intermediate range of γ (less than 10^{-2}% as per Chang et al. 1996). Thus, for γ>10^{-2}%, the curves were extended parallel to the curves obtained by NTU (1989) and University of California, Davis (UCD 1990) through triaxial test data (Chang et al. 1996). Two β curves were considered for the determination of γ time histories: one β curve for sand in top 34m depth and second β curve for clay existing in 34-47m depth. Thus, while computing γ time histories, only β values were updated in an iterative manner to obtain γ compatible β. According to Chang et al. (1996), change in *f*, as excitation level changes during an EQ, can represent change in V_s value or nonlinear response of soil. In order to illustrate this, Chang et al. (1996) divided LSST 16 EQ motion into different 5s time windows (5-10s, 10-15s, 15-20s, 20-25s, 25-30s, 30-35s, 35-40s). PGA in the time window range of 5-10s was 0.01g while in time windows of 20-25s and 35-40s were 0.13g and 0.04g respectively. Further, Chang et al. (1996) presented $H(\omega)$ between surface and 6m depth for the above mentioned time windows and EQ record. It was observed that the value of *f* changed from 5.3Hz in 5-10s window to 3.6Hz in 20-25s window and finally attained a value of 4.4Hz in 35-40s window. Similarly, the $H(\omega)$ and the corresponding *f* values were computed for LSST 7, 8 and 16 records for the intervals of 0-6m, 0-11m, 0-17m and 0-47m as

well. Further, obtained f values were plotted against PGA values of the corresponding time windows clearly showing degradation in f value as PGA increased. This confirmed nonlinear soil behavior during the EQ. In addition, Chang et al. (1996) determined V_s profile by making use of the time windows 5-10s and 20-25s for LSST 16 event. V_s profile obtained using the 5-10s window was consistent with the field measured V_s profile. However, in time window of 20-25s, V_s profile obtained was significantly lower than the field measurements. Further, Chang et al., (1996) highlighted that since the distance between DHB 17 and DHB 47 was more, V_s estimated in this interval (17-47m) were less reliable. In addition, LSST 6 and 7 record (entire time record) were used to determine V_s profile at the Lotung site. Obtained V_s profile using LSST 6 was slightly lesser than the field measurement. On the other hand, V_s profile obtained using LSST 7 data was significantly lower than the field measurement. Chang et al. (1996) thus highlighted that the V_s profiles obtained using specific time windows and entire time records were consistent with each other.

In order to develop γ compatible G/G_{max} curves, all the 7 EQ records were analyzed using the earlier mentioned methodology. In this case however, the total duration of EQs were used to obtain γ time histories and corresponding equivalent G values (Chang et al. 1996). Further, average value of γ (γ_{avg}) computed from deconvolution analysis, corresponded to 0.65 times of the peak γ as used in SHAKE (Schnabel 1972), was considered. In order to check the appropriateness of inferred V_s and γ_{avg}, acceleration time histories and response spectra (β=5%) were also computed at different depths for LSST 6 and 7. Consistency in the observed and the computed response spectra, for above mentioned EQ records, increased the confidence in the inferred V_s and γ_{eff} values. Computed G values at different levels were normalized with respect to G_{max} values obtained from weak EQ records. Finally, G/G_{max} values along with corresponding

γ_{avg} values were plotted for different depths. Chang et al. (1996) highlighted that G/G_{max} values in the depth range of 6 to17m depth were similar. Further, obtained G/G_{max} curves when compared with the curves obtained by NTU (1989) and UCD (1990) were found consistent (Figure 2-7). On the other hand, comparison of obtained G/G_{max} with University of Texas, Austin (UT) laboratory test data inferred values to be lower than laboratory findings.

2.5.3.4 *Kokusho et al. (1996)*

The 1995 Hyogoken -Nanbu EQ records have been extensively in use for different purposes by various researchers. In the work by Kokusho et al. (1996), records obtained during above EQ and one of its aftershock (occurred 2 minutes after the main shock), recorded at four recording stations along the Osaka Bay area of Japan were used. Lithology of the four sites Showa Giken Kogyo, Kakhonak, Tokushima, Port Island (SGK, TKS and KNK, PI) consist of sandy fill at the top followed by Holocene clay and sand underlain by Pleistocene gravelly soil. Apart from the aftershock record, twelve EQ records consisting of NS, EW and vertical (UD) components at each recording station, were used for the inversion analysis. A computer code, developed by Ohta (1975), which could perform the inversion analysis in a frequency domain method, was used. Accuracy of the inversion method was dependent on the degree of reproduction of the $H(\omega)$ for different layers. At first, the $H(\omega)$ for different layers were computed. Then the inversion analysis (assuming an appropriate initial soil layer model) based on borelog, was performed. Initially, low γ based V_s and β values were assigned to different layers. These values were updated to reproduce $H(\omega)$ at each interphase. It has to be mentioned here that only the absolute values of $H(\omega)$ were considered while reproducing them. The degree of reproduction of $H(\omega)$ was judged in such a manner that the lower frequency peaks were better produced than their higher frequency counterparts. For PI site, which was subjected to liquefaction during the

main shock, remarkable changes in G were observed. For Pleistocene and Holocene layers, a reduction of 20 and 40% respectively in V_s value was observed. In addition, for fill layer, reduction in V_s value up to 80% and 50% were found for saturated and unsaturated soil respectively. Further, when the aftershock record was used for the analysis, it was observed that the V_s values for the Holocene and Pleistocene layers were reached to the original values which were obtained from P-S logging test results (low γ values). However, V_s values in the upper fill layer remained degraded due to liquefaction. Same analysis procedure was applied to the vertical acceleration time history as well. It was mentioned by Kokusho et al. (1996) that V_p changed slightly from its initial values in the Pleistocene and Holocene layers (recorded by P-logging). On the other hand, for the fill layer, even 50% reduction in V_p was observed. Similarly, β values were back-calculated to be 6% for the Pleistocene and Holocene layers, and about 33-50% for the top layers when main shock record was utilized for the inversion. On the other hand, β values computed from the aftershock record were very high (10-12%) for the Holocene and fill layers and 5% for the Pleistocene layer. Estimated V_s and β values were further utilized to compute acceleration time histories and maximum γ at different accelerometer levels. Computed time histories were consistent with the recorded time histories except for a small phase lag in the surficial time history. Though computed γ values were less than 0.5% for the Pleistocene and Holocene layers, more than 2% γ were observed at the fill layer due to liquefaction. Similarly, inversion analysis was carried out for ground motions recorded at SGK site. It was observed the V_s value degraded up to 30-50% in the upper Holocene and Pleistocene deposits whereas for deeper Pleistocene layers, this degradation was less than 20%. Further, β values were estimated to be 2-6% for the Pleistocene soils while 10% for Holocene layers. Estimated V_s and β values were reutilized for the computation of acceleration time histories and γ values. Comparison

between computed and recorded time histories in terms of waveforms were concluded as matching. However, PGA values, computed from the analysis, were found higher than the recorded values. In addition, γ at this site remained less than 0.6% throughout the depth.

Records at TKS were also affected by the liquefaction. However, below 13m depth, reduction in Vs was reported to be less than 10%. The β values on the other hand, computed at TKS, were substantially lower than the PI site. The β values were in the range 6-10% even for the liquefied soil layers. For the KNK site, ground motion record had low Peak Horizontal Acceleration (PHA) as the site was located about 65 km away from the epicenter. As a result, the analysis here revealed nearly linear behavior of soil. V_s values reduced to a maximum of 20% for the upper layers while for lower layers, the reduction was around 5%. Similarly, β values were also estimated to be 1% in deeper layers (depth ≥40m) and 2% in upper layers, except from the very shallow top layer where it was around 4%. According to Kokusho et al. (1996), the γ value at the KNK site never exceeded 0.06%. Further, back calculated V_s values for all the sites and for all depths were normalized (ratio) with V_s values obtained from P-S logging test, which later were used to compute G/G_{max} values for each soil type. Typical plot for G/G_{max} vs γ values, for different soil types can be observed Figure 2-8. Apart from the G/G_{max} values corresponding to the liquefied layers, other layers showed fairly decreasing trend in G/G_{max} with increasing γ (Figure 2-8). Similarly, the back calculated β values from all the sites were sorted-out, according to soil type, and plotted against corresponding γ (Figure 2-9). Based on Figure 2-8 and Figure 2-9, Kokusho et al. (1996) further pointed out that the G/G_{max} and β curves for clay, gravel and sand while comparing were found to be located on the extreme right, extreme left side and in center of the plots. Thus, for each of the above three soil types, a clear degradation in G values with increasing γ can be observed from Figure 2-8. Similarly, the β values for all three soils

showed an increasing trend, similar to the pattern reported in the literature (Figure 2-9). However, β values obtained for the liquefied layer from PI site were found much higher than those obtained for liquefied soil, from TKS site clearly indicating inconsistency in terms of β estimation obtained from in-situ ground motion records. Further, G/G_{max} and β values were compared with laboratory obtained DSPCs (Kokusho 1980, 1994). According to Kokusho et al. (1996), the back-calculated values were closely matching with the laboratory determined DSPCs.

In another work, methodology similar to Kokusho et al. (1996) was adopted by Kokusho and Matsumoto (1998) , in order to obtain G/G_{max} and β curves for SGK, KNK, TKS and PI site. In addition, correlation between PGA amplification (surface PGA/base peak horizontal acceleration or PHA) and base level PHA was proposed. Similarly, correlation between PGV amplification (surface PGV/ base PHV) and base level PGV was also established. Further, PGA amplification with V_s ratio and PGV amplification with V_s ratio were also correlated in the work.

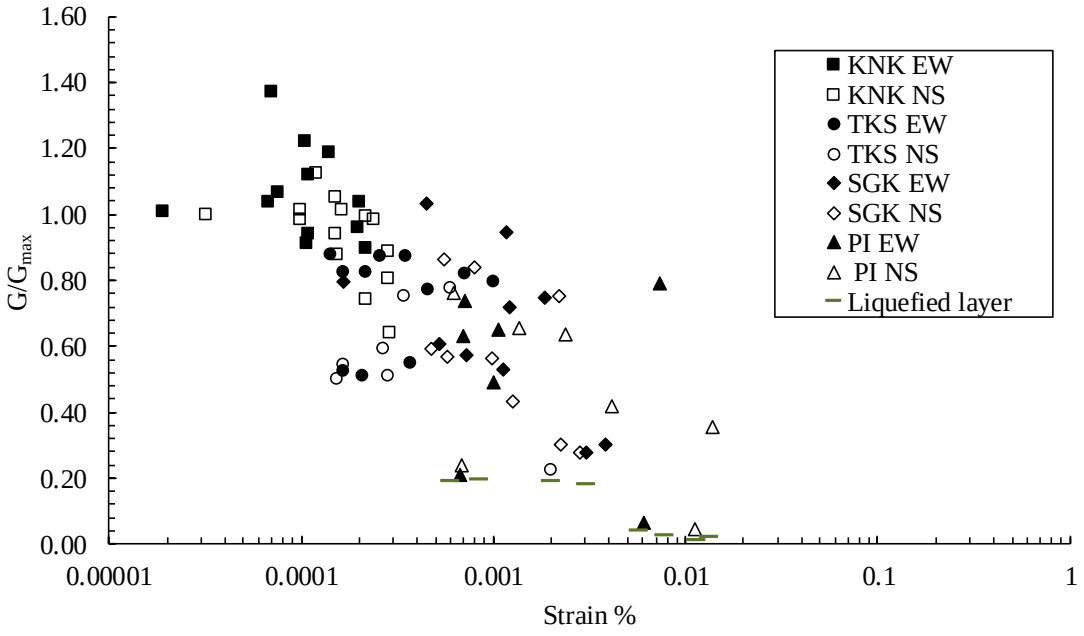

Figure 2.8, Comparison of back computed G/G_{max} by Kokusho et al. (1996) with other data

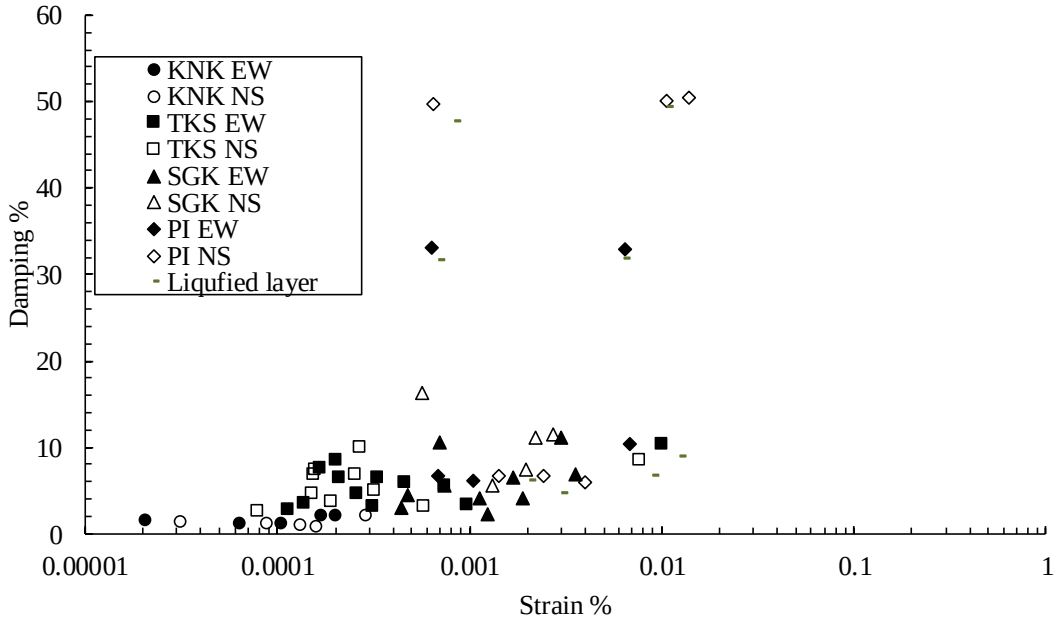

Figure 2.9, Comparison of back computed β curve by Kokusho et al. (1996) with other data

2.5.3.5 *Ghayamghamian and Kawakami (1996)*

In the work, 7 downhole array sites located in Japan (Chiba, Etchujima, Fujisawa, Samukawa, Shinfuji, Tomioka and TTRL) were chosen for the analyses. According to Ghayamghamian and Kawakami (1996), at each of these sites, multiple number of accelerometers were installed, both at surface and at different depths. For this work however, acceleration time histories, recorded at the surface and those recorded at depth of 10, 100, 30, 40, 28, 100 and 44m in Chiba, Etchujima, Fujisawa, Samukawa, Shinfuji, Tomioka and TTRL respectively were considered. At each of these sites, EQ data were selected in a way that they represented both lowest and highest PGA recorded at that site. In addition, few other records with intermediate PGA values were considered from each of the sites. PGA values of selected ground motions ranged between 0.080-0.416g. In addition, only the NS components of the records were considered for the analyses. Further details of these motions can be obtained in Ghayamghamian and Kawakami (1996). As per Ghayamghamian and Kawakami (1996), for Samukawa and Tomioka sites, EQ records with only the highest PGA (0.170 and 0.130g respectively) value were considered. This was due to

the fact that records at Samukawa and Tomioka consisted of long coda portion of the wave which could be used as weak motion for the determination of low γ dynamic soil properties. In order to perform more number of analyses at each site and at different level of γ, the EQ records were divided into different time windows. These time windows included shear wave portion of the records and could represent different level of shaking (Ghayamghamian and Kawakami 1996). Soil profile at 7 sites consisted of sand, gravel, clay and silt layers with different thicknesses and configurations. In contrast, the soil profile at the Shinfuji site consisted of only loam type of soil. Presence of humus soil at the surficial layer of the Fujisawa site was also observed. V_s values in these soil layers vary from 40m/s (humus layer at Fujisawa) to 726m/s (at 24-28m depth in Shinfuji). Inverse analysis procedure adopted by Ghayamghamian and Kawakami (1996) was based on the estimation of $H(\omega)$ between surface and downhole accelerometer level. The $H(\omega)$ were determined both by autocorrelation analysis and cross-correlation analysis. Further, f of these $H(\omega)$ were identified. At first, the auto and cross-spectra of the records (time windows) at surface and in downhole were computed. Then the spectra were smoothened by using a rectangular average filter with 0.5Hz bandwidth. Further, $H(\omega)$ were computed and square root of the $H(\omega)$ values were taken for the further analysis. It was observed that the values of f degraded as the PGA values increased in selected time windows. According to Ghayamghamian and Kawakami (1996), soil nonlinearity is directly related to the degradation in f. Thus, the values of f from all the $H(\omega)$ were identified. Obtained f values were divided by the maximum value of f to obtain V_s/V_s^{max} (V_s^{max} is low γ corresponding V_s value) values at all the sites. Further, these values were squared to obtain G/G_{max} values keeping ρ to be same. In addition, Ghayamghamian and Kawakami (1996) computed γ time histories between the surface and downhole accelerometer level by dividing the relative displacements between surface and

downhole locations (obtained from Fourier spectra) with the accelerometer spacing. Peak values from these γ time histories were correlated with the degradation in G. G/G_{max} curves for all the 7 sites when plotted separately showed a degradation behavior with increasing γ. For the Tomioka site however, such degradation behavior was very limited. Ghayamghamian and Kawakami (1996) pointed out that at Tomioka site, soil behaved linearly due to which no clear degradation in G value could be observed from the G/G_{max} curve. Finally, G/G_{max} curves for all the sites were plotted together and compared with the available literature. As per Ghayamghamian and Kawakami (1996), a consistency between the back calculated G/G_{max} and the one given in the literature could be observed (Figure 2.10).

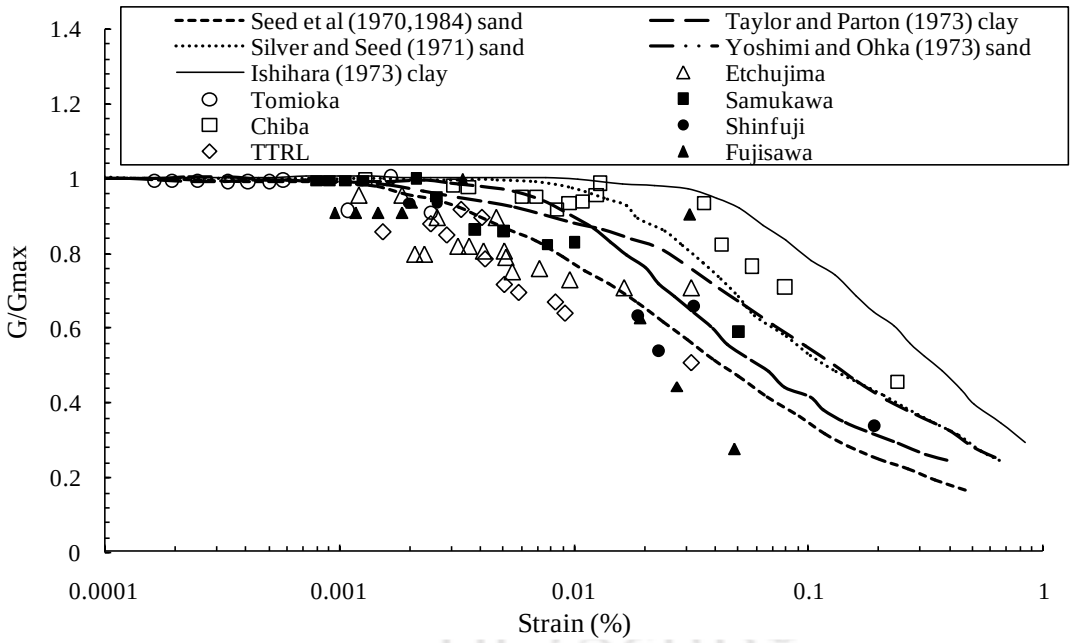

Figure 2.10, Comparison of back computed G/G_{max} by Ghayamghamian and Kawakami (1996) with other data

2.5.3.6 *Xu et al. (2003)*

In another work performed by Xu et al. (2003), frequency domain inverse analysis procedure was adopted. However, based on the work, no DSPC was proposed. The work instead focused on finding out low strain G or V_s from the inverse analysis. The Nuclear Power Engineering

Corporation (NUPEC) in Japan in collaboration with US Nuclear Regulatory Commission (NRC) and Brookhaven National laboratory (BNL) took up this work. Five EQ data, recorded at old and new free field point downhole array stations in Japan, were provided to BNL by NUPEC. Among these 5 records, one record consisted of a surface PGA of 0.174g which could represent nonlinear properties as well (Xu et al. 2003). However, in this work, all the EQ records were examined to check their suitability for the one dimensional upward propagating wave problem. For this purpose, Arias intensity of the EQ records at different depths were computed and plotted against depth. EQ records where a continuous built-up of energy was observed, as the wave travelled upward, were considered suitable for the analyses. EQs with inconsistency in this regard were influenced by the surface waves and thus were not considered. Once suitable records were sorted out, these were analyzed using the Fourier spectral ratio technique with Levenburg-Marquadt nonlinear least square fitting algorithm. The identification procedure for dynamic soil properties was expressed as a conditional least square optimization which aimed at reducing misfit between observed $H(\omega)$ and computed $H(\omega)$. The least square optimization was applied to develop a satisfactory correlation between the observed and computed transfer function. The Fourier spectral ratio technique was incorporated in program CARES (Xu and Graves 1993) which conducted the convolution analysis to determine G value. An iterative approach was followed in CARES (Xu and Graves 1993) to finally arrive at low γ corresponding G value.

Initial G values for the convolution analysis were chosen as per NUPEC. β values for different layers were kept as 1.5% (constant). $H(\omega)$ for both the sites were reproduced and compared with the actual Fourier amplitude ratio. For the Old free field point, when the $H(\omega)$ was produced, a good agreement was observed for the first peak at a frequency about 6Hz. However, there was mismatch when the 2nd peak was considered. According to Xu et al. (2003),

first peak in the transfer function controls the response. Thus, further modification in the computed transfer function was not attempted by Xu et al. (2003). Similar observation was made at the New free field as well. Further, response spectra at those two sites were computed. While computing response spectra, velocity profile and DSPC were obtained by BNL and Geotechnical Engineers Inc. (GEI) respectively. Convolution analysis was performed in CARES as mentioned earlier. The response spectra computed at depths 1.5m and 13m at the Old free field were in very good agreement when compared to the recorded response spectra. At the New free field point, the response spectrum computed at 3m depth was found to be matching very well with the recorded spectrum at the same depth. In addition, three laboratory determined G/G_{max} curves (EPRI 93, GEI, GEOMATRIX) were used along with the soil profile by BNL to compute response spectra at New free field point. These response spectra were computed at the New free field point at a depth of 3m and compared with the recorded one. Among these three response spectra, two (computed with G/G_{max} form EPRI 1993 and GEI) were found very consistent in terms of amplitude and frequency content. Though, the study made no attempt to compute β properties or γ dependent G values, it provided a guideline on how to choose EQ records while performing an inverse analysis.

2.5.3.7 *Ghayamghamian and Motosaka (2001)*

In the work performed by Ghayamghamian and Motosaka (2001), both frequency domain and time domain analyses were carried out. EQ data were collected from the Chiba dense array system in Tokyo from 1m, and 10m depths from the ground surface. For the analyses, two different EQ motions having PGA 0.301g and 0.033g were considered. According to Ghayamghamian and Motosaka (2001), these high and low level of shaking were capable of expressing nonlinear and linear soil response respectively. For the analysis, EQ records at 1m

depth and 10m depth were considered. Frequency domain inverse analysis methodology focused on identifying f values of the $H(\omega)$. It was observed that as the shaking intensity/γ increased, value of f decreased. According to Ghayamghamian and Motosaka (2001), this reduction in f value could be correlated to the degradation of G. For the analyses, the EQ records were divided into several time windows, each being 5.12s (1024 points for convenience in calculating Fourier spectrum). Time windows were selected in such a way that these corresponded to the shear wave portion of actual record. The aim of dividing the motions into several time windows was to observe different level of shaking in those time windows. The shaking level decreased from the arrival of the shear wave to the end of the record. Accordingly, the f values increased in those time windows starting from the arrival of shear wave to the end of the record. The analyses were carried out in four steps. In the first step, the cross spectrum was calculated for each of the time windows. In the second step, the obtained spectra were smoothened using a rectangular average filter having a bandwidth of 0.45 Hz. In the third step, the ratio of two smoothened spectra was calculated. In the last step, square root was taken from the spectral ratio and three times consecutive smoothening was applied based on visual observation of spectral shape. From the observations, it was clear that f decreased as the level of shaking was increased to PGA of 0.301 g. However, no specific change in f was found for the EQ having PGA of 0.033g. According to Ghayamghamian and Motosaka (2001), the change in f was attributed to nonlinear soil behavior. The transfer functions obtained from time windows with largest and smallest level of shaking showed reduction in f and amplification. Reduction in f directly represents reduction in G. Thus, all the f that were obtained by the analyses were divided by one value which is overall highest f representing low γ corresponding G. In this way, the G degradation values were calculated. In order to establish relationship between G/G_{max} and γ, γ time histories were also calculated for the

respective time windows. Double integrations were done to the up-hole and downhole accelerograms to compute the displacement time histories. Once displacement time histories were computed, their difference were divided by the distance between uphole and downhole instruments to compute the γ histories. To remove the drifts in displacement time histories, a band pass rectangular Finite Impulse Response filter was used, which produced no phase shift. Finally, maximum γ values for each of the time windows were plotted against computed G degradation values to obtain G/G_{max} (Figure 2.11). Obtained G/G_{max} curves based on the work were found consistent with the one reported in the literature. However, this work did not attempt to determine β curves from the inverse analysis.

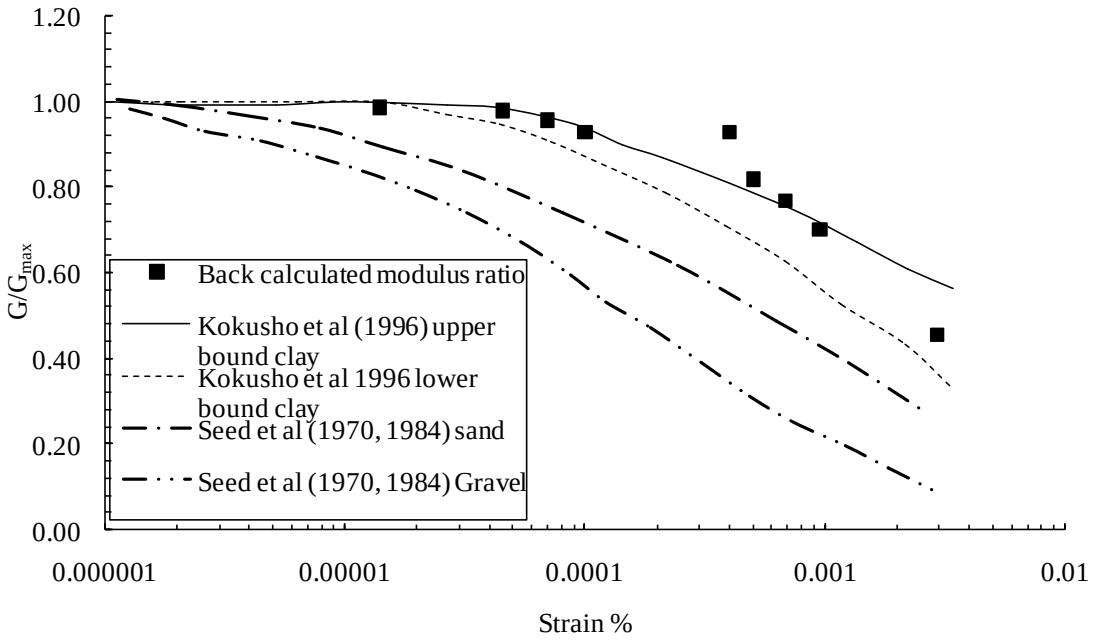

Figure 2.11, Comparison of back computed G/G_{max} by Ghayamghamian and Motosaka (2001) with other data

2.5.4 Time domain method

***2.5.4.1** Zeghal et al. (1995)*

Time domain identification of dynamic soil properties was first attempted by Zeghal et al. (1995). EQ data were collected from the Lotung downhole array system. Work by Zeghal et al.

(1995) used EQs recorded by DHB array. EQs considered for the identification of soil's nonlinear behavior included LSST 5,7,10, 12, 13 and 16. Among these motions LSST 5, 10 and 13 were categorized as weak motions while others were categorized as strong motions. Apart from identification of soil properties, an insight into excess pore water pressure generation during two EQs (LSST 12 and 16) was also studied. EQ records were available at the ground surface and at depths of 6m, 11m, 17m and 47m at the DHB site. The analysis procedure was based on shake table study by Koga and Matsuo (1990). Findings of Koga and Matsuo (1990) were directly applied to determine τ and γ time histories. In addition, τ and γ time histories were derived by solving equation of motion in one dimension using shear beam idealization. As a result, the τ time histories were computed by linear interpolation between downhole acceleration. It has to be mentioned here that these τ estimate were second order accurate. Similarly, second order accurate γ time histories were also computed by utilizing the displacement records between successive downhole acceleration records. Since, the distance between DHB17 and DHB47 was comparatively larger, the same methodology which was used to compute γ time histories at DHB 6 and 11 could not be applied to compute γ time histories at DHB17. However, a similar second order accurate expression (Zeghal and Elgamal 1993), which employed displacement histories at DHB6, DHB11 and DHB17, was utilized to compute γ history at the DHB17. Zeghal et al. (1995) highlighted that possible errors in estimating τ and γ time histories could come from three sources namely; instrument configuration, data processing and analysis technique. According to Zeghal et al. (1995), the peak energy of the EQ records was in frequency range of 0.3 to 5.0Hz. In this range, the approximate error in estimating τ and γ history was less than 2%. More reference for this type of error analysis was also given in the original paper. Zeghal et al. (1995) further pointed out that as γ time history was estimated by integrating acceleration time history,

it contained error due to baseline drift. Thus, in order to eliminate baseline drift and high frequency stress component, low and high pass filters were used. The analysis technique was very consistent with the results as stated by Zeghal et al. (1995). From the τ and γ time histories, stress-strain graphs were plotted for different depths (6m, 11m and 17m). Ellipses, which represent linear viscoelastic response (Lazan 1968) were fitted to the computed τ-γ hysteresis plots. While fitting the ellipses, two things were taken into consideration. First, the ellipses were chosen in a way that these could produce same energy dissipation as the actual τ-γ hysteresis loop. Secondly, the ellipses represented same τ at the peak γ as the actual hysteresis loop had. From these ellipses, equivalent G and β values were obtained. Analyses results from the weak motions were also utilized in the work. From these motions, low γ corresponding G values were obtained at different depths, which were consistent with the other correlations and geophysical tests results. According to Zeghal et al. (1995), generation of pore pressure also contributed to the stiffness degradation. To justify this, Zeghal et al. (1995) considered LSST 16 EQ data as it came with pore pressure recordings. Two hysteresis loops with equal amplitude of stresses were selected for the purpose. These loops were selected in such a manner that one represented stress-strain behavior before the peak γ phase (20-27s for LSST 16) and the other represented τ-γ behavior after attaining peak γ phase. Though the maximum amplitude of τ were same in both the cycles, cycle after the peak γ phase however showed degradation in G value when compared to the other cycle. According to Zeghal et al. (1995), in case of the LSST 16 EQ, during phase of peak γ, excess pore pressure rose to the maximum and after that remained nearly constant. Degradation in G after peak γ phase was thus attributed to the generation of excess pore water pressure. Therefore, Zeghal et al. (1995) divided each of the strong motion data into two parts, one which occured before the peak γ phase and second which occurs after the peak γ phase.

Analyses were carried out separately and the results were also divided into two parts accordingly. Consequently, the data showed more scatter after peak γ, due to the generation of pore water pressure. G/G_{max} and β values obtained at the site were compared with the laboratory tests based estimates in NTU (Figure 2.12 and Figure 2.13) as well as findings by UT. Based on the comparison, the G/G_{max} curve developed was found matching with the previous literature as well as field and laboratory measurements. Estimated β curve however showed more scatter with a fairly increasing trend with γ can be observed in Figure 2.13.

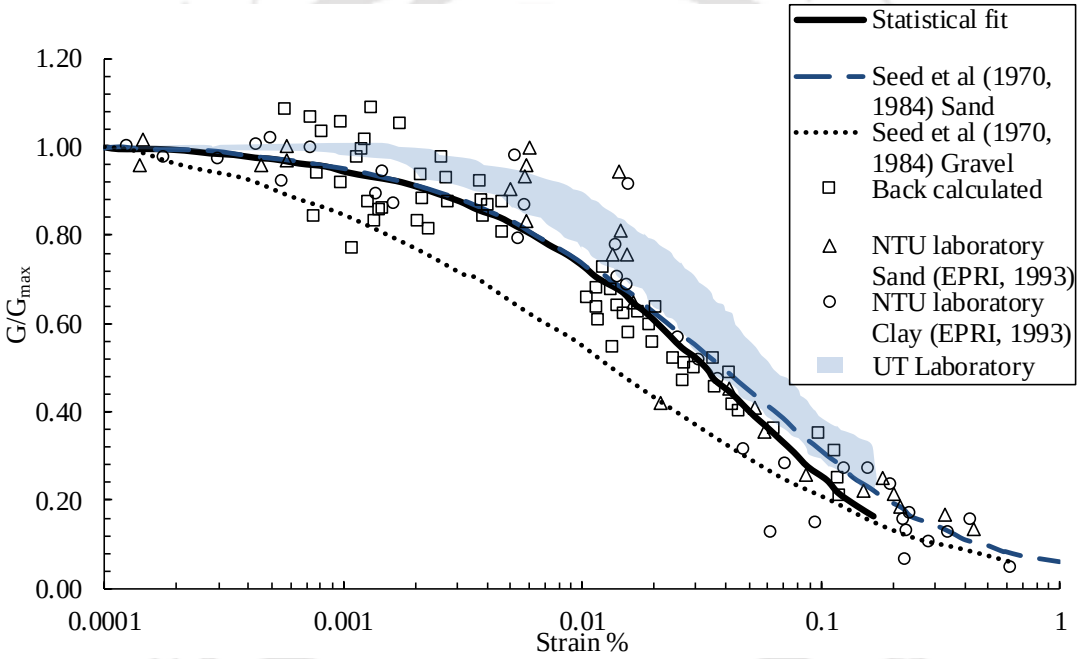

Figure 2.12, Comparison of back computed G/G_{max} by Zeghal et al. (1995) with other data

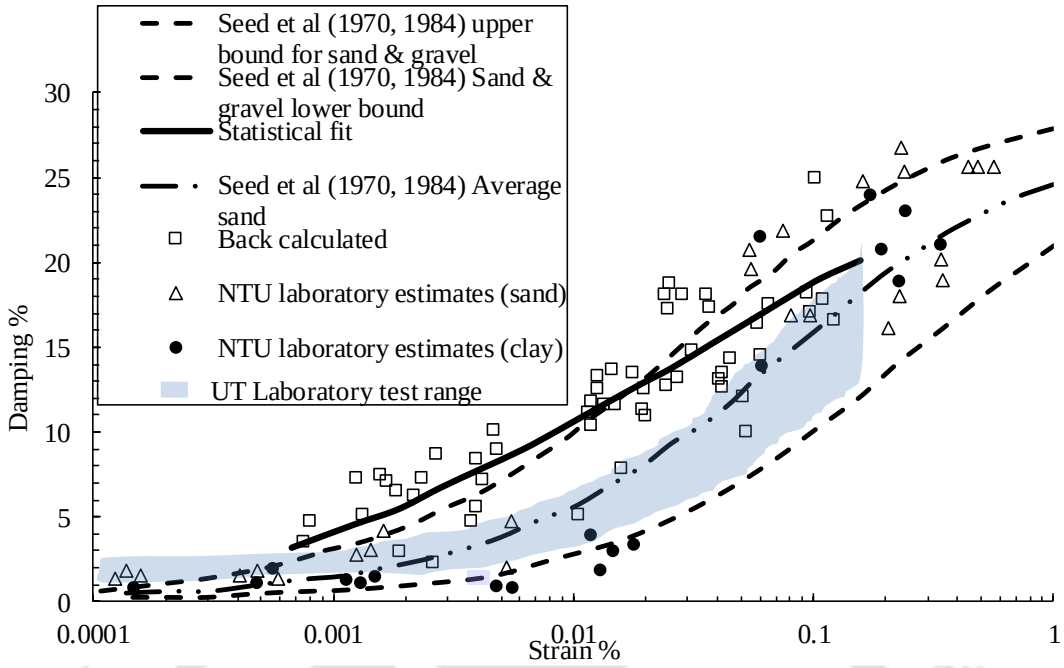

Figure 2.13, Comparison of back computed β curve by Zeghal et al. (1995) with other data

A similar time domain identification procedure was also adopted by Elgamal et al. (1996). In that work also, G/G_{max} and β curves were obtained for Lotung site. In addition, at the Treasure Island site, cross-correlation analysis and spectral analyses were performed to estimate V_s profile.

2.5.4.2 *Yanagisawa and Kazama (1996)*

In this work as well, time domain methodology, which was earlier used by Zeghal et al. (1995), was used. EQ data were collected from PI downhole array in Japan. Detailed description of the soil condition and location of the accelerometer can be found in section 2.2.2 earlier. Yanagisawa and Kazama (1996) considered a total of 9 EQ records consisting of the main shock and aftershocks of the 1995 Kobe EQ. Both the NS and EW components were considered for the analyses. Further, different time windows were selected for different motions, which covered the main acceleration portions of the records. The PGAs of the considered motions ranged from 0.004g to 0.342g. The objective of the work was to estimate the level of τ that affected the ground and how the ground behaved during the EQ. Apart from that, special attention was given

towards; i) softening of ground stiffness during EQ, ii) liquefaction process of the reclaimed layer during the main shock, iii) Nonlinear properties during the main shock and aftershocks. According to Yangisawa and Kazama (1996), for the analyses, uniform deformation in each layer was assumed and thus τ-γ estimates could not be done from higher frequency components. Referring to the work done by Kazama et al. (1996), Yanagisawa and Kazama (1996) adopted highest frequency values as 1.2Hz for the main shock and 1.5Hz for the aftershocks respectively. Similarly, highest frequency considered for the vertical components was 7Hz. Further, Yanagisawa and Kazama (1996) highlighted that the values of τ and γ strain were proportional to the particle velocity. This observation was earlier mentioned by Tokimatsu and Midorikawa (1981) as well. The accuracy of τ, γ estimates, by considering frequency up to the earlier mentioned values, were verified based on the velocity time histories. The velocity time histories, considering frequency up to the mentioned values were compared with the original histories. It was observed that only 10 to 20% reduction in velocity amplitudes occurred due to the filtering. Thus, Yanagisawa and Kazama (1996) highlighted that considering frequency only up to the above mentioned values had minimal effect on estimated τ and γ. At first, the liquefaction and, related τ and γ levels, during the main shock, were studied. τ time histories for the reclaimed layer were computed at an interval of 2m from the ground surface till a depth of 12m (for the NS components of the main shock). It was observed that the main portion of the τ time histories had 2-3 cycles of waves with period of 1s (Yanagisawa and Kazama 1996). Further, stress ratios (defined as peak value of τ normalized by effective overburden pressure) for the horizontal components and vertical components were computed at different depths. The stress ratio was found increasing with depth, having a value of 0.15 at top to a value of 0.45 at the bottom of the reclaimed layer. Similarly, the stress ratio from the vertical components were estimated in range

of 0.15-0.25. γ time histories were also computed for the reclaimed layer, the alluvial clay, diluvial sand and gravel layer. Maximum γ generated in the reclaimed layer was 1-2% suggesting liquefaction. Maximum γ values in the layers below were observed to be 0.6% and 0.1-0.2% for the alluvial clay and diluvial sand and gravel layers respectively. Further, τ-γ hysteresis loops at different depths, for the main shock were calculated. Each of the hysteresis loops were accommodated in a rectangle so that the diagonal of the rectangle represented the equivalent G value. From this G values, V_s values were computed for different layers. Obtained V_s values showed an increase with depth and were slightly lesser than those estimated by Kokusho et al. (1996). In addition, τ-γ hysteresis loops for the reclaimed layer, for different time windows of the main shock, were also computed. It was observed that G value for the reclaimed layer degraded as the ground approached towards liquefaction. In addition, a residual small G value was observed post liquefaction (Yanagisawa and Kazama 1996). Yanagisawa and Kazama (1996) further highlighted difficulties regarding the estimation of β values from random loading due to lack of appropriate loops. However, from few well-defined loops, β values were estimated and were found in the range of 20-35%.

In order to develop G/G_{max} curves, the aftershock records were also considered. τ-γ hysteresis loop for 8 aftershocks were computed for the reclaimed layer, alluvial clay layer, diluvial sand and gravel layer. The characteristics of the loops generated from aftershocks 01 and 02 (occurred 3min after main shock) were different from the others aftershock (1-6, occurred after 3hours or later) in regard of the breadth and inclination of the loops. Yanagisawa and Kazama (1996) highlighted that a lower G and higher β values, obtained from aftershock 01 and 02, were due to the fact that the excess pore water pressure could not dissipate rapidly (after 3min of main shock) before those two aftershocks. However, during aftershock 1, which

occurred after 3 hours of main shock, the τ-γ hysteresis loop showed increased G and decreased β values (based on the inclination and breadth of the hysteresis loop). Based on the τ-γ hysteresis loop obtained from aftershock 6 (after one month from main shock), Yanagisawa and Kazama

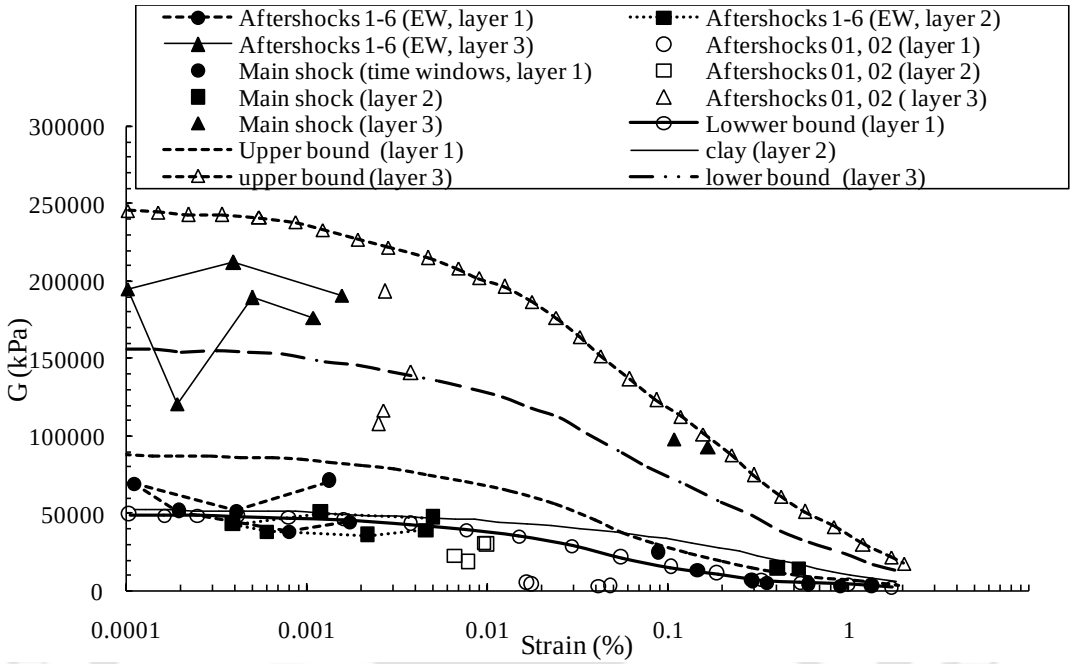

Figure 2.14, Comparison of back computed G by Yangisawa and Kazama (1996) with other data

(1996) highlighted that the reclaimed layer regained its full strength after nearly one month from the main shock. Further, G values obtained for the alluvial clay layer showed similar changes during the aftershocks. These back calculated G values were compared with the G curves used by Kitazawa et al. (1981) for design purpose at the same site. According to Yanagisawa and Kazama (1996), a good agreement between the back calculated and laboratory obtained values was observed (refer to Figure 2.14).

***2.5.4.3** Taboada-Urtuzuástegui et al. (1999)*

Work performed by Taboada-Urtuzuástegui et al. (1999) was based on time domain approach. It targeted the evaluation of dynamic soil properties at the Mexico City. EQ data were collected from Central De Abasto Oficinas (CAO) site. The site was in the vicinity of the downtown

Mexico City. Stratigraphy of the site represents geologic condition of the entire Mexico City, consisting of quaternary soft clayey and silty soil overlying a gravel and sandy alluvium stratum (Taboada-Urtuzuástegui et al. 1999). The soil stratification data was available up to a depth of 60m at CAO site. Water content was varying from 50 to 450% up to 40 m depth (Taboada-Urtuzuástegui et al. 1999) along with V_s values which were as low as 250m/s even at a depth of 50m making Mexico City vulnerable to seismic damages. At CAO site 4, accelerometers were installed at ground surface and at 12m, 30m and 60m depth. Five previously recorded EQs at the site were considered for the analysis. Both the EW and NS components of the records were considered for the analysis. Selected records included maximum PGA between 2.15 cm/s^2 to 19.64cm/s^2. In that work as well, one dimensional shear beam idealization was applied and solution technique similar to the Zeghal et al. (1995) was followed. Shear stress histories were obtained at the middle of two successive instrument levels and at the instrument levels by linear interpolation of acceleration values. γ time histories were calculated by applying linear interpolation between displacements values. According to Taboada-Urtuzuástegui et al. (1999), instrumentation and digitization inaccuracies can lead to baseline drifts. Thus, baseline drift in the form of spurious low frequency components and minor high frequency stress components, were removed by making use of two low and high pass finite duration impulse response filters. Taboada-Urtuzuástegui et al. (1999) further mentioned that these filters did not induce any phase shift. The surface accelerometer was not synchronized with the bottom accelerometers at the time of this work. Hence, Taboada-Urtuzuástegui et al. (1999) emphasized the need for synchronization of all accelerometers before any analysis. The synchronization of surface record and bottom records were done in three steps. In first step, the time of triggering of initiation of ground motion at surface and at 12m depth, were compared. From the comparison, the latest

arrival time was chosen as the origin. In the second step, the segment of one of the record, which belonged to before the origin time, was trimmed-off. In this step, the motions were superimposed and examined for any possible body wave-phase inversion and if present, the entire record was multiplied by -1. In the third step, both the records were again superimposed to find out any further time lag and if present, the amount of time lag was trimmed-off from one of the motions to adjust the time lag. When the motions were further examined, it was observed that ground motions were being significantly amplified from deeper depth to surface and in some of the motions, beating (excessive amplification due to superposition of two waves having nearly equal frequencies) was observed. The evidence of beating in ground motions at Mexico City was also provided by Singh and Ordaz (1993). Thus, Taboada-Urtuzuástegui et al. (1999) used only the first half of the records for the computation of dynamic soil properties. The τ and γ histories were obtained at the instrument level and at midway between them (6m, 12m, 21m, 30m and 45m). Therefore, nonlinear soil behavior was assessed at those levels only. When τ-γ cycles for one of the motions were plotted for different depths, clear degradation in the slopes was found as the motion traveled towards the surface. This indicated that the stiffness was gradually increasing as the depth increased and vice versa.

In the work by Taboada-Urtuzuástegui et al. (1999) as well, ellipses which represent linear-viscoelastic behavior, were fitted to the estimated τ-γ cycles and the equivalent G and β characteristics were computed in the usual way. However, in this work, ellipses were not fitted to individual τ-γ cycles. Instead, these were fitted to a group of τ-γ cycles, which represented same γ levels. At each of the instrument locations and at midway between them, different group of cycles were selected which could represent different γ levels. Computed G/G_{max} values were compared with other existing literatures. Based on the comparison, it was found the computed

G/G_{max} were between the upper bound and lower bound limits of G/G_{max} considered for Mexico City clay (Romo 1995). Further, results were compared with cyclic triaxial test results (Taboada 1989) obtained from soil specimens, collected from 10m distance away from the CAO site. Finally, results were compared with the values obtained through hyperbolic models, accepted for the region (Romo, 1995). In each of the cases, results showed good agreement and a similar trend to other G/G_{max} curves (Figure 2.15). Similarly, β values, which were evaluated from the analyses were within the prescribed (Romo, 1995) upper and lower bound limits. Computed β values were more precisely following the lower bound curve (for soils having Plasticity Index of 250%), which were lesser than the laboratory estimate (Figure 2.16). Taboada-Urtuzuástegui et al. (1999) justified this by pointing out the difficulties associated with sampling and reproducing the same stress state in the laboratory.

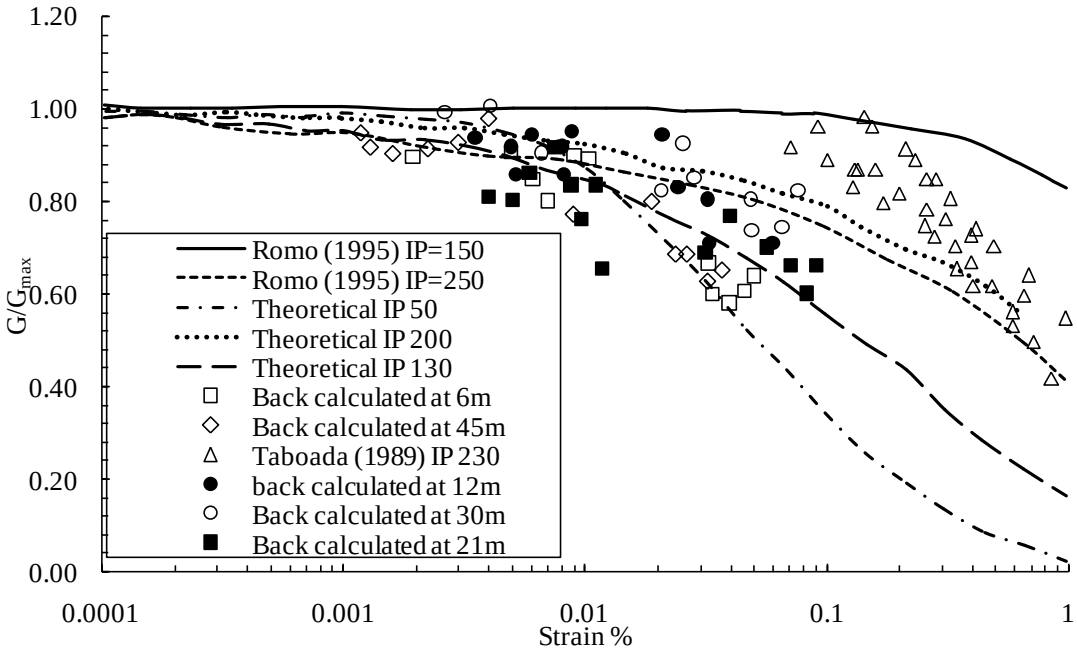

Figure 2.15, Comparison of back computed G/G_{max} curves by Taboada-Urtuzuástegui et al. (1999) with other data

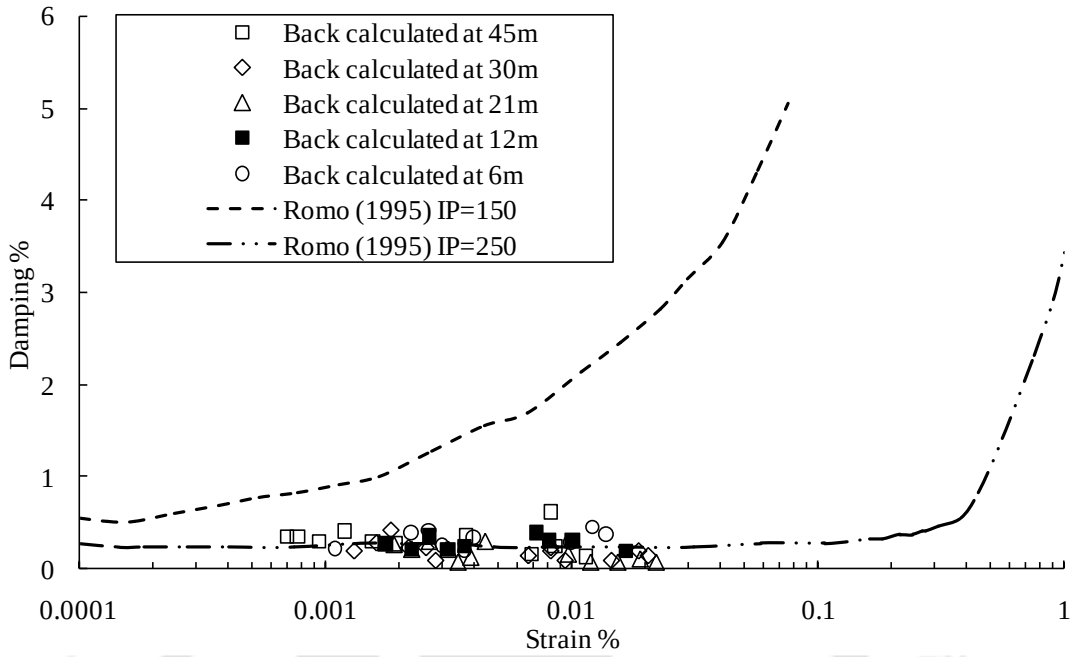

Figure 2.16, Comparison of back computed β by Taboada-Urtuzuástegui et al. (1999) with other data

2.5.4.4 *Ghayamghamian and Kawakami (2000)*

In this work, time domain analysis was performed similar to Zeghal et al (1995). 5 sites (Chiba, Fujisawa, Samukawa, Shinfuji and TTRL) from Japan, earlier used by Ghayamghamian and Kawakami (1996), were considered for the analyses. At each of the above sites, EQ data were collected at the ground surface and at 10, 30, 40, 28, 44m depths from the ground surface. According to Ghayamghamian and Kawakami (2000), data collected at ground surface and at downhole were synchronized with each other. Further, Ghayamghamian and Kawakami (2000) highlighted that EQ data were selected in a way that they could represent both lowest and highest level of recorded PGAs, at a particular site. EQ data considered for the analyses, at all the sites, consisted of PGAs in the range 0.089-0.417g. In addition, EQ data considered for analyses were divided into different time windows, to represent different level of shaking. It should be highlighted here that the time windows were selected in such a manner these covered the shear wave portion of the EQ records. Further, Ghayamghamian and Kawakami (2000) mentioned that

the time windows selected for the analyses were same as those selected by Ghayamghamian and Kawakami (1996). Thus, a comparative study of the results with those obtained by Ghayamghamian and Kawakami (1996) was also carried out in this work. The end portion of the EQ records were also considered for the analyses as those represented low γ level (Ghayamghamian and Kawakami 2000).

Lithology at 5 sites mentioned earlier was dominated by clay, silt and sand in varying thicknesses and configuration. However, the presence of loam (Shinfuji and Chiba site), gravel (Samukawa site) and humus (Fujisawa site) were also observed from the borelog. Analyses technique of Koga and Matsuo (1990), as discussed earlier, was utilized for the work. Procedure adopted by Elgamal et al. (1995), Zeghal et al. (1995) and Taboada-Urtuzuástegui et al. (1999) to compute τ and γ time histories was adopted in this work too. τ and γ time histories were computed by interpolating the acceleration time histories and displacement time histories (available at surface and downhole) respectively. The displacement time histories were computed by double integrating the acceleration time histories. Ghayamghamian and Kawakami (2000) highlighted that, these displacement time histories were affected by spurious low frequency components. Similarly, the expressions used for computing τ and γ time histories could only capture frequency content up to a certain range, depending on the distance between the recording station and wavelength of the motion (Zeghal et al. 1995). Thus, all the EQ records were filtered with a rectangular band pass finite impulse response filter to remove the undesired high and low frequency contents. The τ and γ time histories were computed for the selected time windows for all the sites. The τ-γ hysteresis curves, for different time windows and for an individual time window, were presented by Ghayamghamian and Kawakami (2000) from Chiba and Shinfuji sites. It was observed that the slope of the hysteresis curve degraded as the amplitude of γ

increased for two strong motions (PGA 0.301g and 0.417g respectively) at Chiba and Shinfuji sites. However, no such degradation pattern was observed when two weak motions (PGA 0.033g and 0.040g respectively) were considered for the analyses at sites Chiba and Shinfuji. Further, Ghayamghamian and Kawakami (2000) computed τ-γ hysteresis curve from the end portion of the two above mentioned strong motions at the respective sites. These curves also showed no degradation pattern in the slope and were similar to the curves obtained by weak motions (Ghayamghamian and Kawakami 2000). Ghayamghamian and Kawakami (2000) justified that low level of PGAs was unable to introduce nonlinearity on soil behavior. Further, equivalent linear G and β values were computed from the τ-γ hysteresis curves following the procedure described in Kramer (1996). While computing G and β values for a particular time window, average values for all the loading cycles (in the time window) were considered. In addition, maximum γ computed in the time window was related to the G and β values to establish γ dependent G and β. To obtain G/G_{max} curves, the back-calculated G values must be normalized with G_{max} values. G_{max} value at each site was determined based on f of the site $H(\omega)$ (Ghayamghamian 1997). Computed G/G_{max} and β curves were further compared with the standard curves such as Seed and Idriss (1970a), Seed et al. (1986) and Kokusho et al. (1996). It was observed that computed G/G_{max} and β values were bounded by clay and sand curves at sites Chiba, Samukawa, Shinfuji, and TTRL, which were consistent with the available soil profile (Ghayamghamian and Kawakami 2000) (Figure 2.17). However, at the Fujisawa site, though silty soil was present, the back calculated G/G_{max} followed G/G_{max} curve that was developed for clay (Figure 2.17). On the other hand, back-calculated β values were matching with that for silt (Ghayamghamian and Kawakami 2000) (Figure 2.18). Further, these back-calculated G/G_{max} values were compared with the one obtained based on frequency domain methodology by

Ghayamghamian and Kawakami (1996). From the comparison, it was concluded that the values calculated by time domain method were slightly higher than the frequency domain method. This inconsistency was attributed to the fact that the actual soil profile available at the site were not

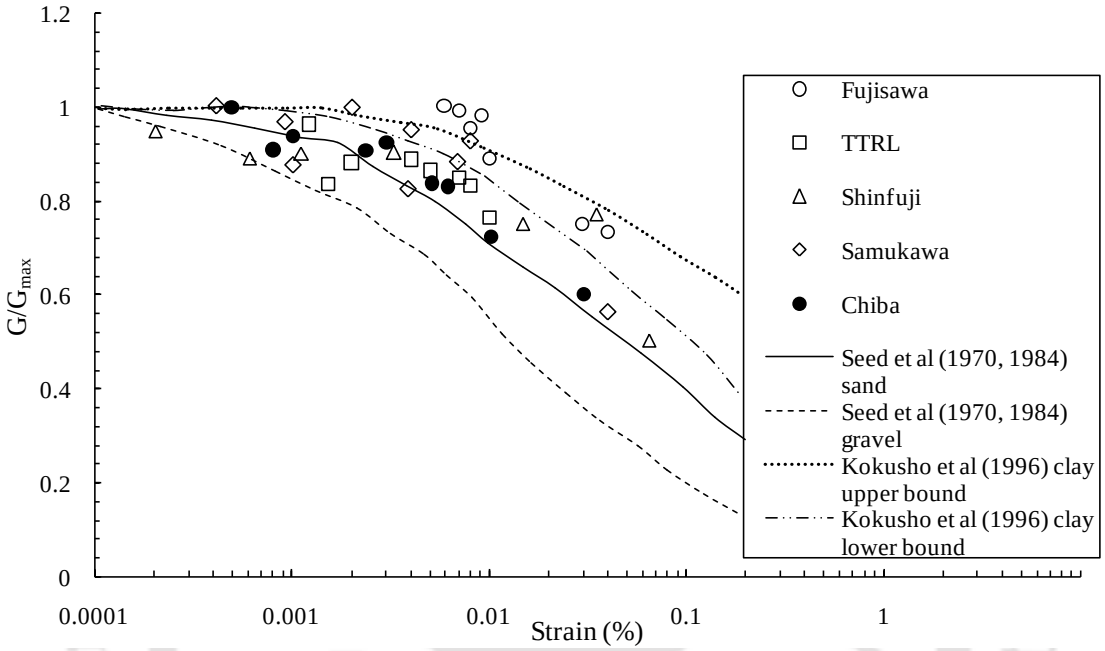

Figure 2.17, Comparison of back computed G/G_{max} by Ghayamghamian and Kawakami (2000) with other data

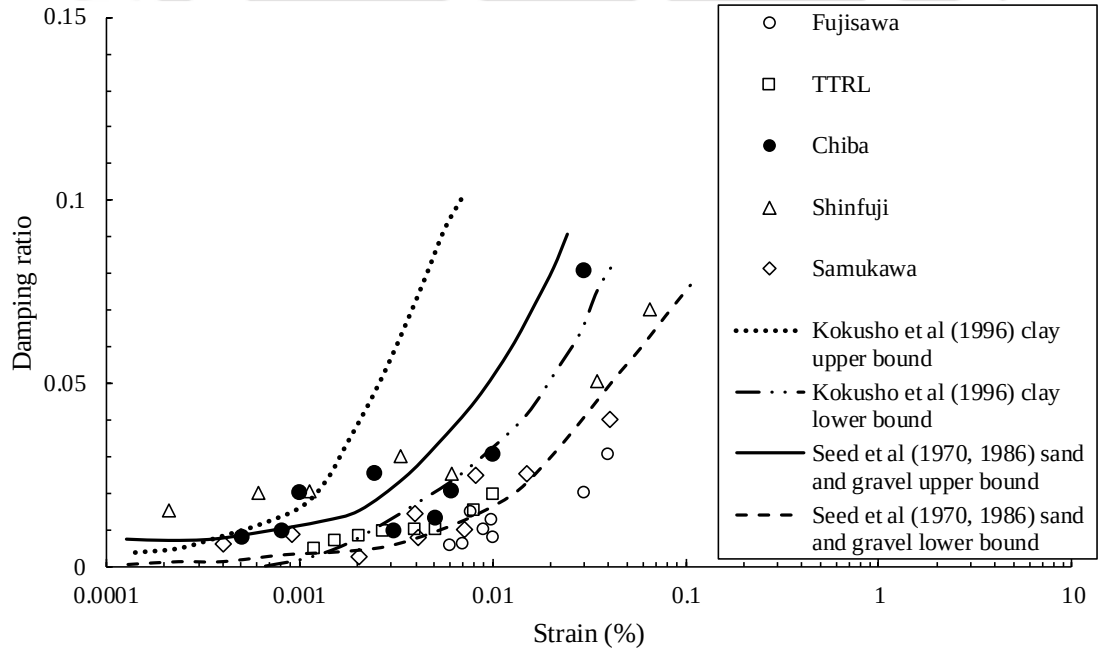

Figure 2.18, Comparison of back computed β by Ghayamghamian and Kawakami (2000) with other data

uniform as considered in the analyses. At Samukawa site, where the soil profile was uniform, similar values of G/G_{max} were obtained both from time domain and frequency domain method (Ghayamghamian and Kawakami 2000).

2.5.4.5 *Ghayamghamian and Matosaka (2001)*

Work performed by Ghayamghamian and Matosaka (2001) was based on both time domain and frequency domain methods. The frequency domain procedure is already discussed in earlier paragraphs. EQ records were collected from Chiba dense array system in Tokyo. Records at the Chiba site were available at ground surface and at 1m, 5m, 10m, 20m and 40m depths below ground surface. For the analyses purpose, EQ records at 1m and 10m depth were considered. Two EQ records with maximum PGA 0.033g and 0.301g were considered for the analyses as these motions could represent linear and nonlinear soil properties respectively. As mentioned earlier, time domain analyses procedure followed one dimensional shear beam idealization similar to the other researchers. EQ records were divided in different time windows. τ and γ time histories were obtained by linear interpolation between acceleration time histories and displacement time histories (at different levels) respectively. According to Ghayamghamian and Matosaka (2001), these estimated time histories were second order accurate. Further, Ghayamghamian and Matosaka (2001) emphasized that the accuracy of the estimated time histories depends on the wavelength of the motion and the distance between the recording points. It was pointed out that the employed formulae for computing τ and γ time histories could not be used above a certain frequency level. This frequency cutoff was identified as the frequency corresponding to the wavelength of 4 times the distance between the recording stations. In the work therefore frequency cutoff was computed as 6Hz. Here a rectangular band pass finite impulse response filter was utilized to take care of the unnecessary high and low frequency

components. The τ-γ hysteresis curve for different time windows were plotted for both the motions. Hysteresis curve corresponding to the 0.303g motion showed considerable differences in different time windows. As the time windows proceeded from the shear wave arrival time to the end of the records, increase in G and degradation in β were observed. However, no such changes were observed when the hysteresis curves from the second motion were considered. Ghayamghamian and Matosaka (2001) stated that nonlinearity can be induced in soil by strong motion only. On the other hand, soil behaves within its linear zone when the shaking intensity is less. The G and β values were computed at each of those time windows for the first motion. In this work, equivalent G and β were computed at each of those time windows. Few simple steps were followed while evaluating equivalent G and β in each of those time windows. At first, the number of cycles were counted in the time window. In the next steps, G and β for each cycle were computed and an average of G and β were estimated. Finally, the maximum γ encountered in the concerned time window was related to the earlier computed average G and β values. Ghayamghamian and Matosaka (2001) estimated G/G_{max} by dividing the above computed G values with a low γ corresponding G_{max}. For this purpose, G_{max} was computed by identifying f of the site $H(\omega)$ of the existing soil profile model. Since no DSPC were available for the site at the time of this investigation, computed G/G_{max} and β values were compared with some laboratory obtained curves. It was found that G/G_{max} curves are between sand and clay curves as mentioned by Ghayamghamian and Matosaka (2001) which were acceptable for the site (Figure 2.19). However, the β values obtained through the analysis showed significant scatter when plotted against γ (Figure 2.20). Further, a comparison between the G/G_{max} curves obtained from frequency domain analyses and time domain analyses was carried out. It was observed, the

moduli values obtained from the time domain analyses were slightly higher than those obtained through frequency domain analyses.

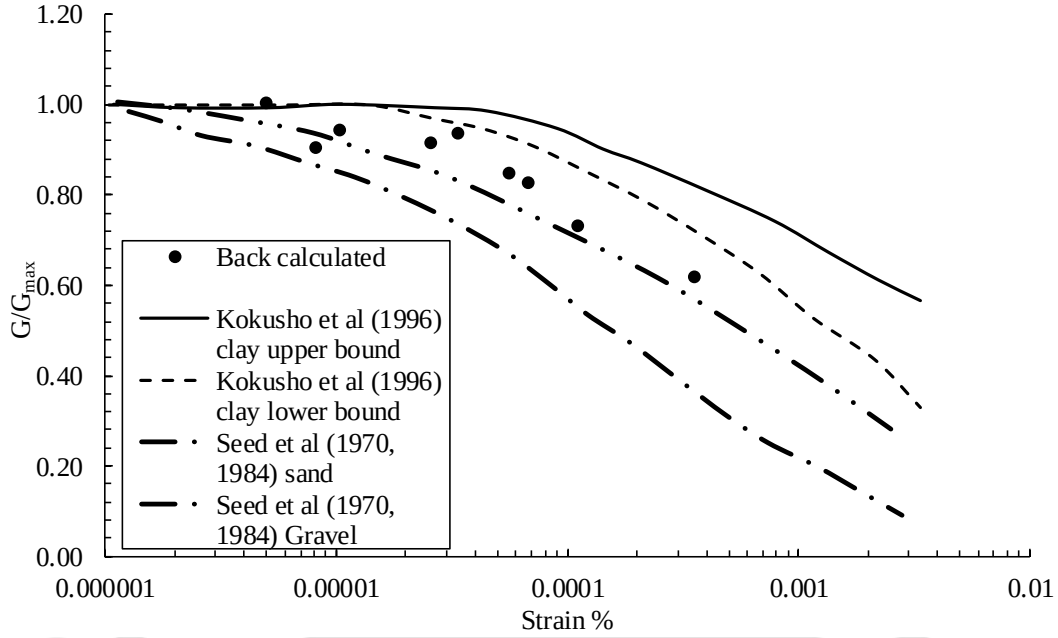

Figure 2.19, Comparison of back computed G/G_{max} by Ghayamghamian and Matosaka (2001) with other data

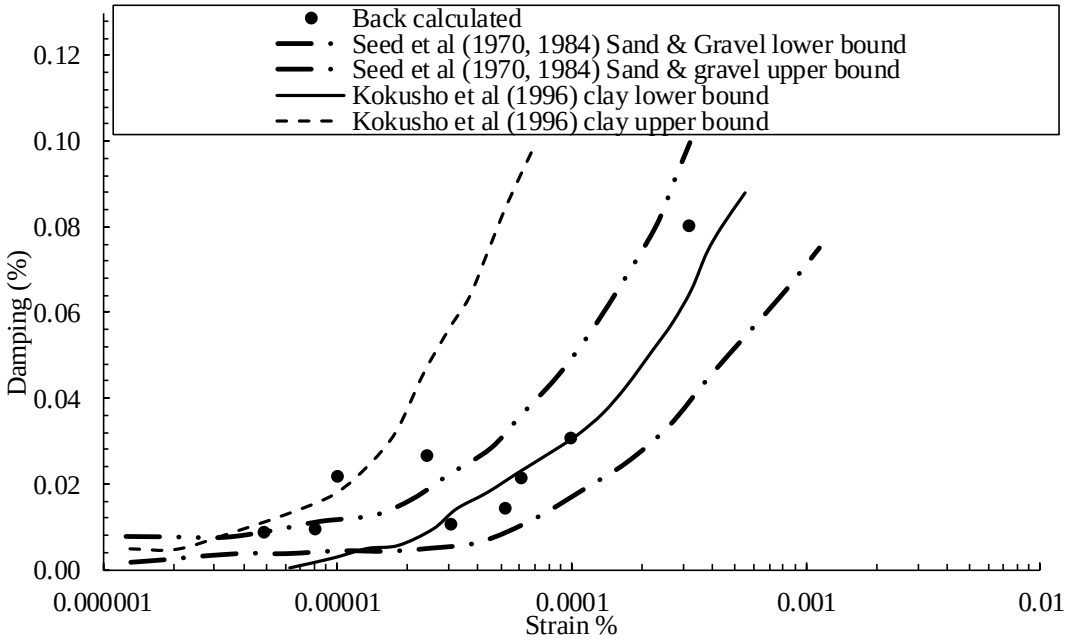

Figure 2.20, Comparison of back computed β by Ghayamghamian and Matosaka (2001) with other data

2.5.5 Other methods

Apart from the works discussed above, dynamic soil properties were determined by other method also. Referring to Figure 2.5, it can be noticed, the methodologies highlighted in red color are discussed in this chapter so far. Other works are not presently discussed here in detail. However, some of the works are mentioned in this section. In time series modeling, a stochastic ARMA model (auto regressive mobile average) produces synthetic ground motions. The ARMA model's parameters are calculated using recorded ground motions. Glaser and Baise (2000) used the ARMA model to measure G/G_{max} and β values for the Lotung downhole array. Glaser and Baise (2000) also found correlations between PGA and G/G_{max}, as well as PGA and β separately. Based on the work, Glaser and Baise (2000) concluded that as PGA increases, G/G_{max} values decrease, and β values increases. Glaser and Leeds (1996) used a system identification (SI) method at the Lotung site to quantify dynamic soil properties. The Kalman filter and optimization method were used in this SI approach. For the study, a total of 8 EQ records with magnitudes (M_w) ranging from 4.5-7.0 were considered. Honjo et al. (1998) used the extended Bayesian method to calculate G/G_{max} and β curves. For the purpose, EQ data were collected from the Tohyou-Cho location in Japan. The study involved 9 EQ recordings with PGAs ranging from 0.014 to 0.078g. The back-calculated G/G_{max} and β values were then compared to site-specific curves generated considering the model by Ramberg and Osgood (1943). Kokusho et al. (2005) also used the same approach (extended Bayesian method) for determining G/G_{max} and β curves for SGK, KNK, TKS, and PI sites in Japan. In order to do that, acceleration records (both mainshocks and aftershocks) of the 1995 Hygoken-Nanbu EQ were used by Kokusho et al. (2005). In the study, initially some appropriate values for V_s and β were considered. The initial low γ corresponding V_s was computed based on wave logging test results from the aftershocks.

However, low γ corresponding β values were selected from laboratory based information. These considered values were then adjusted by optimizing $H(\omega)_{CR}$ to back-calculate final V_s and β values. The back-calculated V_s values were then divided by the low γ corresponding V_s and the entity is squared to get G/G_{max} values. Kokusho et al. (2005) computed the γ values based on wave propagation theory, which is explained in section 3.2. Identified G/G_{max} and β curves were then compared with sand and clay curves established by Seed and Idriss (1970) and Kokusho (1980) respectively.

Class B methodologies on the other hand, are based on a rational presumption of constitutive modeling. Since the goal of the present study is to develop a framework for IGRA utilizing frequency domain method, preliminary information on some of the works based on Class B methodologies are summarized here, but a detailed discussion is omitted here. Wen (1994) used the EKF technique to back-calculate G/G_{max} and β curves for the Lotung downhole array. The Bouc-Wen (Wen 1976) constitutive model was used in the work. In this work, for intervals of 0-6m, 6-11m, and 11-17m, the G/G_{max} and β curves were back-calculated. In the analysis, EQ data (recorded at 0, 6, 11, 17, and 47m) acquired during the May 20, 1986 EQ (Mw 6.5) were employed. Further, the back-calculated values were found to be similar to UT laboratory test findings. Tsai and Hashash (2009, 2007) extracted G/G_{max} and β curve at the Lotung location using a unique inverse analytical framework called 'SelfSim' (Self-learning simulation). The SelfSim framework is built on Neural network (NN), which can be trained to create more sensible soil properties. The research focused on developing a NN model that could reflect the cyclic soil behavior at the Lotung site. At first, recorded acceleration time history was incorporated into the NN model. Further, the NN model iteratively upgraded itself in order to reflect soil constitutive model for the site. In this investigation, just one EQ record with a M_w of

6.8 and a PGA of 0.2g was utilized to determine soil characteristics. In addition, Chandra et al. (2015) used constitutive modeling to determine G/G_{max} curve for two California locations (Garner Valley and Wildlife Liquefaction). It is to be noted here that the γ values was not estimated directly in the study. PGV/V_s values were rather considered as a proxy for γ values. Wang et al. (2019) adopted a similar technique to determine γ values for back-calculating G/G_{max} curves for 8 Kik-Net sites. Over 5000 EQ recordings were utilized for inverse GRA in both of these studies (Chandra et al. 2015; Wang et al. 2019). Eseller-Bayat and Ada (2019) used EQ data from California's three downhole array sites (La Cienega DHA, Eureka DHA, and Garner Valley) in combination with linear (Kelvin Voigt) and nonlinear (Hardin and Drnevich 1972; Pyke 1979) constitutive models. Similar to Tsai and Hashash (2007), Eseller-Bayat and Ada (2019) utilized just one EQ record from each of the three sites was used to back-compute G/G_{max} and β curve for the relevant site. Eseller-Bayat and Ada (2019) used the stress-strain imaging approach described earlier to calculate the γ values between neighboring accelerometer levels. Later, ELGRA was implemented to determine γ values so that the current γ values could be compared with the γ values determined from stress-strain imaging technique. This way, the analysis progressed in an iterative fashion until a point of agreement between two calculated γ values (from ELGRA and stress-strain imaging technique) was reached.

2.5.6 Research findings:

Papers which are selected for the review, based on earlier discussion are studied in details. Based on the existing studies, answer to each of the earlier framed research questions for each study is given under corresponding heading or research findings below. Thus, answer to research question 1 is given as research finding 1 and so on.

2.5.6.1 *Research finding 1: Limitation of existing studies which have proposed inverse GRA frameworks for determining DSPCs.*

Chang et al. (1991, 1996); Zeghal et al. (1995) utilized data from Lotung downhole array to estimate DSPC. In those studies, DSPCs were estimated for soil layers located between consecutive accelerometer levels (0-6m, 6-11m, 11-17m). It should be highlighted here that the lithology at the Lotung site consists of alternate layers of gravel, silt and sand till a depth of 34m (Anderson and Tang 1989; Elgamal, et al. 1995; Mar et al. 1991; Tang et al. 1989). Further, soil information obtained from the few boreholes at the site (Mar et al. 1991; Tang et al. 1989) indicated the presence of gravel in the top 2m followed by a mixture of silty sand and sandy silt layer up to 14m depth from the ground surface. Silty sand and sandy silt layer are underlain by another gravel layer till 25m depth below ground surface. Therefore, the DSPCs (obtained by Chang et al. 1991, 1996; Zeghal et al. 1995) represented nonlinear soil behavior for combined soil layers composed of gravel, silt, and sand and not for individual soil type.

Similarly, study performed by (Ghayamghamian and Matosaka 2001; Ghayamghamian and Kawakami 1996) estimated DSPCs at the Chiba site for the top 10m soil profile. It is worth mentioning that at Chiba site, the top two accelerometers are located at 1m and 10m below ground surface. Further, based on the borehole record obtained at the Chiba site (Katayama et al. 1990), information on the site lithology was obtained. The top 5m layer consists of loam underlain by a sandy clay layer having a thickness from 2 to 4m. Below the clay layer, a diluvial sand layer is present, interspersed with intermediate clay layers. Thus, studies conducted by Ghayamghamian and Kawakami (1996); Ghayamghamian and Matosaka (2001) also estimated DSPCs for combined soil layers made of loam, clay and sand.

The subsurface lithology at PI can be divided into five major strata as highlighted in section 2.2.2. At PI site, the accelerometers are placed at 0, 16 and 32m and 82m depth below the ground surface (Iwasaki and Tai 1996). Thus, studies which considered PI downhole array data (Kokusho et al. 1996; Yangisawa and Kazama 1996) found out DSPCs for different intervals between accelerometers (0-16m, 16-32m, and 32-82m). Further, Yangisawa and Kazama (1996) back-calculated G values based on time domain methodology for soil layers which had thicknesses at least of 16m. The results obtained by Yangisawa and Kazama (1996) has certain limitations which will be discussed in research finding 3.

Midorikawa and Miura (2008); Tokimatsu et al. (2006, 1989); Tokimatsu and Midorikawa (1981) utilized only surface record for determination of G/G_{max}. Therefore, G/G_{max} values were obtained for soil profile located above the bedrock irrespective of the location of the bedrock.

Above discussion clearly highlights that all the studies irrespective of whether based on time domain or frequency domain methodology attempted to determine DSPCs for layers located between consecutive accelerometer levels. In doing so, if multiple sublayers of different soil exist between consecutive accelerometers, collective DSPC of equivalent soil layer system was attempted. In other words, no attempt was made to determine DSPC for such sublayers or different soil types separately. Hence, in case EQ records are only available at ground surface, and at bedrock, at present no methodology is available with which DSPCs for individual soil layers located between the bedrock and the surface can be determined.

2.5.6.2 *Research finding 2: Importance of PGA of input motion while determining DSPC, as per existing studies*

Among 35 papers which are initially obtained for this review, 14 papers adopted frequency domain methodology. Out of these, 6 papers (obtained after earlier discussed exclusion criteria) are considered for this part. The first work in this category was done by Tokimatsu and Midorikawa (1981). At the time of the mentioned work, downhole arrays were not available and thus only surface EQ records were utilized by Tokimatsu and Midorikawa (1981). Consequently, estimation of $H(\omega)$ were not attempted. The work was based on identifying the T from velocity response spectrum of surface motion, which was further correlated to G. For the purpose, 4 recording stations (Hososhima, Hiroo, Kushiro J.M.A. and Kushiro harbor) located in Japan were considered. Obtained G/G_{max} values for the site, based on the analyses, were found consistent with G/G_{max} curves developed by Iwasaki et al. (1979); Kokusho (1980) for clay and sand respectively, based on laboratory investigation. In addition, obtained G/G_{max} values were found scattered with respect to PGA. However, G/G_{max} vs PGV (peak ground velocity) plot showed reasonable dependency irrespective of site. In addition, a correlation between PGV and γ were also established for all the sites. For γ up to 10^{-4}%, PGV vs γ plot followed a slope of 1 (linear behavior). Beyond this value of γ, the slope was no longer unity, indicating nonlinear soil behavior.

In another work performed by Chang et al. (1996), EQ data from Lotung site (DHB) were considered. The objectives of this work were to; i) gather field evidence of nonlinear soil behavior during an EQ, ii) to check the usefulness of the V_s profile determined by geophysical methods iii) to check the usefulness of the G/G_{max} curves determined from laboratory experiments. In order to accomplish the preceding objectives, 7 EQ records at Lotung site with

PGA ranging from 0.03g to 0.21g were considered. The *f* values identified from $H(\omega)$ were utilized by Chang et al. (1996) to determine V_s values. However, while identifying the *f* values, Chang et al. (1996) highlighted that *f* values decreased with increasing PGA. As higher PGA induces higher γ, *f* values tend to shift towards the lower values signifying lower V_s values. Next frequency domain based work was performed by Ghayamghamian and Kawakami (1996). EQ and soil data were collected from 7 downhole array sites (Chiba, Etchujima, Fujisawa, Samukawa, Shinfuji, Tomioka and TTRL) located in Japan. According to Ghayamghamian and Kawakami (1996), G/G_{max} curves for all the 7 sites when plotted separately showed a degradation behavior with increasing γ. For the Tomioka site, however, such degradation behavior was very limited. Another work by Ghayamghamian and Matosaka (2001) utilized EQ and soil data from Chiba downhole array in Tokyo, following both frequency and time domain analysis and determined back-calculated G/G_{max} values. Ghayamghamian and Kawakami (2000) and Ghayamghamian and Matosaka (2001) both observed that *f* decreased with increasing PGA.

The frequency domain methodologies discussed above are based on reproduction of transfer function. In most of the studies (except for Kokusho et al. 1996) *f* values identified from the transfer function were related/ utilized to estimate V_s values. In all of these studies, it was observed that *f* value decreased as the shaking intensity/ PGA increased. Higher PGA implies higher nonlinearity in soil response and consequently reduced G (or V_s) values for the soil layers. Chang et al. (1996) and Ghayamghamian and Matosaka (2001) further illustrated this by computing the $H(\omega)$ for different time windows of an EQ record. Ghayamghamian and Matosaka (2001) showed decrease in *f* for different time windows starting from the end to the arrival of shear wave for a strong motion. However, no such observation was made for weak motion. On the other hand, Chang et al. (1996) correlated *f* values with PGA for different time

windows of a strong motion and came to the conclusion that f decreased as PGA increased. Therefore, it can be said that different levels of PGA induce different level of γ in soil, and thus result in different G values. Further, in order to estimate G/G_{max} or β curve, it is essential to consider multiple EQ records with different PGA values.

2.5.6.3 *Research finding 3: Importance of frequency content of input motion, while determining DSPC, as per existing studies.*

Out of 35 papers considered (as discussed earlier), 10 papers are classified under time domain methodology. This number is further truncated to 5 papers once papers published in the conferences by the same authors are left out. The first time domain analysis was performed by Zeghal et al. (1995) based on EQ records as well as subsoil information from Lotung downhole array, Taiwan. It is worth mentioning here that study by Zeghal et al. (1995) is the only one which had considered the effect of excess pore water pressure on nonlinear behavior of soil.

Time domain methodology, as discussed earlier, estimates the τ and γ time histories from recorded acceleration time history and displacement time history (computed using recorded acceleration time history) respectively (following the work of Koga and Matsuo 1990). While doing so, the τ time histories were computed by linear interpolation between downhole accelerometer levels. It has to be mentioned here that the computed τ estimates were second order accurate (Zeghal et al. 1995). Similarly, second order accurate γ time histories were also computed by utilizing the displacement records (by double integrating acceleration records) between successive downhole acceleration records. In doing so, computed displacement time histories contained spurious low frequency components (Ghayamghamian and Kawakami 1996; Ghayamghamian and Matosaka 2001; Taboada-Urtuzuástegui et al. 1999; Zeghal et al. 1995), which could lead to inaccurate estimation of γ time histories. Thus, these low frequency

components were removed by making use of a low-pass finite impulse response filter. In addition, Zeghal et al. (1995) and Taboada-Urtuzuástegui et al. (1999) mentioned about removing high frequency stress components as well. As per Yangisawa and Kazama (1996), higher frequency components cannot be used for the determination of τ-γ histories since uniform deformation in each layer was assumed for one dimensional GRA case. As a result, linear interpolation was not valid for higher frequencies as per Yangisawa and Kazama (1996).

In other work, Ghayamghamian and Kawakami (1996); Ghayamghamian and Matosaka (2001) pointed out that the formulae used for the determination of τ-γ histories could capture frequencies only up to a certain range. In addition, the maximum frequency (f_{cutoff}) to be used for the analysis was correlated to the distance between downhole accelerometer levels. Further, Ghayamghamian and Matosaka (2001) also found out that the maximum frequency to be used should be corresponding to wavelength (λ) equal to 4 times the distance between the accelerometer levels.

It should be highlighted here that the downhole arrays used in all the time domain methods (PI, Lotung, Chiba) consist of multiple accelerometers located at different depths. However, except for Lotung site (where accelerometers are installed at depth of 0m, 6m, 11m, 17m, 47m below ground level), all the sites have a minimum distance of 10m between top two accelerometers. Considering a V_s value of 400m/s for the surficial layer gives f_{cutoff} as 10Hz (λ = 4X10 = 40m, f_{cutoff} = 400/40 =10Hz), which covers a wide range of frequency. In actual condition however, V_s values of the surficial layers in all the three downhole array sites are lesser than 200m/s. In such case, keeping minimum distance between accelerometers as 10m, f_{cutoff} comes around 4-5Hz. This indicates that in case a downhole array has sparsely spaced accelerometers, f_{cutoff} provides a narrower/ incomplete representation of the entire frequency

content of selected ground motion. Hence, above guidelines cannot be used where spacing between the accelerometers is relatively higher (Ghayamghamian and Matosaka 2001).

2.5.6.4 *Research finding 4: Attempts done by existing studies to determine either* G/G_{max} *or* β *or both*

Among 11 papers which are discussed in detail here, only 5 studies attempted to back-calculate β curve. Out of these 5 works, 1 work (Kokusho et al. 1996) belong to the frequency domain category. In frequency domain methodologies, G or V_s values can be computed through the utilization of $H(\omega)$. However, no proper formulation for determining β exists in the frequency domain. In inverse GRA, the β values become essential when γ is being computed based on one dimensional wave propagation theory (Chang et al. 1991, 1996). Therefore, Chang et al. (1991, 1996) adopted standard β curves in order to determine γ at different depths. However, the same is not true in cases where γ is computed by dividing the relative displacements between accelerometer levels with accelerometer spacing (Ghayamghamian and Kawakami 1996; Ghayamghamian and Matosaka 2001).

In time domain methodologies, the β values can be estimated from the computed τ-γ hysteresis loop. In doing so, ellipses which represented linear viscoelastic response (Lazan 1968) were fitted to compute τ-γ hysteresis loop. From these ellipses, equivalent β values were computed following the procedure mentioned in Kramer (1996). Almost all the works on time domain (except for Yangisawa and Kazama 1996) discussed here attempted to determine β curves. However, the results obtained from these studies (in terms of β estimation) showed significant scattering. Further, β values obtained by Taboada-Urtuzuástegui et al. (1999) were much smaller than the laboratory estimates as pointed out by Taboada-Urtuzuástegui et al. (1999). It is worth mentioning here, Yangisawa and Kazama (1996) did not estimate β curve.

Yangisawa and Kazama (1996) highlighted the lack of appropriate τ-γ loops from random loading for this.

From the above discussion it becomes apparent that there is a gap in terms of estimation of β from downhole array, which has not been explored widely.

2.6 Summary

Present chapter initially discusses in detail time domain and frequency domain IGRA methodologies. Later, systematic review of various works done towards developing IGRA frameworks is done in this thesis. This systematic review suggests that though numerous IGRA frameworks exist, each of these frameworks has some limitations, as discussed below in the form of research gaps.

2.6.1 Research gaps

***2.6.1.1** Determination of β based on IGRA*

Present systematic review suggests that existing frameworks in frequency domain, though can be used to determine G or V_s values, no methodology so far exists to determine β curve. Existing frameworks based on time domain methodology on the other hand estimates equivalent β using τ-γ hysteresis loop using linear viscoelastic response. However, there is significant variation among the results obtained by different researchers. Hence, collectively, the need to develop a consistent framework to estimate β based on IGRA methodologies is realized based on the present systematic review.

2.6.1.2 *Determination of DSPC for individual soil types located between consecutive accelerometers*

Previous IGRA studies determined DSPC of combined stratifications between two successive accelerometer levels in an array. So far, no framework is developed which can determine DSPCs of individual soil layer and not for the combined layer system.

2.6.1.3 *Determination of DSPC for multiple layers based on frequency domain IGRA*

Earlier frequency domain IGRA studies were restricted to determining G or V_s values for the surficial layer only. Study conducted by Chang et al. (1996) though back-computed G or V_s values for multiple soil layers, β values were not computed based on IGRA. Therefore, a consistent frequency domain IGRA framework is required to determine DSPCs for multiple soil layers.

2.6.1.4 *Effect of excess pore water pressure generation and dissipation on DSPC based on IGRA*

Among the research works discussed in this chapter, study performed by Zeghal et al. (1995) only considered generation and dissipation of excess pore water pressure on the outcomes from IGRA. It was concluded that generation of excess pore water pressure degraded G or V_s values considerably. However, further works need to be conducted on the topic to define a well-defined pattern of modulus degradation.

2.6.2 Objectives of the present study

Following are the four objectives of this thesis work,

1. To determine β based on frequency domain IGRA
2. To determine DSPC for individual soil types located between consecutive accelerometers
3. To determine DSPC for multiple layers based on frequency domain IGRA

4. To formulate correlations for determining LSE, when regional DSPCs are not available

CHAPTER 3: DEVELOPMENT OF A NEW INVERSE GROUND RESPONSE ANALYSIS FRAMEWORK FOR THE SURFICIAL LAYER, FOLLOWING FREQUENCY DOMAIN APPROACH

3.1 Introduction:

Numerous attempts, to estimate LSE numerically through GRA, have been done globally. While performing such GRAs, it is assumed that the subsoil is responding to SH component of vertically propagating shear waves from the bedrock to the surface. Depending upon γ level mobilized during an EQ, soil behaves can be approximated accurately either linearly or nonlinearly. According to Vucetic (1994), two thresholds values for γ (γ_{tl}: linear cyclic and γ_{tv}: volumetric) exist, which govern soil's nonlinearity. When, $\gamma < \gamma_{tl}$, soil behaves linearly. On the other hand, when $\gamma_{tl} < \gamma < \gamma_{tv}$, nonlinearity creeps and no permanent deformation is encountered. Furthermore, when $\gamma > \gamma_{tv,}$ soil exhibits significant nonlinear behavior followed by permanent deformation (Chandra et al. 2015). In similar manner, various researchers (Carlton and Tokimatsu 2015; Kaklamanos et al. 2013; Kim et al. 2016; Kim and Hashash 2013) tried to estimate threshold γ values in context with the applicability of ELGRA and NLGRA. As per Wang et al. (2019), ELGRA is applicable for small to moderate γ levels (< 0.1 to 0.3%), and when γ exceeds about 0.2 to 0.5%, NLGRA must be performed. Collectively, based on the amplitude of γ mobilizes in the soil, LGRA or ELGRA or nonlinear GRA (NLGRA) methodology can be adopted to quantify LSE.

Independent of the methodology adopted (other than LGRA which is limited to very level of γ) for GRA, two important inputs required for a site are; 1) the expected level of base/ input motion and 2) the DSPCs of subsoil medium involved. It must be mentioned here that while the expected level of base motion can be determined from site-specific seismic hazard analysis,

DSPC of soil, in a majority of cases, are not available on a regional scale. For this reason, in the absence of regional DSPCs, numerous researchers (Anbazhagan et al. 2007; Besrat et al. 2018; Kumar et al. 2016; Phanikanth et al. 2011; Ranjan 2005; Stanko et al. 2017, 2019; Uthayakumar and Naesgaard 2004) attempted to quantify LSE by using standard DSPCs [i.e. DSPCs proposed by Gazetas et al. (1973); Schnabel (1973); Seed and Idriss (1970); Sun et al. (1988); Vucetic and Dobry (1991)], which were developed for specific regions only and not for any region.

It must be mentioned here that the development of regional DSPCs though can be done from laboratory testing procedures, is a difficult task to perform collectively due to the non-availability of instrumentation or operational complexities. On the other hand, downhole arrays have given a real insight into the wave propagation mechanism through layered media problem. I*n-situ* measurement of EQ data at different depths beneath the ground surface is useful in understanding the mechanism of LSE (Archuleta et al. 2000b; Baise and Glaser 2000; Elgamal et al. 1995; Halder et al. 2019; Kumar et al. 2016, 2018a). In addition, EQ data records from such arrays can be used to calibrate existing GRA models (Elgamal et al. 2001).

Use of downhole array records to back-calculate dynamic soil properties by means of IGRA have also been attempted by various researchers (Chapter 1 gives a detailed literature review and potential research gaps in existing IGRA methodologies).

In the light of existing research gap in existing IGRA methodologies as highlighted in chapter 2, this chapter attempts to develop methodology which can determine β as well as DSPC for individual surficial layer. To do so, firstly a formulation of β value based on frequency domain IGRA is proposed. Further, a novel frequency domain IGRA method is proposed for the determination of DSPCs of the surficial layer based on downhole array data. Proposed method is

then validated by utilizing downhole array records obtained from Lotung and IWTH27 (in Japan) sites. More details can be found in further sections.

3.2 Governing equations:

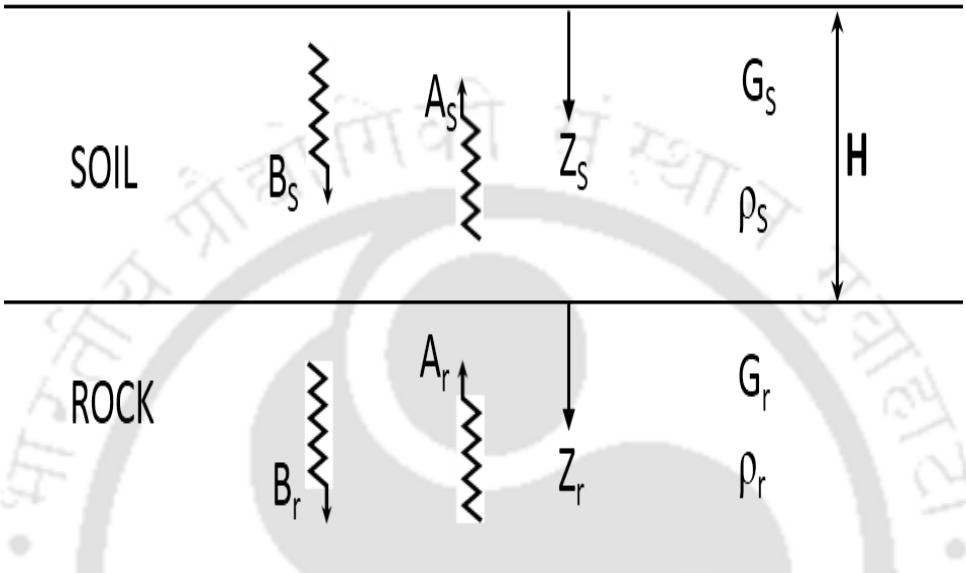

Figure 3.1, Diagrammatic representation of soil layer resting on elastic half space (after Kramer 1996)

In the light of two major limitations with existing IGRA frameworks in terms of DSPCs of each soil type and the estimation of β, the proposed framework in this chapter provides a formulation for the estimation of β values in the frequency domain. In addition, unlike the existing methods discussed earlier, the proposed framework can directly estimate V_s and β values from the empirical transfer function [$H(\omega)_{RR}$]. It must be mentioned here that the proposed IGRA framework follows ELGRA approach.

In Figure 3.1, a soil layer is resting on an elastic half-space (rock). The displacement at any point within the soil layer can be expressed as (following Kramer 1996);

$$u_s = A_s e^{i(\omega t + k_S^* z_s)} + B_s e^{i(\omega t - k_S^* z_s)} \quad 3.1$$

Similarly, the displacement within the rock layer can be expressed as;

$$u_r = A_r e^{i(\omega t + k_r^* z_r)} + B_r e^{i(\omega t - k_r^* z_r)} \quad 3.2$$

Where the subscripts 's' and 'r' denote soil and rock layers respectively; ω is the angular frequency of loading; Z_r and Z_s are the depth coordinates measured in the downward direction from the top of rock and soil layers respectively; k_s^* and k_r^* are the complex wave numbers for soil and rock layers respectively, defined as;

$$k_s^* = \frac{\omega}{V_{ss}^*} = \frac{\omega}{V_{ss}(1+i\beta_s)} \quad 3.3$$

$$k_r^* = \frac{\omega}{V_{sr}^*} = \frac{\omega}{V_{sr}(1+i\beta_r)} \quad 3.4$$

Where, V_{ss} and V_{sr} are the shear wave velocities of soil and rock layers respectively.

Considering free surface condition and displacement compatibility at the interface of soil and rock, the displacement variables in the rock layer in terms of displacement variables in soil layer can be expressed as (Kramer 1996);

$$A_r = \frac{1}{2}\left[A_s(1+\alpha_s^*)e^{ik_s^* H} + B_s(1-\alpha_s^*)e^{-ik_s^* H}\right] \quad 3.5$$

$$B_r = \frac{1}{2}\left[A_s(1-\alpha_s^*)e^{ik_s^* H} + B_s(1+\alpha_s^*)e^{-ik_s^* H}\right] \quad 3.6$$

where, H = thickness of surficial layer.

$\alpha_s^* = \frac{\rho_s V_{ss}^*}{\rho_r V_{sr}^*}$ is the complex impedance ratio. 3.7

Differentiating equation 3.1 with respect to Z_s, shear strain in soil layer (γ_s) can be expressed as;

$$\gamma_s(z,t) = ik_s^*\left[A_s e^{i(\omega t + k_s^* z_s)} - B_s e^{i(\omega t - k_s^* z_s)}\right] \quad 3.8$$

Considering $A_s = B_s = A$ (for free surface condition), equations 3.5 and 3.6 can be rewritten as;

$$A_r = \frac{1}{2}A\left[(1+\alpha_s^*)e^{ik_s^* H} + (1-\alpha_s^*)e^{-ik_s^* H}\right] \quad 3.9$$

$$B_r = \frac{1}{2}A\left[(1-\alpha_s^*)e^{ik_s^*H} + (1+\alpha_s^*)e^{-ik_s^*H}\right] \quad 3.10$$

Accordingly, the value of $H(\omega)$ between the ground surface and bottom of soil layer can be derived as;

$$H(\omega) = \frac{A_s+B_s}{A_r+B_r} = \frac{2}{e^{ik_s^*H}+e^{-ik_s^*H}} = \frac{1}{\cos(k_s^*H)} \text{ (Using Euler's theorem);} \quad 3.11$$

Further, V_s^* can be obtained as,

$$V_s^* = \frac{\omega H}{\cos^{-1}\left\{\frac{1}{H(\omega)}\right\}} \quad 3.12$$

Based on the above discussion, once ground motion records at the surface and beneath the surficial layer are available, V_s^* can be determined. Please note here that equation 3.1 to equation 3.12 can be found in many standard textbooks and well-referred papers. These equations are also referred in the proposed framework. However, once the value of V_s^* is known from the records, how G/G_{max} and β values can be determined is not given in textbooks and papers, and is a part of proposed framework. This has been explained by means of taking dataset from Lotung and IWTH27 site from Kik-net and analyzing the same using proposed framework, as explained in further sections.

3.3 Analysis based on proposed framework:

In this section, the proposed framework is explained by analyzing ground motion records from Lotung and IWTH27 sites, considering two possible cases. In the first case, how the proposed framework is applied towards the determination of β variation with γ is explained. In the second case, how the proposed framework can be used to arrive at DSPCs of single layer/ soil type is explained.

3.3.1 Analysis and Results from Lotung downhole array data

***3.3.1.1** Ground motions considered*

Between the years 1985 and 1986, the Lotung site recorded eighteen EQs (LSST1-LSST18) data. These records along with source information for all of 18 EQs are available on the website

Table 3.1, Details of ground motion considered for the analyses at DHB (As per Elgamal et al. 1995)

Motion no	Event name	Date	Magnitude (M_L)	Epicentral distance (km)	PGA (g)	Time window (s)
1	LSST4, NS	16/1/1986	6.5	23.7	0.26	3-10
2	LSST5, EW	29/3/1986	--	--	0.04	3-6
3	LSST7, EW	20/5/1986	6.5	66.2	0.16	8-15
4	LSST7, NS	20/5/1986	6.5	66.2	0.21	8-15
5	LSST8, EW	20/5/1986	6.2	69.2	0.03	2-5
6	LSST9, NS	11/7/1986	4.5	5	0.05	2-5
7	LSST10, EW	16/7/1986	4.5	6.1	0.03	2.4-4.5
8	LSST10, NS	16/7/1986	4.5	6.1	0.04	2.4-4.5
9	LSST11, EW	17/7/1986	5	6	0.07	3-6
10	LSST11, NS	17/7/1986	5	6	0.1	3-6
11	LSST12, EW	30/7/1986	6.2	5.2	0.16	5-10
12	LSST13, EW	30/7/1986	6.2	--	0.05	6-10
13	LSST14, NS	5/8/1986	4.9	4.7	0.03	5-8
14	LSST15, EW	14/11/1986	--	--	0.02	5-8
15	LSST15, NS	14/11/1986	--	--	0.04	5-8

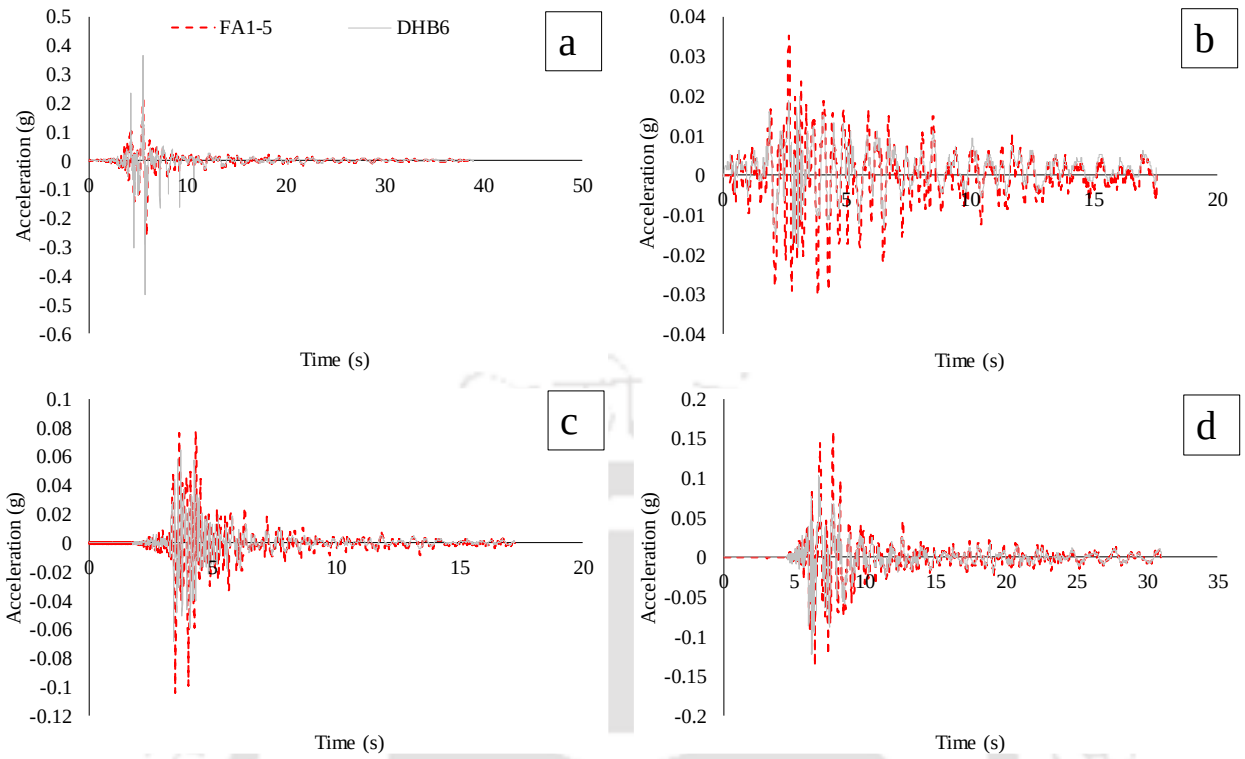

Figure 3.2, EQs records at DHB for; a) motion 1, b) motion 5, c) motion 10 and, d) motion 11

http://soilquake.net/Downholearray/Lotung/ (last visited on 04.03.2020). In order to explain the proposed framework, fifteen EQ ground motions, which were recorded at the DHB array, are utilized for back-calculating G/G_{max} and β values. It should be highlighted here though EQ records at DHA array is available, according to Wen (1994), these records are influenced by the close proximity of the containment structure and hence are not considered for the present work. Details of these EQs records from DHB have been taken from Elgamal et al. (1995) and are summarized in Table 3.1. It can be observed from Table 3.1 that the magnitudes of the considered EQ records vary from 4.5 to 6.5 (M_L). Accordingly, the PGA values (recorded at FA1-5) vary between 0.03-0.26g. Such variation in PGA values helps to estimate G/G_{max} and β values over a wider range of γ. Similarly, variation in terms of epicentral distance range (5.2km to 69.2km) is also considered to account for both distant and near-source EQs. Typical four EQ

records obtained at FA1-5 and DHB6 (at 6m depth of DHB downhole array) are shown in Figure 3.2. It must be mentioned here that excess pore water pressure records (though available for LSST 12 event) have not been utilized in the present study as this study considers total stress based approach.

3.3.1.2 *Analysis Methodology*

Using ground motions selected in section 3.3.1.1 above, G/G_{max} and β values for the soil layer located between FA1-5 and DHB6, following the proposed framework, are developed, are determined. For the purpose, ρ value is taken as 1.87gm/cc (as per Huang et al. 2001) for both the surface layer and the layer below it (layer between DHB6 and DHB11). Acceleration time histories recorded at FA1-5 and DHB6, during each of the EQs listed in Table 3.1, are first observed. To proceed further, time windows of shear wave portion in each EQ record are to be determined. This is attributed to the fact that the current study considers one dimensional GRA where LSE develops due to SH waves. It should be highlighted here that earlier frequency domain methodologies considered multiple time windows belonging to the shear wave portion of an EQ record (Chang et al. 1996; Ghayamghamian and Kawakami 1996) as well as entire EQ record (Chang et al. 1991; Tokimatsu and Midorikawa 1981) for the determination of G/G_{max}. Please note that multiple time windows (5s as per Chang et al., 1996; 5.12s as per Ghayamghamian and Kawakami, 1996; Ghayamghamian and Matosaka 2001) were considered solely to represent different levels of shaking within an EQ record. In the present work however, only one time window belonging to the shear wave portion from each EQ record is considered. The shear wave arrival time is picked based on visual inspection (following Harinarayan 2020). As per Ameri et al. (2011) and Bindi et al. (2009), the end of the shear wave portion can be identified when 90% of the seismic energy of the EQ record is reached (In this study however,

the end of the shear wave portion from the EQ records is selected in such a manner that encompasses the peak acceleration portion of the shear wave. Hence, each selected time window in this work represents a shaking that is characterized by the peak acceleration value for the entire record. Obtained time windows of shear wave portion in each EQ record are summarized in column 7, Table 3.1. Once the shear wave portion of the record is identified, further procedure of the analysis is explained step-wise as;

1. As a first step, each pair of acceleration time history records (corresponding to respective time windows) are transferred into the frequency domain by performing Fast Fourier transformation using MATLAB command 'fft'. Obtained Fourier spectrum at the ground surface is divided by the Fourier spectrum at 6m depth to determine $H(\omega)_{RR}$ plot between FA1-5 and DHB6.
2. In the second step, the value of f and the corresponding value of $H(\omega)_{RR}$ of the soil layer located between FA1-5 and DHB6 are obtained from $H(\omega)_{RR}$ plot. Based on these values of f and $H(\omega)_{RR}$, and employing Equation 3.12, V_s^* value for the layer is determined. Further, V_s and β values for the layer are computed by separating the real and imaginary part of V_s^* (as per equation 3.3). It should be highlighted here that separation of real and imaginary parts is done solely to determine β values. Since earlier frequency domain methodologies did not estimate β values, the procedure of separation of real and imaginary parts is unique part of proposed framework. Additionally, earlier developed frameworks though determined V_s / G values, in doing so, only the f value of $H(\omega)_{RR}$ was utilized in these frameworks. The amplitude value of $H(\omega)_{RR}$ was not considered in earlier developed framework. It must be mentioned here that the amplitude of $H(\omega)_{RR}$ is controlled by β value. For this reason, may be, earlier frameworks were unable to determine β value, as attempted in this work.

3. Earlier developed methodologies estimated V_s based on f value (identified from $H(\omega)_{RR}$) alone. However, whether this calculated V_s could represent $H(\omega)_{RR}$ at other frequencies as well, was not checked in earlier developed frameworks. It has to be highlighted here that the characteristics of ground motion not depend only on the value of f but on other frequencies as well. Above observation is valid for $H(\omega)_{RR}$ too. It must also be mentioned here that in order to reproduce $H(\omega)_{RR}$, both V_s as well as β values are required. Since, β values were not estimated in earlier frameworks, it could not be checked whether estimated V_s by earlier methodologies represented $H(\omega)_{RR}$ at other frequencies as well. In the third step of the present framework, the above limitation is overcome by calculating theoretical transfer function ($H(\omega)_{CR}$) between FA1-5 and DHB6 for frequency range of 0 to 15Hz by utilizing computed V_s and β values obtained in the second step. Further, this $H(\omega)_{CR}$ is compared with the earlier considered $H(\omega)_{RR}$ between 0 and 15Hz. It must be mentioned here that $H(\omega)_{RR}$ consists of irregular peaks and valleys, which should be removed (Chang et al. 1991a, 1996; Ghayamghamian and Kawakami 1996; Ghayamghamian and Matosaka 2001). In this work, $H(\omega)_{RR}$ is smoothened three consecutive times following the work by Chang et al. (1996), and Ghayamghamian and Kawakami (1996), to remove irregular peaks. Similarly, $H(\omega)_{CR}$ is also smoothened three consecutive times for comparison. The smoothing operation can be done by using a moving average filter (Chang et al. 1996; Ghayamghamian and Kawakami 1996). In the present study, a moving average filter is utilized in the form of inbuilt MATLAB command "smooth" for the purpose. A one way analysis of variance (ANOVA) determination with "student's t-test" is performed on $H(\omega)_{CR}$ and $H(\omega)_{RR}$ to assess whether the difference between these two plots (throughout the frequencies) is acceptable or not. [The ANOVA test is based on the null hypothesis, which states "the difference between two

sample means" is not significant (in case the difference is significant, then the alternate hypothesis is valid). Typically, a p value >0.05 (probability that the null hypothesis is correct for the two samples) is considered for statistical analysis.] In the current context, the difference between $H(\omega)_{CR}$ and $H(\omega)_{RR}$ is considered significant in case the p-value obtained from student's t-test is less than 0.05. Similarly, the difference is acceptable in case of p-value > 0.05. Based on this criterion, one can decide whether $H(\omega)_{CR}$ and $H(\omega)_{RR}$ at all ranges of frequencies are matching. In case both are found matching (i.e. p>0.05), V_s and β values used for computation of $H(\omega)_{CR}$ are considered as actual dynamic soil properties during the corresponding EQ scenario. Further, effective shear strain ($\gamma_{eff} = 0.65\gamma_{max}$) at the middle of the layer is estimated based on the above-calculated V_s and β values, and recorded motion at FA1-5 using equation 3.8. Following the above mentioned three steps, final V_s and β values are determined in this work for ground motions 2 to 8, 12, 13 and 15 (see Table 3.1).

4. In case $H(\omega)_{CR}$ and $H(\omega)_{RR}$ are found significantly different (i.e. p<0.05) (indicating that obtained V_s and β values in step 3 are not representing overall $H(\omega)_{RR}$ throughout the frequency content), only then the fourth step of the proposed framework has to be followed. In this step, the $H(\omega)_{CR}$ and $H(\omega)_{RR}$ plots are observed and it is concluded that the alignment of f obtained (from both $H(\omega)_{CR}$ and $H(\omega)_{RR}$) are consistent. In such a case however, a significant difference in terms of amplitudes exists. It has to be noted that since V_s and β values are computed based on amplitude of $H(\omega)_{RR}$ at f, the amplitude of $H(\omega)_{CR}$ and $H(\omega)_{RR}$ at f should be identical. However, during the smoothing operation in the third step, differences in amplitude between $H(\omega)_{CR}$ and $H(\omega)_{RR}$ may arise even at f. This is due to the consideration of moving average filter in smoothing operation. Moving average filter utilizes

the amplitudes at adjacent frequencies in addition to the amplitude at the frequency of interest to calculate the average value.

For other ground motions considered (which do not fall under the criteria of above discussed three steps), it is observed that smoothened $H(\omega)_{CR}$ overestimates smoothened $H(\omega)_{RR}$ in terms of amplitude (both at f and even at other frequencies). As highlighted earlier, the amplitude of $H(\omega)_{RR}$ is controlled by β value. Hence, in order to reduce the amplitude difference between $H(\omega)_{CR}$ and $H(\omega)_{RR}$, a refinement of estimated β value is proposed here. To do so, an iterative procedure is followed where obtained β value (from the second step) is manually increased in stages. Depending upon the difference between the amplitudes of $H(\omega)_{CR}$ and $H(\omega)_{RR}$ after every iteration, increase in β value in range of 0.1% to 5.0% is done in stages. In case the difference between the amplitudes of $H(\omega)_{CR}$ and $H(\omega)_{RR}$ is less, β value is updated by 0.1%. On the other hand, if the difference between the amplitudes of $H(\omega)_{CR}$ and $H(\omega)_{RR}$ is more, β value is increased even by 5% for quicker convergence. It should be noted here that during this iterative process, earlier obtained V_s value (as per the second step) should remain unaltered. With each pair of V_s value and updated β value, the above discussed procedure till step three (as discussed above) is repeated iteratively till p attains a value of 0.05 or more. β value corresponding to the last iteration is considered as the final β value for the surficial layer for a given EQ motion. The entire framework for Lotung site is explained by means of a flowchart given in Figure 3.3.

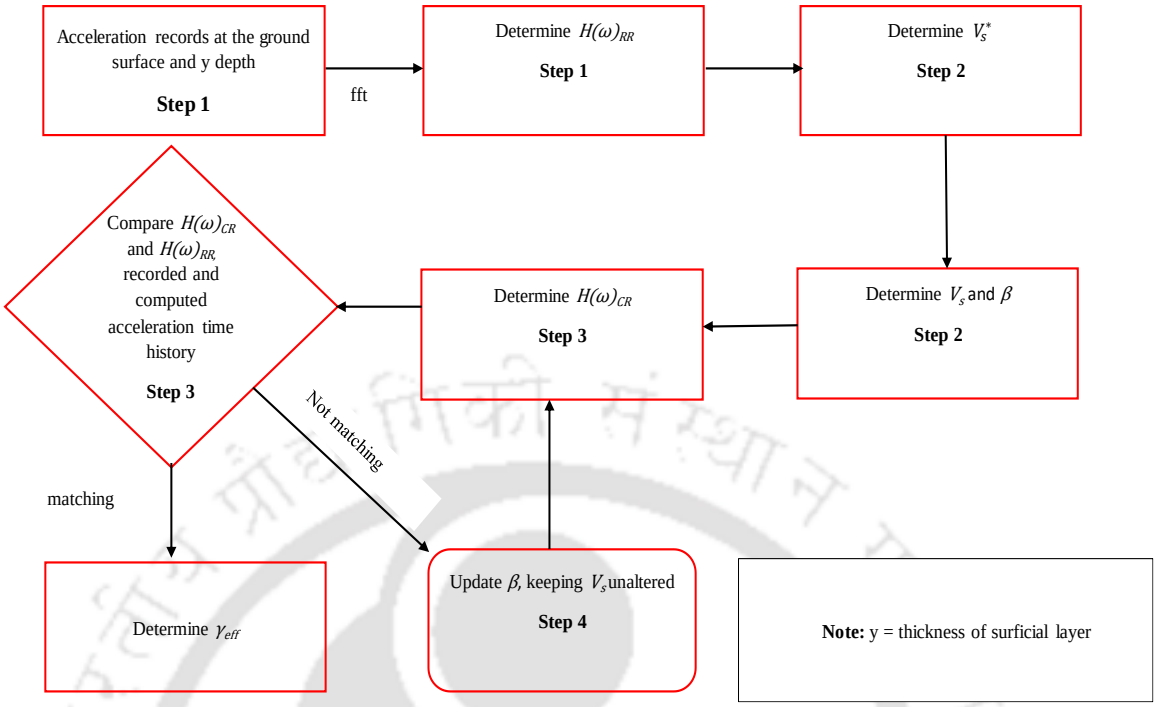

Figure 3.3, Flowchart of the proposed framework used at Lotung

Using latest values of V_s and β value, γ_{eff} at the center of the soil layer can be estimated as per equation 3.8. In the present work, all the above four steps are found applicable for ground motion no. 1, 9, 10, 11 and 14 (see Table 3.1). Collectively, based on whether the proposed methodology has to be followed till step three or step four, both V_s and β values, and corresponding γ_{eff} (which represents $H(\omega)_{RR}$ throughout the frequency content) can be obtained from a given pair of accelerometer records. A detailed discussion about the results obtained for the Lotung site, collectively based on fifteen ground motions, can be found in the next subsection.

3.3.1.3 *Results and discussion*

Based on the last section, for each pair of ground motion records, the values of V_s, β and γ_{eff} can be obtained. Repeating the same procedure for each of the fifteen pairs of ground motions, fifteen sets of V_s, β, and γ_{eff} are obtained. While V_s, β and γ_{eff} from 10 pairs of ground motions

are obtained by following the proposed methodology till step three, V_s, β and γ_{eff} from other five pairs of ground motions are obtained by following the proposed methodology till step four. Summary of back-calculated V_s, β and γ_{eff} from all the ground motions is presented in Table 3.2. It can be observed from Table 3.2 that γ_{eff} varies between 0.003% (for motion 7) to 0.092% (for motion 1). Further, V_s varies from 61.58m/s (for motion 4) to 123.26m/s (for motion 7). It should be highlighted here that Anderson and Tang (1989) conducted geophysical tests at the Lotung site (Figure 2.3) and found V_s value of 120m/s for the surficial layer, which is closely matching with the V_s of 123.23m/s obtained based on the proposed framework. Similarly, γ_{eff} of 0.003% (corresponding to V_s of 123.26m/s), obtained based on the proposed framework, is in close range of γ for geophysical tests. In addition, the back-calculated β values vary between 0.19% (for ground motion 5) to 17% (for ground motion 11). The final p values obtained based on the comparison of $H(\omega)_{CR}$ and $H(\omega)_{RR}$, for all the 15 pairs of ground motions are given in Table 3.2. It can be observed from Table 3.2 that the final p values vary between 0.05 (for motion 11) to 0.90 (for motion 7).

Each of the back-computed V_s values (see Table 3.2) are further divided by the highest obtained V_s value (i.e. 123.26m/s) and the entity is squared to obtain the G/G_{max} values. These G/G_{max} values are plotted against corresponding γ_{eff} values (corresponding to V_s considered in calculating G/G_{max}) as shown in Figure 3.4. In addition, laboratory obtained G/G_{max} data and statistical fit based G/G_{max} curves for the top 6m soil at DHB site, developed by Zeghal et al. (1995) and Chang et al. (1996) based on IGRA are also presented in Figure 3.4. G/G_{max} values obtained from the present study show an excellent match with the curves obtained by Zeghal et al. (1995) and Chang et al. (1996) (see Figure 3.4). Further, the back-calculated β values and corresponding γ_{eff} obtained from proposed framework are plotted in Figure 3.5. Laboratory

determined β values by NTU (Chang et al. 1996) and statistical fit based β curve for the top 6m soil of DHB site developed by Zeghal et al. (1995) based on inverse GRA are also presented in Figure 3.5. It can be observed from Figure 3.5 that the back-computed β values based on the proposed framework though are scattered, follow the scattering pattern given by NTU for this site.

Comparison of $H(\omega)_{CR}$ and $H(\omega)_{RR}$ for three ground motions (motion no. 5, 10 and 11) are shown in Figure 3.6 (a-c). It can be observed from Figure 3.6 (a-c) that $H(\omega)_{CR}$ and $H(\omega)_{RR}$ are matching very well both in terms of amplitude and *f*. Further, based on $H(\omega)_{CR}$ and Fourier amplitude spectrum computed from recorded ground motion at DHB6, acceleration time histories (for respective time windows) are computed at the ground surface for these ground motions (motion no. 5, 10 and 11). Comparison between computed and recorded time histories

Table 3.2, Back calculated dynamic soil properties for surficial layer at DHB

Motion no.	γ_{eff} (%)	V_S (m/s)	β (%)	p	% Error (in PGA value)
1	0.092	68.237	13.600	0.052	-0.29
2	0.003	121.605	2.658	0.074	5.30
3	0.060	76.589	10.251	0.118	-11.61
4	0.082	61.580	8.000	0.097	9.46
5	0.006	112.469	0.193	0.307	-7.73
6	0.005	107.323	5.163	0.070	7.79
7	0.003	123.267	2.810	0.900	0.26
8	0.003	121.880	4.000	0.463	5.67
9	0.009	104.039	10.500	0.054	-9.01
10	0.012	105.482	8.300	0.052	-4.68
11	0.037	83.967	17.800	0.050	0.22
12	0.006	123.213	0.924	0.134	-7.28
13	0.007	117.893	4.211	0.147	-12.76
14	0.015	99.908	10.950	0.051	-6.80
15	0.014	101.969	4.979	0.693	-4.70

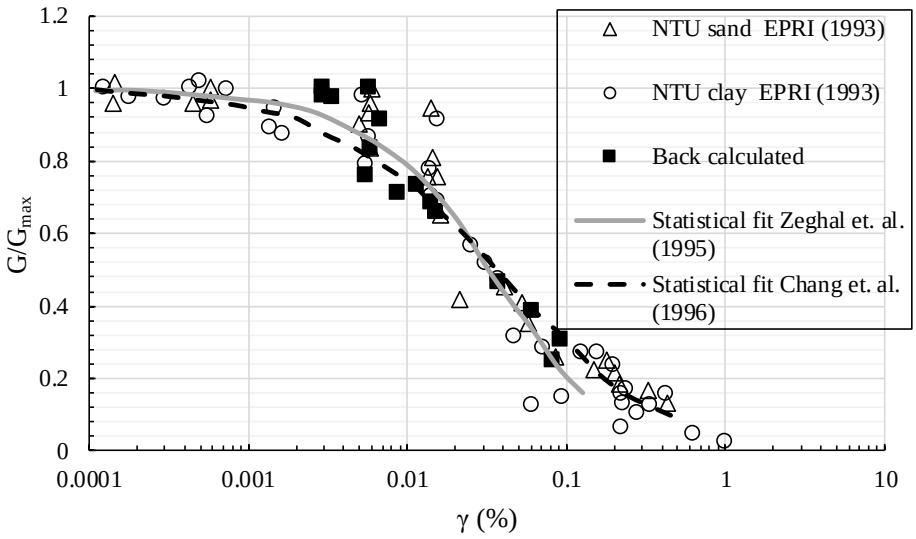

Figure 3.4, Comparison of back-calculated G/G_{max} Values for Lotung site based on proposed framework with other studies

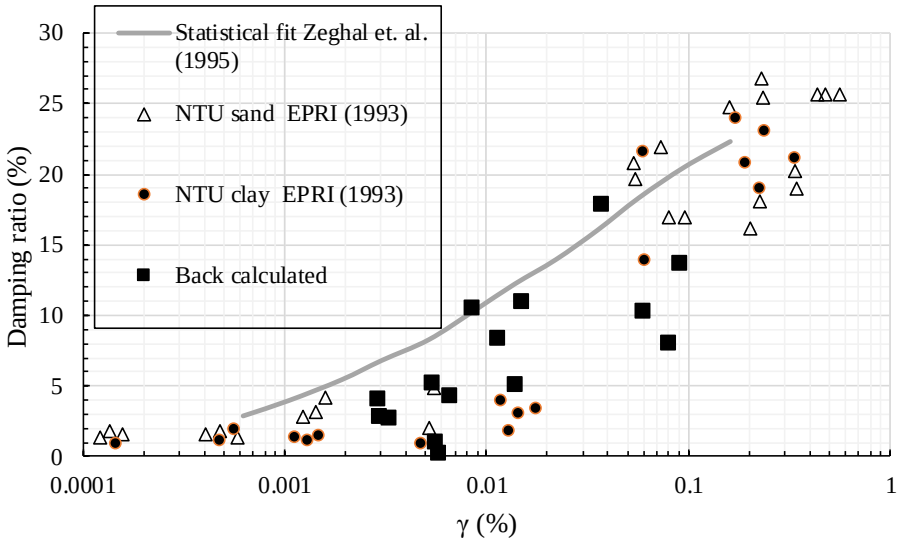

Figure 3.5, Comparison of back-calculated β Values for Lotung site based on proposed framework with other studies

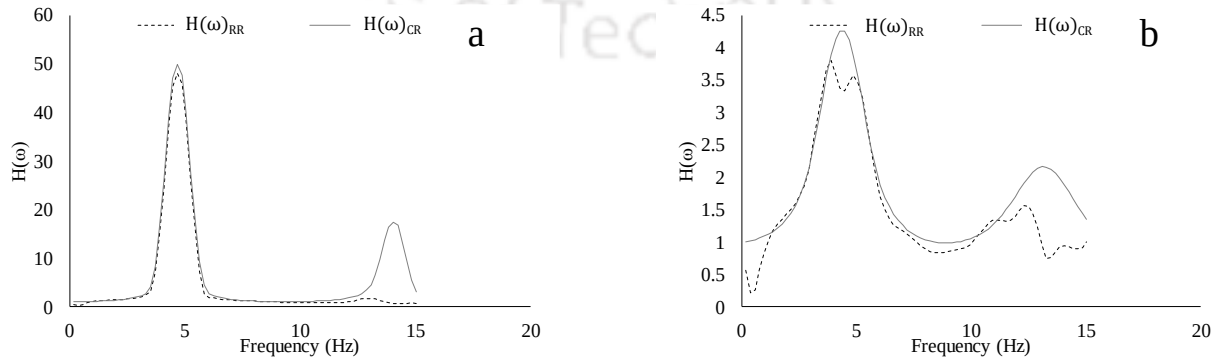

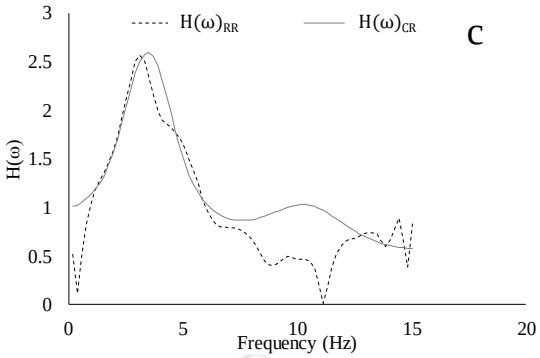

Figure 3.6, Comparison between $H(\omega)_{CR}$ and $H(\omega)_{RR}$ for; a) motion 5, b) motion 10, and c) motion 11

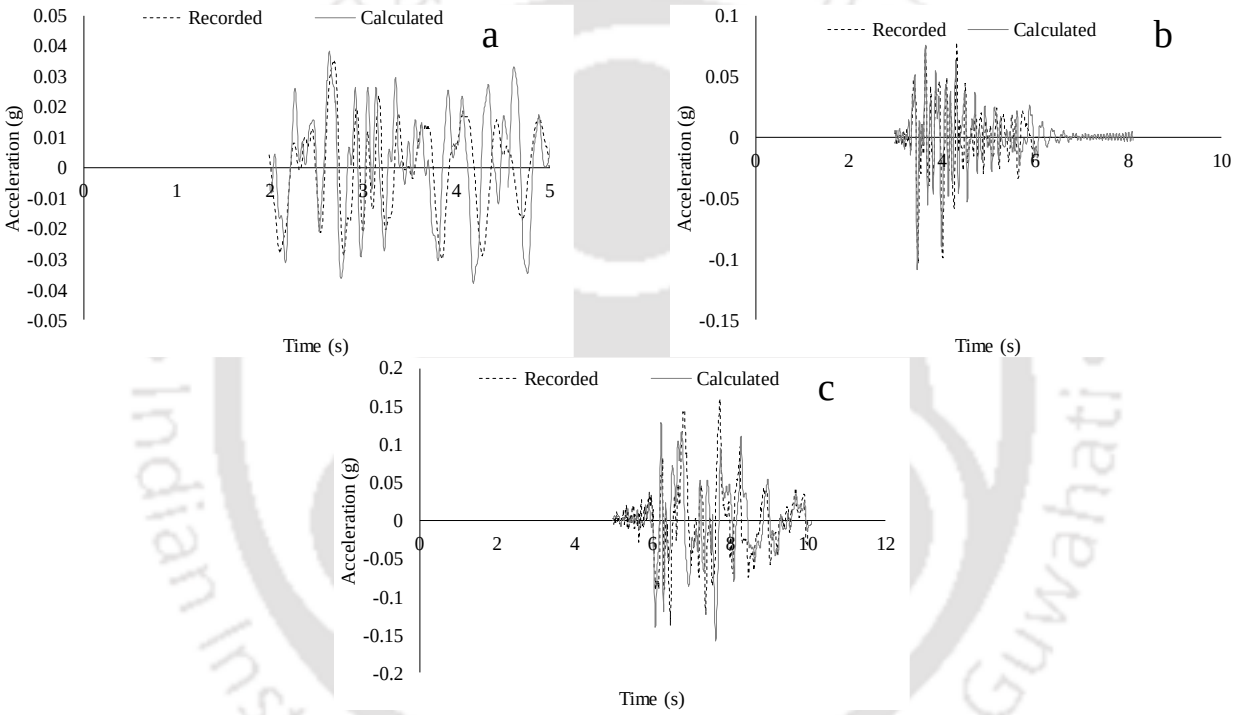

Figure 3.7, Comparison of calculated and recorded surface acceleration time history for; a) motion 5, b) motion 10, and c) motion 11

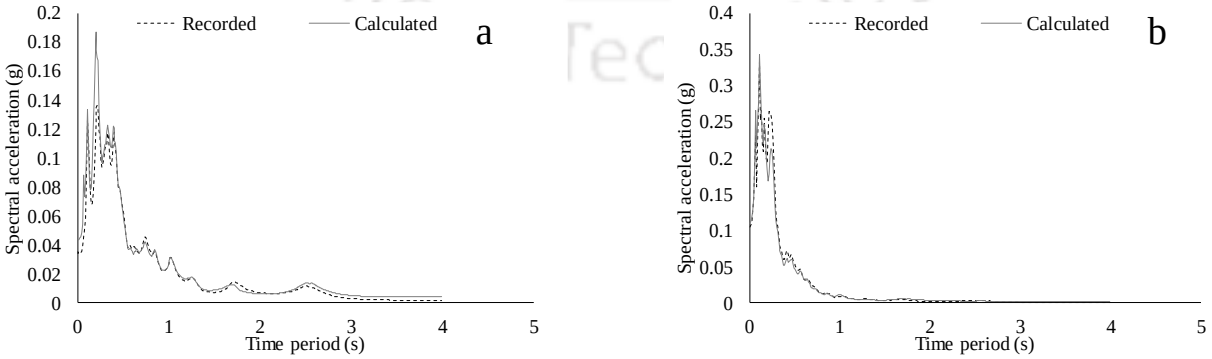

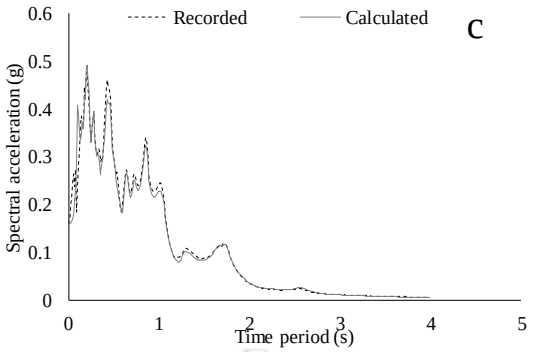

Figure 3.8, Comparison of response spectra based on calculated and recorded ground motions for; a) motion 5, b) motion 10, and c) motion 11

(presented in Figure 3.7 a-c) shows that both sets of records are closely matching. Further, 5% damped response spectra computed based on recorded and computed acceleration time histories (for respective time windows and for motion no. 5, 10 and 11 as shown in Figure 3.8 a-c) are also matching. Based on Figure 3.6, Figure 3.7 and Figure 3.8, it can be concluded that the calculated soil properties based on the proposed framework are able to capture soil response very close to the actual response over a wide range of motions.

Further, percentage error between two sets of PGA (computed and recorded) is estimated for all the EQs, as given in Table 3.2. The –ve sign indicates an overestimation of calculated PGA, and +ve sign indicates an underestimation of calculated PGA in comparison to recorded motion based PGA. The minimum error computed is obtained as 0.22% for motion 11, and the maximum error computed is 12.76% for motion 13.

3.3.2 Analysis with IWTH27 downhole array data

***3.3.2.1** Study area*

For this part of the analyses, acceleration records are collected from strong-motion seismograph network of K-NET, KiK-net, located in Japan. The network systems consist of Kyoshin network (K-NET) and Kiban Kyoshin network (KiK-net). Under K-NET, more than 1000 observation

stations are operational. These stations are distributed across Japan at intervals of 20km. At each of K-NET observation station, a well-instrumented seismograph is installed at the ground surface, which can record strong motion data. KiK-net, on the other hand, has 700 observation stations that are instrumented with a pair of seismographs. These seismographs are installed at the ground surface and a known depth below the ground surface. At all the K-NET and KiK-net stations, soil as well as seismic waves (Primary and Secondary waves) velocity profiles are available. Both K-NET and KiK-net are regulated by the National Research Institute of Earth Science and Disaster Resilience (NIED) (http://www.kyoshin.bosai.go.jp/).

Thompson et al. (2012) studied 100 KiK-Net sites and, based on the comparison between $H(\omega)_{CR}$ and $H(\omega)_{RR}$ developed a two letter classification scheme for these arrays. It should be highlighted here, though the study by Thompson et al. (2012) compared $H(\omega)_{CR}$ and $H(\omega)_{RR}$, the comparison was limited to assess the match between f values only and not in terms of amplitude. Based on the work, Thompson et al. (2012) identified 16 recording stations where one dimensional wave propagation theory is applicable. Among these 16 recording stations, IWTH27 (39.0307 N, 141.532 E) was one station (Thompson et al. 2012). For the present study, IWTH27 is considered as the second case to discuss the application of the proposed framework in order to arrive at the dynamic soil properties of individual soil layer at IWTH27. It must be highlighted here that discussion for Lotung site done earlier already demonstrated how the proposed method can be applied in order to arrive at β value of subsoil. IWTH27 is considered here to explain how to deal with the second limitation with existing methodologies (on how the dynamic soil properties can be determined for individual soil layer rather than combined soil layers) based on the proposed framework. It must be mentioned here that IWTH27 site has bedrock at 4m depth. Further, ground motion records available for this site are available at the ground surface and at

100m depth. Thus, unlike Lotung site, records at IWTH27 are only available at the top of the surficial layer and at larger depth but not at the bottom of the surficial layer.

IWTH27 site is located in Iwate prefecture on north-eastern Honsu Island, in the vicinity of several major EQs source including the 2011 Tohoku EQ event (Kaklamanos et al. 2015). According to Kaklamanos et al. (2015), at least 3 EQ records with PGA > 0.75g have been recorded at this site. It belongs to site class C with average V_s value in top 30m (V_{s30}) being 670m/s (following NEHRP, BSSC 2004 classification scheme). The subsurface profile for IWTH27 site is available up to 100m depth as can be observed from Table 3.3. No information regarding the water table location, SPT-N values and soil unit weights are available for the site. It can be observed from Table 3.3 that 4m thick topsoil, which consists of a fill layer, has V_p and V_s values of 320m/s and 150m/s respectively. Below this layer, bedrock is made of volcanic tuff (light, porous rock formed due to consolidation of volcanic ash), sandstone of tuff, shale of tuff, and shale, which were formed in Carboniferous period (360-300 million years ago). The bedrock layer between 4m and 30m depth consists of tuff followed by a 16m thick sandstone of tuff layer. V_p value for the tuff layer and the sandstone of tuff layer is 4320m/s. On the other hand, V_s value from 4-16m depth is of the order of 1100m/s, below which it attains a value of 1950m/s for the next 30m. Another tuff layer is present below sandstone of tuff layer, which extends up to a depth of 78m. In this layer, V_p and V_s values are 5250m/s and 2590m/s, respectively. In fact, the V_p value up to 100m depth after sandstone of tuff layer, remains as 5250m/s. The tuff layer is then followed by a 7m thick shale of tuff layer with V_s value of 2790m/s, which continues till 100m depth. Beneath the shale of tuff layer, alternate layers of shale and tuff can be observed (See Table 3.3) up to the depth of 100m. According to Kaklamanos et al. (2015), the presence of

soft soil at the surface and proximity of this site to many EQ sources can lead to a significant nonlinear response in the surficial layer during future EQs.

Table 3.3, Soil stratification details at IWTH27 site

Depth (m)	Soil type	P wave velocity (m/s)	S wave velocity (m/s)
4	Top soil	320	150
30	Tuff	4320	1100
46	Sandstone of Tuff	4320	1950
78	Tuff	5220	2590
85	Shale of Tuff	5250	2790
85.3	Shale		
86	Tuff		
88.7	Shale		
89.8	Tuff		
91.8	Shale		
93.9	Tuff		
94.5	Shale		
103	Tuff		

3.3.2.2 *Ground Motions considered*

A total 10 number of EQ records from IWTH27 are considered for the present analyses. Further, only horizontal components (NS/EW or both) of the EQ recordings are considered for the

purpose. Details of the records considered in this work along with PGA values are listed in Table 3.4. It can be observed from Table 3.4 that EQ records with a wide range of PGA (0.064-0.797g) are considered for the present analysis. Apart from this, variation in EQ magnitude and hypocentral distance in selected ground motions can also be observed from Table 3.4. It has to be highlighted here that information regarding synchronization, the incident angle of wave and directional drift are not available on the website (http://www.kyoshin.bosai.go.jp/). However, it is observed that the EQ records obtained from above website are accompanied by distortions and shift of reference baseline. Such shifts in reference baseline can lead to inaccurate determination of velocity and displacement time history (Boore and Bommer 2005). Thus, in the present work, EQ records obtained from the website are corrected for baseline drift before using them further. Baseline corrections are applied by using linear polynomial. Figure 3.9 presents some of the typical EQ records after baseline correction. For further analyses, following inverse GRA methodology, time windows containing shear waves portion are identified (as listed in Table 3.4) and used.

3.3.2.3 *Analyses*

For the borelog given in Table 3.3, the entire depth is divided into 25 layers of 4m each for modeling in this work. Each layer is modeled considering actual V_s value given in Table 3.3. Further, β value for each layer is considered as 2% as an initial assumption. ρ for each layer is computed from V_p of that layer (as given on http://www.kyoshin.bosai.go.jp/ for IWTH27 site and following the procedure mentioned in Boore, 2007). It must be mentioned here that the objective of this analysis is to determine the dynamic properties of the soil layer existing between the surface and 4m depth while the recorded motions are available at the ground surface and 100m depth. Hence, motions that are available at 100m depth need to be transferred to 4m

Table 3.4, Details of ground motion considered for the analyses at IWTH27

Motion no	Origin time & component	Latitude (N)	Longitude (E)	Hypocentral depth (km)	Magnitude (M_w)	PGA (g)	Time window (s)
1	05/26/2003 (22:34,EW)	38.888	141.596	76	4.8	0.064	20-30
2	05/26/2003 (22:34,NS)	38.888	141.596	76	4.8	0.086	20-30
3	6/14/2008 (8:43, NS)	39.028	140.88	8	7.2	0.220	25-50
4	7/24/2008 (00:26, EW)	39.732	141.635	108	6.8	0.441	30-40
5	3/11/2011 (14:46, EW)	38.103	142.86	24	9	0.642	40-75
6	4/7/2011 (23:32, EW)	38.203	141.92	66	7.1	0.797	25-50
7	7/30/2012 (07:05, EW)	39.097	142.472	34	5.5	0.122	25-30
8	4/3/2014 (08:22, EW)	39.17	141.763	64	5.5	0.282	20-30
9	5/13/2015 (06:13, EW)	38.862	142.15	46	6.8	0.214	20-30
10	3/24/2011 (17:21, EW)	39.077	142.357	34	6.2	0.121	20-30

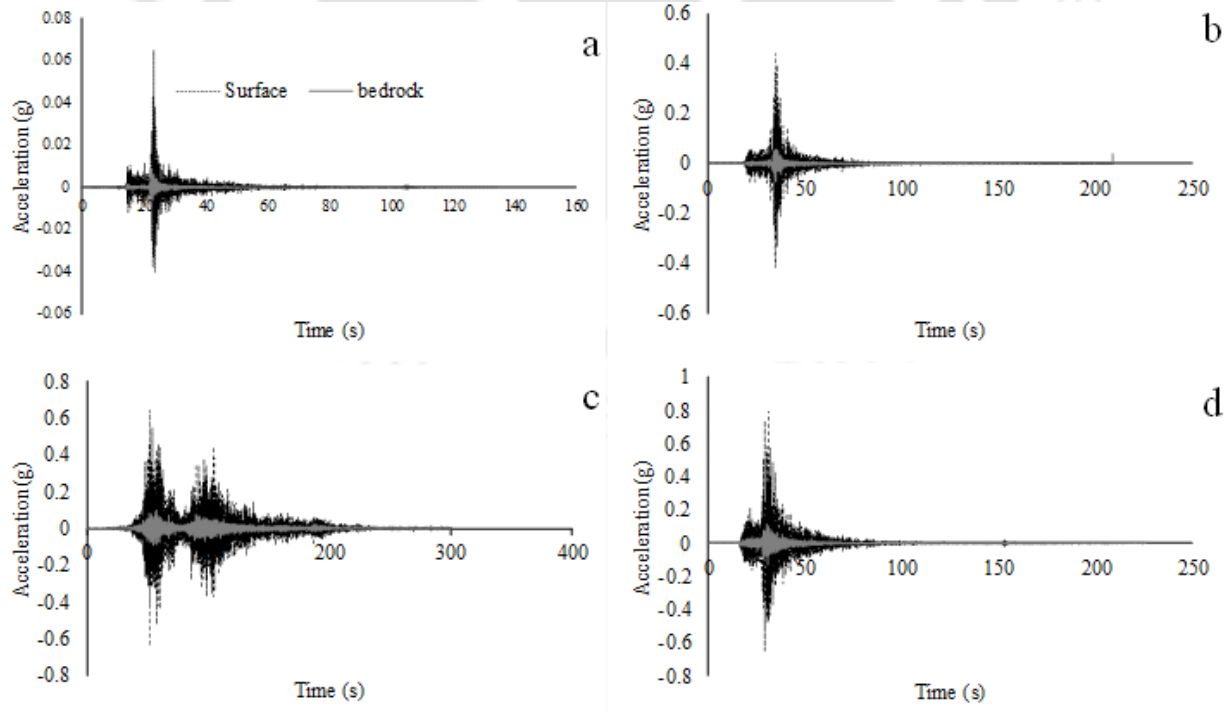

Figure 3.9, EQs records at IWTH27 for; a) motion 1, b) motion 4, c) motion 5 and, d) motion 6

depth so that the proposed IGRA framework can be applied. To do so, the response of rock layers between 100m and 4m has to be taken into account and this requires defining the rock properties. In order to make sure that the steps discussed here are independent of the initial approximation of rock properties, two sets of analyses (LGRA and ELGRA) are performed. All the LGRA and ELGRA are performed using the MATLAB code developed by Kumar and Mondal (2017). While performing LGRA, G corresponding to V_s value as given in Table 3.3 and β of 2% is considered for all the 25 soil layers. In ELGRA however, G/G_{max} and β curves, as per Schnabel (1973) for rock, are assumed for layers existing between 4m and 100m depth. It should be highlighted here that according to Bajaj and Anbazhagan (2019), DSPC by Schnabel (1973) is most suitable for the rock layers at IWTH27 site. For soil layer between 4m and ground surface, V_s=150m/s (see Table 3.3) and β =2% are considered throughout the ELGRA. It must again be mentioned here that LGRA and ELGRA are done not to find the dynamic soil properties of surficial layer but to understand the effect of response of rock layers in terms of mobilized γ values for various ground motions. Further, ELGRA ascertaining no stress-free condition at the top of rock layer is only possible if some values of soil properties are assigned. Collectively based on LGRA and ELGRA (typical findings summarized in Table 3.5), it can be observed that for all the ground motions, γ_{eff} throughout the rock medium remain less than 0.003%. In addition, both LGRA and ELGRA acquired same values of γ_{eff} at layers within the rock medium. Based on above sets of analyses, it is understood that the rock layers behave as linear-elastic material when subjected to given ground motions at the base. Further, it can also be concluded that the response of rock layers is independent of any the selection of G/G_{max} and β curves. Hence, while attempting to determine the dynamic properties of surficial layers based on the proposed framework, all the rock layers are modeled as linear elastic material (without any

DSPC). Further, how the proposed framework can be applied in this case, is explained by means of a flowchart given in Figure 3.10. It should be noted that the flowchart is prepared for general use considering the depth at which ground motion record is available as 'X' and the thickness of surficial layer as 'Y' as given in Figure 3.10. Further, steps of the analysis are discussed below.

1. In the first step, as done for Lotung site, the time windows corresponding to the shear wave portion for each of the ten pairs of ground motions (as listed in Table 3.4), recorded at surface and 100m depth, are selected. Based on the identified time window, $H(\omega)_{RR}$ between the surface and 100m depth is computed for each ground motion by utilizing MATLAB command 'fft'. In addition, based on the layer properties used in the last paragraph for LGRA (see Table 3.3), $H(\omega)_{CR}$ is computed between the ground surface and 100m depth by performing LGRA. Depending on earlier set criteria ($p>0.05$), values of $H(\omega)_{CR}$ and $H(\omega)_{RR}$ are compared. It should be highlighted here that the matching between $H(\omega)_{CR}$ and $H(\omega)_{RR}$ solely depends on the above considered soil properties of surficial layer (V_S=150m/s and β =2%) in LGRA. It should be mentioned here that rock layers have already shown linear elastic behavior. In case, the $H(\omega)_{CR}$ and $H(\omega)_{RR}$ are found matching (i.e. $p>0.05$), above considered V_S and β values can be considered as representative of actual soil properties of the surficial layer for that EQ motion. In such cases, the Fourier spectrum for earlier identified time window is determined from recorded ground motion at 100m depth using MATLAB command 'fft'. This Fourier spectrum along with above $H(\omega)_{CR}$ is used to compute the acceleration time history at the ground surface.

   While doing so, in some cases even for $p>0.05$, it is observed that the computed acceleration time history at the ground surface is remarkably different from the corresponding recorded acceleration time history in terms of PGA. In such case, an

additional criterion is set. If the percentage error between the two PGAs is lesser than 10% (following Mondal and Kumar 2017), the computed acceleration time history is considered in agreement with the recorded acceleration time history. Hence, it can be said that, in case of p> 0.05 and also the percentage error between recorded and computed PGA is less than 10%, initial considered V_s and β values for the surficial layer (i.e. 150m/s and 2% respectively) are considered as representative of actual dynamic soil properties for the corresponding ground motion. Further, γ_{eff} at the center of the surficial layer is computed using equation 3.8 and recorded surface ground motion. This way, following the first step, final V_s and β values for ground motions 2 and 8 (Table 3.4) are determined.

2. In case, it is found $H(\omega)_{CR}$ and $H(\omega)_{RR}$ are not matching, or the percentage error between recorded and computed PGA values is more than 10%, subsequent steps have to be followed. In the second step, the Fourier amplitude spectrum at 4m depth (FAS_4) is computed based on LGRA and using rock properties mentioned in the first step. Utilizing this computed FAS_4 and actual Fourier amplitude spectrum at the ground surface (obtained from recorded surface motion utilizing MATLAB command 'fft'), transfer function [$H(\omega)_{0\text{-}4}$] is computed between the ground surface and 4m depth. The procedure to compute $H(\omega)_{0\text{-}4}$ (referring to Figure 3.10, Y=4 for this site) is shown in Figure 3.10. Further, using this value of $H(\omega)_{0\text{-}4}$, a new set of V_s and β values is computed for the surficial layer following Equation 3.3 and Equation 3.12, as per the procedure mentioned earlier.
3. In the third step, the values of V_s and β values for the surficial layer considered in step 1 are updated by the computed V_s and β values in the second step. Further, step one is repeated with these new values of V_s and β for the surficial layer alone while and V_s and β values for the rock layers remain unaltered. Based on step one, $H(\omega)_{CR}$ is estimated and compared with

$H(\omega)_{RR}$ over a wider frequency range, as done in the case of Lotung site, in order to decide whether these two $H(\omega)$ are comparable or not. To do so, p-value, as discussed earlier, is determined. In case p value>0.05, V_s and β values obtained from step 2 are considered as representatives of dynamic soil properties. However, in case of p value<0.05, it is observed that *f* values of $H(\omega)_{CR}$ and $H(\omega)_{RR}$ are same but there is difference in terms of amplitude. As highlighted earlier, β value controls the amplitude of $H(\omega)_{CR}$. Hence, in step 3, only the β value for the surficial layer is updated in stages (typical range of increment may vary from 0.1% to 5%), keeping V_s value to be same as obtained in step two earlier. The procedure is highlighted by blue colored arrows in the flowchart (Figure 3.10). For every increase in β value, step one is repeated till p value comes out to be greater than 0.05. In addition, while updating β value, estimated surface PGA from LGRA is compared with recorded PGA. Only in case of p>0.05 as well as percentage error in PGA is lesser than 10% (for motions 1, 4, 6, 7 and 10 in this study), the values of V_s and β in the step are considered as final properties of surficial layer.

4. Another condition may arise with p>0.05 but percentage error in PGA >10% (as obtained for motions 3, 5, and 9). In previous condition (p>0.05), p can even have a very high value in comparison to 0.05. Hence, in this case, in fourth step, such very high p values are tried to be brought down close to 0.05 by updating β values iteratively. In each iteration, percentage error between two PGA values (obtained based on V_s and updated β value, and recorded ground motion) are calculated. The iteration is stopped when either p value reaches close to 0.05 or percentage error in PGA is lesser than 10%, whichever is earlier. V_s and last iteration corresponding β value are considered as representative of the final soil properties of the

surficial layer. Corresponding to V_s and last iteration corresponding β value, γ_{eff} at the center of the surficial layer is computed using equation 3.8 and recorded surface motion.

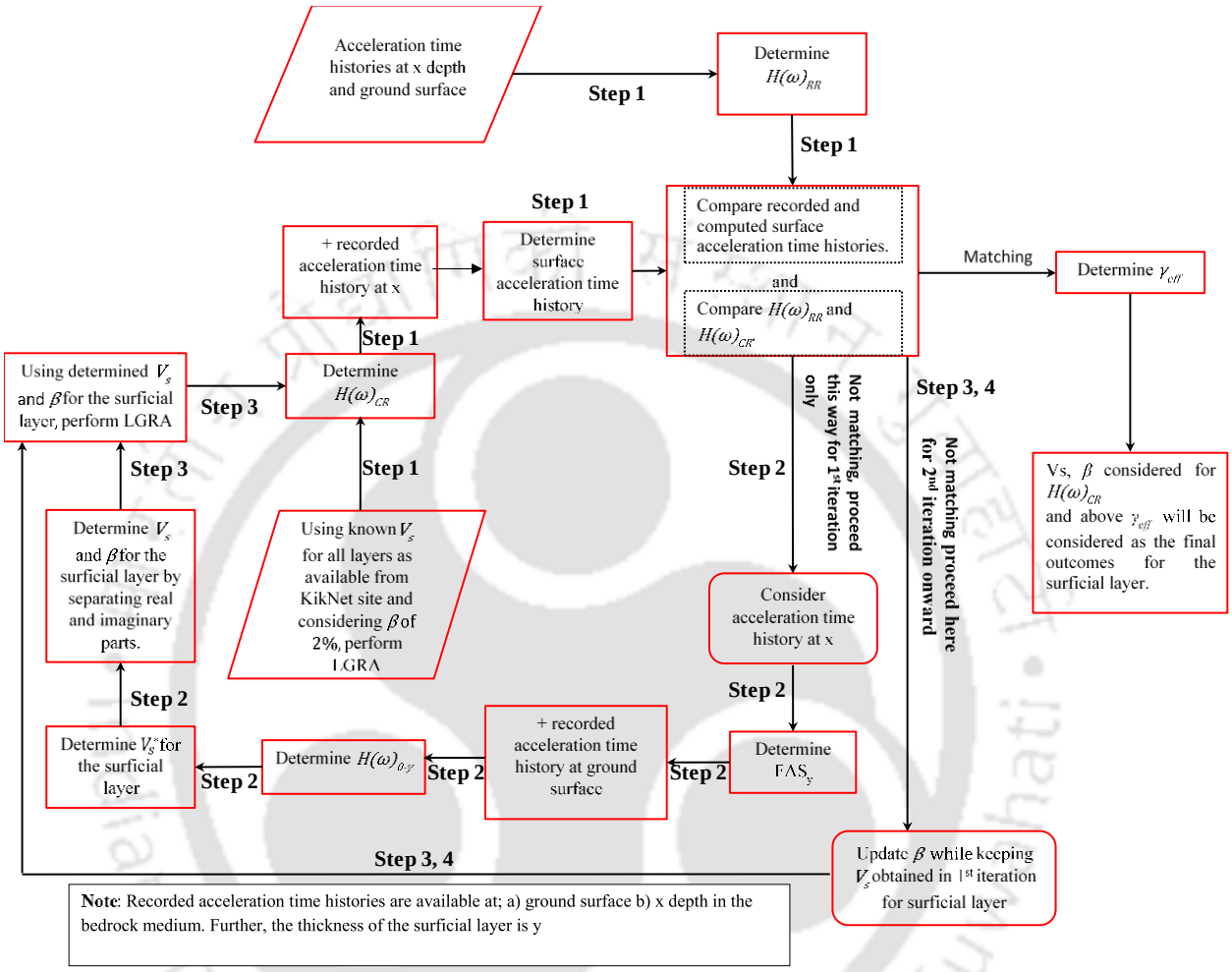

Figure 3.10, Flowchart of the proposed framework used at IWTH27

Table 3.5, Comparison of shear strain obtained from LGRA and ELGRA

Average shear strain (%)										
	Motion 1		Motion 2		Motion 3		Motion 4		Motion 5	
Layer no.	Rock	Linear	Rock	Linear	Rock	Linear	Rock	Linear	Rock	Linear
Layer 2	5.85E-05	6.18E-05	9.14E-05	9.14E-05	0.000397	0.000397	0.000846	0.000846	0.000387	0.000387
Layer 3	0.0001	0.000102	0.000125	0.000125	0.000656	0.000656	0.00163	0.00163	0.001301	0.001301
Layer 4	0.00014	0.000141	0.000155	0.000155	0.00098	0.00098	0.002358	0.002358	0.002288	0.002288
Layer 5	5.79E-05	5.79E-05	5.74E-05	5.74E-05	0.000405	0.000405	0.000934	0.000934	0.001024	0.001024
Layer 6	7.05E-05	7.08E-05	6.46E-05	6.46E-05	0.000492	0.000492	0.001092	0.001092	0.001309	0.001309
Layer 7	8.22E-05	8.27E-05	7.41E-05	7.41E-05	0.000574	0.000574	0.001227	0.001227	0.001582	0.001582
Layer 8	9.28E-05	9.36E-05	8.76E-05	8.76E-05	0.000649	0.000649	0.001337	0.001337	0.001842	0.001842
Layer 9	0.000102	0.000103	0.0001	0.0001	0.000718	0.000718	0.00142	0.00142	0.002087	0.002087
Layer 10	0.000111	0.000113	0.000111	0.000111	0.000779	0.000779	0.001478	0.001478	0.002314	0.002314
Layer 11	0.000119	0.00012	0.000121	0.000121	0.000832	0.000832	0.001512	0.001512	0.002523	0.002523
Layer 12	0.000125	0.000127	0.000129	0.000129	0.000878	0.000878	0.001554	0.001554	0.002712	0.002712
Layer 13	0.000129	0.000131	0.000134	0.000134	0.000907	0.000907	0.001639	0.001639	0.00284	0.00284
Layer 14	7.17E-05	7.29E-05	7.53E-05	7.53E-05	0.000504	0.000504	0.000931	0.000931	0.001601	0.001601
Layer 15	7.39E-05	7.52E-05	7.87E-05	7.87E-05	0.000521	0.000521	0.000997	0.000997	0.001684	0.001684
Layer 16	7.57E-05	7.71E-05	8.16E-05	8.16E-05	0.000536	0.000536	0.001071	0.001071	0.001759	0.001759
Layer 17	7.8E-05	7.94E-05	8.4E-05	8.4E-05	0.000549	0.000549	0.001141	0.001141	0.001827	0.001827
Layer 18	7.99E-05	8.14E-05	8.59E-05	8.59E-05	0.000565	0.000565	0.001206	0.001206	0.001887	0.001887
Layer 19	8.15E-05	8.31E-05	8.75E-05	8.75E-05	0.00059	0.00059	0.001267	0.001267	0.001941	0.001941
Layer 20	8.31E-05	8.46E-05	8.86E-05	8.86E-05	0.000613	0.000613	0.001322	0.001322	0.001986	0.001986
Layer 21	8.5E-05	8.66E-05	8.92E-05	8.92E-05	0.000634	0.000634	0.00137	0.00137	0.002025	0.002025
Layer 22	7.47E-05	7.6E-05	7.77E-05	7.77E-05	0.000563	0.000563	0.001217	0.001217	0.001772	0.001772
Layer 23	7.58E-05	7.72E-05	7.82E-05	7.82E-05	0.000578	0.000578	0.001247	0.001247	0.001793	0.001793
Layer 24	7.72E-05	7.83E-05	7.85E-05	7.85E-05	0.000591	0.000591	0.001272	0.001272	0.001809	0.001809
Layer 25	7.86E-05	7.97E-05	7.85E-05	7.85E-05	0.000603	0.000603	0.001291	0.001291	0.001819	0.001819

Table 3.5: (continued)

Average shear strain (%)										
	Motion 6		Motion 7		Motion 8		Motion 9		Motion 10	
Layer No.	rock	Linear	Rock	Linear	rock	Linear	rock	Linear	Rock	Linear
Layer 2	0.000137	0.000137	0.000433	0.000433	0.000153	0.000153	0.000398	0.000398	0.000236	0.000236
Layer 3	0.00021	0.00021	0.001445	0.001445	0.000245	0.000245	0.000628	0.000628	0.000352	0.000352
Layer 4	0.000284	0.000284	0.002451	0.002451	0.000331	0.000331	0.000846	0.000846	0.00049	0.00049
Layer 5	0.000113	0.000113	0.001086	0.001086	0.000131	0.000131	0.000339	0.000339	0.000199	0.000199
Layer 6	0.000135	0.000135	0.001384	0.001384	0.000156	0.000156	0.000409	0.000409	0.00024	0.00024
Layer 7	0.000157	0.000157	0.001674	0.001674	0.00018	0.00018	0.000476	0.000476	0.00028	0.00028
Layer 8	0.000177	0.000177	0.001952	0.001952	0.000203	0.000203	0.00054	0.00054	0.000318	0.000318
Layer 9	0.000198	0.000198	0.002217	0.002217	0.000225	0.000225	0.0006	0.0006	0.000354	0.000354
Layer 10	0.000217	0.000217	0.002468	0.002468	0.000245	0.000245	0.000657	0.000657	0.000387	0.000387
Layer 11	0.000236	0.000236	0.002702	0.002702	0.000264	0.000264	0.000709	0.000709	0.000418	0.000418
Layer 12	0.000253	0.000253	0.002918	0.002918	0.000282	0.000282	0.000757	0.000757	0.000445	0.000445
Layer 13	0.000266	0.000266	0.003068	0.003068	0.000294	0.000294	0.00079	0.00079	0.000464	0.000464
Layer 14	0.000151	0.000151	0.001737	0.001737	0.000166	0.000166	0.000444	0.000444	0.000261	0.000261
Layer 15	0.00016	0.00016	0.001836	0.001836	0.000174	0.000174	0.000466	0.000466	0.000273	0.000273
Layer 16	0.00017	0.00017	0.001928	0.001928	0.000181	0.000181	0.000487	0.000487	0.000284	0.000284
Layer 17	0.000179	0.000179	0.002013	0.002013	0.000188	0.000188	0.000507	0.000507	0.000293	0.000293
Layer 18	0.000188	0.000188	0.00209	0.00209	0.000195	0.000195	0.000525	0.000525	0.000302	0.000302
Layer 19	0.000196	0.000196	0.002158	0.002158	0.000201	0.000201	0.000542	0.000542	0.00031	0.00031
Layer 20	0.000204	0.000204	0.002219	0.002219	0.000206	0.000206	0.000557	0.000557	0.000316	0.000316
Layer 21	0.000212	0.000212	0.002271	0.002271	0.000211	0.000211	0.000571	0.000571	0.000321	0.000321
Layer 22	0.000189	0.000189	0.001994	0.001994	0.000185	0.000185	0.000502	0.000502	0.00028	0.00028
Layer 23	0.000195	0.000195	0.002029	0.002029	0.000188	0.000188	0.00051	0.00051	0.000283	0.000283
Layer 24	0.0002	0.0002	0.002064	0.002064	0.00019	0.00019	0.000517	0.000517	0.000284	0.000284
Layer 25	0.000205	0.000205	0.002093	0.002093	0.000192	0.000192	0.000523	0.000523	0.000285	0.000285

For IWTH27 site, for the three motions (3, 5 and 9), the iterations are stopped when p value reaches close to 0.05. The final percentage error is found out to be 24%, 23% and 15% for motions 3, 5, and 9, respectively. It must be mentioned here that for motions 3, 5 and 9, after step 3, the percentage errors in terms of two sets of PGA values were 70%, 53%, and 57%, respectively, which were significantly higher than the corresponding values after step 4 clearly indicating that β value obtained after step 4 is closer to the actual value in comparison to β values obtained after step 3. Additionally, it should be highlighted here that though V_s and β values are estimated from $H(\omega)_{0\text{-}4}$, the update of β value stops based on $H(\omega)_{CR}$ between 0 and 100m depth. This value of $H(\omega)_{CR,}$ though considers the updated value of β for the surficial layer, for the rock medium however, the β value remains as 2%. This value may vary in an actual condition but is not considered here. This assumption may be the attribute to a higher percentage error in PGA after step four and can be verified once ground motion at the base of rock medium, and at the top and bottom of surficial layer are available.

3.3.2.4 *Results and discussions:*

Based on the four-step method discussed for inverse analysis framework in the last section, one set of V_s, β and γ_{eff} values at the center of the surficial layer, for each of the ten ground motions (See Table 3.4), are back-calculated. These back-calculated V_s, β and γ_{eff} values are given in Table 3.7. It can be observed from Table 3.7 that γ_{eff} values vary between 0.0039-0.166% (for motions 1 and 7 respectively). Further, V_s values vary between 71.65-150m/s (for motions 7 and 2 respectively). Similarly, β values vary between 0.5%-10% (for motions 1 and 9 respectively). Besides, the p values and percentage error in PGA for each of the ten ground motions are also tabulated in Table 3.7. It can be observed that a maximum p value of 0.89 is obtained for motion 8. Further, a minimum p value of 0.05 is obtained for motions 7 and 9. Further, the maximum

difference in PGA estimation is limited to 24% (for motion 3) while the minimum difference is as low as 2% (motion 8). All the back-calculated V_s values are normalized with respect to the maximum V_s (150m/s). Further, these normalized V_s values are squared to obtain G/G_{max} values for the surficial layer. Utilizing these back-calculated G/G_{max} values and γ_{eff} values, an average G/G_{max} curve for the surficial layer of the IWTH27 site is proposed here, following the constitutive model by Hardin and Drnevich (1972). Figure 3.11 presents the back-calculated G/G_{max} values found in this work, along with the proposed average G/G_{max} curve. Further, back-calculated β values are plotted against corresponding γ_{eff} values in Figure 3.12. In addition, utilizing back-calculated β values and corresponding γ_{eff} values, an average β curve for this site, following the constitutive model by Hardin and Drnevich (1972) is also proposed in the present study as shown in Figure 3.12.

Further, in order to check matching between the computed and recorded ground motion parameters, comparison of $H(\omega)_{CR}$ and $H(\omega)_{RR}$ for three ground motions (motion no. 3,5 and 6) are presented in Figure 3.13 (a-c). It can be observed that $H(\omega)_{CR}$ and $H(\omega)_{RR}$ are matching well both in terms of amplitude and *f* for ground motion 3 (see Figure 3.13 a). However, for ground motions 5 and 6, only alignment of *f* matches whereas (see Figure 3.13 b, c), amplitudes at *f* are overestimated by computed parameters. It should be highlighted here that though amplitudes at *f* are overestimated by the computed parameters [$H(\omega)_{CR}$], a p value > 0.05 for the concerned ground motions (see Table 3.7) signifies amplitudes of $H(\omega)_{CR}$ and $H(\omega)_{RR}$ matches over a wider range of frequencies. Another important observation that can be made is that for motion 6, (See Figure 3.13 c) the first peak is higher than the second peak in $H(\omega)_{RR}$. On the other hand, the first peak is lower than the second peak in the $H(\omega)_{CR}$ for the same motion. This ambiguity needs further attention. Further, based on $H(\omega)_{CR}$ and Fourier amplitude spectrum computed from the

recorded ground motion at 100m depth, acceleration time histories (for respective time windows) are computed at the ground surface for the earlier mentioned ground motions (motion no. 3, 5 and 6). Comparison between computed and recorded acceleration time histories as shown in Figure 3.14 (a-c) indicates that both sets of ground motions are closely matching. In addition, 5% damped response spectra computed based on recorded and computed acceleration time histories (for respective time windows for motion no. 3, 5 and 6) are also compared in Figure 3.15 (a-c). It can be observed from Figure 3.15 (a-c) that for a wider range of time periods, the spectral acceleration values are matching between the computed and recorded parameters. Collectively based on comparisons done from Figure 3.13 to Figure 3.15, it can be said the back computed V_s and β values are able to represent soil response very close to actual response over a wider range of ground motions.

Table 3.6, Back calculated dynamic soil properties for IWTH27

Motion no.	γ_{eff} (%)	V_s (m/s)	β (%)	G/G_{max}	p	% Error (in PGA, value)
Motion 1	0.0039	128.53	0.5	0.73	0.65	9.86
Motion 2	0.0048	150.00	2	1.00	0.34	-9.59
Motion 3	0.0177	134.43	6.6	0.80	0.06	-24.06
Motion 4	0.0324	130.68	3.7	0.76	0.73	-9.96
Motion 5	0.1299	80.08	8.2	0.29	0.05	-23.51
Motion 6	0.0089	130.57	3.6	0.76	0.38	-9.39
Motion 7	0.1669	71.65	6	0.23	0.05	-6.40
Motion 8	0.0064	150.00	2	1.00	0.89	1.97
Motion 9	0.0205	137.71	10	0.84	0.05	-15.29
Motion 10	0.0154	132.93	6.2	0.79	0.84	-9.73

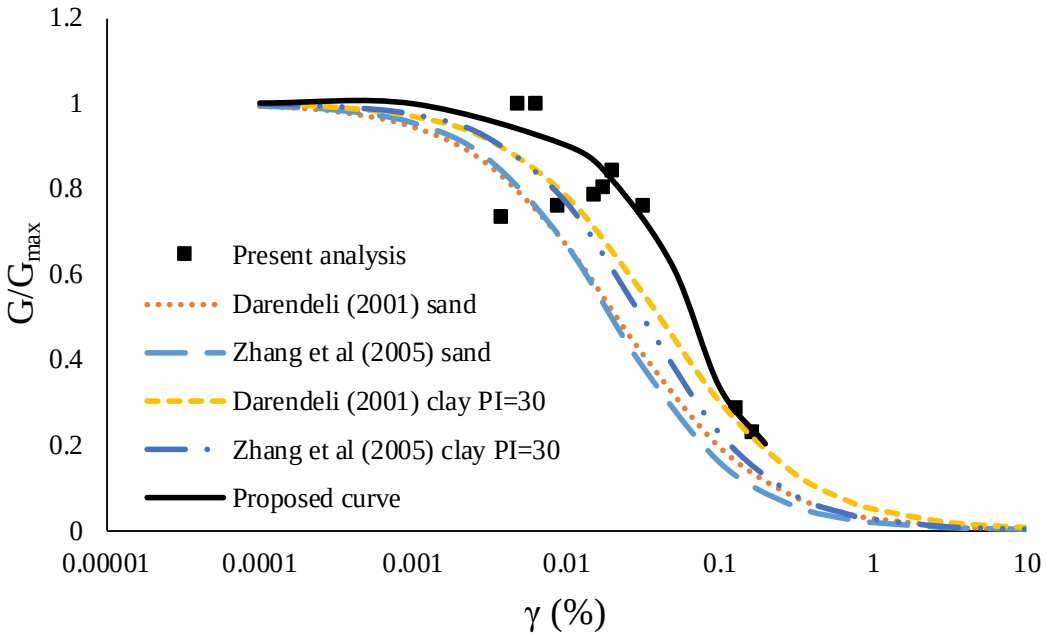

Figure 3.11, Comparison of obtained G/Gmax values and proposed curve from the present study with existing studies

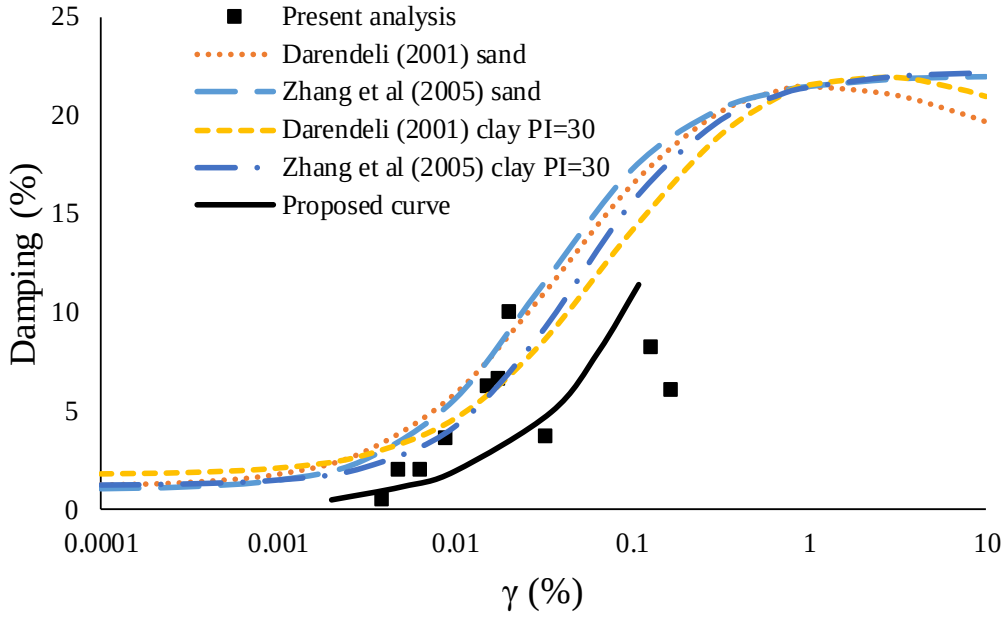

Figure 3.12, Comparison of obtained β values and proposed curve from the present study with existing studies

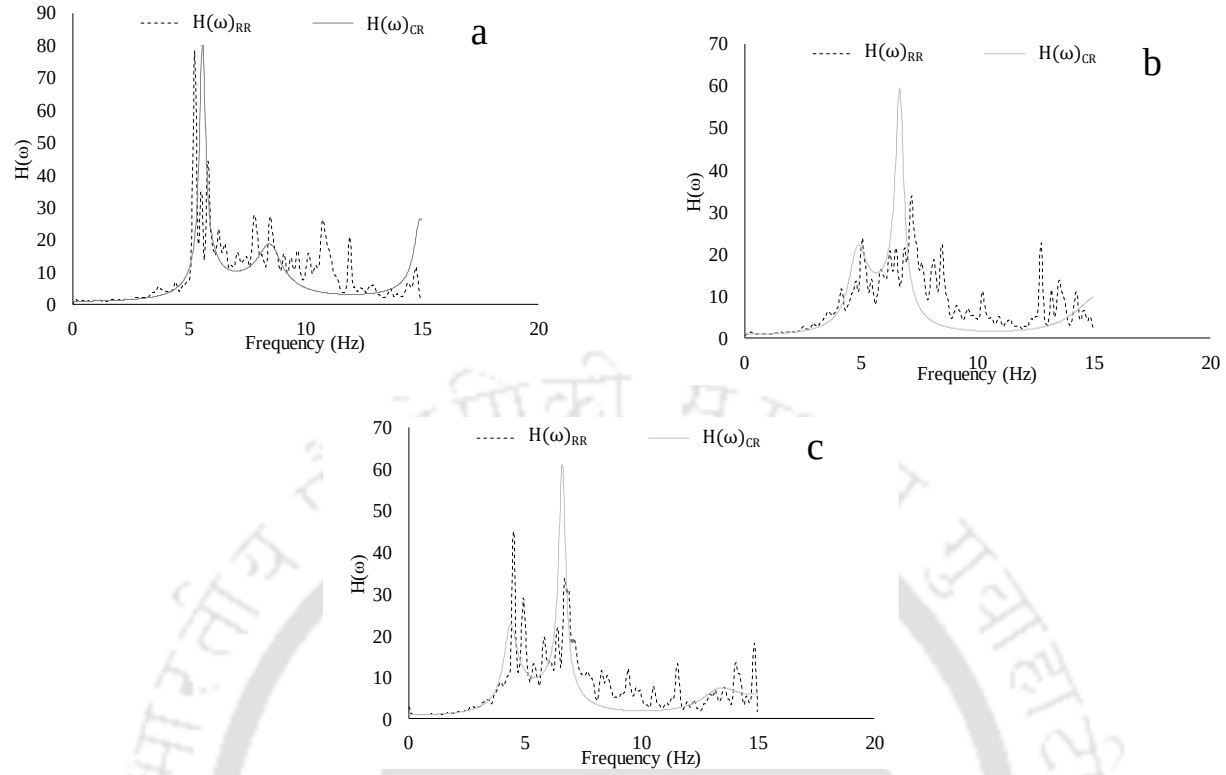

Figure 3.13, Comparison between $H(\omega)_{CR}$ and $H(\omega)_{RR}$ for; a) motion 3, b) motion 5, and c) motion 6

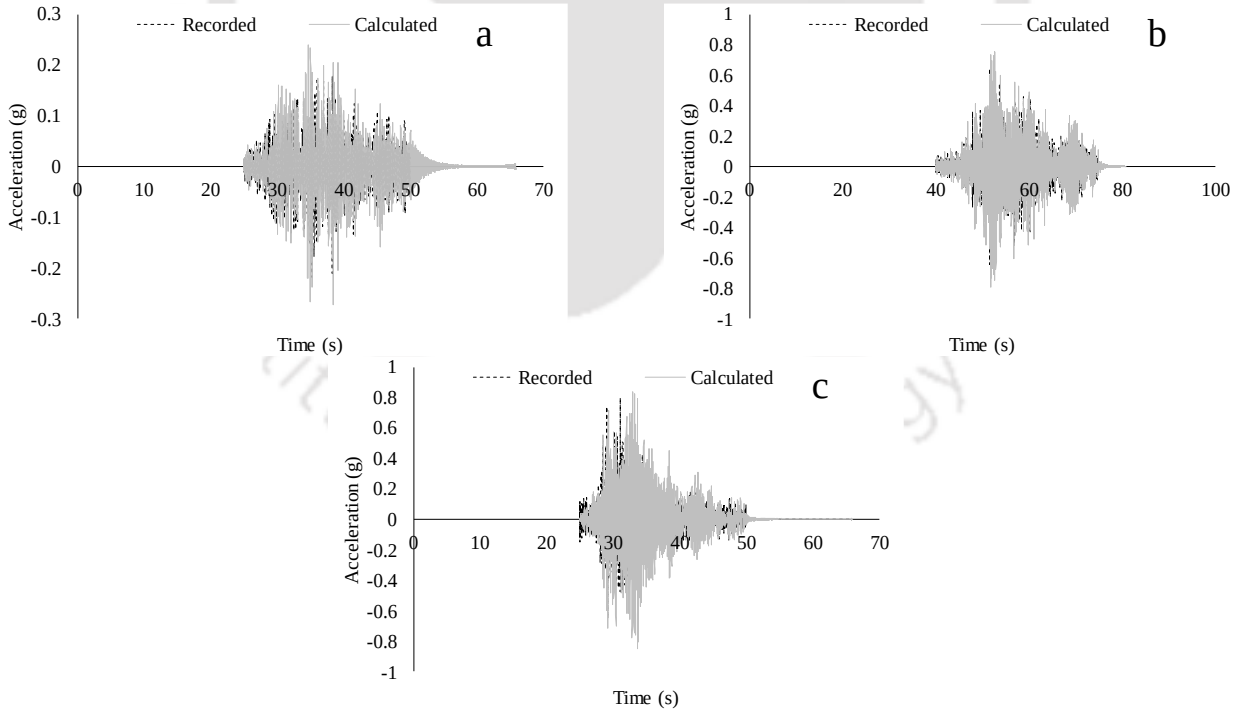

Figure 3.14, Comparison of recorded and calculated surface acceleration time history for; a) motion 3, b) motion 5, and c) motion 6

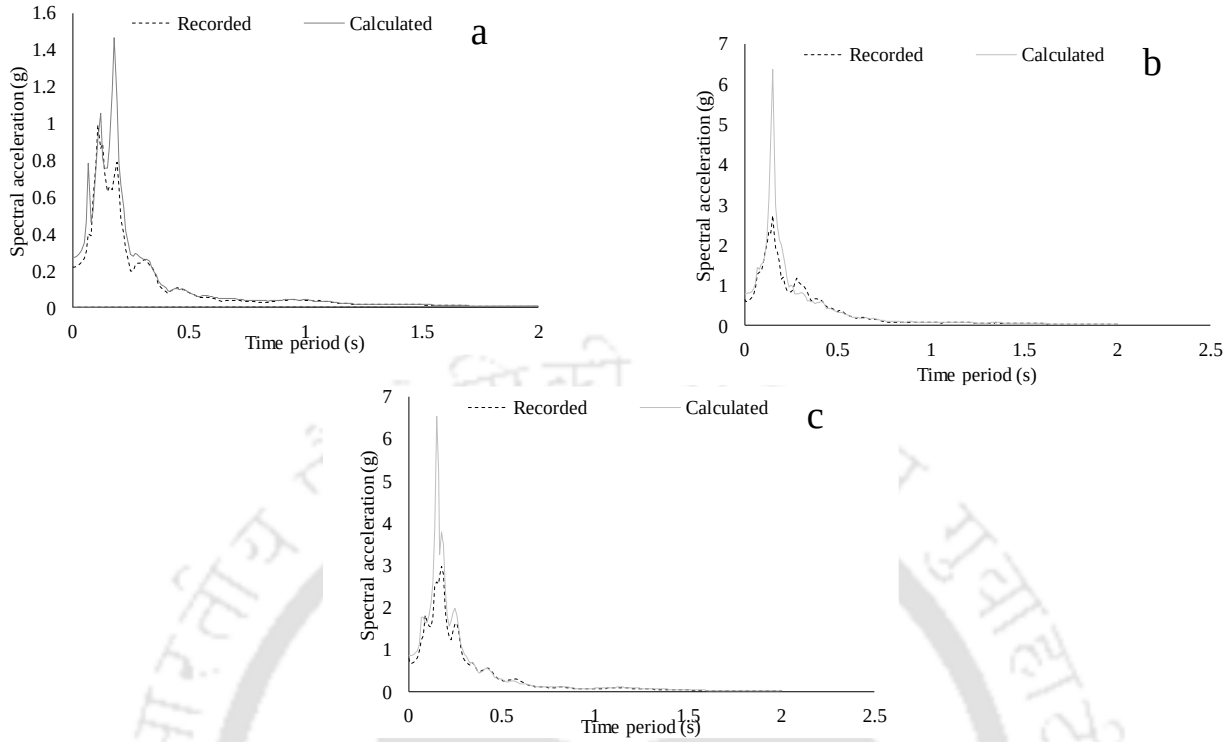

Figure 3.15, Comparison of response spectra based on calculated and recorded surface motion for; a) motion 3, b) motion 5, and c) motion 6

3.3.2.5 *Validation*

It should be highlighted here that for IWTH27 site, no site-specific DSPCs are available till present to be used for comparison with the present findings. However, Kaklamanos et al. (2015) and Kim and Hashash (2013) conducted GRA studies at IWTH27 by using G/G_{max} and β curves developed based on constitutive relationships by Darendeli (2001) and Zhang et al. (2005). Thus, for validation purposes in this section, G/G_{max} and β curves for sand as well as clay, which were used for the surficial layer by Kaklamanos et al. (2015) and Kim and Hashash (2013), are compared with present findings. Comparison of G/G_{max} values and average G/G_{max} curve obtained from the present study with the one given by Darendeli (2001) and Zhang et al. (2005) is made in Figure 3.11. It can be observed from Figure 3.11 that the proposed G/G_{max} curve is significantly different from G/G_{max} curves by Darendeli (2001) and Zhang et al. (2005) in γ

range of 0.01 to 0.1%. However, for γ <0.01% and γ >0.1%, the proposed average G/G_{max} in this study is matching with the G/G_{max} curves by Darendeli (2001) and Zhang et al. (2005).

Further, obtained β versus γ_{eff} values from the present study along with the average β curve are compared with β curves for sand as well as clay by Darendeli (2001) and Zhang et al. (2005) as given in Figure 3.12. It can be observed from Figure 3.12 that β versus γ_{eff} values obtained in the present study is matching with β curves for clay by Darendeli (2001) and Zhang et al. (2005) up to γ< 0.03%. Beyond this value of γ, a significant variation between the present values with respect to corresponding curves for clay by Darendeli (2001) and Zhang et al. (2005) can be observed.

It must be highlighted here that the G/G_{max} and β curves by Darendeli (2001) and Zhang et al. (2005) were given in the form of empirical correlation. Moreover, it was not checked whether selected G/G_{max} and β curves by Darendeli (2001) and Zhang et al. (2005) were best suited for IWTH27 site. Therefore, additional validation of the present findings is required. For this, using the above estimated average G/G_{max} curve and β curve, ELGRA are performed for additional 4 ground motions listed in Table 3.8, using GRA code developed by Kumar and Mondal (2017). It must be mentioned here that these 4 ground motions were not used earlier while determining average G/G_{max} curve and β curve for the site based on the proposed methodology. Further, ELGRA are also performed for the same set of 4 ground motions using G/G_{max} curve and β curve by Zhang et al. (2005) for clay (PI 30). Since back computed β values from this study are found matching precisely with curve developed by Darendeli (2001) and Zhang et al. (2005) for clay, curve for clayey soil is used for validation here. During ELGRA, the rock layers are modeled as linear material. The surface acceleration time histories obtained from both set of ELGRA are presented in Figure 3.16 (a-d). Besides, recorded surface motions

are also shown in Figure 3.16 (a-d). It can be observed from Figure 3.16 (a, b and d), acceleration time histories obtained from both sets of ELGRA are consistent with the recorded acceleration time histories. However, Figure 3.16 c clearly depicts that acceleration time history obtained based on the proposed G/G_{max} and β curve is closely matching with the actual acceleration time history than acceleration time history obtained based on Zhang et al. (2005)'s based G/G_{max} and β curve for clay. Acceleration time history obtained based on Zhang et al. (2005) G/G_{max} and β curve for clay clearly underestimates the actual acceleration time history when PGA of the ground motion is high (see Figure 3.16 c). Therefore, it can be said the proposed G/G_{max} and β curve is a better representation of DSPC for a wider variety of γ for the surficial layer of IWTH27 downhole array than available standard G/G_{max} and β curves.

Table 3.7, Details of ground motions considered for the validation

Serial	Origin time & component	Latitude (N)	Longitude (E)	Hypocentral depth (km)	Magnitude (M_w)	PGA (g)
1	2009/06/23 (16:37:00, EW)	38.895	142.532	39	5.6	0.062
2	2009/06/23 (16:37:00, EW)	38.895	142.532	39	5.6	0.052
3	2011/03/11 (14:46:00, NS)	38.103	142.86	24	9	0.752
4	2011/03/11 (15:06:00, NS)	39.042	142.397	27	6.4	0.178

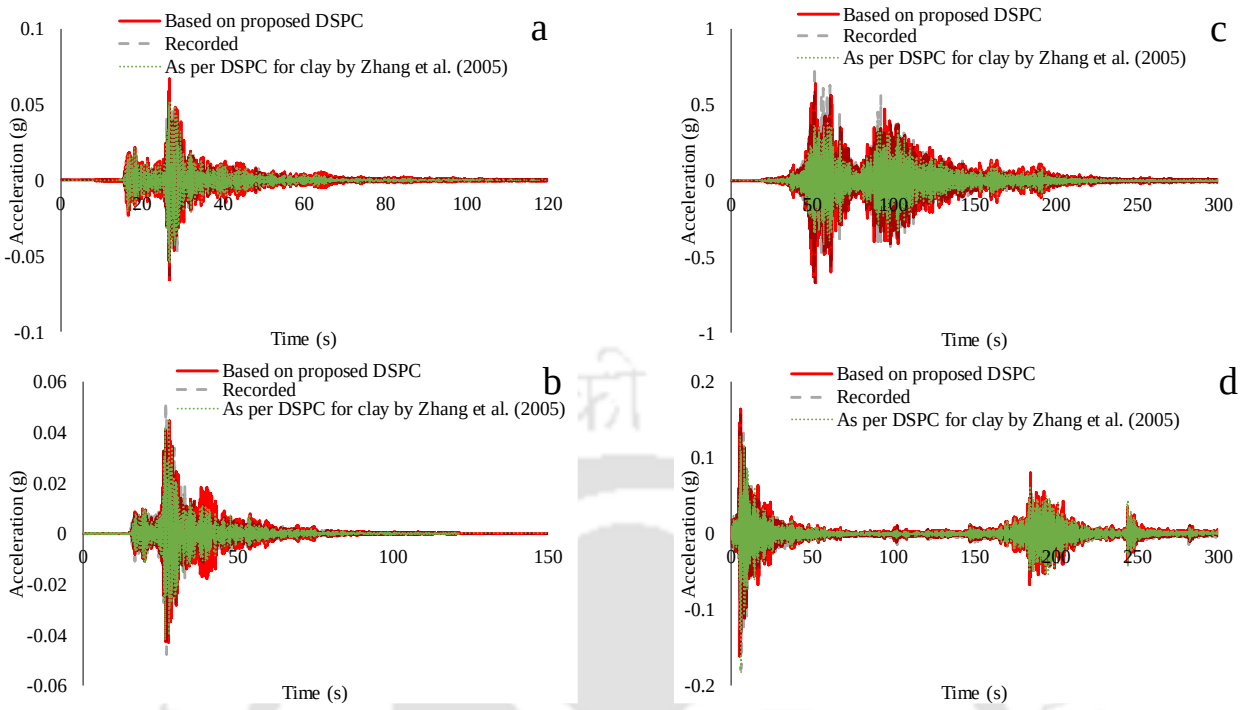

Figure 3.16, Comparison of acceleration times histories recorded, calculated based on proposed DSPC and DSPC by Zhang et al. (2005) for; a) motion 1 b) motion 2 c) motion 3 d) motion 4

3.4 Conclusion:

Earlier studies utilized surface records and downhole records to obtain G/G_{max} for soil medium entrapped between the accelerometer levels. In case of multiple layers existing between accelerometer levels, existing methodologies give G/G_{max} for combined soil layers and not for individual layer. Further, a majority of such studies did not estimate β values. Overcoming these limitations, the current chapter proposed two sets of four-step framework following which, for a two-layered system (with rock as bottom layer), G/G_{max} versus γ_{eff} and β versus γ_{eff} for the surficial layer can be determined. In order to test the effectiveness of proposed framework, four step methods are applied to Lotung site and IWTH27 site. While Lotung has recorded ground motion at the top and bottom of 6m thick surficial layer, IWTH27 has recorded ground motions at 0 and 100m depth with 4m as surficial layer thickness. For Lotung site, since the determination of initial dynamic properties as well as updation of such properties in iteration is

based on 0 and 6m depth, at the end of the iteration, both f as well as amplitude matches. However, for IWTH27 site, initial dynamic properties are determined based on $H(\omega)_{0\text{-}4}$, they are updated in iteration based on $H(\omega)_{CR}$ and $H(\omega)_{RR}$ at 0 and 100m. As a result, at the end of the iteration, significant difference in terms of calculated and recorded PGA values is possible, which is an attribute of assumed β for the rock layer.

Based on proposed steps, G/G_{max} and β for the surficial layers existing at Lotung and IWTH27 are estimated. For IWTH27 site, average G/G_{max} and β are also proposed in this study. While obtained G/G_{max} and β for Lotung site are found comparable with existing information, for IWTH27, proposed G/G_{max} and β curves are found better than the one reported in the existing literature in capturing soil response

CHAPTER 4: FRAMEWORK OF INVERSE GROUND RESPONSE ANALYSIS FOR TWO-LAYERED SYSTEM

4.1 Introduction

Based on the literature review presented in Chapter 2, various research gaps in existing available IGRA methodologies in terms of estimation of β curve and DSPCs for specific layer is missing. In the light of this research gap, Chapter 2 developed a new framework based on which both β curve and DSPCs for the surficial layer can be determined. It has been seen that the outcomes of the proposed framework are matching closely with DSPCs for Lotung and IWTH27 sites with existing literature. Continuing with the same objective of determining DSPCs of subsoil layers, the present chapter develops framework to back-compute DSPCs for the surficial layer and layer below it at the Lotung site. In doing so, the methodology to back compute DSPC for the surficial layer remains similar to that discussed in section 3.3.1.2. For the determination of DSPCs of the layer below the surficial one, the current chapter combines the methodology discussed in section 3.3.1.2 and findings by Hadjian (2002). Details of the framework and the steps involved are explained in the sections below.

4.2 Ground motions considered

Details of 18 EQs recorded in the vicinity of the Lotung site (available on *soilquake.net*) been discussed in Chapter 3. It should be noted here that the EQ data provided by above website do not include downhole array data for LSST 1. Further EQ data downloaded for LSST 2 and LSST 3 were found corrupted, and for LSST 4, the downhole EQ recordings were distorted. Therefore, the above mentioned EQ data are not used in this study. Further, the remaining dataset (LSST 5-LSST 18) each has three components recorded (NS, EW and UD) at every downhole location.

Since the present work is based on one-dimensional shear wave propagation, the vertical components of the records are not used in the analysis. Hence, altogether, 28 ground motions (EW and NS) from DHB array data are used for the determination of G/G_{max} and β values. Table 4.1 summarizes the specific detailss of these ground motions (as per Elgamal et al. 1995). The magnitude of EQ records under consideration ranges from 4.5 to 7 (M_L). Further, the PGA values of these EQ records (recorded at FA1-5) range from 0.02-0.21g. Such variation in PGA values aids in the estimation of G/G_{max} and β values over a larger γ range. It can be observed from Table 4.1 that a wide variation in epicentral distance (5.2-77.9km) is also taken into account, allowing the effect of both distant as well as near-source EQs into consideration, in the analysis. It should be noted here that according to Wen (1994), the close proximity of a containment structure affects EQ records at the DHA array. For this reason, the current work does not use EQ data from the DHA array.

Table 4.1, Details of ground motion considered for the analyses at DHB

Serial	Motion name	Date	Magnitude (M_I)	Epicentral distance (Km)	PGA (g)		Time window (s)	
					EW	NS	EW	NS
1	LSST5	3/29/1986	---	---	0.04	0.03	3-6.5	3-6
2	LSST6	4/8/1986	5.4	31.4	0.04	0.03	5-8	5-8
3	LSST7	5/20/1986	6.5	66.2	0.16	0.21	8.5-15	8.5-14
4	LSST8	5/20/1986	6.2	69.2	0.03	0.03	2-9	1.5-3.5
5	LSST9	7/11/1986	4.5	5	0.07	0.05	3-4.5	3-5
6	LSST10	7/16/1986	4.5	6.1	0.03	0.04	2.3-3.5	2-4.5
7	LSST11	7/17/1986	5	6	0.07	0.1	2.5-5.7	3-6
8	LSST12	7/30/1986	6.2	5.2	0.16	0.19	5.3-9.5	5.3-9.5
9	LSST13	7/30/1986	6.2	---	0.05	0.03	6.5-14.5	4-7.2
10	LSST14	8/5/1986	4.9	4.70	0.05	0.03	5-7	5-7
11	LSST15	11/14/1986	---	---	0.02	0.04	5.2-7.5	5.5-7.5
12	LSST16	11/14/1986	7	77.90	0.13	0.17	15-30	15-30
13	LSST17	11/14/1986	---	---	0.04	0.04	10-19	10-20
14	LSST18	11/15/1986	---	---	0.03	0.02	3-7	1-6

4.3 Proposed methodology for the surficial layer and based analysis

Following the governing equations described previously (Equation 3.1 to Equation 3.12) in section 3.2, G/G_{max} and β values are back-calculated for the soil layer perched between FA1-5 and DHB6 in this section. It should be mentioned here that ρ value is taken as 1.87gm/cc (as per Huang et al. 2001) for the surficial layer (soil deposit between FA1-5 and DHB6) as well as for the layer below it (soil deposit between DHB6 and DHB11). As the current study is based on one-dimensional GRA [which is based on the assumptions that soil response is due to the vertically propagating shear waves], identification of the shear wave portion of ground motions is important. Earlier frequency domain studies (Chang et al. 1996; Ghayamghamian and Kawakami 1996) divided the shear wave portion of the EQ record into multiple time windows (either 5s or 5.12s of duration). This was intended to acquire multiple shaking levels from a single EQ record which could reflect different γ levels. On the other hand, (Chang et al. 1991a, 1996; Tokimatsu and Midorikawa 1981) utilized the entire EQ record for the analyses. For the present study, the shear wave portion is identified from each of the EQ records mentioned in Table 4.1. The starting point (t_p) of P wave can be identified visually (Banerjee and Kumar 2018). Further, as per (Banerjee and Kumar 2018), t_p, V_p, V_s, and hypocentral distance can be used to determine the starting point of the shear wave arrival. Similarly, literature exists towards the determination of the termination of shear wave component in an EQ record (Ameri et al. 2011; Bindi et al. 2009). The subsequent steps for analysis are discussed below.

1. In the present study, as a first step, both the starting point and end point of shear wave portion in an EQ record are picked based on visual inspection. Further, only one time window for each EQ record is considered in the present work. This time window is chosen in such a way that the EQ record's peak amplitude value is covered within the

selected time window. Details of time window for each of the selected ground motions are also summarized in Table 4.1. After selecting the time window, Fourier amplitude spectra for the corresponding ground motions are calculated for EQ records obtained from FA1-5 and DHB6 (for the respective time window). Later, $H(\omega)_{RR}$ is computed by dividing the Fourier spectrum of FA1-5 record by the Fourier spectrum of DHB6 record.

2. In the second step, the peak amplitude of $H(\omega)_{RR}$ and the associated f are obtained from the $H(\omega)_{RR}$ plot. It is to be noted here that the amplitude of $H(\omega)_{RR}$ depends on β value. In earlier frequency domain methodologies, the amplitude of $H(\omega)_{RR}$ was not taken into account. As a result, such studies could not determine β values of the soil layers involved. In this work however, based on the peak amplitude of $H(\omega)_{RR}$ and f, and utilizing Equation 3.12, the value of V_s^* can be computed. Once V_s^* is known, V_s and β values can be computed by separating real and imaginary parts of V_s^* respectively, following Equation 3.3.
3. In the third step, the adequacy of the back-computed V_s and β values to reflect soil response is assessed. For the purpose, $H(\omega)_{CR}$ is computed involving FA1-5 and DHB6, using the above-computed V_s and β values, and following Equation 3.11. In addition, acceleration time history (for the respective time window) at FA1-5 is computed by utilizing recorded ground motion at DHB6 and the above estimated $H(\omega)_{CR}$. At this stage, two additional criteria in addition to the criterion set in section 3.3.1.2 are set to check the suitability of V_s and β values in representing the actual soil response. It should be noted here that the above estimated V_s and β values correspond to peak amplitude of $H(\omega)_{RR}$ and f. Therefore, at f, the amplitudes of $H(\omega)_{CR}$ and $H(\omega)_{RR}$ are comparable. However, whether based on the above V_s and β values, $H(\omega)_{CR}$ and $H(\omega)_{RR}$ match with

each other at other frequencies also, has to be checked. For this reason, in the first criteria (that was originally proposed by Mondal and Kumar 2021a), $H(\omega)_{RR}$ and $H(\omega)_{CR}$ are compared up to 10Hz frequency. It should be highlighted here that $H(\omega)_{RR}$ has uneven spikes and falls, which need to be smoothened prior to the above comparison [following (Chang et al. 1991a, 1996; Ghayamghamian and Kawakami 1996; Ghayamghamian and Matosaka 2001)]. For the present study, both $H(\omega)_{RR}$ and $H(\omega)_{CR}$ are smoothened three times in a row, following the works by Chang et al. (1996); Ghayamghamian and Kawakami (1996). For this purpose, a finite impulse response moving average filter is applied using in built MATLAB command "smooth". ANOVA test using a "student's t-test" is done on the smoothened $H(\omega)_{RR}$ and $H(\omega)_{CR}$ graphs to examine the general agreement between these two graphs up to 10Hz. The ANOVA test is dependent on the null hypothesis, which asserts that "the difference between two sample's mean is negligible (if the difference is considerable, then the alternate hypothesis is applicable)". For statistical analysis, p value > 0.05 (probability that the null hypothesis is valid for the two samples) is usually used. Further based on p-value, the matching between $H(\omega)_{RR}$ and $H(\omega)_{CR}$ can be assessed. In case p-value > 0.05, $H(\omega)_{RR}$ and $H(\omega)_{CR}$ are considered to be in agreement up to 10Hz. This way, the first criteria confirms that estimated V_s and β values are capable of representing actual soil response in the frequency domain. However, their suitability in the time domain needs to be further confirmed. For this reason, second and third criteria are needed.

In the second criteria, the PGA values obtained from the computed and recorded acceleration time histories at FA1-5 are compared. Percentage error in PGA for surficial layer (PGA_diff1) (in computed acceleration time history-based PGA with respect to

recorded acceleration time history-based PGA) is computed for each of the 28 motions. A –ve percentage error indicates an overestimation of recorded PGA while a +ve percentage error indicates an underestimation of recorded PGA in computed PGA. Thus, the recorded and computed acceleration time histories at FA1-5 are considered to be in agreement only if the absolute value of percentage error falls below 20%. This value of 20% has been set in this work based on a detailed assessment.

It has to be highlighted here that the second criterion stated above provides an assessment solely based on PGA values. However, it does not confirm whether the waveform of the computed acceleration time history is consistent with the waveform of the recorded acceleration time history at FA1-5 throughout the time window under consideration. It has to be highlighted here that in order to confirm matching between computed and recorded acceleration time histories, spectral acceleration values computed based on two sets of response spectrum (computed and recorded) can be considered (following Afacan et al. 2014). For this reason, in the third criterion, 5% damped response spectra are computed at FA1-5 based on recorded acceleration time history and computed acceleration time history (for the respective time window). Further, an assessment is made for the matching of above-computed response spectra (computed based on recorded acceleration time history and computed acceleration time history at FA1-5). For the purpose, another Student's t test is performed on the response spectra, and a minimum threshold of p value (p1) is set as 0.05. Thus, when p1 > 0.05, both the response spectra (computed based on recorded acceleration time history and computed acceleration time history) are considered to be consistent. It is to be highlighted that by considering the matching of response spectra, the suitability of the back-computed V_s and β values to

reflect soil response is assessed simultaneously in time domain as well as in frequency domain.

4. For motions which do not satisfy even one of the above-mentioned three criteria, it is observed that though the value of f is consistent in both $H(\omega)_{RR}$ and $H(\omega)_{CR}$, the amplitudes of $H(\omega)_{RR}$ and $H(\omega)_{CR}$ are different. For such motions, step four is proposed here. As mentioned earlier, the amplitudes of $H(\omega)_{RR}$ and $H(\omega)_{CR}$ are the functions of β. Hence, in order to reduce the difference between the amplitudes of $H(\omega)_{RR}$ and $H(\omega)_{CR}$, modification in β values is required. Thus, in the fourth step, only β values are increased or decreased iteratively, keeping V_s obtained till step two unaltered and revised values of $H(\omega)_{CR}$ is calculated. This β value is changed iteratively at a common increment/ decrement of 1% depending on the sign of PGA_diff1. If PGA_diff1 is less than 0, the β value is increased; otherwise, the β value is decreased iteratively. In every iteration, using the updated β value and unaltered V_s value, step three is repeated until all three set criteria are satisfied. It has to be highlighted here that the iterative updation of β value is achieved by means of a MATLAB function (firstlayer.m) developed by the author. Further, the maximum and minimum values of β are set as 20% and 1% respectively in the function. The function can automatically (without any input from user) update and adjust β value unless the set criteria are satisfied.
5. Based on the discussion so far, final V_s for all the motions are obtained from step 2. Further, β values corresponding to those motions which either satisfy all the three criteria of step 3 or do not satisfy these criteria and got update in β value is updated in step 4, are known. At this stage, in order to check if the above obtained β value can further be improved, an additional iteration is performed in the step five where most recent β value

corresponding to each motion is further increased/ decreased by 1% based on the PGA_diff1 value (increased if PGA_diff1 < 0, decreased if PGA_diff1 > 0), and accordingly p-value, p1-value, and PGA_diff1 values are obtained. If the p-value, p1-value and PGA_diff1 values improve simultaneously in the subsequent iteration, then β value is updated. It is to be noted here that improvements in p-value and p1-value in an iteration indicates that p-value and p1-value obtained in that iteration are greater than p-value and p1-value obtained in the previous iteration. On the other hand, improvement in the PGA_diff1 value means that the absolute value of PGA_diff1 obtained in any iteration is lesser than the absolute value of PGA_diff1 obtained in the previous iteration. Once no further improvements in p-value, p1-value, and PGA_diff1 value are observed, further iteration in step 5 is terminated and updated β values corresponding to each motion is considered as final. Further, γ time history at the center of the soil layer is computed by substituting the back-computed V_s and β values into Equation 3.8. Finally, effective shear strain ($\gamma_{eff} = 0.65 \times \gamma_{max}$) is computed from the γ time history. Figure 4.1 shows a flowchart that explains the whole framework for determining V_s, β and γ_{eff} values for the surficial layer (described above).

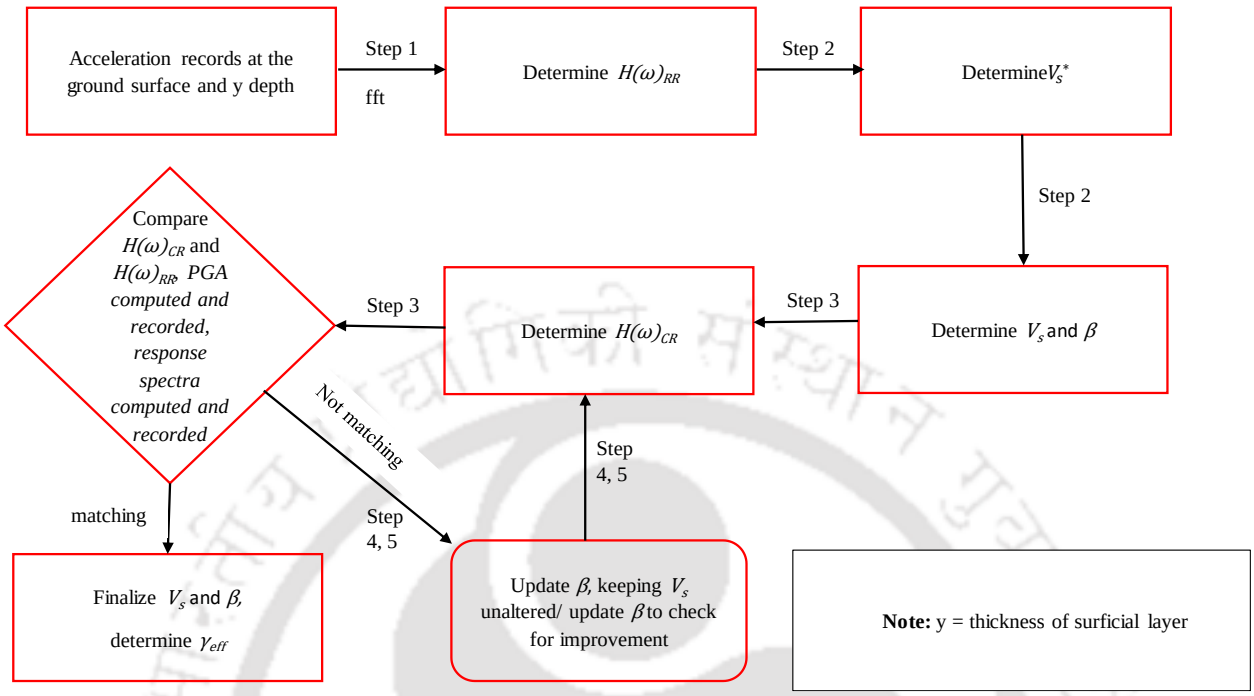

Figure 4.1, Flowchart of the proposed framework used at Lotung for two layer system (1st layer)

4.4 Methodology to obtain V_s value for the layer existing between DHB6 and DHB11

In the earlier section, a methodology which can be followed to determine V_s and β values for the surficial layer is discussed. Above methodology can only be applied to the surficial layer and not to layers below it. In this section, methodology to determine V_s value for the second layer (layer existing between DHB6 and DHB11) is discussed. It has to be highlighted here f/T of a soil layer within a multi-layered soil system can be determined based on $H(\omega)_{RR}$, following graphical method (Chang et al. 1991a, 1996; Madera 1970) or by following approximate analytical method (Hadjian 2002). In the present study, firstly, T is determined following the approximate analytical methodology proposed by (Hadjian 2002) as follows;

$$\frac{T_c}{T_1} = \sqrt{\frac{\pi^2}{8}\left[0.75 + \left(\frac{T_2}{T_1}\right)^2\left(1 + 2\frac{H_1}{H_2}\right)\right]} \quad 4.1$$

Where T_c is defined as the fundamental natural period of first two layers (from the ground surface combined), as obtained from $H(\omega)_{RR}$ between the ground surface and bottom of the second layer. Similarly, T_1 and T_2 are defined as fundamental natural periods of the surficial layer and the layer below it, respectively. Further, H_1 and H_2 are the thicknesses of the surficial layer and layer below it. In Equation 4.1, the value of T_2 can be determined once all the other values are known. For the purpose, T_1 is determined following Equation 4.2 using V_s value of the surficial layer calculated earlier. Finally, the V_s value for the second layer can be determined using Equation 4.2 (Chang et al. 1996),

$$V_s = \frac{4H}{T} \quad 4.2$$

It has to be mentioned here that Equation 4.1 can be utilized only when $\frac{H_1}{H_2} > 1$(Hadjian 2002). For the present study this value $\left(\frac{H_1}{H_2}\right)$is 1.2 (6/5) making Equation 4.1 applicable for the Lotung site.

4.5 Analysis for the second layer

This part determines V_s and β values for the second layer based on the discussion in the previous section. Please note that V_s and β values for the surficial layer are known at this stage. Further, utilizing V_s value for 2nd layer (as computed based on T_2 value in the last section) and considering β as 1%, $H(\omega)_{CR}$ [$H(\omega)_{CR,\ 6\text{-}11}$] is determined between DHB6 and DHB11. It should be highlighted here that though the V_s value for 2nd layer considered for determination of $H(\omega)_{CR,\ 6\text{-}11}$ is obtained based on the method proposed by Hadjian (2002), the β value of 1% considered is an initial approximation only, which may or may not represent the actual soil response. Since, β

value controls the amplitude of $H(\omega)$, $H(\omega)_{CR,\ 6\text{-}11}$ calculated using above V_s and β values will not be comparable to $H(\omega)_{RR}$ [obtained using record at DHB6 and record at DHB11, $H(\omega)_{RR.\ 6\text{-}11}$] in terms of amplitude even at T_2. Hence, further comparison between $H(\omega)_{CR,\ 6\text{-}11}$ and $H(\omega)_{RR.\ 6\text{-}11}$, and subsequent adjustment in β value is required. Thus, β value is obtained by iteratively updating the value from 1% at an increment of 1%, till overall matching is obtained both in frequency domain and time domain. It has to be mentioned here that initially the agreement between the computed and recorded parameters is adjudged following the three criteria of step three discussed for the surficial layer earlier. However, it is observed here that for few ground motions, the criterion corresponding to difference in PGA (PGA_diff2) is not satisfying. Thus, for the second layer, only two criteria (criterion one and three as discussed for the surficial layer) are set to check the matching of response parameters in frequency domain and time domain respectively. Further, it is observed that in the case of weak motions (PGA<0.1g), the set criteria are satisfied in the first iteration (i.e., β = 1%) itself. Further, when the β value is increased in subsequent iterations (at the rate of 1%), it is observed that both the criteria are satisfied at higher β values as well. Hence, multiple β values are obtained from the same ground motion, all of which satisfy the set criteria. It is to be noted here that for the first layer, the initial β value is obtained based on the amplitude of $H(\omega)_{RR}$. However, for the second layer, the β value selected in each iteration is assumed. Therefore, selecting any one β value from multiple values randomly may not be justified. Thus, two different criteria are set to check the matching of the computed and recorded parameters in the frequency domain and time domain. For this purpose, in every iteration, "student's t-test" is performed on $H(\omega)_{CR,\ 6\text{-}11}$ and $H(\omega)_{RR.\ 6\text{-}11}$. Additionally, 5% damped response spectra are computed based on recorded and computed acceleration time histories (for respective time windows) at DHB6. Further, another "student's t-test" is performed

on the two response spectra calculated based on computed and recorded time histories. The 'p values' obtained from both "student's t-test" performed on $H(\omega)_{CR,\ 6\text{-}11,}$ and $H(\omega)_{RR.\ 6\text{-}11}$, and response spectra after each iteration are then stored. This way, the iterative determination of β value will take place, updating β value from 1% to a maximum of 20%. The iteration will progress as long as both the 'p values' stored in that iteration are greater than the 'p values' stored in the previous iteration. Finally, the β value corresponding to the last iteration is selected as the final β. It has to be highlighted here that the updation of β value in each iteration is achieved by means of a MATLAB function 'secondlayer.m'. This function automatically updates β value until the set criteria are satisfied. Once β value is finalized for the second layer, γ time history is computed at the center of second layer using Equation 3.8 and utilizing Fourier spectra obtained from the acceleration record (for respective time window) at DHB6. Subsequently, γ_{eff} values are computed from γ time history. The entire procedure discussed in this section is shown by means of a flowchart in Figure 4.2.

4.6 Results and discussion

Utilizing the inverse GRA framework discussed above, two set of V_s, β, and γ_{eff} are computed for the surficial layer and second layer for each ground motion mentioned in Table 4.1. As a result, 56 sets of V_s, β, and γ_{eff} are computed based on 28 ground motions mentioned in Table 4.1. Table 4.2 provides an overview of the back-calculated soil properties for the first layer. Further, Table 4.3 depicts the back-calculated soil properties for the second layer. It can be observed from Table 4.2 and Table 4.3 that some rows are shaded. It can be seen from Table 4.2 and Table 4.3 that the motions corresponding to the shaded rows do not satisfy either the criteria set for the first layer or for the second layer. Thus, altogether these motions are shaded in both Table 4.2 and Table 4.3. It has to be highlighted here that altogether, 11 motions are shaded in both Table 4.2

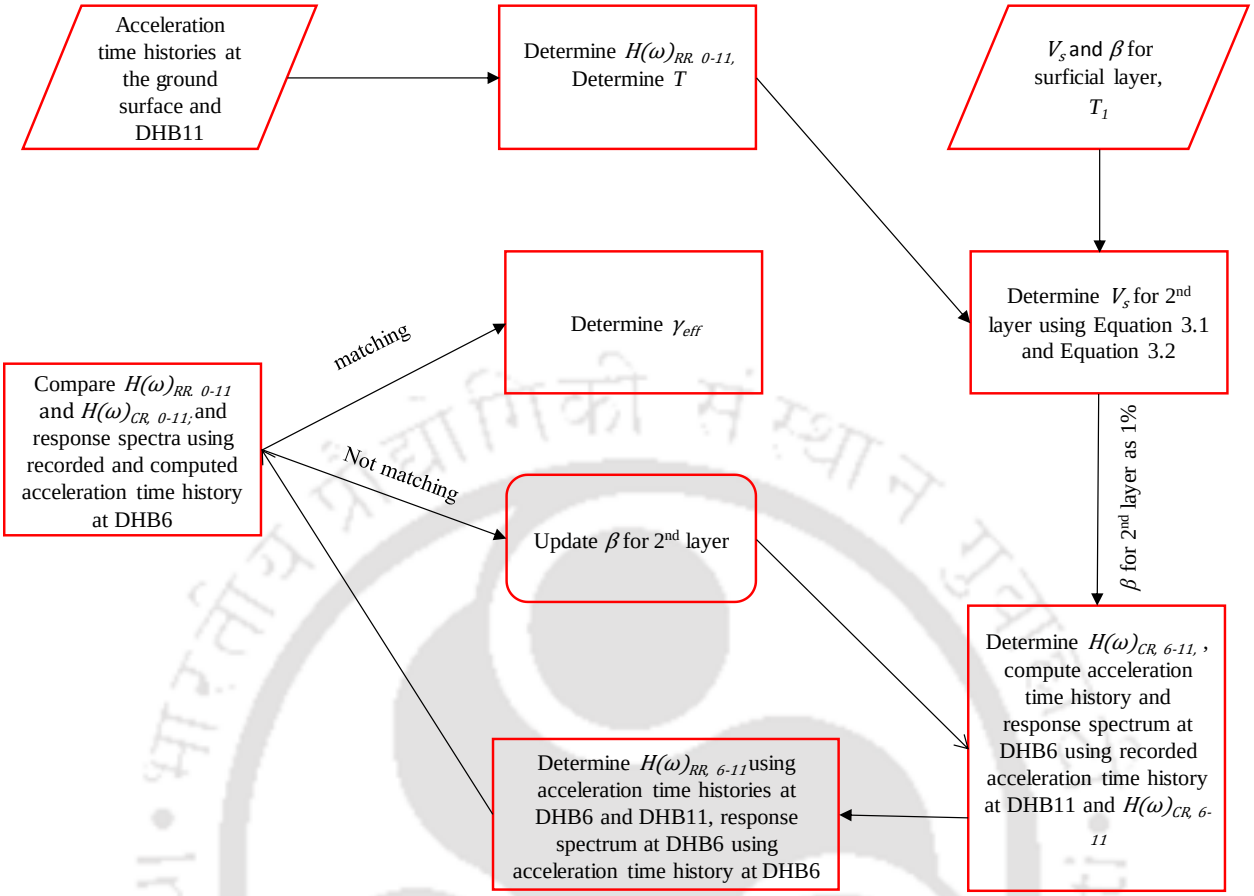

Figure 4.2, Flowchart of the proposed framework used at Lotung for two layer system (2nd layer)

and Table 4.3. These motions and the corresponding back-calculated properties are not considered for the present inverse analysis. Table 4.2 shows that the γ_{eff} values for the first layer range from 0.0020% (for motion 12) to 0.048 % (for motion 24). Likewise, the back-computed V_S values range from 82.5m/s (for motion 24) to 136.7m/s (for motion 19). It should be noted here that the low γ corresponding V_S value obtained in this analysis (136.7m/s) matches well with the geophysical findings by Anderson and Tang (1989) (see Figure 2.3). Furthermore, the back-calculated β values for the surficial layer range from 3% (for motion 22) to 16.9% (for motion 13).

Table 4.2 also includes the final p values for both $H(\omega)$ and response spectra at the end of the proposed procedure. The smallest p value for $H(\omega)$ (= 0.06) is achieved for motion 2,

while the largest p value (= 0.93) is obtained for motion 16. Similarly, the smallest p value for response spectra is obtained (= 0.25) for motion 13, while the largest p value is obtained (= 0.91) for motion 2. Further, the maximum percentage error in estimating PGA is limited to 17.3% for motion 25, while the minimum percentage error of -1.4% is obtained for motion 7.

For the second layer, the γ_{eff} values vary between 0.002% (for motion 19) and 0.08% (for motion 24), as summarized in Table 4.3. The back-computed V_s values vary from 90.78m/s (for motion 24) to 168m/s (for motion 19). Again from Figure 2.3, it can be confirmed that the back-calculated low γ corresponding V_s value obtained in this study (168m/s) is consistent with the geophysical test result of Anderson and Tang (1989). Further, it can be observed from Table 4.3 that the back-computed β values are in the range of 2% (for motion 19) to 20% (for motion 24). The p values for $H(\omega)$ in the second layer vary from 0.067 (for motion 7) to 0.94 (for motion 2). Similarly, it can be observed from Table 4.3, the p value for response spectra varies from 0.06 (for motion 7) to 0.93 (for motion 12). Further, percentage error in estimating PGA value for the second layer (PGA diff2) is varying from -0.89% (for motion 21) to -54% (for motion 22). It has to be highlighted here that for the determination of β values for the second layer, no criteria regarding PGA diff2 value is proposed in this study. Further, From Table 4.1, it can be seen that the PGA values for the motions corresponding to the higher absolute PGA diff2 values are very less (<0.1g). Thus, such a higher PGA diff2 value may not have a significant effect on the computed PGA value.

Comparison between $H(\omega)_{RR}$ and $H(\omega)_{CR}$, and $H(\omega)_{CR,\ 6\text{-}11}$ and $H(\omega)_{RR.\ 6\text{-}11}$ for all the motions that are considered for inverse analysis are shown in Figure 4.3 (a-q). It is evident from the comparison between $H(\omega)_{RR}$ and $H(\omega)_{CR}$ and the comparison between $H(\omega)_{RR,\ 6\text{-}11}$ and $H(\omega)_{CR,\ 6\text{-}11}$ that the recorded parameters $H(\omega)_{RR}$ and $H(\omega)_{RR.\ 6\text{-}11}$ match very well with the

corresponding computed parameters $H(\omega)_{CR}$ and $H(\omega)_{CR,\ 6\text{-}11}$. Additionally, comparisons between response spectra obtained from recorded motions and computed motions are shown in Figure 4.4 (a-q) for all the motions considered for inverse analysis. It can be seen from Figure 4.4 (a-q) that the response spectra computed based on recorded ground motions show consistency with the response spectra computed based on estimated ground motions. Further, it can be observed from Figure 4.4 (f, g, j, k, n, and q) that the recorded PHA values (at '0' second time period) for the corresponding ground motions at DHB6 are 0.05g or less. It has to be highlighted here that for these ground motions, absolute values of PGA_diff2 obtained earlier were greater than 20%. The low PHA values for these motions assert that though the absolute values of PGA_diff2 are greater than 20%, obtained PHA values in both cases are on the lower side.

Once V_s and β values for each of the layers are known, one can determine G/G_{max} and β curves for the layers. In order to obtain G/G_{max} values for Lotung site, the back-calculated V_s values (see Table 4.2 and Table 4.3) are divided by the $V_s^{\max}$ value for that layer (i.e.136.7m/s for the first layer and 168m/s for the second layer). Further, this ratio (V_s/V_s^{max}) is squared to obtain G/G_{max} value corresponding to γ_{eff} of above considered V_s (see Table 4.2 and Table 4.3). The same procedure is repeated to obtain G/G_{max} versus γ_{eff} for each of the ground motions considered for the inverse analysis. The G/G_{max} versus γ_{eff} values for the first layer are plotted as shown in Figure 4.5. In addition, laboratory obtained G/G_{max} data [from UT and NTU], ((EPRI 1993) and statistical fit based G/G_{max} curves generated by Chang et al. (1996); Zeghal et al. (1995) for the top 6m soil layer at DHB site based on inverse GRA are also shown in Figure 4.5. It can be observed from Figure 4.5 that the G/G_{max} values produced in this investigation have an excellent agreement with the curves found by Chang et al. (1996); Zeghal et al. (1995). Further,

reference shear strain (γ_{ref}) values based on Hardin and Drnevich (1972) constitutive model for each G/G_{max} value and corresponding γ_{eff} value are obtained. Average value obtained from such γ_{ref} values is then computed. Average G/G_{max} curve based on Hardin and Drnevich (1972) constitutive model is proposed utilizing the average γ_{ref} value obtained earlier as shown in Figure 4.5 by means of solid black line. It can be observed from Figure 4.5 that the proposed curve matches very well with the statistical fit curves by (Chang et al. 1996; Zeghal et al. 1995) based on inverse GRA study.

Similar to G/G_{max}, obtained β value and corresponding γ_{eff} (Table 4.2) for motions that are considered for inverse analysis are used to understand β variation with γ_{eff} for the first layer. Obtained β versus γ_{eff} for the first layer is plotted in Figure 4.6. In addition, Figure 4.6 shows laboratory determined β values by NTU (Chang et al. 1996) and a statistical fit based β curve for the top 6m soil at DHB location generated by Zeghal et al. (1995) based on inverse GRA. It can be observed from Figure 4.6 that the back-calculated values based on the current work, albeit dispersed, mostly follow the statistical fit curve proposed by Zeghal et al. (1995) for this location. Further, γ_{ref} values are calculated for each of the motions considered for the present inverse GRA. It has to be highlighted here that these values are computed based on the β values and corresponding γ_{eff} values obtained in the present study utilizing Hardin and Drnevich (1972) constitutive model. For the purpose, the maximum β value is considered 20%. An average curve is proposed considering Hardin and Drnevich (1972) constitutive model using the average value obtained from the γ_{ref} values calculated earlier. The average β curve is also shown in Figure 4.6 with black solid line. It can be seen from Figure 4.6 that average β curve obtained from the present work closely matches with the statistical fit curve proposed by Zeghal et al. (1995). It has to be highlighted here that β values obtained in this chapter for the surficial layer are less

scattered as compared to β values obtained for the same soil layer in Chapter 3 (See Figure 3.5). This is due to the fact that in present chapter, additional criteria for matching are set apart from the criterion of 'p-value' from comparison of $H(\omega)$ set in Chapter 3. Additional criteria for adjudging the matching leads to better identification of β values.

Similar way, for the second layer as well, the G/G_{max} versus γ_{eff} values are plotted in Figure 4.7. Figure 4.7 also shows laboratory acquired G/G_{max} data and statistical fit based G/G_{max} curves for the soil layer across DHB6 and DHB11 at the DHB site generated by Chang et al. (1996); Zeghal et al. (1995) based on inverse GRA. It can be seen from Figure 4.7 that beyond 0.008% γ_{eff} values, the G/G_{max} values obtained in the present findings are significantly lesser than both laboratory-based data and data obtained by previous inverse GRA studies. Similar to the first layer, an average G/G_{max} curve is proposed for the second layer considering the average γ_{ref} value obtained from all the G/G_{max} values following (Hardin and Drnevich 1972) constitutive model. The average G/G_{max} curve is shown by black solid line in Figure 4.7. It can be seen from Figure 4.7 that the average curve developed in this study based on proposed framework contains lower values of G/G_{max}, as compared to the laboratory based curves and curves obtained by previous inverse GRA studies.

The back-calculated β versus γ_{eff} values for the second layer are plotted as shown in Figure 4.8. Further, laboratory-based data for β and earlier inverse GRA based data for β are also shown in Figure 4.8. It can be observed from Figure 4.8 that some of the β values obtained in the present study are matching with UT laboratory-based β variation while other values match with the values obtained by Zeghal et al. (1995). Further, γ_{reff} values for all the β values are calculated following Hardin and Drnevich (1972) constitutive model. Similar to first layer, an average β curve is proposed by considering the average value obtained from γ_{ref} values calculated earlier.

The average β curve is shown in Figure 4.8 using black solid line. It can be seen from Figure 4.8 that the average β curve proposed in this work follows the UT laboratory test findings.

Table 4.2, Back calculated soil properties for the first layer

Serial	Motion detail	Strain (%)	Shear wave velocity (m/s)	Damping ratio	p-value for $H(\omega)$	p_value for Response spectrum	PGA_difference (%)
1	LSST5,0m,EW	0.003	134.137	0.007	0.001	0.955	26.827
2	LSST5,0m,NS	0.004	126.215	0.11	0.06	0.912	-8.153
3	LSST6, 0m, EW	0.005	122.258	0.067	0.352	0.757	-17.082
4	LSST6, 0m, NS	0.001	211.247	0.122	0.093	0.595	-13.494
5	LSST7, 0m, EW	0.007	199.997	0.159	0	0.002	-0.046
6	LSST7, 0m, NS	0.062	67.052	0.014	0	0	0.93
7	LSST8, 0m, EW	0.004	127.616	0.083	0.324	0.796	-1.408
8	LSST8, 0m, NS	0.004	126.139	0.064	0.003	0.971	2.096
9	LSST9, 0m, EW	0.007	129.908	0.105	0.108	0.345	-2.386
10	LSST9, 0m, NS	0.005	123.379	0.009	0.009	0.202	5.058
11	LSST10, 0m, EW	0.002	151.399	0.051	0.001	0.534	-1.279
12	LSST10, 0m, NS	0.002	136.425	0.09	0.465	0.913	-11.81
13	LSST11, 0m, EW	0.007	110.122	0.169	0.649	0.25	-17.278
14	LSST11, 0m, NS	0.012	109.568	0.086	0.464	0.865	-15.685
15	LSST12, 0m, EW	0.032	91.409	0.167	0.06	0.785	-14.372
16	LSST12, 0m, NS	0.027	100.108	0.143	0.937	0.894	-11.499
17	LSST13, 0m, EW	0.005	126.529	0.158	0.075	0.842	-15.597
18	LSST13, 0m, NS	0.003	125.781	0.104	0.891	0.688	-10.877
19	LSST14, 0m, EW	0.003	136.693	0.146	0.091	0.856	1.516
20	LSST14,0m, NS	0.005	129.794	0.204	0.004	0.77	-11.01
21	LSST15, 0m, EW	0.012	109.172	0.12	0.832	0.487	-16.857
22	LSST15, 0m, NS	0.011	114.301	0.031	0.25	0.509	-12.644
23	LSST16, 0m, EW	0.029	91.079	0.138	0.071	0.191	-19.573
24	LSST16, 0m, NS	0.048	82.511	0.1	0.497	0.852	-4.985
25	LSST17, 0m, EW	0.005	121.223	0.122	0.089	0.497	-17.314
26	LSST17, 0m, NS	0.006	109.387	0.014	0.85	0.349	-19.991
27	LSST18, 0m, EW	0.004	122.347	0.025	0.944	0.348	-10.453
28	LSST18, 0m, NS	0.003	124.783	0.055	0.06	0.76	-6.163

Table 4.3, Back-calculated soil properties for the second layer

Serial	Motion detail	Strain (%)	Shear wave velocity (m/s)	Damping ratio	p-value for $H(\omega)$	p_value for Response spectrum	PGA_difference (%)
1	LSST5,0m,EW	0.004	123.927	0.11	0.524	0.494	22.083
2	LSST5,0m,NS	0.005	120.663	0.11	0.943	0.507	17.265
3	LSST6, 0m, EW	0.008	119	0.09	0.904	0.214	16.187
4	LSST6, 0m, NS	0.003	182.342	0.2	0.005	0.583	-28.979
5	LSST7, 0m, EW	0.033	158.641	0.15	0.061	0.567	10.468
6	LSST7, 0m, NS	0.056	107.678	0.2	0.255	0.003	-4.721
7	LSST8, 0m, EW	0.01	102.423	0.12	0.067	0.06	-9.018
8	LSST8, 0m, NS	0.005	141.932	0.04	0.623	0.402	-12.896
9	LSST9, 0m, EW	0.005	159.787	0.02	0.75	0.256	22.569
10	LSST9, 0m, NS	0.005	140.634	0.2	0.003	0.381	23.201
11	LSST10, 0m, EW	0.003	144.557	0.2	0	0.437	4.641
12	LSST10, 0m, NS	0.002	138.177	0.05	0.599	0.936	17.845
13	LSST11, 0m, EW	0.016	100.499	0.07	0.41	0.063	29.687
14	LSST11, 0m, NS	0.012	100.276	0.03	0.762	0.106	22.745
15	LSST12, 0m, EW	0.047	109.202	0.04	0.378	0.066	-3.053
16	LSST12, 0m, NS	0.044	117.413	0.07	0.837	0.055	-8.313
17	LSST13, 0m, EW	0.005	120.794	0.02	0.393	0.394	44.598
18	LSST13, 0m, NS	0.005	106.629	0.02	0.213	0.077	34.624
19	LSST14, 0m, EW	0.002	168.758	0.02	0.195	0.825	-16.959
20	LSST14,0m, NS	0.005	135.26	0.2	0.001	0.013	59.589
21	LSST15, 0m, EW	0.009	141.558	0.02	0.349	0.788	-0.894
22	LSST15, 0m, NS	0.008	151.873	0.07	0.274	0.071	-54.636
23	LSST16, 0m, EW	0.071	87.039	0.2	0	0.524	2.618
24	LSST16, 0m, NS	0.082	90.786	0.2	0.839	0.263	-1.064
25	LSST17, 0m, EW	0.011	116.348	0.07	0.449	0.064	-18.423
26	LSST17, 0m, NS	0.013	111.288	0.2	0.004	0.063	-20.298
27	LSST18, 0m, EW	0.011	105.314	0.2	0.55	0.013	-31.825
28	LSST18, 0m, NS	0.007	120.064	0.09	0.496	0.09	-46.258

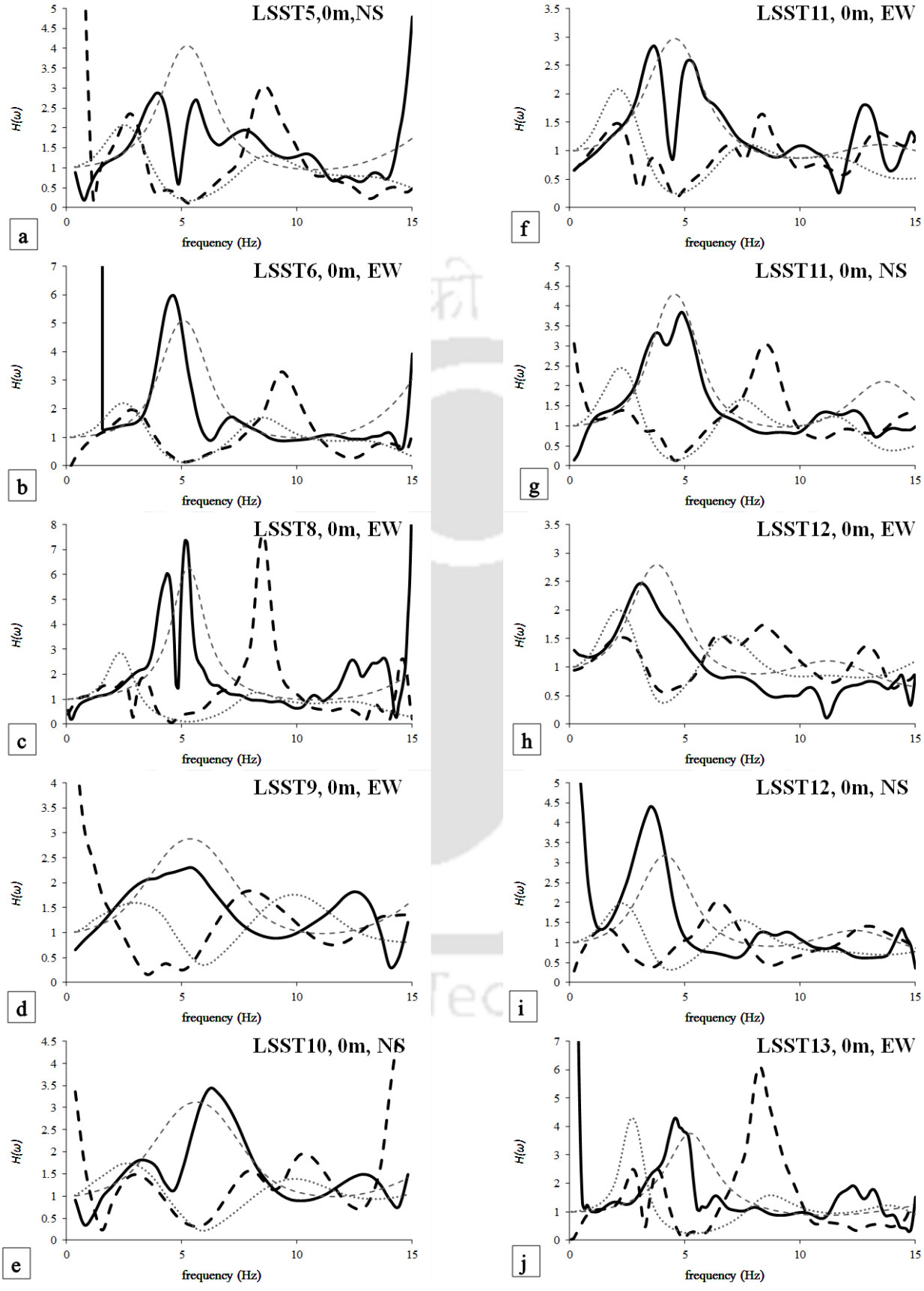

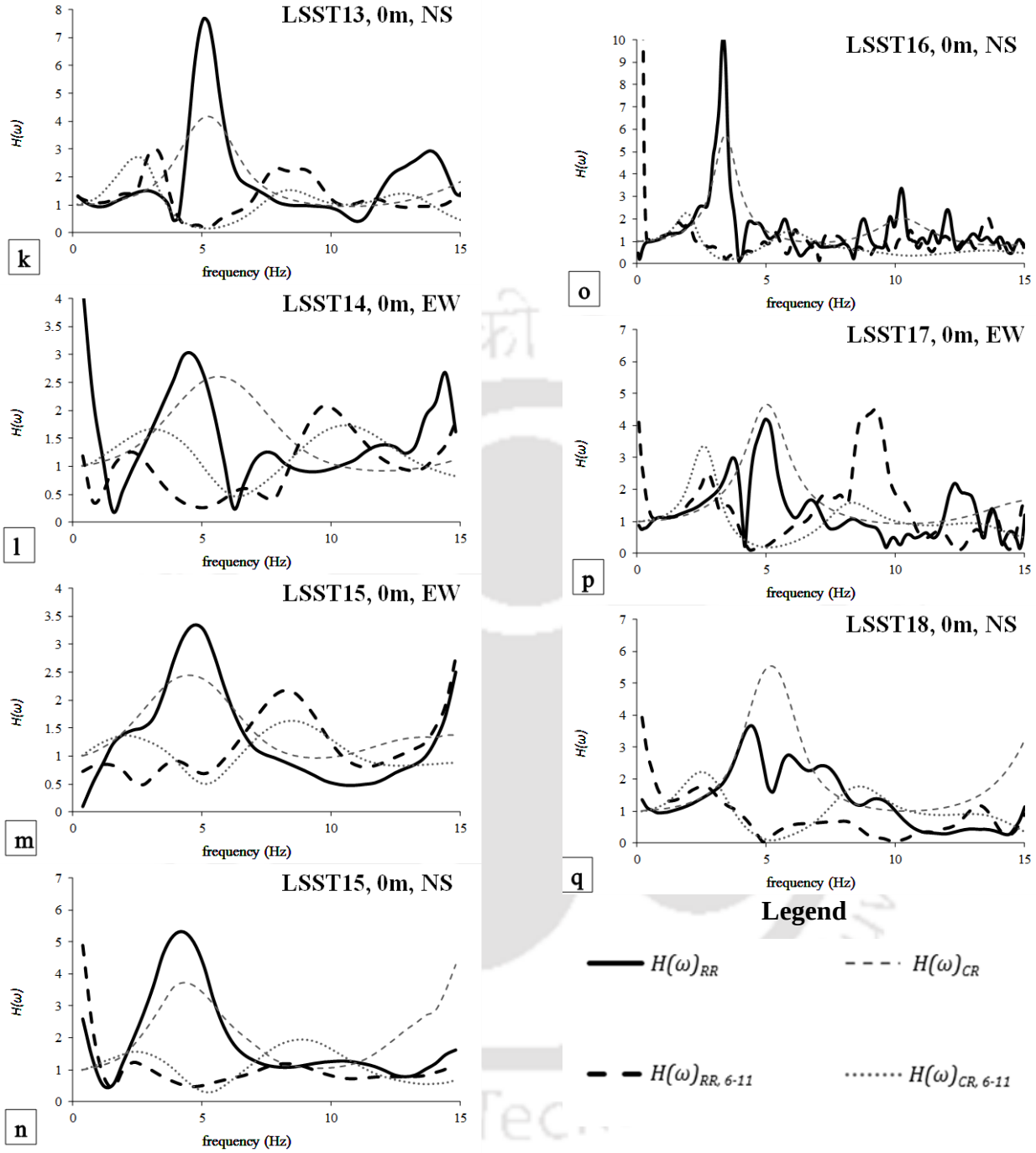

Figure 4.3 (a-q), Comparison of $H(\omega)_{CR}$ and $H(\omega)_{RR}$ and $H(\omega)_{CR,\ 6\text{-}11}$ and $H(\omega)_{RR,\ 6\text{-}11}$ for motions considered in inverse analysis

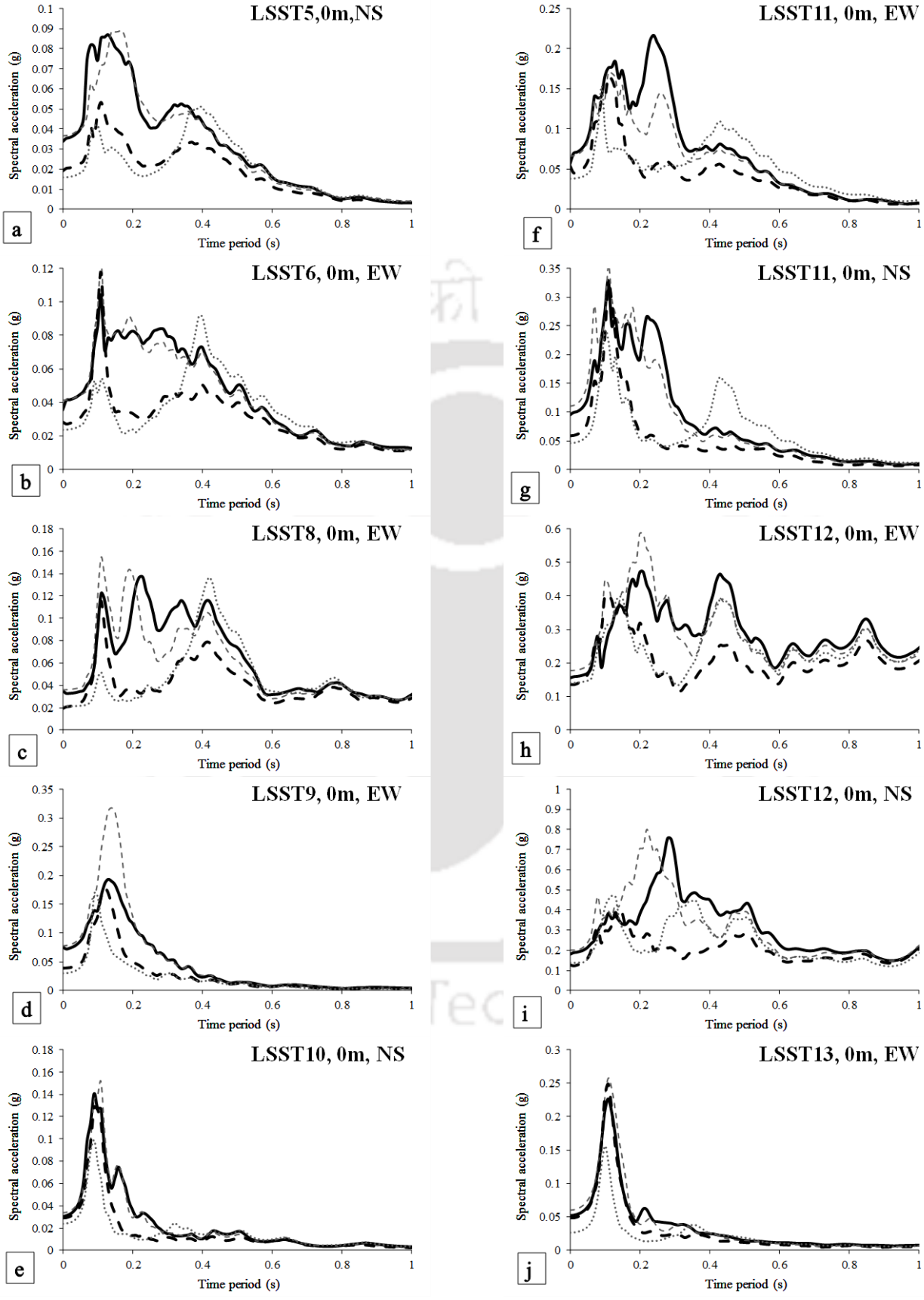

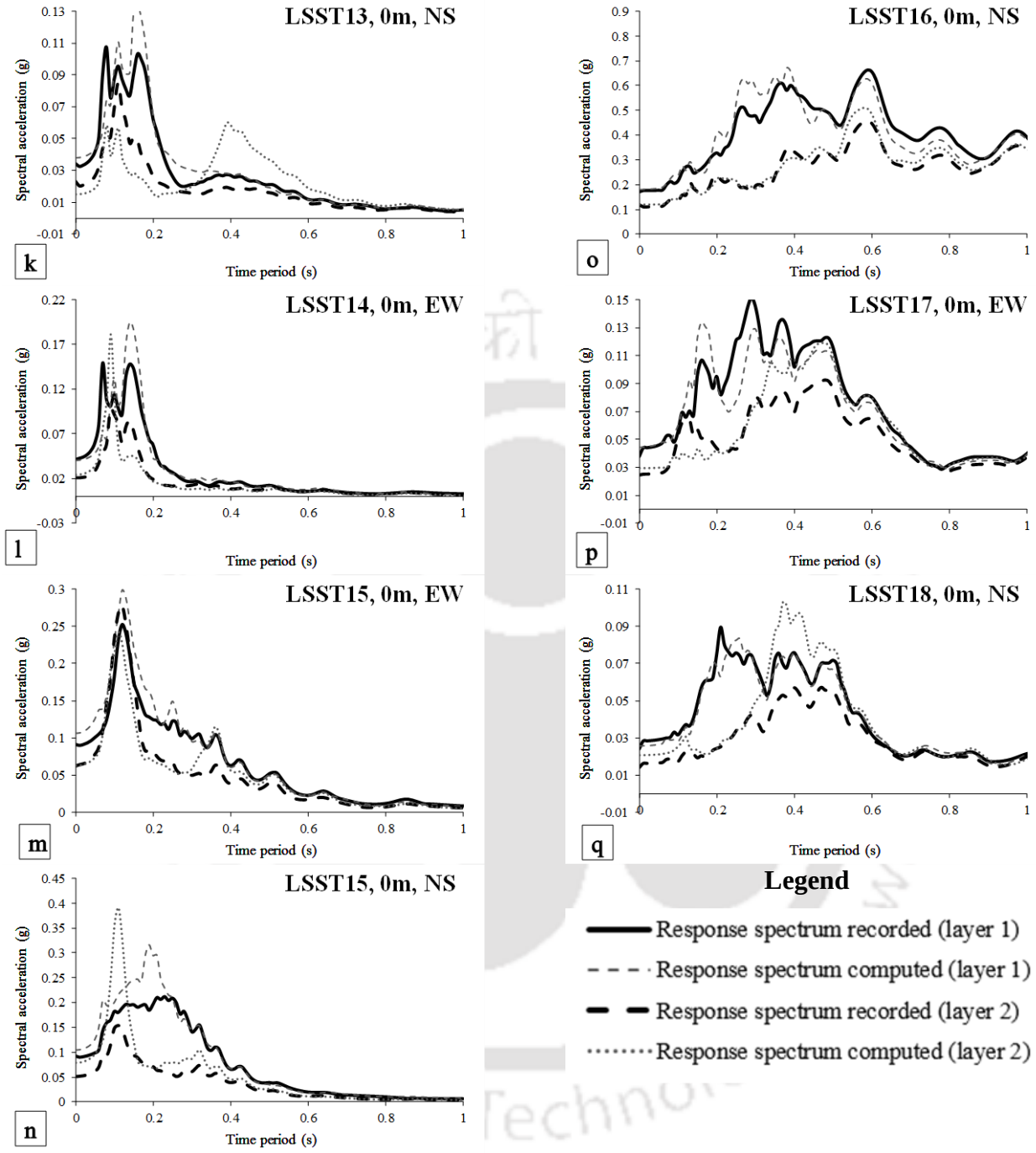

Figure 4.4 (a-q), Comparison of response spectra computed based on recorded motion and response spectra computed based on computed motion for motions considered in inverse analysis

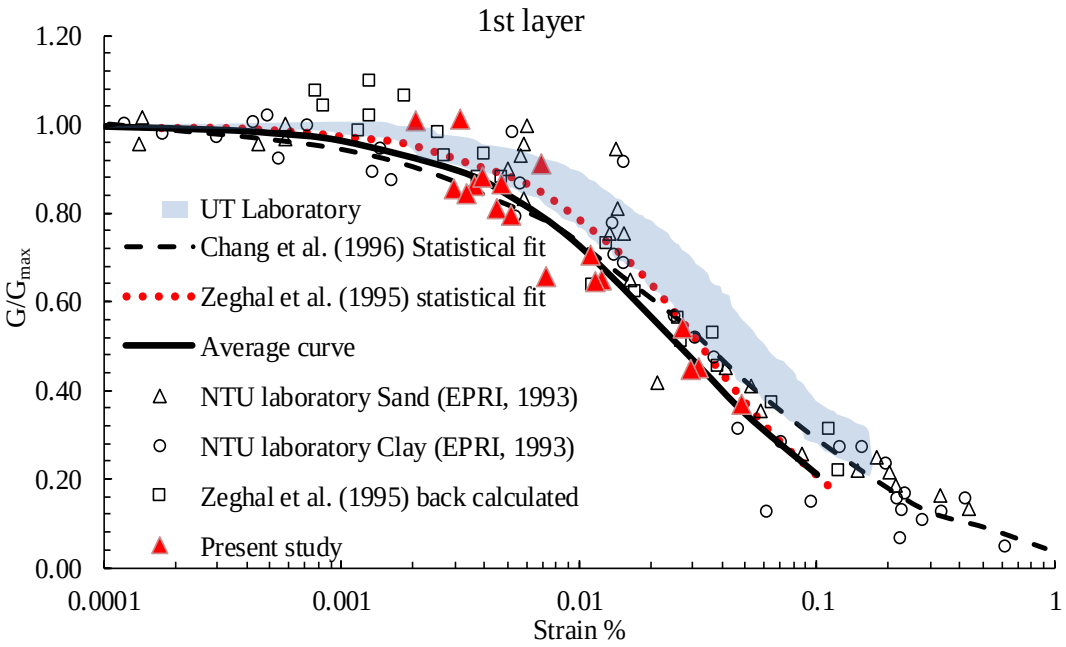

Figure 4.5, Comparison of obtained G/G_{max} for the first layer based on proposed framework with other studies

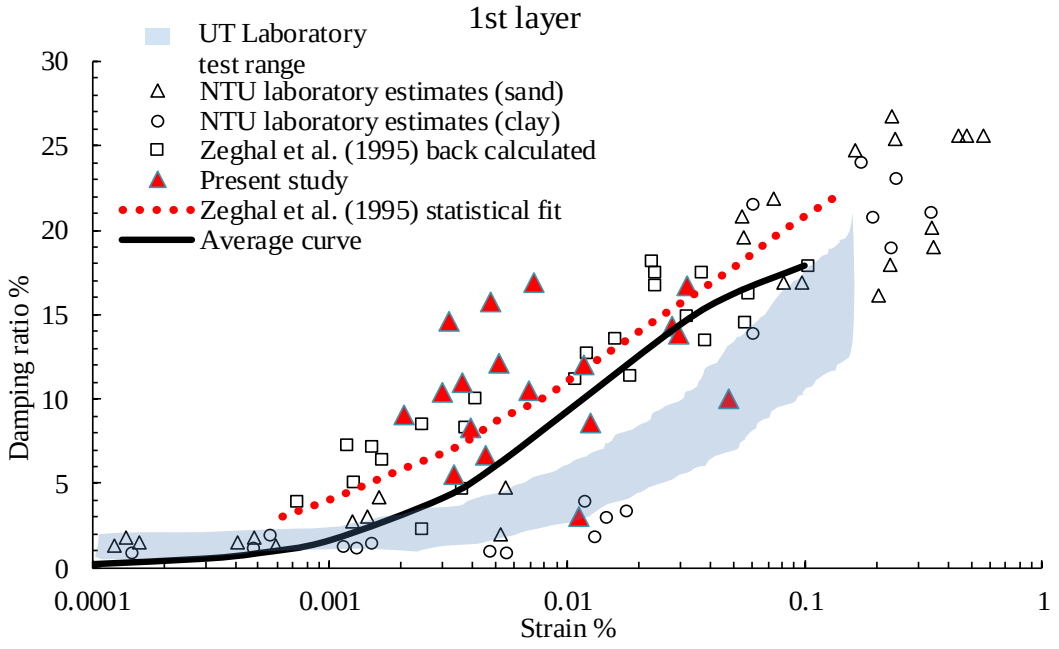

Figure 4.6, Comparison of obtained β for the first layer based on proposed framework with other studies

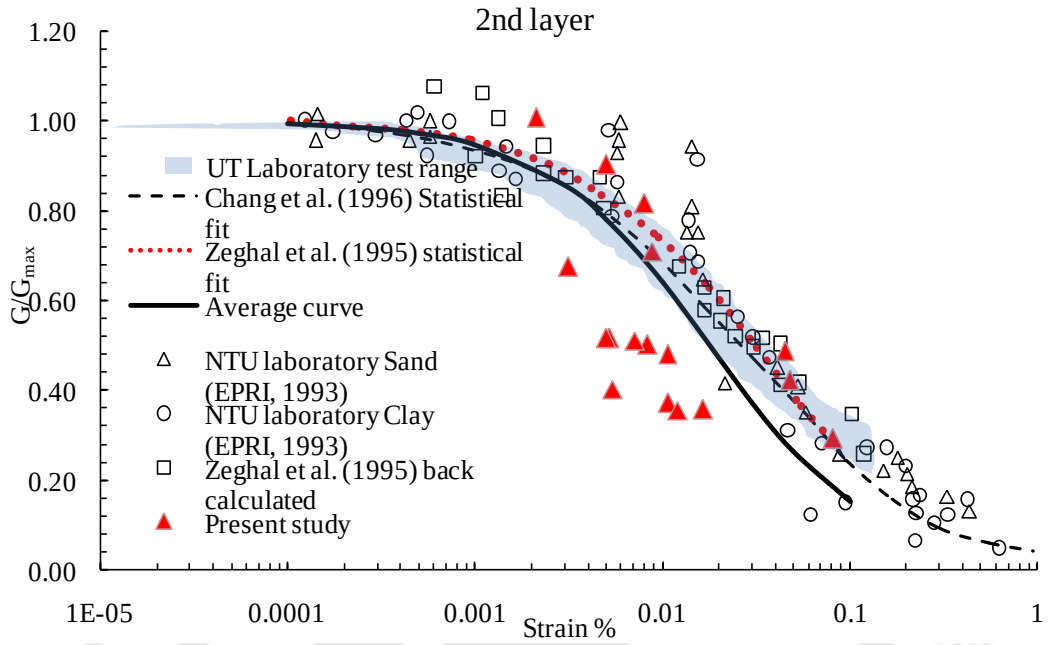

Figure 4.7, Comparison of obtained G/G_{max} for the second layer based on proposed framework with other studies

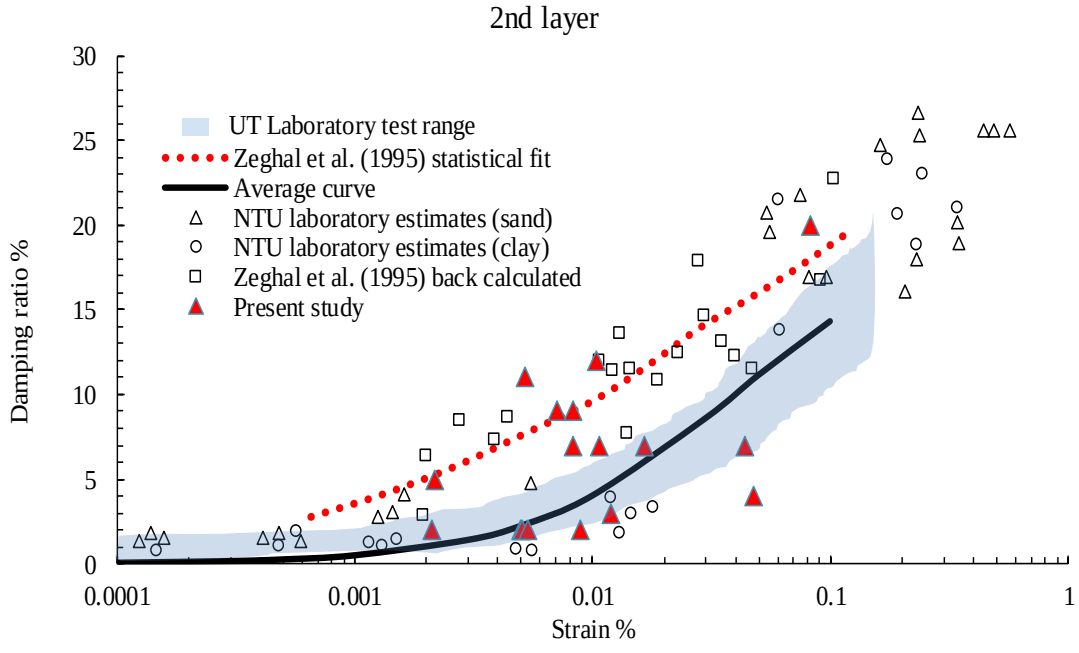

Figure 4.8, Comparison of obtained β for the second layer based on proposed framework with other studies

4.7 Validation

In the last section, two sets of average G/G_{max} curve and average β curve each are proposed for the surficial layer and layer below it for the Lotung site. It has to be highlighted here, that the average G/G_{max} curve for the surficial layer proposed in the present study is consistent with the

other G/G_{max} curves based on previous IGRA and laboratory based curve. However, the average G/G_{max} curve for the second layer proposed in the current research is not matching with any of the findings (both IGRA and laboratory test). Further, the average β curves for 2nd layer proposed in the present work are not matching with β curves proposed by the earlier inverse GRA framework (Zeghal et al. 1995). The average β curves proposed in the current study rather match well with UT laboratory-based findings. Thus, a validation of proposed average DSPCs from the present study is required to assess their suitability to represent LSE. For this purpose, motions that are excluded from the present inverse GRA (as highlighted by shaded rows in Table 4.2 and Table 4.3) are considered here for the validation. Further, 5% damped response spectra are developed for all the above motions at FA1-5 and DHB6. Additionally, ELGRA are performed for all the motions (highlighted by shaded rows in Table 4.2 and Table 4.3, total 11 motions) using the recorded motions at DHB11. The average curves proposed in this study are used as DSPCs for ELGRA. It has to be highlighted here that all the ELGRA are performed using the ELGRA code developed by Kumar and Mondal (2017), and results are obtained in the form of 5% damped response spectra at DHB6 and at FA1-5. Response spectra calculated based on recorded ground motions and based on results from ELGRA are then compared for all the motions considered in this section. For the purpose, "student's t-test" performed on the response spectra calculated based on recorded motions and based on results from ELGRA. Additionally, comparisons are shown graphically also in Figure 4.9 (a-k). The p values obtained from "student's t-test" for both DHB6 (p2) and FA1-5 (p1) are also shown in Figure 4.9 (a-k). Based on p values, it can be said that response spectra calculated based on recorded motions and based on results from ELGRA match very well for motions with low PGA (<0.1g) values. Further, the PGA values and PHA values (for FA1-5 and DHB6, respectively) obtained from response

spectra computed based on ELGRA are consistent with the PGA values and PHA values obtained from response spectra computed based on recorded motions for low PGA corresponding motions. However, for motions with PGA > 0.1g (LSST7, 0m, EW; LSST7, 0m, NS), the p values obtained based on "student's t-test" are significantly lesser than 0.05. It has to be highlighted here that the above observations for LSST7, 0m, EW and LSST7, 0m, NS are the

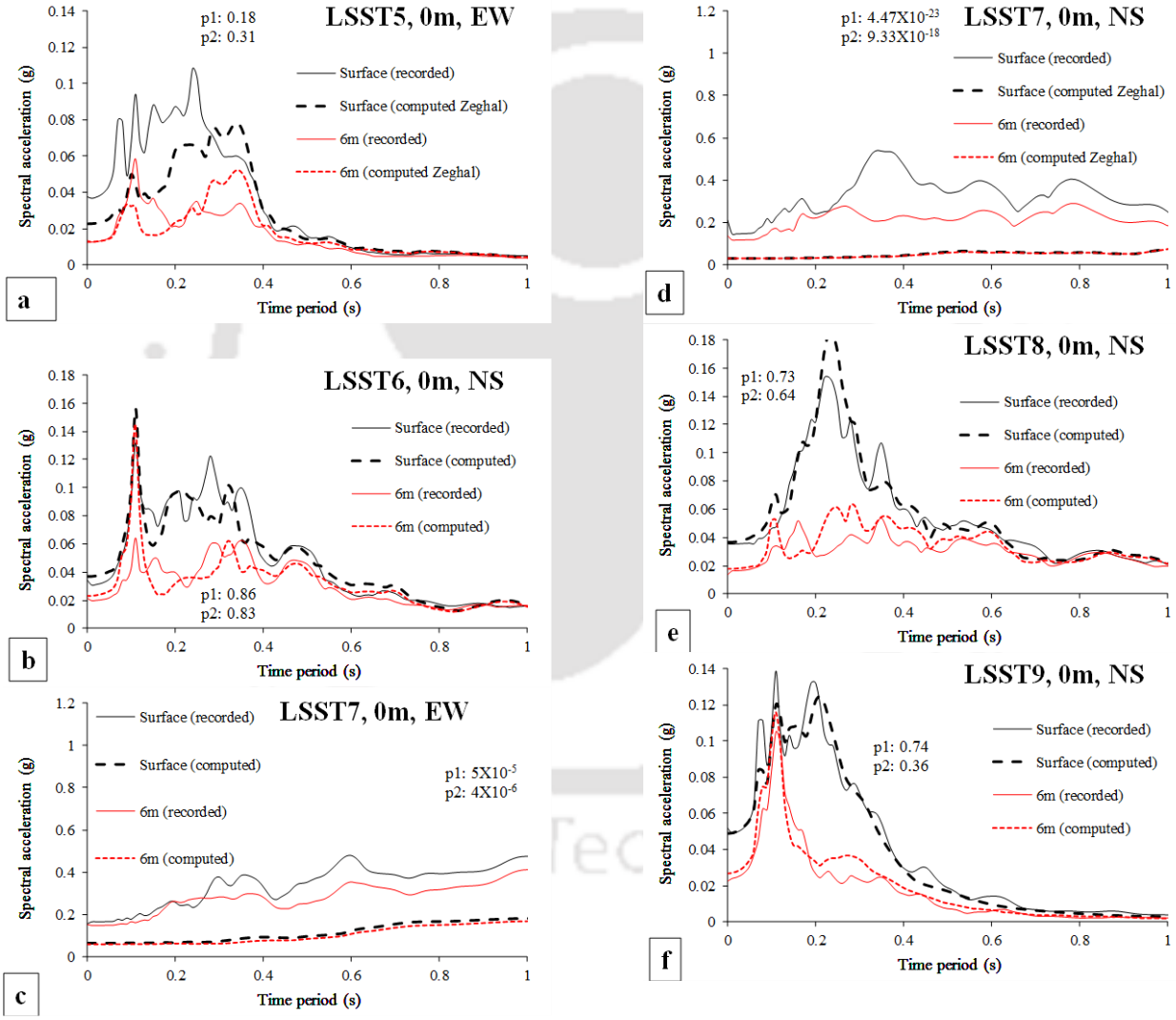

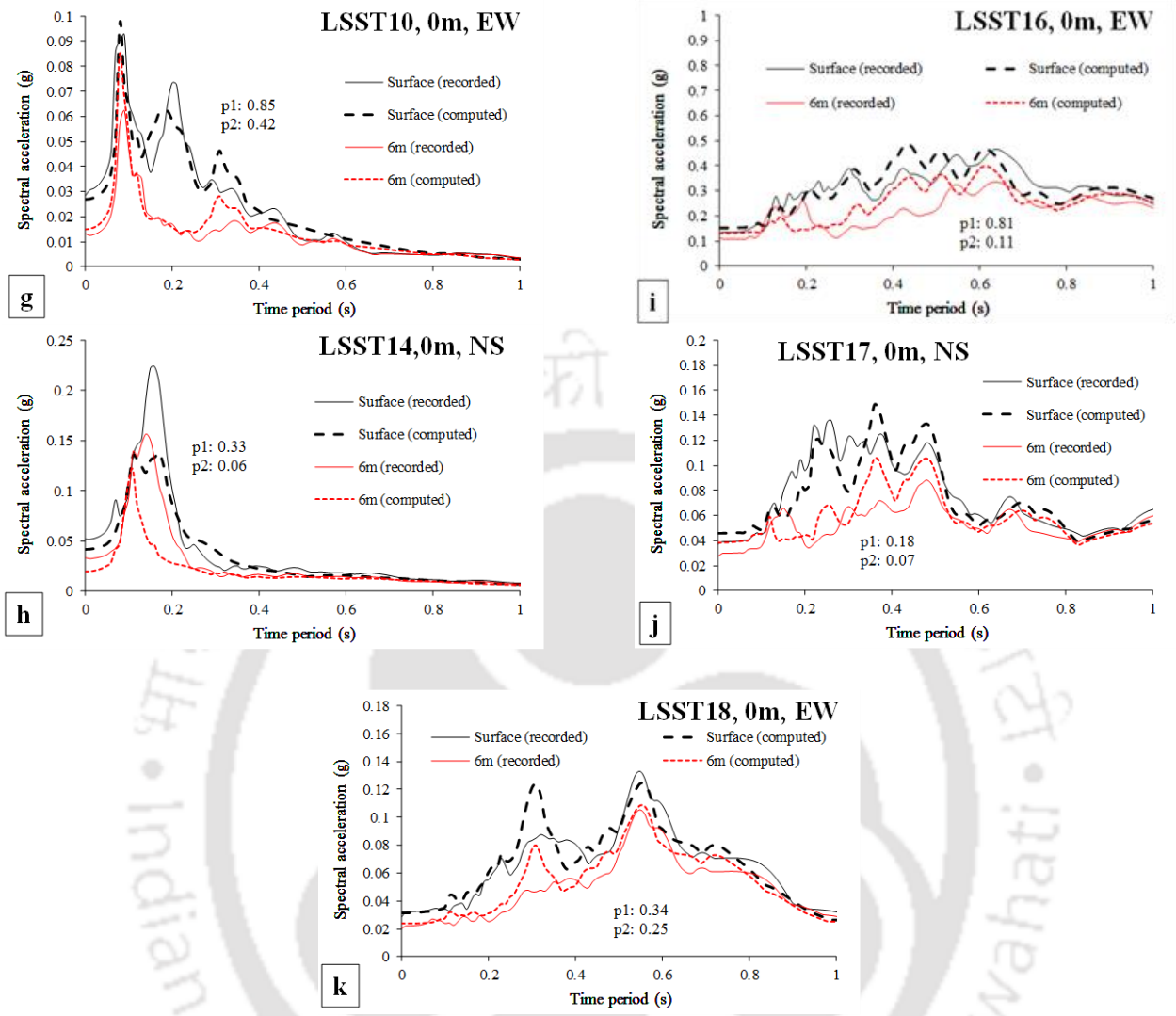

Figure 4.9 (a-k), Comparison of response spectra computed based on recorded ground motions and ELGRA

only two cases where the proposed methodology / proposed average DSPCs are not able to represent soil response appropriately. This may be attributed due to the effect of surface waves present in those motions. Nevertheless, apart from the above two ground motions, for all the other ground motions (26 in number) the proposed IGRA framework yielded satisfactory results.

4.8 Conclusion

DSPCs are very important in the context of performing site-specific GRA. However, adoption of standard DSPCs for the purpose is being practiced worldwide. Even laboratory determined DSPCs for site-specific soils have shortcomings. In such case, DSPCs can be determined by performing inverse GRA framework on downhole array data. It should be highlighted here, earlier frequency domain inverse GRA studies utilized ground surface EQ records and EQ records obtained at the bottom of the surficial layer to determine DSPC for the surficial layer only. Although frequency domain studies were attempted to determine DSPC for multiple soil layers located between consecutive accelerometers, such studies mostly were limited to determining G/G_{max} values only. Highlighting these limitations associated with earlier frequency domain studies, the present chapter proposes a four-step methodology which is applied to EQ data obtained from Lotung downhole array to determine DSPC for the layers located between 0-6m depth and 6-11m depth. The back calculated G/G_{max} and β values are found comparable with laboratory-based DSPC as well as DSPC obtained from earlier inverse GRA studies for the Lotung site. It is observed that the back-computed G/G_{max} and β values match very well with the existing literature. It is to be highlighted here, the present methodology depends on the identification and reproduction of $H(\omega)$, which is very simple in comparison to some of the earlier developed inverse GRA frameworks to determine both G/G_{max} and β values for multiple soil layers.

CHAPTER 5: FREQUENCY DOMAIN FRAMEWORK FOR INVERSE GROUND RESPONSE ANALYSIS FOR MULTI-LAYERED SYSTEM

5.1 Introduction

Application of geotechnical system identification techniques (refer to Figure 2.5) to determine DSPCs have been attempted several times in the last 50 years. In such studies, system unknowns are back-calculated based on input/ output datasets. In case of IGRA, the DSPCs are the system unknowns, and the input and output datasets are downhole and surface acceleration time histories respectively. Existing IGRA studies are discussed in detail in Chapter 2 of this thesis. In this Chapter, a new frequency domain-based IGRA methodology is proposed that can be utilized to determine DSPCs for 'n' (where n is a positive integer) number of layers based on 1D wave propagation theory. In such a case however, acceleration records must be available at 'n+1' number of locations along the downhole. During intensive ground shaking, soil behaves nonlinearly. As a result, there is tendency of *f* shifting towards lower values (Beresnev and Wen 1996; Bonilla et al. 2003, 2005; Field et al. 1997; Frankel et al. 2002; Régnier et al. 2013; Ren et al. 2017; Tsuda and Steidl 2006; Wu et al. 2009). It has to be highlighted here that the determination of DSPCs based on the proposed frequency domain IGRA method makes use of the above phenomenon of *f* shifting towards the lower values during nonlinear soil behavior. In the present study, the proposed methodology is first applied on downhole array records obtained from Lotung Downhole array. At the Lotung site, DSPCs are determined for top three soil layers located between the top four accelerometers. Later, the proposed methodology is validated for a different site located in Delhi using ground motions obtained from GRA by an earlier study.

5.2 Methodology for Multiple layers

At first, the V_s and β values for the surficial layer are determined following the procedure discussed in section 4.3. Once the V_s and β values for the surficial layer are determined, the procedure to determine V_s and β values for subsequent layers will be followed as given below. The entire procedure is also shown by means of a flowchart in Figure 5.1.

1. In step 1, V_s value for the nth layer is determined based on equation 4.1. However, in this case, if the V_s value for the nth layer has to be determined, T_1 is considered as the combined fundamental natural time period (see equation 4.1) for the top n-1 layers, and Tc is considered as the combined fundamental natural time period for all n layers. Further, T_2 is the fundamental natural time period of the nth layer. Once T_2 is determined, V_s value for the nth layer is also determined by multiplying f by four times H. H is defined as the thickness of the nth layer. In the subsequent steps, β value for the nth layer is determined by following the procedure described in section 4.5.
2. In step 2, initially, β value of 1% is assumed, and the theoretical transfer function between accelerometer levels n and n+1 [$H(\omega)_{CR,\ n\text{-}n+1}$] is determined. It is to be noted that at this point, V_s and β values are known for all the layers till n-1th layer from the ground surface. Utilizing above computed $H(\omega)_{CR,\ n\text{-}n+1,}$ and acceleration time history recorded at the n+1th accelerometer, acceleration time history at the nth accelerometer level is computed. Based on this computed acceleration time history, 5% damped response spectrum is also computed at nth accelerometer level. Additionally, empirical transfer function between accelerometer levels n and n+1 [$H(\omega)_{RR,\ n\text{-}n+1}$] is determined utilizing acceleration time histories recorded at the nth and n+1th accelerometers. Further,

5% damped response spectrum is computed at n^{th} accelerometer level considering recorded acceleration time history at n^{th} layer.

3. In step 3, the computed response parameters [$H(\omega)_{CR,\ n\text{-}n+1,}$ PGA obtained based on computed acceleration time history at the n^{th} accelerometer level and response spectrum computed acceleration time history] are compared with recorded response parameters [$H(\omega)_{RR,\ n\text{-}n+1,}$ PGA obtained based on recorded acceleration time history at the n^{th} accelerometer level, and response spectrum based on recorded acceleration time history]. The matching between the recorded and computed parameters is assessed by means of three criteria. These three criteria are; i) p value obtained based on Student's t test performed on $H(\omega)_{CR,\ n\text{-}n+1}$ and $H(\omega)_{RR,\ n\text{-}n+1}$ >0.05, ii) p value obtained from Student's t test performed on response spectra computed based on recorded acceleration time history and response spectra computed based on computed acceleration time history > 0.05, and iii) absolute PGA difference calculated between recorded acceleration time history and computed acceleration time history at n^{th} accelerometer level < 20%. In case above three criteria are satisfied simultaneously for any ground motion, the V_s and β values back-computed for the surficial layer are considered as representative of actual soil response. It is observed that for soil layers below the surficial soil layer, all the above mentioned three criteria are not satisfied simultaneously in this work for most of the ground motions. Thus, for the second layer onwards, if any two of the above mentioned criteria are satisfied, the corresponding V_s and β values are considered to be representative of actual soil response. However, similar to 'two-layer system', for the present case (multiple layer system) also, it is observed that there can be multiple β values for which the above set criteria can be satisfied. In such circumstances, β value corresponding to maximum p

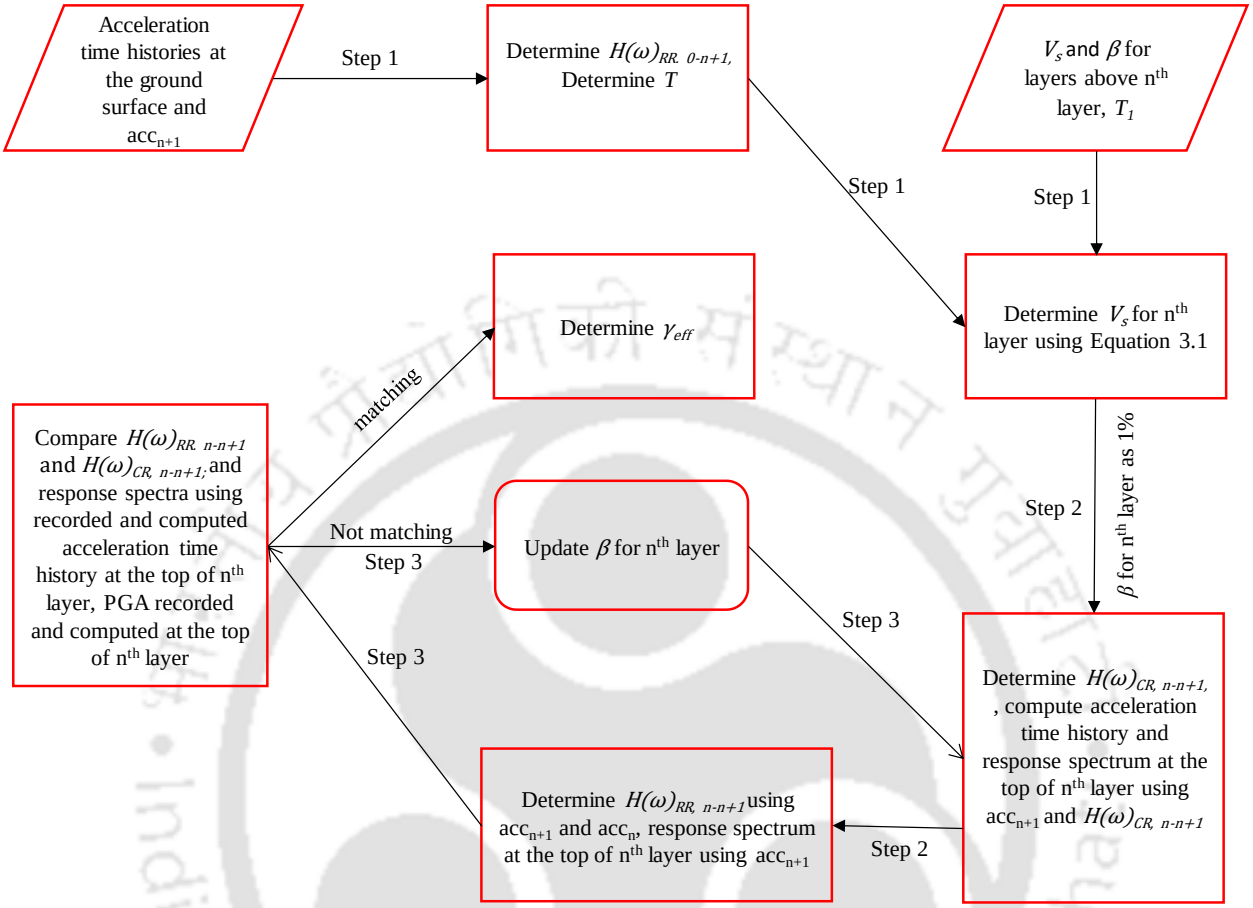

Figure 5.1, Flowchart of the analysis for multiple layers

values [obtained from Student's t test for both $H(\omega)$ and response spectra] or minimum absolute PGA difference value is considered as representative of actual soil response.

5.3 Analysis and results

In order to validate the procedure mentioned in the last section, EQ data from downhole arrays are required from multiple sites. However, presently the authors do not have access to data from any other downhole array sites apart from Lotung. Thus, in this section, the analysis procedure is applied to EQ data obtained from ELGRA study and EQ data obtained from Lotung downhole

array. In both cases, the proposed methodology works very well, as discussed in the following sub-sections.

5.3.1 Based on data from Lotung downhole array

In this section, the proposed methodology will be applied to EQ data obtained from Lotung downhole array. For the purpose, the same set of 28 ground motions (See Table 4.1) which were utilized for two-layered system (Chapter 4) are considered. It has to be highlighted here that the objective of the present study is to determine DSPCs for the top three layers at the Lotung site based on recorded acceleration time histories available from the top four accelerometers. DSPCs for the soil layer located between 17m depth and 47m depth cannot be back-computed accurately using the present methodology due to relatively higher spacing among the accelerometers (Ghayamghamian 2001; Taboada-Urtuzuastegui et al. 2000; Yangisawa and Kazama 1996; Zeghal et al. 1995). The back-computed soil properties are shown in Table 5.1, Table 5.2 and Table 5.3 for layer 1, layer 2 and layer 3 respectively. The shaded rows in Tables 5.1, 5.2 and 5.3 correspond to ground motions that did not satisfy the set criteria for at least one layer. Thus, the back-computed V_s and β values obtained based on the above ground motions are discarded. On the other hand, the back-computed V_s and β values obtained based on ground motions that satisfied all the criteria set (values in Tables 5.1, 5.2 and 5.3 that are not shaded) will be considered for further analysis. The V_s values obtained based on the proposed IGRA methodology are further divided by the maximum computed V_s value and the entities are squared to get G/G_{max} values. Above computed G/G_{max} values are then plotted against their respective γ values in Figures 5.2, 5.4 and 5.6. Further, the back-computed β values are also plotted against their respective γ values in Figure 5.3, 5.5 and 5.7. Additionally, laboratory based G/G_{max} values and β values, and previously conducted IGRA based G/G_{max} values and β values are also shown

in Figures 5.2 to 5.7. Further, γ_{ref} values are computed for each of the back-computed G/G_{max} values and β values based on Hardin and Drnevich (1972) constitutive modeling. Utilizing the γ_{ref} values, the average γ_{ref} value is calculated and average G/G_{max} curves and average β curves are developed for each of the soil layers as shown in Figures 5.2-5.7.

Table 5.1, Back-computed soil properties for layer 1 at Lotung

Serial	Motion detail	Shear strain (%)	V_s (m/s)	β	p1	p2	PGA_diff
1	LSST5,0m,EW	0.003	134.137	0.007	0.001	0.955	26.827
2	LSST5,0m,NS	0.004	126.215	0.110	0.060	0.912	-8.153
3	LSST6, 0m, EW	0.005	122.258	0.067	0.352	0.757	-17.082
4	LSST6, 0m, NS	0.001	211.247	0.122	0.093	0.595	-13.494
5	LSST7, 0m, EW	0.007	199.997	0.159	0.000	0.002	-0.046
6	LSST7, 0m, NS	0.062	67.052	0.014	0.000	0.000	0.930
7	LSST8, 0m, EW	0.004	127.616	0.063	0.115	0.920	-13.536
8	LSST8, 0m, NS	0.004	126.139	0.074	0.002	0.836	-0.336
9	LSST9, 0m, EW	0.007	129.908	0.085	0.051	0.243	-7.631
10	LSST9, 0m, NS	0.005	123.379	0.009	0.009	0.202	5.058
11	LSST10, 0m, EW	0.002	151.399	0.051	0.001	0.534	-1.279
12	LSST10, 0m, NS	0.002	136.425	0.010	0.503	0.299	-16.647
13	LSST11, 0m, EW	0.007	110.122	0.169	0.649	0.250	-17.278
14	LSST11, 0m, NS	0.013	109.568	0.076	0.346	0.995	-19.832
15	LSST12, 0m, EW	0.032	91.409	0.167	0.060	0.785	-14.372
16	LSST12, 0m, NS	0.028	100.108	0.123	0.771	0.776	-18.846
17	LSST13, 0m, EW	0.005	126.529	0.158	0.075	0.842	-15.597
18	LSST13, 0m, NS	0.003	125.781	0.084	0.829	0.497	-18.109
19	LSST14, 0m, EW	0.003	136.693	0.136	0.065	0.769	-1.369
20	LSST14,0m, NS	0.005	129.794	0.204	0.004	0.770	-11.010
21	LSST15, 0m, EW	0.012	109.172	0.110	0.950	0.441	-19.377
22	LSST15, 0m, NS	0.011	114.301	0.021	0.411	0.413	-8.908
23	LSST16, 0m, EW	0.029	91.079	0.138	0.071	0.191	-19.573
24	LSST16, 0m, NS	0.048	82.511	0.070	0.058	0.592	-8.956
25	LSST17, 0m, EW	0.005	121.223	0.122	0.089	0.497	-17.314
26	LSST17, 0m, NS	0.006	109.387	0.014	0.850	0.349	-19.991
27	LSST18, 0m, EW	0.004	122.347	0.015	0.628	0.410	-13.633
28	LSST18, 0m, NS	0.003	124.783	0.055	0.060	0.760	-6.163

Table 5.2, Back-computed soil properties for layer 2 at Lotung

Serial	Motion detail	Shear strain (%)	V_s (m/s)	β	p1	p2	PGA_diff
1	LSST5,0m,EW	0.004	118.401	0.130	0.793	0.851	30.932
2	LSST5,0m,NS	0.006	115.330	0.100	0.895	0.200	13.171
3	LSST6, 0m, EW	0.009	113.766	0.080	0.872	0.043	14.927
4	LSST6, 0m, NS	0.003	174.080	0.200	0.005	0.729	-23.482
5	LSST7, 0m, EW	0.036	151.327	0.150	0.111	0.828	6.561
6	LSST7, 0m, NS	0.060	103.854	0.200	0.391	0.002	-4.167
7	LSST8, 0m, EW	0.012	97.712	0.170	0.004	0.447	1.821
8	LSST8, 0m, NS	0.005	135.965	0.110	0.058	0.933	-6.768
9	LSST9, 0m, EW	0.005	153.293	0.020	0.462	0.311	15.898
10	LSST9, 0m, NS	0.005	134.749	0.120	0.004	0.984	2.832
11	LSST10, 0m, EW	0.003	138.165	0.190	0.000	0.378	2.423
12	LSST10, 0m, NS	0.003	132.168	0.060	0.865	0.637	6.306
13	LSST11, 0m, EW	0.018	96.005	0.120	0.878	0.479	43.335
14	LSST11, 0m, NS	0.013	95.794	0.040	0.695	0.098	20.809
15	LSST12, 0m, EW	0.052	104.712	0.060	0.138	0.065	1.109
16	LSST12, 0m, NS	0.048	112.550	0.090	0.518	0.132	1.595
17	LSST13, 0m, EW	0.005	115.453	0.020	0.331	0.391	45.528
18	LSST13, 0m, NS	0.006	101.778	0.030	0.081	0.038	29.466
19	LSST14, 0m, EW	0.002	171.680	0.070	0.397	0.462	2.364
20	LSST14,0m, NS	0.005	129.428	0.020	0.003	0.149	47.076
21	LSST15, 0m, EW	0.009	135.932	0.050	0.256	0.866	1.446
22	LSST15, 0m, NS	0.008	145.903	0.200	0.689	0.977	-9.399
23	LSST16, 0m, EW	0.078	83.192	0.180	0.000	0.125	1.843
24	LSST16, 0m, NS	0.089	86.940	0.200	0.825	0.093	-6.104
25	LSST17, 0m, EW	0.011	111.211	0.180	0.002	0.897	-12.638
26	LSST17, 0m, NS	0.015	106.454	0.050	0.848	0.000	-56.018
27	LSST18, 0m, EW	0.013	100.540	0.200	0.425	0.004	-36.521
28	LSST18, 0m, NS	0.007	114.766	0.190	0.493	0.876	-9.410

Table 5.3, Back-computed soil properties for layer 3 at Lotung

Serial	Motion detail	Shear strain (%)	V_s (m/s)	β	p1	p2	PGA_diff
1	LSST5,0m,EW	0.003	130.396	0.190	0.909	0.964	-10.931
2	LSST5,0m,NS	0.006	112.101	0.070	0.081	0.900	2.320
3	LSST6, 0m, EW	0.010	112.101	0.130	0.000	0.095	1.436
4	LSST6, 0m, NS	0.004	153.369	0.060	0.738	0.803	24.721
5	LSST7, 0m, EW	0.054	138.980	0.200	0.000	0.513	-22.777
6	LSST7, 0m, NS	0.065	135.645	0.060	0.028	0.853	3.247
7	LSST8, 0m, EW	0.015	92.975	0.090	0.000	0.015	2.695
8	LSST8, 0m, NS	0.003	182.105	0.080	0.115	0.882	-0.217
9	LSST9, 0m, EW	0.003	156.969	0.030	0.029	0.663	3.677
10	LSST9, 0m, NS	0.003	155.081	0.020	0.291	0.895	10.334
11	LSST10, 0m, EW	0.003	139.757	0.020	0.000	0.748	9.993
12	LSST10, 0m, NS	0.002	175.417	0.020	0.006	0.291	16.241
13	LSST11, 0m, EW	0.017	93.784	0.080	0.004	0.512	4.306
14	LSST11, 0m, NS	0.011	137.452	0.080	0.920	0.303	4.566
15	LSST12, 0m, EW	0.035	146.932	0.190	0.841	0.689	-26.722
16	LSST12, 0m, NS	0.032	163.367	0.090	0.956	0.910	6.122
17	LSST13, 0m, EW	0.005	102.505	0.020	0.525	0.283	14.613
18	LSST13, 0m, NS	0.007	102.896	0.020	0.629	0.093	13.202
19	LSST14, 0m, EW	0.001	187.778	0.070	0.138	0.916	7.024
20	LSST14,0m, NS	0.004	157.888	0.160	0.982	0.895	19.525
21	LSST15, 0m, EW	0.010	131.280	0.020	0.288	0.006	5.215
22	LSST15, 0m, NS	0.006	156.969	0.020	0.453	0.797	9.091
23	LSST16, 0m, EW	0.104	87.656	0.200	0.070	0.191	-7.239
24	LSST16, 0m, NS	0.075	106.732	0.150	0.635	0.843	-2.929
25	LSST17, 0m, EW	0.018	105.902	0.180	0.000	0.858	-0.218
26	LSST17, 0m, NS	0.031	101.099	0.200	0.066	0.007	-19.638
27	LSST18, 0m, EW	0.014	120.440	0.170	0.005	0.831	-28.429
28	LSST18, 0m, NS	0.011	102.505	0.160	0.058	0.810	-3.054

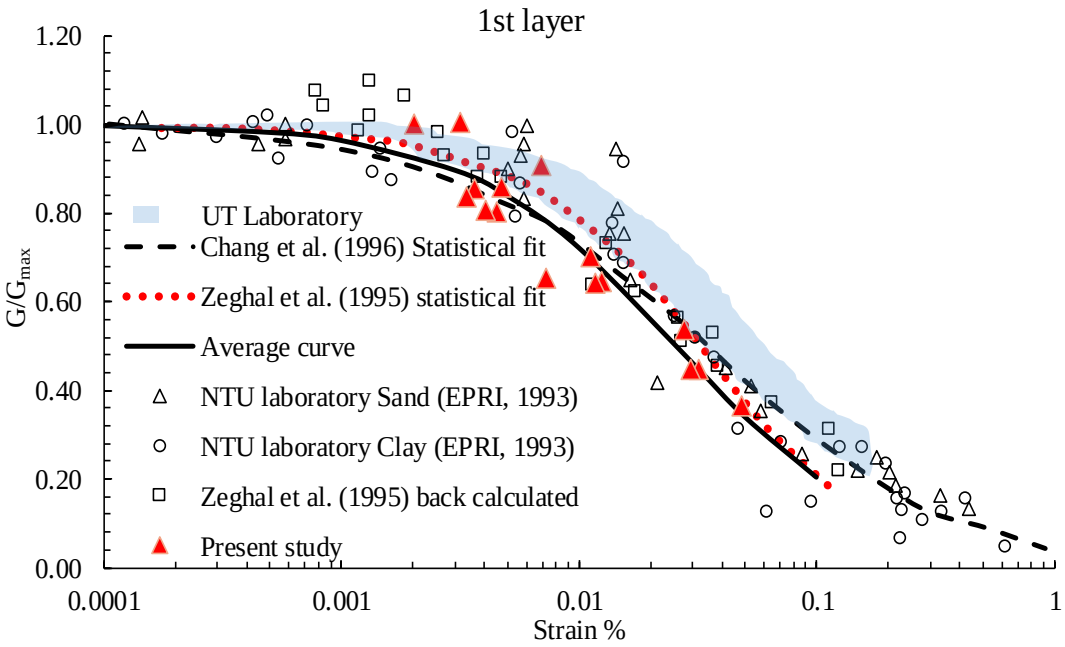

Figure 5.2, G/G_{max} values for layer 1 at Lotung

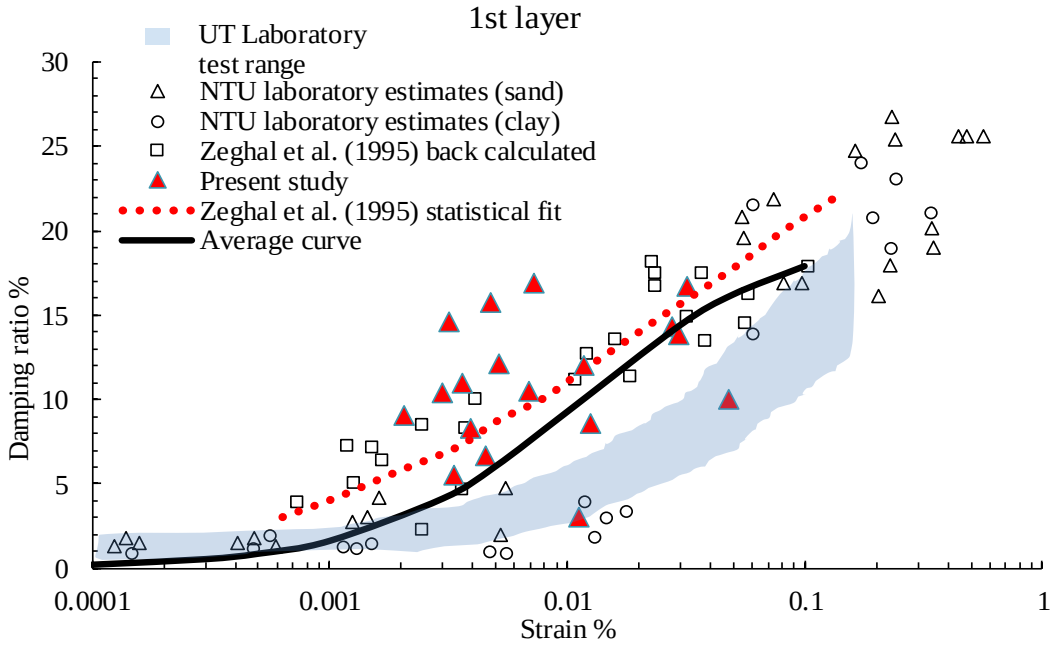

Figure 5.3, β values for layer 1 at Lotung

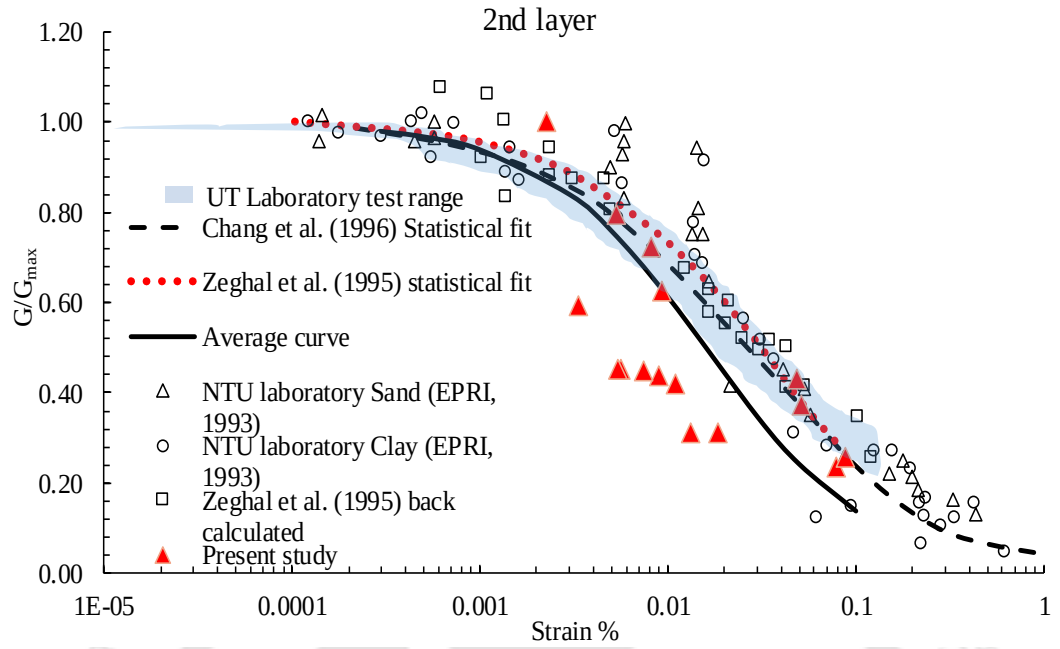

Figure 5.4, G/G_{max} values for layer 2 at Lotung

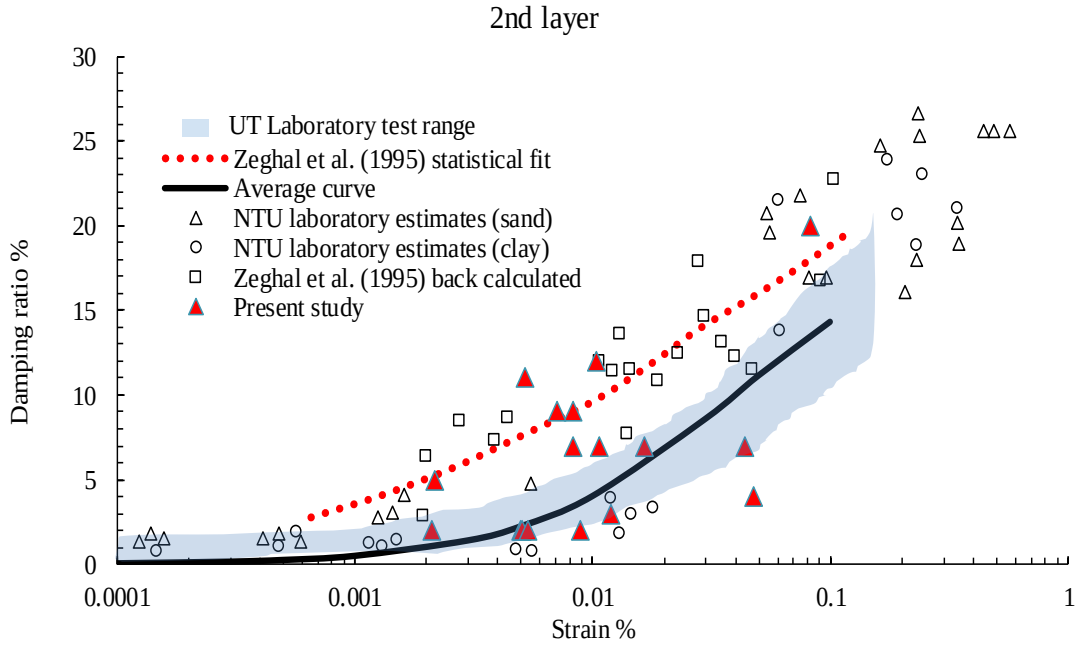

Figure 5.5, β values for layer 2 at Lotung

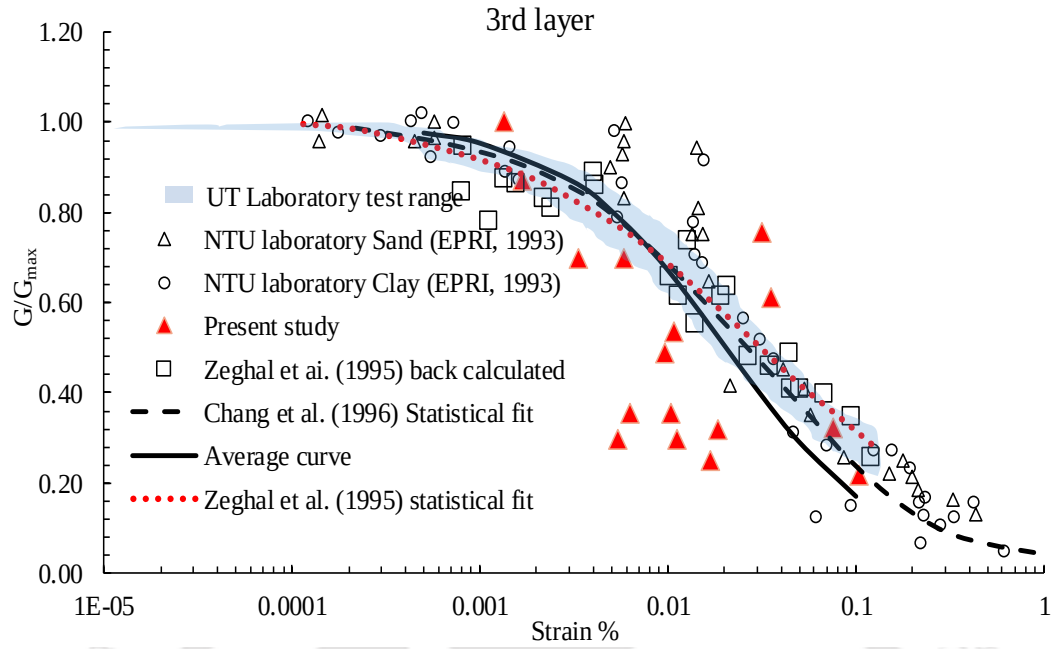

Figure 5.6, G/G_{max} values for layer 3 at Lotung

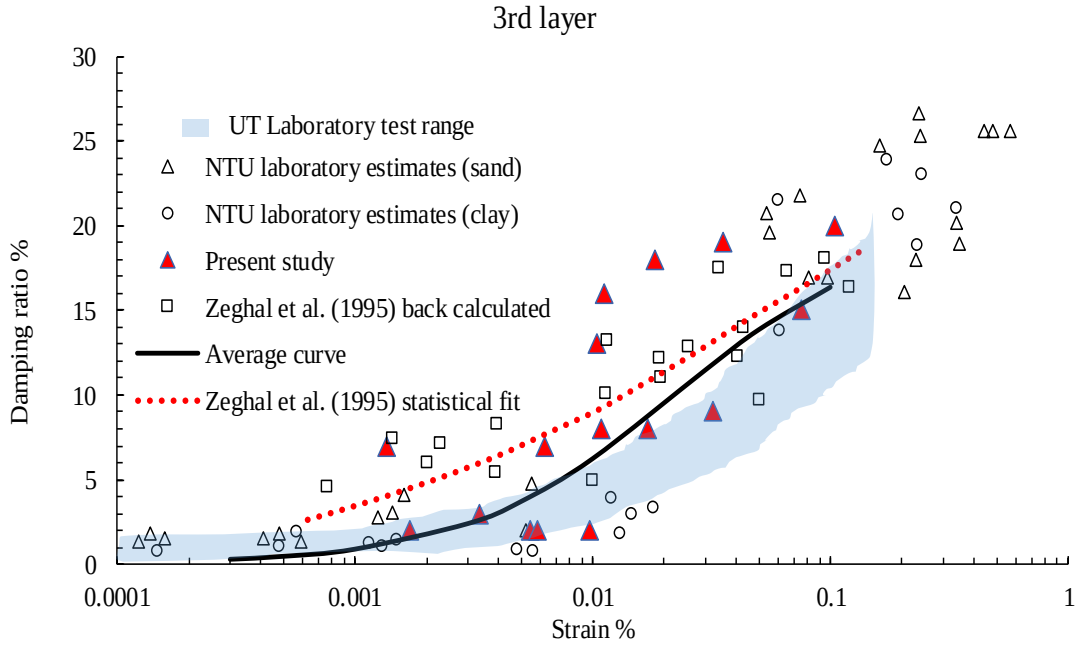

Figure 5.7, β values for layer 3 at Lotung

5.3.1.1 Validation

It has to be highlighted here that the average G/G_{max} curve for the surficial layer proposed in the present study is consistent with the other G/G_{max} curves based on IGRA and laboratory based curve. However, the average G/G_{max} curve for the second layer and third layer proposed in the

current research are not matching with any of the findings (both IGRA and laboratory test). Additionally, the average curves given in the current study (for other than surficial layer), do not match with β curves proposed by the earlier IGRA framework (Zeghal et al. 1995). The average β curves proposed in the current study rather match well with UT laboratory-based findings. Thus, a validation of proposed average DSPCs from the present study is required to assess their suitability to represent LSE. For this purpose, motions that are excluded from the present IGRA (as highlighted by shaded rows in Table 5.1, Table 5.2 and Table 5.3) are considered here for the validation. Further, 5% damped response spectra are developed for all the above motions at DHB11, DHB6 and at FA1-5. Additionally, ELGRA are performed for all the 12 motions (highlighted by shaded rows in Table 5.1, Table 5.2 and Table 5.3) using the recorded motions at DHB17. The average curves proposed in this study are used as DSPCs for ELGRA.

It has to be highlighted here that all the ELGRAs are performed using the ELGRA code developed by Kumar and Mondal (2017) and results are obtained in the form of 5% damped response spectra at DHB11, DHB6 and at FA1-5. Response spectra calculated based on recorded ground motions and based on results from ELGRA are then compared for all the motions considered in this section. For the purpose, "student's t-test" performed on the response spectra calculated based on recorded motions and based on results from ELGRA. The comparisons of the response spectra computed based on recorded motions and computed motions are shown in Figure 5.8 (a-k). Additionally, student's t test is performed on the pairs of response spectra computed based on recorded acceleration time history and computed acceleration time history. The p values obtained from such student's t test are also shown in Figure 5.8 (a-k). In these Figures, p1 represents p value for the response spectra at the ground surface, p2 represents p value for the response spectra at 6m depth and p3 represents p value for response spectra at 11m

depth. It can be observed from Figure 5.8 (a-k) that apart from LSST 5 (EW), LSST 7 (NS), and LSST 8 (NS) ground motions (shown in Figures 5.8 f, h, j), all other ground motion produce acceptable response (p value > 0.05) when ELGRA is performed based on proposed average DSPCs. The discrepancy in case of LSST 5 (EW), LSST 7 (NS) and LSST 8 (NS) ground motions may be attributed due to interference of surface wave which the ELGRA methodology fails to address.

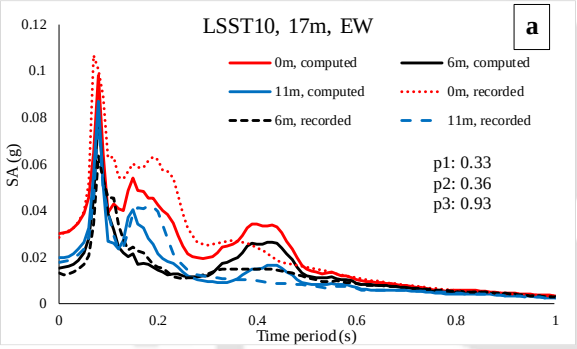

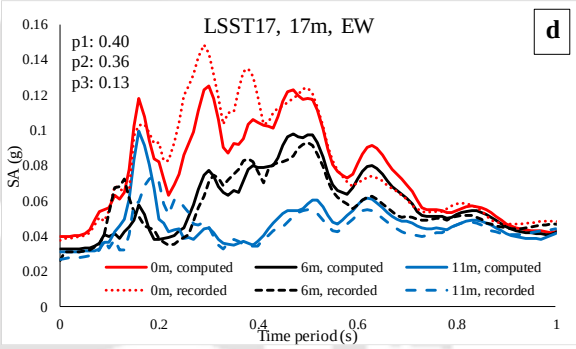

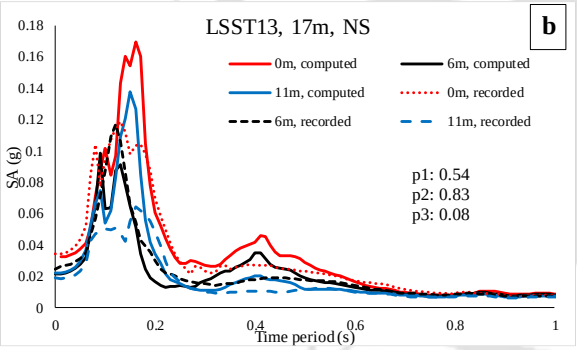

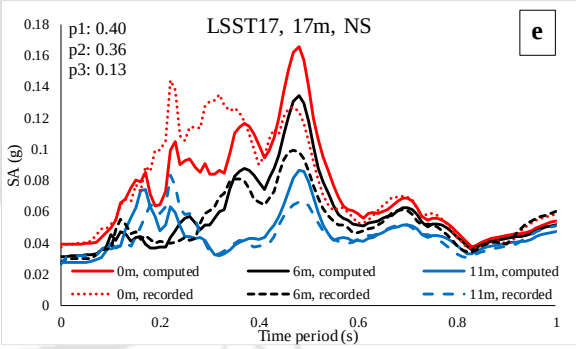

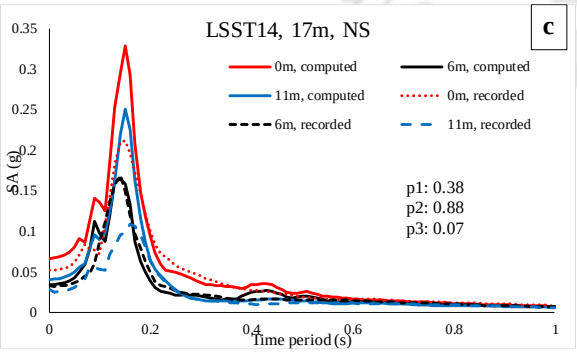

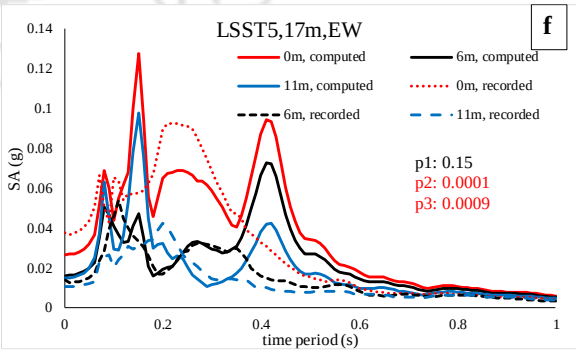

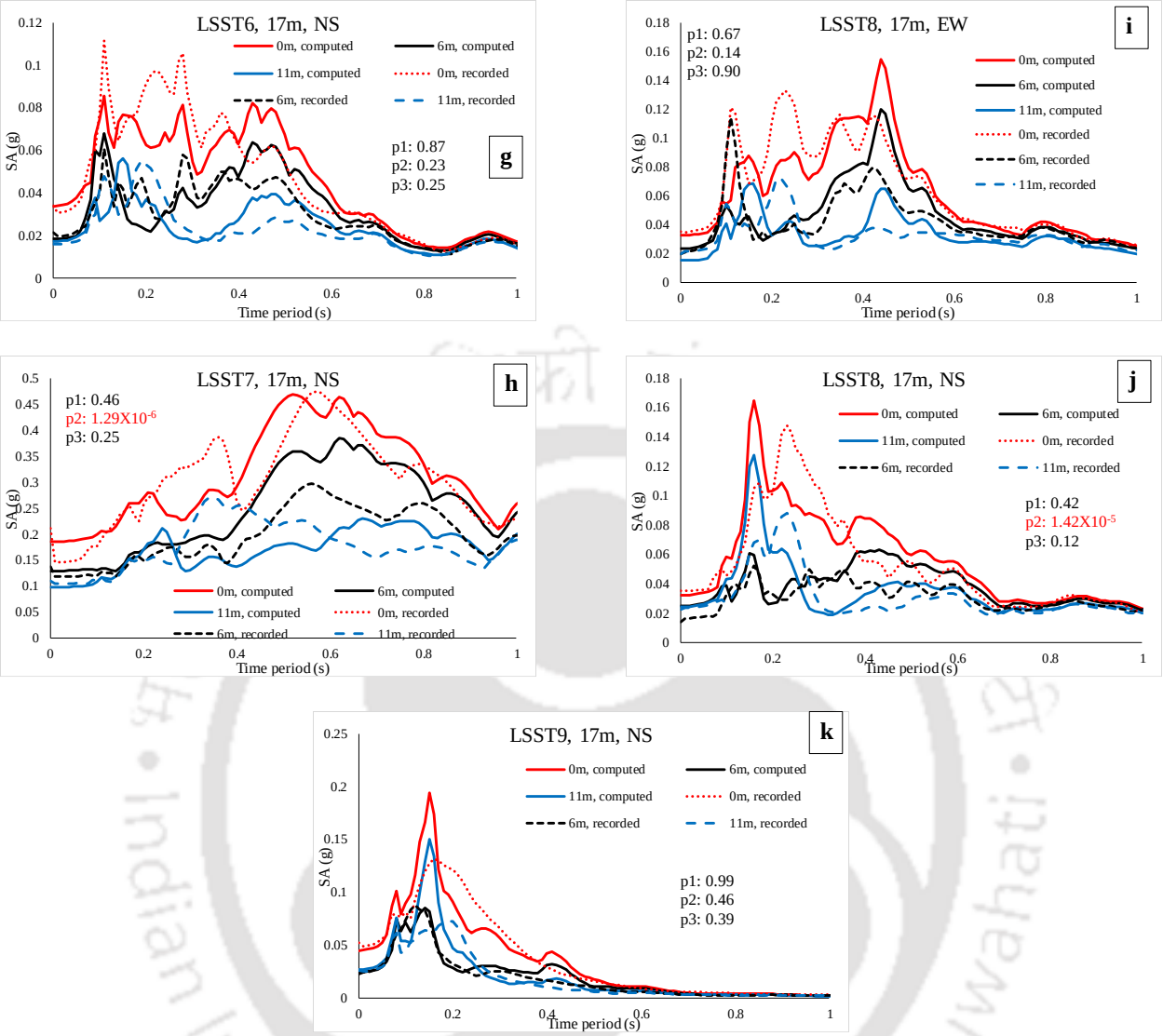

Figure 5.8 (a-k), Comparison of response spectra computed based on recorded motion and computed motion

5.3.2 Based on data from ELGRA

In order to check if proposed methodology can be applied to any site and not only to DHB, a borehole profile from Delhi, which was originally used by Kumar and Mondal (2017) for GRA, is considered in the present study. Using this borelog and considering 30 globally recorded ground motions which were originally selected by Kumar et al. (2016), ELGRA is performed in this work to obtain ground motions at different depths. It should be noted here that the details of

the above 30 ground motions are shown in Table 6.2. Kumar and Mondal (2017) divided the entire borehole into 19 soil layers with varying thicknesses, G and unit weight. Further, this soil profile was modeled by Kumar and Mondal (2017) using MATLAB code by Kumar and Mondal (2017) in order to perform ELGRA. Additional details of the modeling done by Kumar and Mondal (2017) is shown in Table 5.4. The first column in Table 5.4 refers to the soil layer number. The second column consists of different soil types as per Kumar and Mondal (2017). It has to be highlighted here that Kumar and Mondal (2017) utilized only two soil types (soil type 1 and soil type 2) for the analysis. While soil type 1 represented clayey soil, soil type 2 represented sandy soil as per Kumar and Mondal (2017). Further, Kumar and Mondal (2017) utilized G/G_{max} curve proposed by Vucetic and Dobry (1991) for a plasticity index (PI) range of 0-10 and β curve proposed by Sun et al. (1988) for PI range of 10-20 for modeling of soil type 1. On the other hand, soil type 2 was modeled by Kumar and Mondal (2017) using average G/G_{max} and average β curves for sand as per Seed and Idriss (1970). Layer thicknesses, G_{max}, initial low γ corresponding β value and unit weights of different soil layers are listed in columns 3, 4, 5 and 6 respectively in Table 5.4.

In the present study, soil modelling for ELGRA is done in the exactly same manner as done in Kumar and Mondal (2017). Using modelled soil layers and applying all 30 ground motions mentioned above at the bottom of the 19th layer, ELGRA is performed in this work using MATLAB code by (Kumar and Mondal 2017). Outcome in the form of variation in ground motions at the top of each of the 19 layers is obtained, for each of the ground motions.

In order to validate proposed IGRA methodology, obtained acceleration time histories at the top of 1st, 2nd, 3rd, 4th, 5th and 6th layers are utilized as input, and G/G_{max} and β values are

back-computed for the top 5 soil layers. Other acceleration time histories (excluding those at the top of 1st, 2nd, 3rd, 4th, 5th and 6th layers) are not utilized to keep the discussion limited.

Table 5.4, Soil modeling used by Kumar and Mondal (2017)

1	2	3	4	5	6
Layer no	Soil type	Thickness (m)	G_{max} (kPa)	β	Unit weight in kN/m^3
1	2	4.15	61621.56	0.05	16
2	1	1.5	68468.4	0.05	16
3	2	1.5	116396.3	0.05	17
4	2	2	164324.2	0.05	17.2
5	1	2	116396.3	0.05	17
6	1	1.5	130090	0.05	17.2
7	1	1.5	143783.6	0.05	17.8
8	1	1	191711.5	0.05	18
9	2	1.5	232792.6	0.05	19.5
10	2	1.5	260179.9	0.05	19.5
11	2	1.5	287567.3	0.05	20
12	2	1.5	342342	0.05	20
13	1	1.5	301261	0.05	20
14	1	1.5	328648.3	0.05	21
15	2	1.5	376576.2	0.05	21
16	2	1.5	424504.1	0.05	21
17	2	1.5	513513	0.05	21
18	2	1.5	602521.9	0.05	21
19	2	-	602521.9	0.05	21

This way, corresponding to each of the 30 input ground motions, a set of 6 ground motions (obtained at the top of 1st, 2nd, 3rd, 4th, 5th and 6th layers) is obtained. All the above 30 sets of input motions are given as inputs in the presently developed algorithms (firstlayer.m and multiplelayers.m) and the outputs in terms of V_s, β and γ corresponding to each input motion are obtained. Received outputs following the proposed IGRA methodology are shown in Tables 5.5, 5.6, 5.7, 5.8 and 5.9 for 1st, 2nd, 3rd, 4th and 5th respectively. It has to be highlighted here that the shaded rows in Tables 5.5, 5.6, 5.7, 5.8 and 5.9 contain back-computed V_s, β and γ for the

ground motion that do not satisfy the earlier mentioned criteria of matching either for the first layer or for the subsequent layers. Consequently, these back-computed V_s and β values are not considered for the further analysis.

Back-computed V_s values (for motions other than those marked in shaded rows) are divided by the maximum V_s value (V_s^{max}) for the corresponding layer and the entities are squared to obtain G/G_{max} values. It has to be highlighted here that V_s^{max} values for each of the 5 layers are determined by using the G_{max} values and unit weights listed in column 4 and 6 respectively in Table 5.4 ($V_s^{max} = \sqrt{\frac{G_{max}}{\rho}}$). (Computed V_s^{max} values for 1st, 2nd, 3rd, 4th and 5th layers are 196m/s, 206m/s, 261m/s, 309m/s and 261m/s respectively.) Back-computed G/G_{max} values and β values 1st, 2nd, 3rd, 4th and 5th layers are summarized in Tables 5.5, 5.6, 5.7, 5.8 and 5.9 respectively. Plot of back-computed G/G_{max} versus γ values and β versus γ values (for 1st, 2nd, 3rd, 4th and 5th layers) are shown in Figures 5.9, 5.10, 5.11, 5.12, 5.13, 5.14, 5.15, 5.16, 5.17 and 5.18 respectively. Additionally, the DSPCs that were considered for ELGRA by (Kumar and Mondal 2017) for 1st, 2nd, 3rd, 4th and 5th layers are also shown in respective figures. It can be observed from Figures 5.9, 5.10, 5.11, 5.12, 5.13, 5.14, 5.15, 5.16, 5.17 and 5.18 that back-computed G/G_{max} versus γ values and β versus γ values based on the proposed methodology are matching very well with corresponding DSPCs for each layer used by (Kumar and Mondal 2017).

This validation firstly confirms that the proposed methodology can determine G/G_{max} versus γ values and β versus γ values for any site. Secondly, the proposed methodology can be used to determine G/G_{max} versus γ values and β versus γ values for any number of layers (3 number of layers for Lotung site and 5 number of layers for Delhi).

Table 5.5, Back-calculated properties for 1st layer

Serial	Strain (%)	Shear wave velocity (m/s)	Damping ratio	p-value for $H(\omega)$	p_value for Response spectrum	PGA_difference (%)
1	0.008	169.330	0.048	0.360	0.990	2.257
2	0.016	154.990	0.095	0.459	1.000	-1.924
3	0.004	180.742	0.047	0.795	0.974	-4.419
4	0.009	166.757	0.049	0.145	0.986	3.099
5	0.006	163.197	0.203	0.000	0.964	-0.964
6	0.013	171.176	0.036	0.692	0.945	-5.334
7	0.001	146.864	0.204	0.000	0.663	-3.316
8	0.010	165.605	0.045	0.184	0.740	2.357
9	0.002	162.319	0.195	0.530	0.914	-7.589
10	0.126	100.440	0.182	0.334	0.940	-0.158
11	0.004	175.955	0.056	0.653	0.971	2.493
12	0.015	155.458	0.013	0.000	0.773	5.469
13	0.038	133.786	0.109	0.184	0.968	0.006
14	0.006	173.393	0.063	0.596	0.997	-0.446
15	0.004	179.204	0.051	0.820	0.997	-6.699
16	0.010	166.907	0.072	0.533	0.981	-4.393
17	0.012	162.668	0.062	0.193	1.000	-0.741
18	0.057	125.426	0.139	0.433	0.998	-7.736
19	0.036	135.711	0.085	0.000	0.946	0.203
20	0.051	126.240	0.122	0.176	0.957	0.115
21	0.007	171.583	0.067	0.499	0.992	-0.978
22	0.050	126.965	0.119	0.217	0.975	0.758
23	0.051	125.600	0.140	0.390	0.987	-0.013
24	0.077	113.464	0.142	0.163	0.990	3.500
25	0.026	145.978	0.088	0.000	0.998	-0.961
26	0.003	183.177	0.025	0.798	0.992	0.547
27	0.046	129.534	0.136	0.225	0.982	-1.611
28	0.016	155.985	0.092	0.222	0.992	-1.787
29	0.010	165.469	0.056	0.377	0.919	-5.033
30	0.025	143.831	0.112	0.591	0.978	-2.288

Table 5.6, Back calculated properties for 2nd layer

Serial	Strain (%)	Shear wave velocity (m/s)	Damping ratio	p-value for $H(\omega)$	p_value for Response spectrum	PGA_difference (%)
1	0.013	195.811	0.020	0.463	0.932	5.668
2	0.376	41.538	0.200	0.000	0.019	-30.540
3	0.007	192.715	0.070	0.878	0.984	-4.796
4	0.015	193.308	0.020	0.051	0.924	4.899
5	0.083	67.762	0.200	0.038	0.004	-67.988
6	0.019	179.446	0.100	0.328	0.936	7.210
7	0.041	35.781	0.200	0.000	0.000	-15.719
8	0.051	95.383	0.160	0.706	0.261	-45.784
9	0.082	41.649	0.200	0.000	0.008	-46.201
10	0.112	135.888	0.140	0.321	0.971	5.097
11	0.006	208.927	0.200	0.000	0.657	6.322
12	0.022	185.471	0.130	0.161	0.925	2.519
13	0.060	156.118	0.100	0.095	0.959	2.573
14	0.010	203.664	0.200	0.000	0.855	4.804
15	0.007	207.729	0.200	0.000	0.860	-8.265
16	0.017	193.104	0.020	0.816	0.926	-0.370
17	0.021	185.559	0.060	0.260	0.953	-0.242
18	0.101	142.828	0.110	0.093	0.946	-7.623
19	0.058	157.998	0.130	0.428	0.938	-0.809
20	0.085	144.376	0.120	0.206	0.982	1.258
21	0.011	200.095	0.020	0.283	0.928	0.942
22	0.074	148.729	0.130	0.658	0.950	1.128
23	0.088	141.959	0.110	0.067	0.964	-0.226
24	0.138	128.435	0.130	0.087	0.961	2.423
25	0.141	93.052	0.160	0.174	0.320	-0.681
26	0.005	210.339	0.200	0.000	0.875	2.027
27	0.078	147.905	0.100	0.053	0.949	0.118
28	0.026	181.956	0.040	0.109	0.954	-1.103
29	0.123	57.205	0.200	0.000	0.002	-62.049
30	0.712	37.628	0.200	0.000	0.000	-52.086

Table 5.7, Back calculated properties for 3rd layer

Serial	Strain (%)	Shear wave velocity (m/s)	Damping ratio	p-value for $H(\omega)$	p_value for Response spectrum	PGA_difference (%)
1	0.013	226.078	0.100	0.068	0.945	7.813
2	0.026	167.382	0.200	0.000	0.540	6.922
3	0.004	278.898	0.200	0.000	0.801	-5.129
4	0.012	226.334	0.120	0.386	0.986	-1.222
5	0.015	225.394	0.200	0.000	0.903	-2.949
6	0.011	232.287	0.120	0.830	0.999	2.226
7	0.003	144.931	0.200	0.000	0.554	16.278
8	0.005	348.718	0.200	0.000	0.940	-24.529
9	0.007	168.245	0.200	0.000	0.492	5.727
10	0.121	139.051	0.170	0.337	0.970	-1.071
11	0.005	248.147	0.200	0.000	0.886	-0.948
12	0.019	213.104	0.090	0.050	0.973	-2.935
13	0.059	170.432	0.120	0.154	0.991	-2.596
14	0.010	233.083	0.020	0.792	0.960	6.354
15	0.006	246.825	0.200	0.000	0.884	-5.166
16	0.015	226.334	0.090	0.231	0.996	-4.232
17	0.021	211.148	0.100	0.079	0.967	-0.837
18	0.120	146.308	0.130	0.051	0.970	-8.744
19	0.058	173.381	0.130	0.077	0.972	-3.748
20	0.095	151.342	0.150	0.345	0.980	1.116
21	0.010	237.316	0.060	0.126	0.996	-4.924
22	0.070	164.293	0.180	0.735	0.986	-3.457
23	0.099	148.831	0.140	0.144	0.982	0.394
24	0.183	125.810	0.150	0.070	0.976	1.476
25	0.013	331.880	0.200	0.000	0.727	1.913
26	0.004	252.102	0.200	0.000	0.911	-0.988
27	0.088	153.255	0.130	0.085	0.984	2.913
28	0.024	206.511	0.100	0.148	0.990	-4.366
29	0.013	226.100	0.200	0.000	0.831	-27.553
30	0.061	151.839	0.200	0.003	0.446	7.485

Table 5.8, Back calculated properties for 4th layer

Serial	Strain (%)	Shear wave velocity (m/s)	Damping ratio	p-value for *H(ω)*	p_value for Response spectrum	PGA_difference (%)
1	0.011	269.254	0.050	0.059	0.960	7.731
2	0.014	218.105	0.020	0.315	0.989	-2.645
3	0.004	311.473	0.020	0.607	0.999	-10.808
4	0.010	279.497	0.040	0.101	0.983	-9.032
5	0.007	337.375	0.120	0.055	0.878	-1.367
6	0.008	291.947	0.020	0.399	0.911	-0.103
7	0.002	188.851	0.020	0.827	0.895	10.799
8	0.003	454.394	0.200	0.016	0.980	-7.437
9	0.003	219.231	0.200	0.000	0.558	2.593
10	0.084	178.884	0.140	0.577	0.976	-2.800
11	0.004	300.272	0.020	0.408	0.950	-4.204
12	0.016	261.499	0.060	0.051	0.979	-0.998
13	0.048	213.010	0.080	0.085	0.951	4.622
14	0.008	283.859	0.020	0.103	0.951	7.540
15	0.005	295.628	0.020	0.505	0.955	-0.331
16	0.014	269.393	0.030	0.060	0.893	-0.026
17	0.017	257.744	0.070	0.086	0.960	-0.876
18	0.090	185.808	0.130	0.573	0.994	-11.055
19	0.044	218.686	0.100	0.064	0.951	-1.235
20	0.066	196.713	0.100	0.164	0.991	-5.304
21	0.008	284.362	0.020	0.066	0.980	-0.892
22	0.045	217.456	0.140	0.873	0.975	-5.166
23	0.072	191.032	0.140	0.910	0.988	0.298
24	0.141	159.377	0.130	0.319	0.994	0.635
25	0.015	345.369	0.020	0.071	0.762	-9.649
26	0.003	301.893	0.020	0.181	0.977	-1.486
27	0.068	194.936	0.130	0.610	0.991	5.363
28	0.019	254.811	0.060	0.099	0.954	4.833
29	0.008	294.618	0.200	0.005	0.778	-19.651
30	0.033	197.852	0.200	0.000	0.595	5.136

Table 5.9, Back calculated properties for 5th layer

Serial	Strain (%)	Shear wave velocity (m/s)	Damping ratio	p-value for $H(\omega)$	p_value for Response spectrum	PGA_difference (%)
1	0.015	249.758	0.030	0.062	0.903	6.705
2	0.011	243.400	0.200	0.000	0.983	-19.265
3	0.006	264.299	0.020	0.816	0.859	-10.331
4	0.014	251.355	0.030	0.068	0.921	-11.678
5	0.006	376.502	0.020	0.917	0.711	0.029
6	0.014	230.755	0.020	0.105	0.979	-5.451
7	0.002	210.753	0.200	0.000	0.521	11.220
8	0.002	507.092	0.020	0.263	0.676	11.395
9	0.003	244.656	0.130	0.050	0.436	4.982
10	0.117	168.970	0.140	0.995	0.970	-4.478
11	0.006	268.523	0.020	0.853	0.807	8.623
12	0.022	237.695	0.060	0.076	0.962	-1.566
13	0.065	200.452	0.070	0.103	0.915	2.386
14	0.012	252.735	0.020	0.054	0.878	4.971
15	0.007	267.728	0.020	0.971	0.905	5.578
16	0.018	245.471	0.020	0.056	0.959	-10.706
17	0.025	233.954	0.070	0.123	0.915	-0.740
18	0.115	182.237	0.080	0.093	0.959	-12.928
19	0.057	204.411	0.090	0.067	0.928	-3.045
20	0.087	186.258	0.070	0.066	0.973	-4.724
21	0.011	261.422	0.020	0.107	0.867	-1.701
22	0.056	204.994	0.070	0.242	0.984	-7.015
23	0.097	181.368	0.090	0.200	0.988	-0.695
24	0.189	151.147	0.140	0.632	0.989	0.515
25	0.060	187.216	0.200	0.001	0.886	-14.881
26	0.005	269.996	0.020	0.499	0.903	1.929
27	0.092	181.519	0.100	0.333	0.980	3.709
28	0.026	234.214	0.050	0.089	0.911	6.204
29	0.007	328.786	0.140	0.948	0.987	-5.386
30	0.027	220.798	0.200	0.000	0.538	10.218

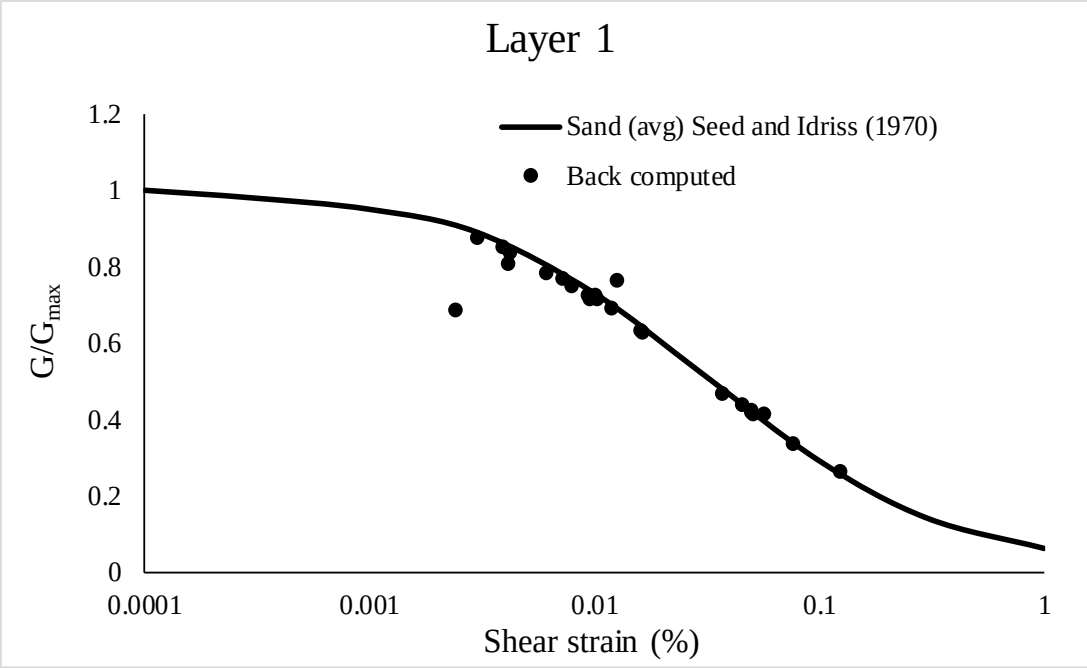

Figure 5.9, Comparison of back-calculated G/G_{max} values for layer 1 with Seed and Idriss (1970)

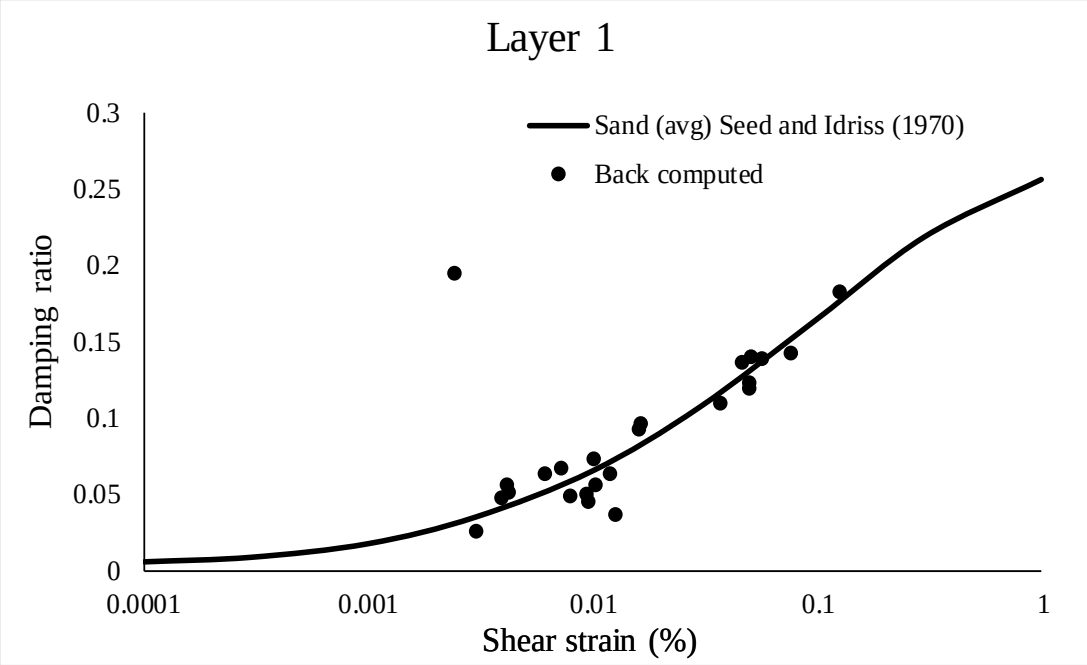

Figure 5.10, Comparison of back-calculated β values for layer 1 with Seed and Idriss (1970)

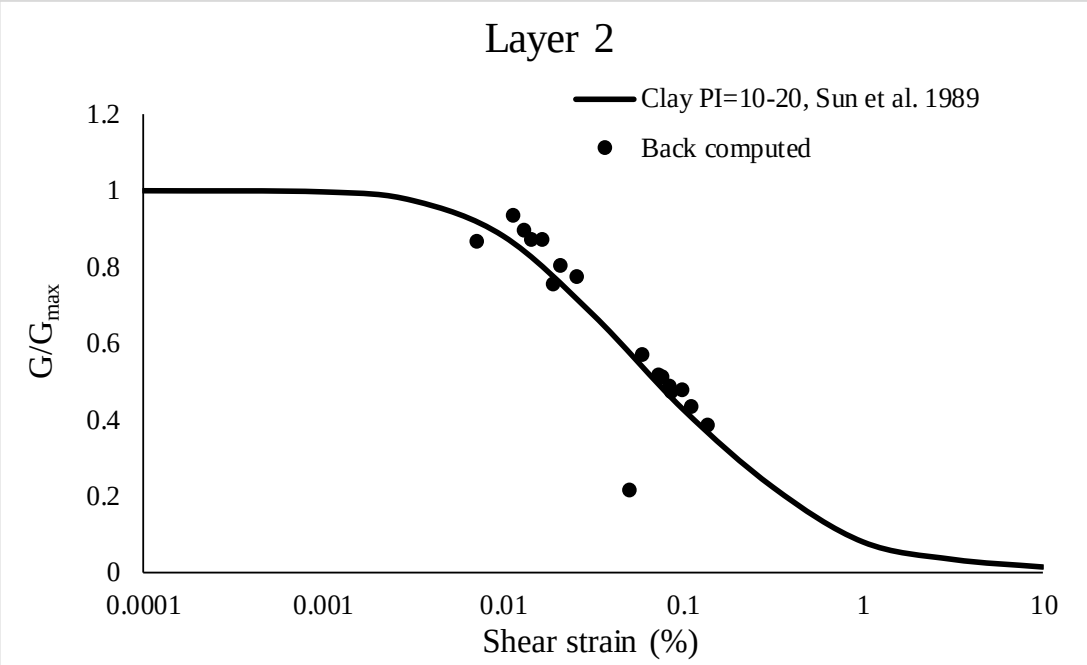

Figure 5.11, Comparison of back-calculated G/G_{max} values for layer 2 with Sun et al. (1989)

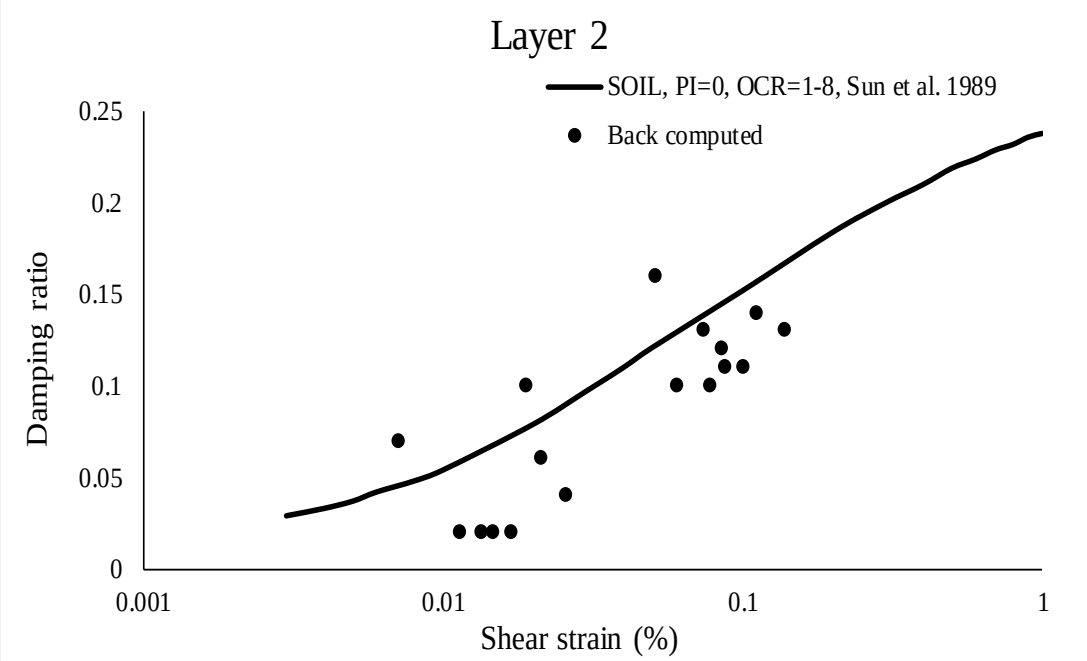

Figure 5.12, Comparison of back-calculated β values for layer 2 with Sun et al. (1989)

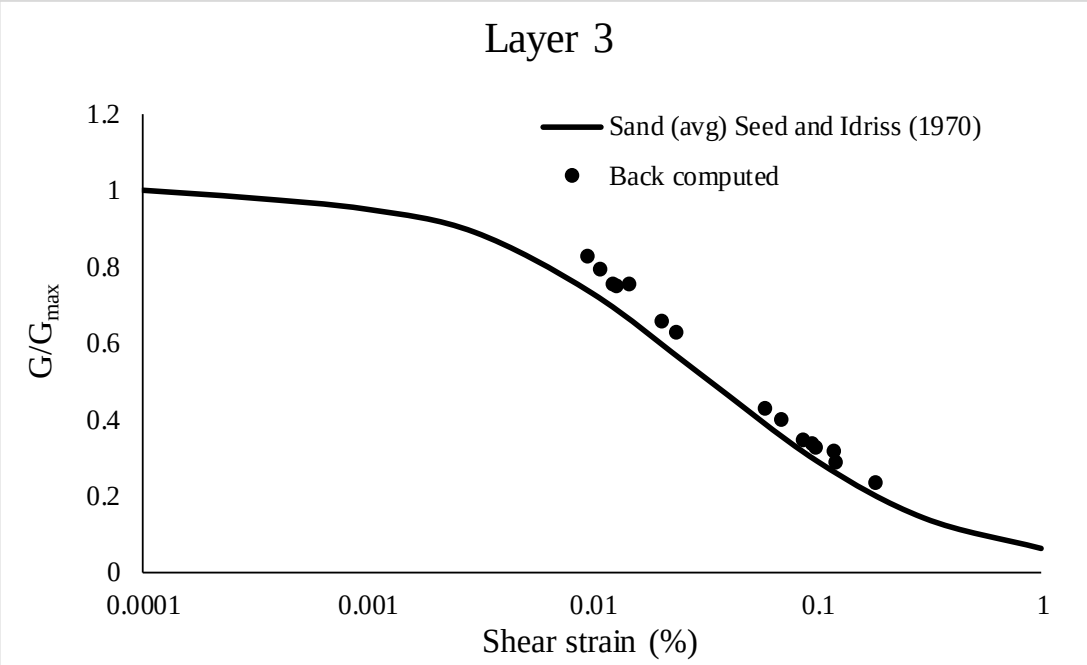

Figure 5.13, Comparison of back-calculated G/G_{max} values for layer 3 with Seed and Idriss (1970)

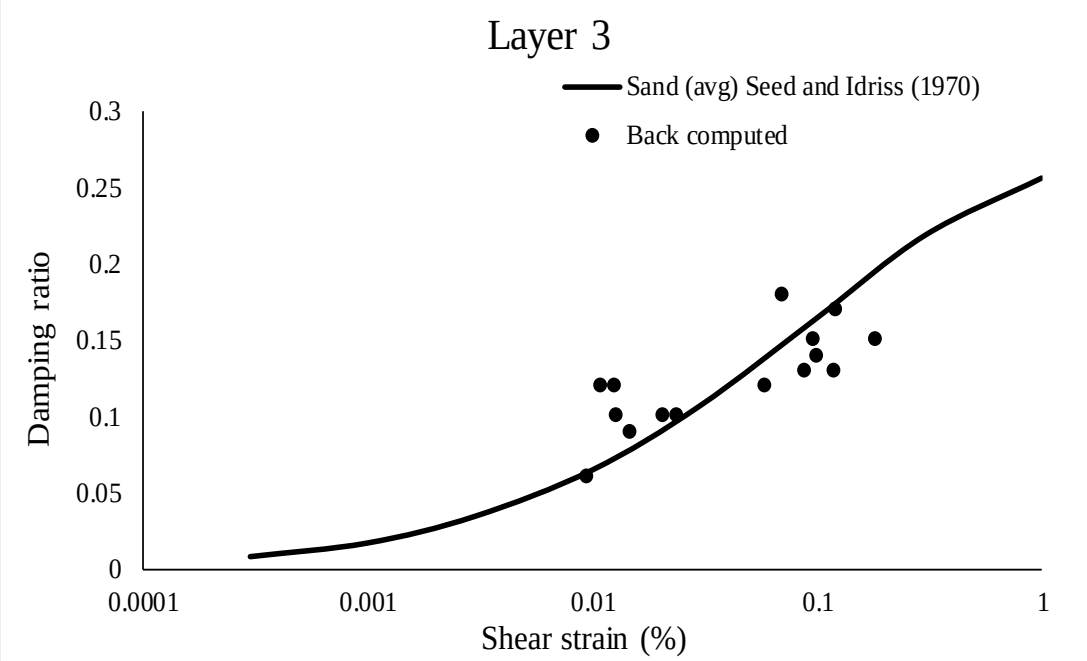

Figure 5.14, Comparison of back-calculated β values for layer 3 with Seed and Idriss (1970)

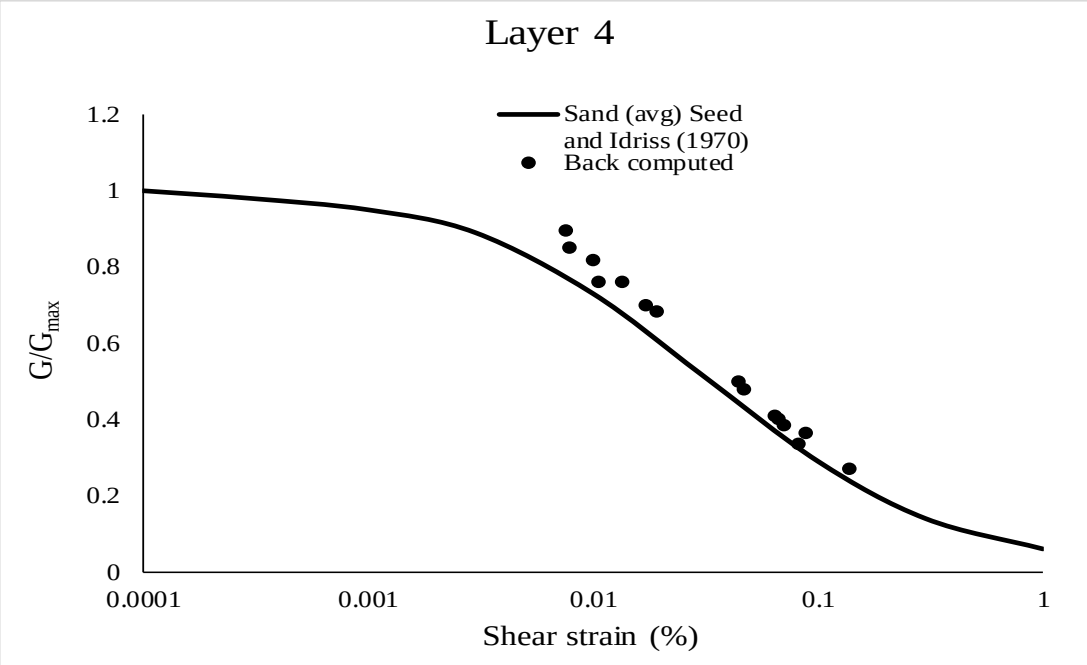

Figure 5.15, Comparison of back-calculated G/G_{max} values for layer 4 with Seed and Idriss (1970)

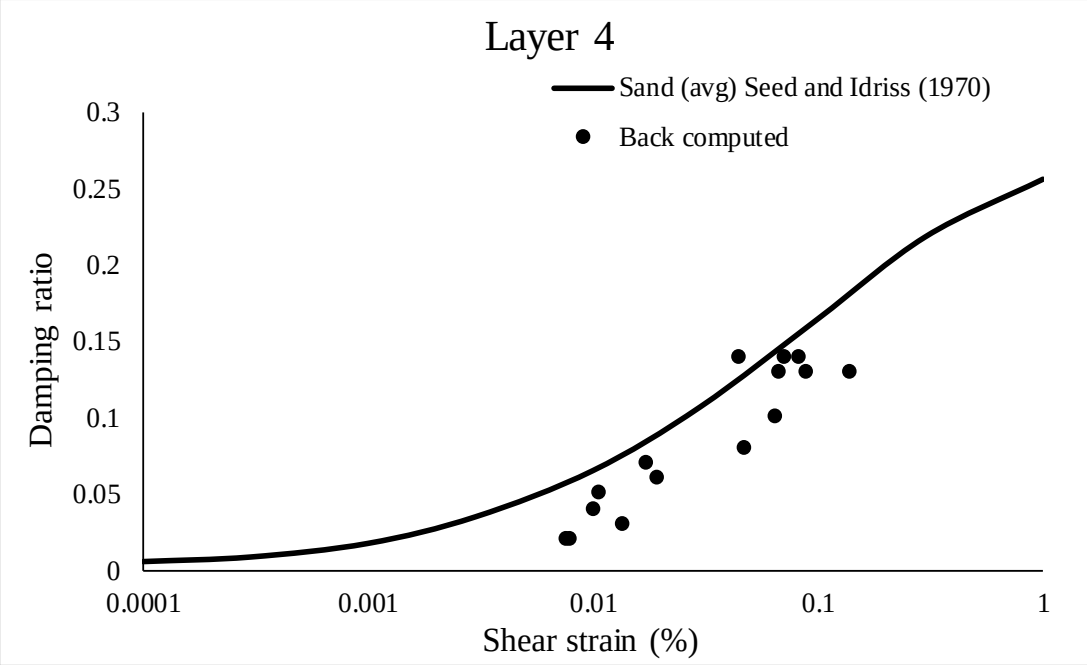

Figure 5.16, Comparison of back-calculated β values for layer 4 with Seed and Idriss (1970)

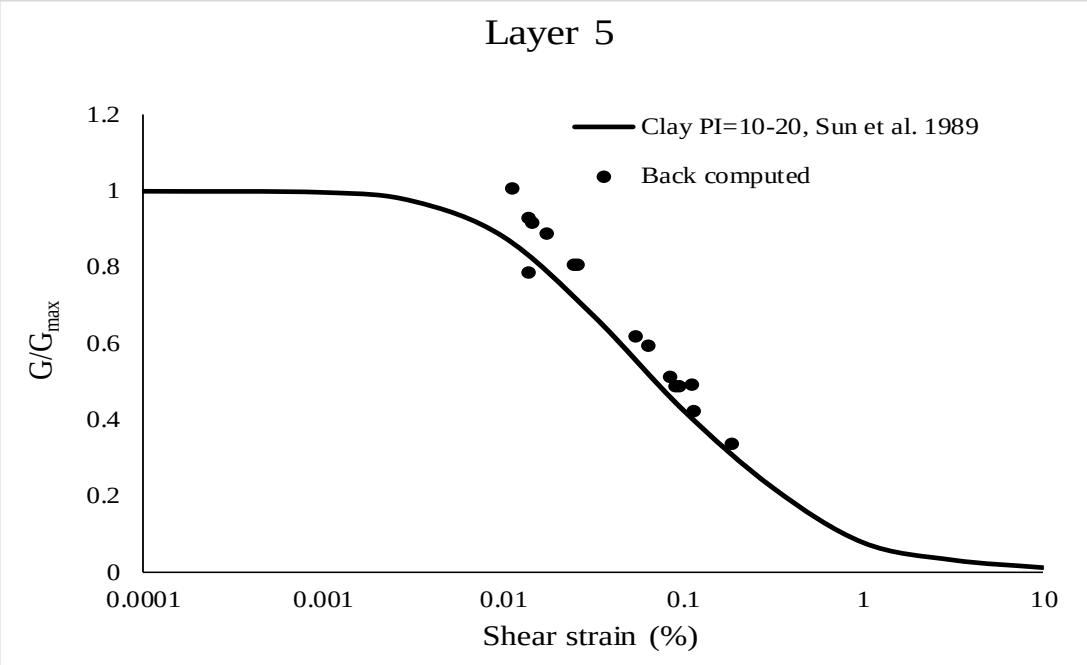

Figure 5.17, Comparison of back-calculated G/G_{max} values for layer 5 with Sun et al. (1989)

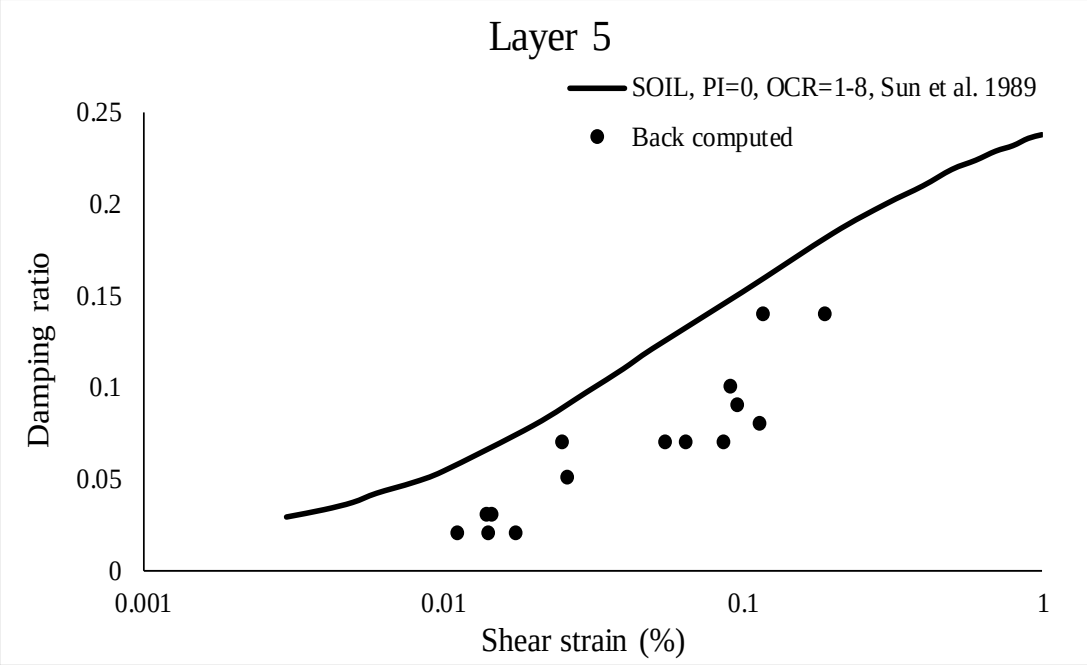

Figure 5.18, Comparison of back-calculated β values for layer 5 with Sun et al. (1989)

5.4 Conclusions

In this chapter, a frequency domain IGRA methodology is proposed that can be utilized to determine DSPCs for multiple layers. For this purpose, a MATLAB based function 'multilayer.m' is developed. In this function, a number of acceleration time histories recorded

along a downhole array are given as input. The function returns V_s and β values for each of the soil layers located between two consecutive downhole locations. The function is then used on EQ data sets derived from ELGRA findings and downhole array recordings. In case of EQ data set obtained based on ELGRA, the developed function and proposed methodology work exceptionally well. In case of downhole array recordings, the proposed methodology yields somewhat scattered values of V_s and β. Thus, average DSPCs are also proposed for different soil layers located along the Lotung downhole array. Further, the same set of proposed average DSPCs are used for carrying out ELGRA at the Lotung site. For this purpose, a different data set of EQ motions (that were not considered while proposing the average DSPCs) are used. Based on the ELGRA results, it is found that the proposed DSPCs work satisfactorily in estimating ground response. Thus, the proposed methodology can be confidently used for the determination of DSPCs for multiple soil layer systems based on downhole array data.

CHAPTER 6: CORRELATIONS FOR ESTIMATING LOCAL SITE EFFECTS DUE TO SOIL NONLINEARITY FOR GUWAHATI

6.1 Introduction

In previous 4 chapters, the influence of DSPCs over GRA results have been highlighted several times. Accordingly, Chapters 3, 4 and 5 proposed frameworks which can be applied to downhole array records in order to determine DSPCs of various subsoil layers. While Chapters 3, 4 and 5 based methodology can be applied to downhole array records, for regions with no such array records available, GRA studies will be need some or the other DCPSs. Based on the literature review given in Chapter 1 and 2, it is clear that majority of GRA studies used standard DSPCs in the absence of site-specific DSPCs. Further, for some regions, more than one GRA studies exist using different set of DSPCs for the same soil. This results in getting different subsoil response for the same soil, primarily due to the use of different set of DSPCs. It must be noted here that though both linear behavior of soil and nonlinear behavior of soil can cause LSE, it is the nonlinear behavior of soil (LSE_{NL}) which changes with set of DSPCs used.

In the present chapter, an attempt has been made to determine site–specific correlations for Guwahati based on which LSE (in the absence of site-specific DSPCs either based on both laboratory method and IGRA method are not available) can be quantified. The sole purpose of the developed correlations is to avoid performing GRA for each and every site of interest by the user which may include using different set of DSPCs as well. For the purpose, subsoil information from Guwahati is taken into consideration. Selection of Guwahati is primarily because of its high seismicity, relatively softer near surface geology, and also because Guwahati

is the largest industrial and educational hub of Northeast India (NEI). Further details can be found in further sections.

6.2 Guwahati and its seismicity

Guwahati is the largest city in NEI, within its suburb in Dispur, the capital of Assam. The city lies between 26.08˚N to 26.25˚ N and 91.58˚E to91.92˚E, covering an area of around 600 sq. km (Raghukanth et al. 2011b). It is located towards the southeastern part of Kamrup district and is built over soft alluvium deposit transported by the River Brahmaputra. The city is surrounded by many hillocks in the south-eastern part. Some of the notable mentions are Buragosain parbat (426 m), Fatasil hill (292 m), Nilachal hills (293 m), Khurguli hill (216 m), Silapahar (220 m), Chunsuli Pahar (215 m), Japorigog hill (277 m), Narangi Hill (240 m), Amchang pahar (202 m), Narakasur hill (267 m), Sonaiguli hill (202 m), Jalukabari hill (168 m) etc. Apart from above hillocks and the mighty River Brahmaputra defining the northern boundary of the city, many water bodies are also located within Guwahati (Deepor Beel, Sil Pukhuri, Dighali Pukuri, Borsola Beel, Ghuguli Beel, Raja Beel, Hahsara Beel, Susuki Beel, Pata Beel, Pitni Beel, Silsako Beel, Damal Beel, Tepar Beel, etc.). In the last few decades, the population of Guwahati has increased rapidly. According to 2011 census, Guwahati has a population of one million. This is primarily because many people from other parts of NEI have started to live in Guwahati either permanently or temporarily because of better job opportunities, education and healthcare facilities.

Seismicity-wise, Guwahati falls in zone V of the seismic zonation map (BIS 1893:2016) of India, indicating the highest seismic hazard zone of the country. The city is surrounded by active tectonic blocks. The region is surrounded from north and northeast by the Himalayan collision zone, from the east by the Indo-Myanmar subduction interface and from the south by

the Shillong Plateau-Mikir tectonic. Ongoing movement in the above tectonic blocks makes the entire NEI (except Sikkim), as one of the most complex tectonic setting regions of India. In the last 110 years, almost 20 major EQs and 2 great EQs have been witnessed by the city (Kayal et al. 2006). The Himalayan Frontal Thrust is responsible for many shallow focus- low magnitude EQs in the region. Similarly, active subduction process along the Indo-Mayanmar belt and the faults lying across this belt were responsible for many minor to major EQs, which were felt in Guwahati. The tectonic block of Shillong plateau-Mikir hill is very active. Many active faults, which have produced significant EQs in the past, are present in this block. Some of the important faults on this block are Jamuna/ Dhubri fault, Dhudnoi/ Chedrang fault and Kulsi fault. Apart from these three faults, the Kopili fault is passing between the Meghalaya plateau and Mikir hill, and the Bomdila fault which is passing along the northern boundary of the Mikir hill, are noteworthy mentions.

The present study area of Guwahati city is located on the northern boundary of the Shillong plateau making it a region of moderate to high seismic hazard. The city has witnessed many damaging EQs over the years. The 1897 great Assam EQ (M_w 8.1) originated on the Dhudnoi/ Chedrang fault is one such event. During this EQ, an area of 1, 50, 000 square miles was badly affected (Oldham 1899). Ground shaking was felt all over the Guwahati city. The Kamakhya temple and many stone made bridges in Guwahati city were severely damaged (Rajendran et al. 2004) during above EQ. In similar manner, the NW-SE trending Kopili fault triggerred the 1869 Cachar EQ and the 1943 EQ, both having magnitude greater than 7.0 (Mw). During the 1869 Cachar EQ, several building damages were encountered at Pan Bazar area of Guwahati. In addition, it is reported by As per Centre for Natural Disaster Management (2002), water table at many places in Guwahati rose to the ground surface during the 1869 Cachar EQ, ,

suggesting a strong case of liquefaction. Sylhet fault is another important fault, which is located in the Bengal basin, and was the source of the 1918 Srimangal EQ (M_w 7.6). The Jamuna/ Dhubri fault was responsible for the 1931 (M_w 7.1) Dhubri EQ. Strike-slip movement in a NW-SE trending fault in the Mishmi block caused the great 1950 Assam EQ (M_w 8.7). Severe damages were inflicted in the Upper Assam area during this EQ.

In additional to above-mentioned active seismic sources around Guwahati, there are several faults located within the Guwahati city as well. These include; 1) a 5km long fault running between the Nilachal and the Fatasil hill, 2) 10km long fault between Kalapahar and Fatasil hill, 3) 20km long fault between southern foothills and the river Brahmaputra and 4) a fault running between the southern foothills and the Kalapahar-Fatasil hill range (GSI 2000; Raghu Kanth and Dash 2010; Kumar et al. 2014b;). According to researchers (Khattri 1987; Khattri and Wyss 1978), the unbroken segment between the 1897 EQ location and 1950 EQ location is capable of producing a great EQ. This unbroken segment is termed as Assam gap (Khattri 1987; Khattri and Wyss 1978). Thus, the presence of soft alluvium, hillocks, water bodies, seismic sources, important structures, and fast-growing population make Guwahati city more prone to seismic damages during future EQs.

6.3 Lithology

As per Guwahati Metropolitan Development Authority (GMDA 2016) report, bedrock medium of Guwahati city is dominated by the Precambrian gneissic complex with a hint of porphyritic granites at several places. The gneissic basement composed of granite gneiss, biotite gneiss, biotitic schist and quartzite quaternary alluvium. Further, the alluvium fills over the gneissic complex consists of alternate beds of unconsolidated sand, silt and clay. Presence of minerals such as quartz, biotite, muscovite along with typical Brahmaputra sand are found at many places

such as Bharalumukh, Machkhowa, Chatribari and Ulubari locations of Guwahati (GMDA 2016).

As per Kumar et al. (2018), subsoil in Guwahati consists of alternate layers of sand, clay and silt till 30m depth. For the present work, 108 boreholes (referring to Kumar et al. 2018), which were drilled for Mass Rapid Transit System (MRTS) project, are collected from GMDA. SPT test was conducted at every 3m interval and at depths where strata encountered a change. Both disturbed and undisturbed samples were collected by means of standard split spoon sampler and thin walled samplers respectively. Further, the samples were tested in the laboratory to obtain necessary geotechnical properties (GMDA 2016). One typical borelog is shown in Table 6.1. It can be observed from Table 6.1 that the subsoil lithology for Guwahati mainly consists of clay layers with low to high compressibility and silty sand layers. Such information is consistent with that reported by Raghukanth et al. (2011) for Guwahati city. Similar observations can also be made from other 107 borelogs. Collectively based on 108 borelogs, it can be concluded that soft soil (having SPT-N<15 as per NEHRP 2003) is present up to a depth of 10m. Further, stiff soil (15<SPT-N<50 as per NEHRP 2003) is found between 10m and 15m depth, and hard soil (SPT-N>50, NEHRP) between 15m and 30m depth. The depth of ground water table (GWT) in these boreholes was reported to vary from 0m to 6.7m (after 24 hours of observation).

6.4 Existing GRA studies for Guwahati

Earlier, Raghukanth et al. (2011a) performed GRA for Guwahati city using 100 borehole data located all over Guwahati city. In that study, 20 input ground motions were simulated for each of the three EQs namely; 1869 Cachar EQ, 1897 Great Assam EQ and probable EQ scenario considering Assam Gap (Khattri et al. 1983). For the purpose, EXSIM code developed by Motazedian and Atkinson (2005) was utilized by Raghukanth et al. (2011a). Further, the soil

layers in different boreholes were modeled using dynamic soil properties curves (DSPC) proposed by Vucetic and Dobry (1991). Raghukanth et al. (2011a), in that study, proposed a concept of correction factors. In case soil information is not known, the above correction factors could be used with bedrock level response spectra to determine surface level response spectra. In another study performed by Kumar and Krishna (2013), 6 borhole locations from Amingaon in north Guwahati were used to perform ELGRA. For the purpose, 7 EQ motions (1897 Assam EQ, 1988 Indo-Burma EQ, 1991 Uttarkashi EQ, 1990 North-East EQ, 1995 Indo-Burma EQ, 2001

Table 6.1, Typical borehole

Borehole No. 77		GWT at 6.60m depth		Samples			
Depth (m)	Description	Soil classification	Thickness	Type	No.	Depth (m)	SPT-N
0	Filled up materials with garbages& blackish sandy soil	SP	4.5	DS	1	1	
				UDS	1	1.5	
				SPT	1	3	4
4.5				UDS	2	4.5	
	Blackish silty clay	CH/CI	10.5	SPT	2	6	5
				UDS	3	7.5	
				SPT	3	9	9
				UDS	4	10.5	
				SPT	4	12	12
				UDS	5	13.5	
15				SPT	5	15	13
	Grayish clay	CH	6	UDS	6	16.5	
				SPT	6	18	26
				UDS	7	19.5	
21				SPT	7	21	36
	Blackish silty clay	CH	3	UDS	8	22.5	
24				SPT	8	24	70
	Brownish coarse sand	SM	6	UDS	9	25.5	
				SPT	9	27	R
				UDS	10	28.5	
30				SPT	10	30	R

Bhuj EQ and 2011 Sikkim EQ) were used as input motion. In that study, Kumar and Krishna (2013) utilized DSPC proposed by Seed and Idriss (1970) and Vucetic and Dobry (1991) to model sand and clay layers, respectively. Further, based on the ELGRA study, Kumar and Krishna (2013) recommended amplification factors (AFs) (surface PGA/ bedrock peak horizontal acceleration) in the range 2-4. Kumar et al. (2014), in a separate study, performed nonlinear GRA (NLGRA) using seven borehole sites located at Amingaon. In that study, two scaled-up components of 2011 Sikkim EQ (recorded at IIT Guwahati) were used as input motions. In that study as well, DSPC developed by Seed and Idriss (1970) and Vucetic and Dobry (1991) were used to model sand and clay layers, respectively. Based on the study, Kumar et al. (2014) reported AF in the range 1.47-2.72 for the seven boreholes considered. In another study that was performed by Basu and Dey (2017), NLGRA was attempted at three typical locations in IIT Guwahati. In that study, ground motion that was recorded at IIT Guwahati during 2011 Sikkim EQ and 3 scaled-up components of the same motion were utilized as input motions. Further, formulation by Ishibashi and Zhang (1993) was utilized to obtain DSPCs for all the soil layers involved. In that study, AFs were reported to be in the range 1-5. Additionally, Basu and Dey (2017) highlighted that even de-amplification happened for some particular cases where bedrock peak horizontal acceleration (PHA) was more than 0.18g. A similar NLGRA study also has been carried out by Basu et al. (2019), utilizing 90 borehole data collected from all over Guwahati city. In that study also DSPCs for different soil layers were obtained based on Ishibashi and Zhang (1993), and AFs were reported to be 1-5. In another work performed by Sharma et al. (2018), ELGRA were carried out for Guwahati city considering 120 borehole data. In this study, EQ motion recorded at Gangtok during 2011 Sikkim EQ was considered. In this study also, sandy soil and clayey soils were modeled using DSPCs proposed by Seed and Idriss

(1970) and Vucetic and Dobry (1991), respectively. Based on the outcomes from ELGRA, Sharma et al. (2018) reported AFs for Guwahati city as 1-4. In another work performed by Siddique and Sharma (2020), both NLGRA and ELGRA were performed. In this study, curves by Seed and Idriss (1970) and Vucetic and Dobry (1991) were used to model sandy and clayey soil, respectively. The AFs were reported to be 1-4.2 for ELGRA and 1-3.5 for NLGRA.

Above discussion highlights that a number of studies attempted GRA for Guwahati city. For the purpose, both ELGRA and NLGRA have been used extensively. However, while performing GRA, these studies considered different sets of DSPCs and input motions. Using different set of DSPCs will result in different outcomes of GRA, as indicated by different values of AF by each study for Guwahati. Moreover, above studies were based on specific locations and specific input motions. Hence, in case a location is not covered in earlier studies require LSE quantification, one has to perform GRA based on selected DSPC and input motion. Further, input motion many a times are not readily available for every user, making site-specific studies a further challenge.

Overcoming such complication, correlations which correlates AFs as a function of PHA values, site class (SC), and soil type, the outcomes would be reliant on the DSPCs and ground motions used in that study. Highlighting the limitations related to previous GRA studies and challenges in performing site-specific GRA for newer sites, the present study proposes four correlations which can an indirectly estimate AFs as a function of PGA value. These correlations can be used to estimate error values between PGA obtained based on ELGRA (PGA_{EL}) and PGA obtained based on LGRA (PGA_{LN}) as a function of PGA_{LN}. In doing so, the effect of different SCs (based on BSSC 2009) and different soil types (clay or sand) have been considered. It must

be noted here that the correlations proposed in this study are based on PGA_{LN} to make current findings independent of DSPCs. Further details can be found in the next section.

6.5 Development of empirical correlations

In this study, two sets of GRA are performed. In first set of analyses, ELGRA on 108 boreholes located across the Guwahati city are performed. 30 globally recorded ground motions are used as inputs, and PGA values at the top of different soil layers are determined as output. In the second set of analyses, the same set of 108 boreholes and 30 ground motions are used for LGRA and PGA values at the top of all the layers involved, are computed. Further, all PGA_{LN} values are subtracted from corresponding PGA_{EL} values. It has to be highlighted here, in this paper, the above calculated differences in PGA_{EL} and PGA_{LN} are termed as LSE_{NL} from here on. Further, correlations are developed which can estimate LSE_{NL} at a given depth as a function of PGA_{LN}. These correlations are developed for different NEHRP (National earthquake hazard reduction program) site classes (SCs) and different soil types (sand and clay). 51 boreholes which were not included while developing the correlations are utilized to validate the proposed correlations.

6.5.1 Selection of input motion

Bedrock motion is one of the two important site-specific parameters required for GRA. Thus, once the bedrock motion is known; it can be used for the quantification of induced effects as well as to understand LSE during corresponding EQ scenario. Most of the times however, it has been observed that sufficient numbers of regionally recorded ground motions are not available for the site, where GRA is to be done. In such situation, compatible ground motions recorded in other parts of the world are considered as bedrock motion for the site. Standard ground motions recorded during 1940 El-Centro EQ, 1985 Mexico EQ, 1989 Loma Prieta EQ, 1994 Northridge EQ, 1995 Kobe EQ, 1999 Chi-Chi EQ etc. are frequently used by researchers from across the

globe including India (Besrat et al. 2018; Kumar et al. 2016; Phanikanth et al. 2011; Stanko et al. 2017, 2019) to understand LSE in the absence of regional ground motion records. In such case, above referred ground motions are scaled up to comply with the response spectrum of the site/ region of interest. In similar manner, generation of synthetic ground motions in accordance with uniform hazard spectra and seismic hazard value at the site is also attempted by researchers globally (Bazzurro et al. 1998; Deodatis 1996; Kennedy et al. 1984; Kumar et al. 2011; Nath and Thingbaijam 2011).

The tectonic setting of a region is indicated by the recorded bedrock motions locally. As a result, data from other parts of the world may or may not accurately represent the tectonic setting at the site in question. In addition, using a small number of regionally recorded ground motions or synthetically generated ground motions that match the local seismicity may not cover all the unknown factors about how future EQs will control ground motion. Further, how far away the site is from the earthquake source is a key factor in figuring out what the ground motions will be like. Due to the different distances and angles between the source and the site, source and path characteristics have a big effect on near-source EQ ground motions. Ground motions may vary even more when source complexity is taken into account (Archuleta and Hartzell 1981; Mai and Meyers 2009; Ripperger et al. 2008). On the other hand, LSE is the most important parameter for controlling EQ ground motions when the EQ source is far away (Ntritsos et al. 2021). In these situations, recorded motions from nearby outcrops or a deconvoluted version of these outcrop motions can be used as input motions for GRA. The above discussion clearly highlights the challenges which exist related to the selection of input ground motions for GRA. Kumar et al. (2016) pointed out that a large set of input motions can cover a wide range of ground motion characteristics, including amplitude, frequency content, and duration. This is one effective way

to deal with above-mentioned challenges. Considering these difficulties, Kumar et al. (2016) chose 30 ground motions from the PEER database for GRA in the Delhi area. For the present study as well, the same set of 30 ground motions is used. The details of these ground motions are shown in Table 6.2. It can be observed from Table 6.2 that well-known ground motions like the 1995 Kobe EQ, the 1989 Loma Prieta EQ, and the 1985 Mexico EQ, among others, are chosen for GRA in this work. In addition, Table 6.2 shows that the characteristics of ground motion vary significantly in every aspect. Taking into account the possible variation in PHA value, the selected motions cover a wider range of amplitudes from 0.008g to 1.03 g. Table 6.2 also shows that the lengths of the selected ground motions range from as short as 6.8 s to as long as 140 s. Further, the predominant frequencies of the ground motions as obtained from Fourier spectra are also shown in Table 6.2. It can be observed that the predominant frequencies vary from 0.26 Hz to 16.5 Hz. The distances between the epicenters of the selected motions range from 0.9 km to as far as 216 km. Further, selected ground motions have magnitudes ranging from 5.0–8.1 in Mw scale.

***Table 6.2*, Ground motion detail (as per Kumar et al. 2016)**

Sr. No.	Ground Motion Details as per SHAKE2000	Epicentral Distance (Km)	Magnitude	PGA (g)	Duration (s)	Predominant Frequency (Hz)
1	ADAK, ALASKA 1971-M 6.8;R-67KM, N81E	86.77	6.8	0.098	24.58	3.32
2	ANCHORAGE, ALASKA 1875, M-6, R81-GOULE HALL STATION	81.93	6	0.036	18.59	5.42
3	ANCHORAGE ALASKA 1975, M 6, R 79, WESTWARD HOTEL STATION (BASEMENT)	78.37	6	0.049	38.96	1
4	ANZA 02/25/80, BORREGO AIR BRANCH 225	43.1	5.3	0.046	10.25	2.39
5	ANZA 02/25/80 1047, TERWILLIGER VALLEY 135	15.8	5.3	0.08	10.01	6.54
6	BISHOP-ROUND VALLEY 11/23/84 1914, MCGEE CREEK SURFACE 270	42.35	5.8	0.075	6.8	3.9
7	BORREGO MOUNTAIN 04/09/68 0230, EL CENTRO ARRAY 9, 270	60	6.4	0.056	39.95	0.46
8	BORREGO MOUNTAIN 04/09/68 0230, PASADENA-ATHENAEUM, 270	216.8	6.4	0.009	60.23	0.61
9	BORREGO MOUNTAIN 04/09/68 0230, TERMINAL ISLAND, 339	205	6.4	0.008	51.8	2.5

Sr. No.	Ground Motion Details as per SHAKE2000	Epicentral Distance (Km)	Magnitude	PGA (g)	Duration (s)	Predominant Frequency (Hz)
10	CAPE MENDOCINO EARTHQUAKE RECORD 04/25/92, MW-7.0, 90 DEG COMPONENT	10	7.1	1.03	59.98	4.44
11	CHALFANT 07/20/86 1429, BISHOP PARADISE LODGE,070	19.8	6.4	0.046	39.95	16.5
12	CHILE EARTHQUAKE, VALPARAISO RECORD, 3/3/85	129.2	7.8	0.12	79.39	2.1
13	COALINGA 05/02/83 2342 PARKFIELD, FAULT ZONE 6/ 090	43.9	6.5	0.055	39.95	0.43
14	COALINGA 05/09/83 PALMER AVE ANTICLINE RIDGE, 090	12.5	5.3	0.215	40	2.29
15	GEORGIA, USSR 06/15/91 0059, BAZ X	49	6.2	0.033	34.07	1.22
16	IMPERIAL VALLEY 10/15/79 2319, BONDS CORNER 230	15.9	5	0.1	19.88	1.41
17	KERN COUNTY 7/21/52 11:53, SANTA BARBARA COURTHOUSE 042	80.5	7.5	0.086	75.35	1.84
18	KOBE 01/16/95 2046, ABENO 000	24.9	6.9	0.22	139.98	0.26
19	KOBE 01/16/95 2046, KAKOGAWA 000	22.5	6.9	0.25	40.91	0.91
20	KOBE 01/16/95, KOBE PORT ISLAND 090	0.9	6.9	0.53	42	0.79
21	LIVERMORE 01/27/80 0233, HAYWARD CSUH STADIUM 236	33.9	5.8	0.027	15.98	3.61
22	LIVERMORE 01/27/80 0233 LIVERMORE MORGAN TERR PARK 265	20.6	5.8	0.197	24	5.61
23	LOMA PRIETA TA 10/18/89 00:05, ANDERSON DAN DOWNSTREAM 270	16.9	7	0.24	39.59	2.14
24	LOMA PRIETA TA 10/18/89 00:05, HOLLISTER DIFF ARRAY 255	13.9	7	0.27	40	1.48
25	MICHIOACAN EARTHQUAKE 19/9/85, CALETA DE CAMPOS, N-COMPONENT	38.36	8.1	0.14	81.06	1.39
26	NORTHERN CALIFORNIA 09/22/52 1141, FERNDALE 134	44.3	5.2	0.07	40	1.31
27	NORTHRIDGE EQ 1/17/94 1231, ANACAPA ISLAND	71.4	6.7	0.013	40	4.46
28	NORTHRIDGE EQ 1/17/94 1231, ARLETA 360	9.5	6.7	0.31	39.94	1.46
29	PARKFIELD 06/28/66 04:26, CHROME # 8	11.2	6.1	0.116	26.09	0.85
30	TRINIDAD 11/08/08, 10:27, RIO DEL OVERPASS E	72	7.2	0.13	22	3.14

6.5.2 1D soil model for ELGRA

In 1D GRA, it is assumed that soils respond due to SH waves through layered soil strata. In 1D ELGRA, the 1D wave propagation equation (Kramer 1996; Kumar and Mondal 2017) is solved in the frequency domain to calculate the transfer function that correlates displacements across

two different soil layers at any two depths. Soil properties required to carry out ELGRA are; ρ, G and β values, DSPC and input ground motions. Initially, low γ corresponding G and β values are assigned to each of the soil layers. Further, utilizing this set of G and β values, γ_{eff} at the center of each soil layer is calculated by LGRA. Corresponding to this obtained γ_{eff} value, a new set of G and β values for the soil layer is selected from DSPCs. The above-mentioned exercise of calculating γ_{eff} values and selecting corresponding sets of G and β values are repeated iteratively until the difference between the G values and between β values in two consecutive iterations falls within 1% of difference (Kumar and Mondal 2017).

For the present study, ELGRA are performed using the software DEEPSOILv7 (Hashash et al. 2017). Each of the 108 boreholes are modeled in DEEPSOILv7. For modeling, input parameters required for each soil layer are thickness, ρ, V_s and β. In addition, depth of ground water table is also an input parameter. It should be mentioned here that in the collected 108 boreholes mentioned above, V_s values for the layers are not available. Instead, SPT-N values based on *in-situ* measurements are available. Kumar et al. (2018) developed SPT-V_s correlations for Guwahati city based on *in-situ* values which can be used for sand, clay and for any types of soil to calculate V_s value from SPT-N value. For the present work, V_s –SPT-N correlation developed by Kumar et al. (2018) is used to convert SPT-N values in each of the 108 boreholes to V_s. Further, generic material curves by Darendeli (2001) are utilized to define the DSPCs of the soil layers. The curves proposed by Darendeli (2001) requires input parameters such as mean effective confining pressure ($\bar{\sigma}'_m$), PI, over consolidation ratio (OCR), loading frequency and number of loading cycles. Among these parameters, $\bar{\sigma}'_m$ is most influential in case of sandy soil (Darendeli 2001), which can be determined using ρ and depth of ground water table. Further, silty sands and sand layers are both modeled as sandy soils. For clayey soil on the other hand, PI

is the most important parameter while selecting DSPCs. In the borelogs considered for the present work, direct classification in terms of CI, CL, CH etc. are available for clayey soil and not actual PI values. Thus, representative PI values (based on the plasticity chart following BIS: 1498, 1970) are assumed as 5, 11, 16, 22 and 30 for CL, CL-CI, CI, CI-CH, and CH respectively. In addition, values of OCR, loading frequency and number of loading cycles (for both sandy and clayey types of soils) are taken as default values of 1.0, 1Hz, and 10 respectively in DEEPSOILv7 as suggested by Darendeli (2001).

Utilizing the above-mentioned properties, each soil layers in each of the 108 boreholes is modeled in DEEPSOILv7. The bedrock is modeled as 'rigid as it accounts for "within" type of motion. Before performing the analyses, all the earlier selected 30 ground motions are firstly included in DEEPSOILv7 database following the procedure mentioned by Hashash et al. (2017). Then each of the 30 ground motions are applied at the bottom of each of 108 boreholes (at 30 m depth). This way, a total of 3240 (108x30) ELGRA are performed under first set of analyses.

It has to be highlighted here that the present study focuses on estimating LSE_{NL} as a function of PGA_{LN} values. Instead, if AFs are expressed as a correlation of PGA_{EL}, computed AFs would correspond to standard DSPCs (Darendeli 2001 for present study) considered in the study. Consequently, the applicability of such correlations for Guwahati city would be hampered. Hence, in the second set of analyses, LGRA of the same 108 boreholes from Guwahati (which were used earlier, while performing ELGRA) is attempted using same set of 30 inputs motions, which were used to perform ELGRA. Apart from this, there is no usage of DSPCs as input in LGRA. Rest all other input parameters are kept same for carrying out LGRA as used in ELGRA early. All the 3240 (108x30) LGRA are done in DEEPSOILv7 software.

6.5.3 Analyses and results

From each of the 3240 ELGRA, value of PGA_{EL} at the top of each soil layer is observed. In addition, PGA_{LN} from LGRA at different soil layers, corresponding to each of the analysis, are also observed from the analysis outcome. Further, LSE_{NL} values are calculated based on PGA_{EL} and PGA_{LN} values for all the soil layers. It has to be highlighted here that as each of the 3240 analyses are different from each other in terms of PGA, depth from the ground surface (*h*), soil type (clay or sand) and SC, it can be considered that above-computed LSE_{NL} values obtained from the analyses are functions of PGA, *h*, soil type (clay or sand), and SC. Hence, role of each of the above parameters on the value of LSE_{NL} is assessed in the next subsection while developing the correlation.

6.5.3.1 *Development of empirical correlations*

In order to develop correlation, firstly the data is separated based on SC of borehole. To do so, firstly average SPT-N value in top 30m (N_{30}), based on SPT-N variation with depth for each borehole, is estimated. Based on N_{30} value, SC of each of the boreholes is determined following NEHRP, (2009) site classification scheme. Out of 108 boreholes considered, 54 boreholes belong to SC D and 54 boreholes belong to SC E. SC information are borehole-specific. However, within a borehole different type of soils can be present, which may control LSE_{NL} differently. To understand the effect of each soil type, analyses results which are corresponding to same SC are further segregated on the basis of soil type. This way, there are two SCs (SC D and SC E) in which 108 boreholes can be assigned. Further, based on soil types present in both SCs, there can be a total of four subgroups (SC D_clay, SC D_sand, SC E_clay and SC E_sand). In order to develop empirical correlations, variation in LSE_{NL} with PGA_{LN} and *h* under each of the above four subgroups are observed. Since 30 input ground motions are considered as inputs

for each borehole, 30 different LSE_{NL} values are obtained from the analysis at any depth in each borehole. In order to correlate such variation in LSE_{NL} value with PGA_{LN}, as a first step, a power function (following the work by Halder et al. 2019) is used .For the purpose, MATLAB command 'fit' with option 'power1' is used. The functional form is shown in Equation 6.1.

$$LSE_{NL} = aPGA_{LN}{}^{c} \quad 6.1$$

Where 'a' and 'c' are the regression coefficients. In each borehole, while change in input motion is changing LSE_{NL}, such change is also observed along the depth of the borehole. This indicates that in each of the 108 boreholes, at different depths a different value of LSE_{NL} is obtained corresponding to each of the 30 input motions. Hence, in order to account for this variation in LSE_{NL} with depth, regression coefficients 'a' and 'c' in Equation 6.1 are considered as functional form of *h*.

Since the correlations are to be determined for each of the four subgroups, to start with, variation in LSE_{NL} with PGA_{LN} for specific soil type and SC are observed at a specific depth. On careful observation of all the boreholes corresponding to SC D (or SC E), it is noted that not all the boreholes have clay/ or sand present at all depths. As a result, while developing correlation for a particular subgroup, LSE_{NL} and PGA_{LN} for same SC and same soil type are not available uniformly in all the boreholes at that depths. As a result, in case the correlation is developed considering entire dataset available, it will be biased to the depths from where more data is available in the regression. In order to minimize this biasedness of the developed correlation, any set of LSE_{NL} and PGA_{LN} are only selected in case such data is available in at least 3 boreholes belonging to same SC and soil type. Number 3 here is obtained by observing the entire dataset for a common information. Set of LSE_{NL} and PGA_{LN} from depths where it is not available in atleast 3 boreholes corresponding to same SC and soil type, are dropped from the dataset of

developing the correlation. This way, four separate datasets for four subgroups are developed. Using each of these dataset and following Equation 6.1, values of 'a' and 'c' corresponding to various depths are firstly obtained. Tables 6.3, 6.4, 6.5 and 6.6 summarize the values of regression coefficients 'a' and 'c' obtained at different depths corresponding to SC D_clay, SC D_sand, SC E_clay and SC E_sand respectively. In each of these tables, first column lists the depth parameter, second column summarizes 'a' values obtained at the respective depth from the regression analysis. Additionally, 95% confidence bound for 'a' term (as obtained from MATLAB command 'fit') are tabulated in the third column and its sub columns. Further, column

Table 6.3, Coefficients for SC D_clay

Depth (m)	a	95% confidence bound		c	95% confidence bound	
0	-0.542	-0.533	-0.552	1.177	1.164	1.190
1.5	-0.549	-0.536	-0.562	1.210	1.190	1.230
3	-0.557	-0.549	-0.565	1.253	1.239	1.267
4.5	-0.581	-0.573	-0.589	1.227	1.211	1.243
6	-0.582	-0.573	-0.590	1.214	1.194	1.233
7.5	-0.577	-0.569	-0.586	1.162	1.141	1.183
9	-0.566	-0.556	-0.575	1.139	1.117	1.162
10.5	-0.556	-0.547	-0.565	1.149	1.126	1.171
12	-0.569	-0.560	-0.578	1.143	1.119	1.168
13.5	-0.541	-0.531	-0.552	1.086	1.057	1.114
15	-0.516	-0.505	-0.527	1.073	1.041	1.105
16.5	-0.493	-0.482	-0.504	1.065	1.031	1.099
18	-0.477	-0.464	-0.490	1.071	1.031	1.110
19.5	-0.441	-0.428	-0.454	1.055	1.012	1.098
21	-0.410	-0.395	-0.425	1.003	0.951	1.055
22.5	-0.365	-0.348	-0.383	0.986	0.922	1.051
24	-0.369	-0.350	-0.389	1.093	1.016	1.170
25.5	-0.302	-0.278	-0.325	1.053	0.949	1.156
0.5	-0.561	-0.541	-0.582	1.224	1.193	1.255
27	-0.243	-0.218	-0.268	1.104	0.975	1.234
28.5	-0.096	-0.077	-0.115	0.897	0.706	1.089
1.8	-0.540	-0.512	-0.568	1.252	1.207	1.297
1	-0.537	-0.519	-0.556	1.252	1.222	1.282
0.2	-0.567	-0.535	-0.599	1.204	1.144	1.264

Table 6.4, Coefficients for SC D_sand

Depth (m)	a	95% confidence bound		c	95% confidence bound	
27	-0.143	-0.133	-0.153	0.869	0.801	0.937
28.5	-0.057	-0.052	-0.063	0.834	0.746	0.922
18	-0.488	-0.477	-0.499	1.197	1.164	1.230
19.5	-0.489	-0.479	-0.500	1.235	1.203	1.266
21	-0.431	-0.420	-0.442	1.161	1.123	1.199
22.5	-0.383	-0.372	-0.395	1.090	1.047	1.133
24	-0.308	-0.295	-0.321	1.018	0.964	1.072
25.5	-0.250	-0.237	-0.263	1.011	0.947	1.076
12	-0.512	-0.500	-0.524	1.203	1.172	1.234
13.5	-0.499	-0.487	-0.511	1.172	1.139	1.205
6	-0.549	-0.531	-0.568	1.136	1.091	1.181
7.5	-0.519	-0.500	-0.538	1.111	1.063	1.158
9	-0.525	-0.509	-0.540	1.126	1.085	1.168
10.5	-0.525	-0.510	-0.541	1.151	1.110	1.192
15	-0.492	-0.479	-0.504	1.134	1.100	1.169
16.5	-0.494	-0.482	-0.507	1.163	1.129	1.197
3	-0.564	-0.534	-0.593	1.274	1.220	1.329
4.5	-0.581	-0.550	-0.613	1.246	1.169	1.322

Table 6.5, Coefficients for SC E_clay

Depth (m)	a	95% confidence bound		c	95% confidence bound	
0	-0.575	-0.567	-0.582	1.160	1.151	1.170
1	-0.575	-0.558	-0.591	1.204	1.176	1.231
3	-0.580	-0.573	-0.588	1.195	1.178	1.212
4.5	-0.583	-0.576	-0.590	1.173	1.155	1.191
6	-0.583	-0.576	-0.590	1.147	1.128	1.165
7.5	-0.575	-0.568	-0.582	1.101	1.082	1.119
9	-0.568	-0.561	-0.575	1.084	1.065	1.103
10.5	-0.562	-0.555	-0.569	1.079	1.061	1.097
12	-0.569	-0.562	-0.576	1.055	1.036	1.073
13.5	-0.540	-0.532	-0.547	1.006	0.985	1.026
15	-0.511	-0.502	-0.520	1.015	0.990	1.040
16.5	-0.447	-0.437	-0.458	0.938	0.902	0.973
18	-0.401	-0.390	-0.412	0.894	0.855	0.933
19.5	-0.357	-0.346	-0.367	0.881	0.844	0.919
24	-0.275	-0.257	-0.293	0.861	0.785	0.936
25.5	-0.161	-0.143	-0.178	0.707	0.610	0.804
27	-0.134	-0.116	-0.153	0.795	0.673	0.918
21	-0.348	-0.335	-0.362	0.909	0.860	0.958
22.5	-0.290	-0.274	-0.306	0.872	0.806	0.938
1.5	-0.580	-0.568	-0.592	1.209	1.187	1.231
0.3	-0.585	-0.562	-0.608	1.207	1.158	1.257
0.5	-0.547	-0.513	-0.582	1.272	1.206	1.339

Table 6.6, Coefficients for SC E_sand

Depth (m)	a	95% confidence bound		c	95% confidence bound	
21	-0.330	-0.343	-0.318	0.977	0.926	1.028
22.5	-0.297	-0.312	-0.283	0.939	0.878	1.001
27	-0.073	-0.083	-0.064	0.682	0.581	0.783
6	-0.571	-0.593	-0.549	1.087	1.022	1.153
7.5	-0.543	-0.565	-0.521	1.004	0.943	1.064
24	-0.217	-0.231	-0.203	0.885	0.812	0.959
25.5	-0.156	-0.171	-0.142	0.818	0.729	0.907
15	-0.403	-0.421	-0.386	1.069	1.008	1.131
16.5	-0.383	-0.402	-0.365	1.059	0.990	1.128
9	-0.538	-0.562	-0.514	1.157	1.099	1.214
10.5	-0.475	-0.500	-0.449	1.143	1.081	1.205
12	-0.448	-0.465	-0.432	1.223	1.182	1.265
13.5	-0.443	-0.460	-0.427	1.182	1.134	1.230
18	-0.410	-0.426	-0.393	1.120	1.061	1.179
19.5	-0.417	-0.433	-0.400	1.161	1.102	1.219

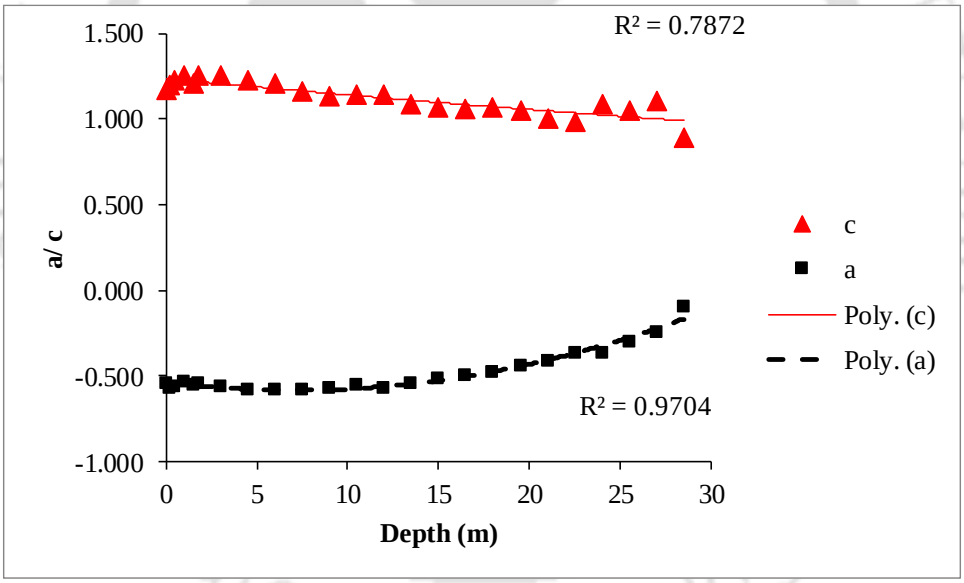

Figure 6.1, a and c values for SC D_clay

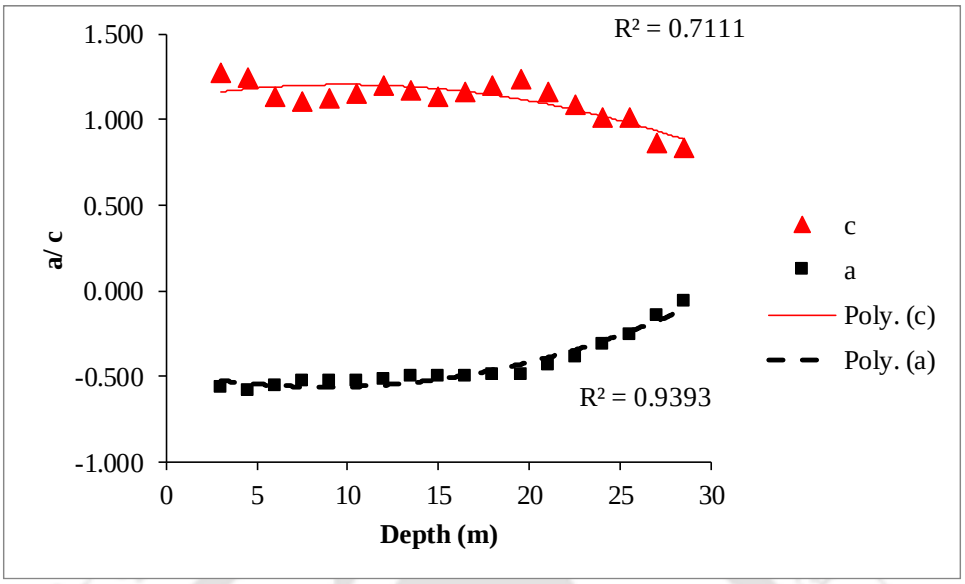

Figure 6.2, a and c values for SC D_sand

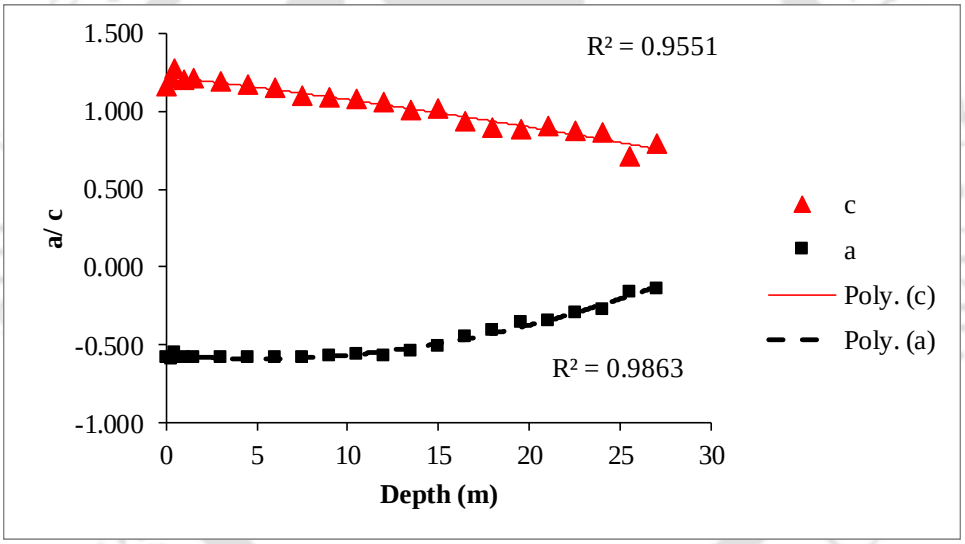

Figure 6.3, a and c values for SC E_clay

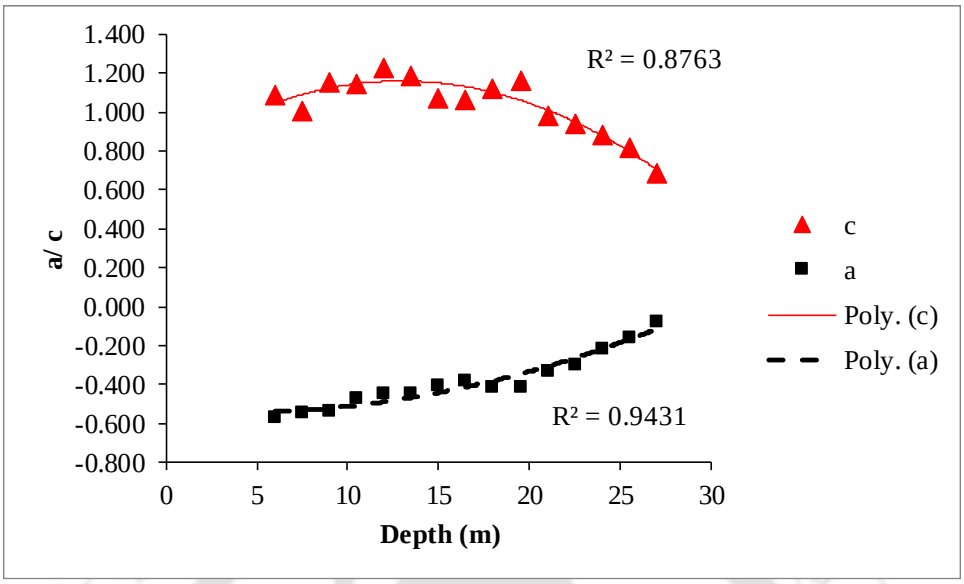

Figure 6.4, a and c values for SC E_sand

4 summarizes values of coefficient 'c' at different depths and, the fifth column and its sub columns present 95% confidence bounds in 'c' term.

From Tables 6.3 and Table 6.5, it can be observed that the values of regression coefficients "a" and "c" are obtained considering data from the entire 30m depth of the borehole. For sandy soil however, the values of regression coefficients "a" and "c" are obtained based on the data after 3m depth for SC D and after 6m depth for SC E respectively (see Table 6.4 and Table 6.6 respectively). Above observation clearly indicates that sandy soil is not present in abundance in depths less than 3m. Based on the regression analysis done so far, using values of "a" and "c" at specific *h* (as summarized in Table 6.3-6.6) and for known value of PGA_{LN}, LSE_{NL} value can be determined. However, in order to develop a generalize correlation within a particular subgroup, which can be used to calculate LSE_{NL} values at any *h* and any PGA_{LN} value, a second set of regression analyses (for each of the four dataset developed earlier) need to be carried out. To do so, "a" values and "c" values from each of the Tables 6.3 to 6.6 are plotted against *h* as shown in Figure 6.1, Figure 6.2, Figure 6.3 and Figure 6.4 respectively. Trend lines representing best fit curve to the plotted parameters are also shown in Figure 6.1, Figure 6.2,

Figure 6.3 and Figure 6.4 following polynomial function. It has to be highlighted here that the maximum order of polynomial functions is kept as 2 wherever required, otherwise, linear fitting is used. Replacing, "a" and "c" coefficients in Equation 6.1 for each subgroups by the functional forms obtained from Figure 6.1, Figure 6.2, Figure 6.3 and Figure 6.4 the final correlations obtained are as follow;

For SC D_clay

$$LSE_{NL} = (0.0009h^2 - 0.0127h - 0.5374)PGA_{LN}^{(-0.0087h+1.2338)} \quad 6.2$$

For SC D_sand

$$LSE_{NL} = (0.0012h^2 - 0.0204h - 0.4708)PGA_{LN}^{(-0.0009h^2+0.0178h+1.119)} \quad 6.3$$

For SC E_clay

$$LSE_{NL} = (0.001h^2 - 0.0095h + -0.5657)PGA_{LN}^{(-0.017h+1.2341)} \quad 6.4$$

For SC E_sand

$$LSE_{NL} = (0.0008h^2 - 0.0055h - 0.535)PGA_{LN}^{(-0.0023h^2+0.06h+0.7707)} \quad 6.5$$

6.6 Validation

In the last section, 4 empirical correlations are developed based on which the value of LSE_{NL} (for known value of PGA_{LN} and h) can be determined. In this section, validation of above obtained LSE_{NL} (based on the correlations) is done by comparing with results obtained from ELGRA and LGRA. For this purpose, 51 additional boreholes (23 from SC D and 28 from SC E groups) are considered. Further, both ELGRA and LGRA are conducted on these 51 boreholes. It has to be mentioned here that these 51 boreholes are not considered in the initial analyses while developing earlier mentioned correlations. Since the overall goal of the present study is to develop correlations based on which LSE can be estimated directly without performing GRA, in

order to check if proposed correlations are dependent on selected DSPC's or not, a different set of DSPCs (other than those used in ELGRA earlier) are considered to perform ELGRA. Table 6.7 summarizes different DSPCs used in this section. Further, all the ELGRA and LGRA are performed on all these 51 boreholes using the MATLAB code developed by Kumar and Mondal (2017). Firstly, for a specific borehole, the values of LSE_{NL} (for known SC, soil type, and known values of PGA_{LN} and *h*) are estimated from respective proposed correlation. Secondly, the computed LSE_{NL} values are added with the respective PGA_{LN} values to simulate PGA_{EL} values. In order to check the suitability of the proposed correlations to compute LSE_{NL} values, these estimated PGA_{EL} values are compared with PGA_{EL} values obtained from ELGRA done in this section. The difference between the two PGA_{EL} values (one estimated based on correlation and other based on ELGRA) is estimated and the percentage error with respect to PGA_{EL} values obtained from ELGRA is calculated. It has to be highlighted here that –ve percentage error indicates over estimation of PGA_{EL} values with respect to PGA_{EL} values obtained based on ELGRA and +ve percentage error indicates under estimation of PGA_{EL} values with respect to PGA_{EL} values obtained from ELGRA. Figures 6.5 to 6.9 present histograms of frequency versus percentage error plots. Additionally, corresponding cumulative frequency of percentage error is also presented on second y-axis in Figures 6.5 to 6.9. The details of the histograms are shown in tabular form in Tables 6.8 to 6.11 for SC D_clay, SC D_sand, SC E_clay and SC E_sand respectively. It can be seen from Figures 6.5 to 6.9 and Tables 6.8 to 6.11 collectively that the proposed correlations (Equation 6.2-6.5) in most of the cases under-estimate (more number of +ve errors than –ve errors) PGA_{EL} values compared to PGA_{EL} values obtained from ELGRA.

Table 6.7, DSPCs used for ELGRA

Material_type1	Sand (avg) Seed and Idriss (1970)
	Sand (avg) Seed and Idriss(1970)
Material_type2	Clay PI=1-10, Sun et al. (1988)
	SOIL, PI=0, OCR=1-8
Material_type3	Clay PI=1-10, Sun et al. (1988)
	SOIL, PI=0, OCR=1-8
Material_type4	Clay PI=10-20, Sun et al. (1988)
	SOIL, PI=15, OCR=1-8
Material_type5	clay PI=20=40, Sun et al. (1988)
	SOIL, PI=30, OCR=1-8
Material_type6	Clay (upper) Sun et al. (1988)
	SOIL, PI=50, OCR=1-8
Material_type7	Rock Schnabel (1973)
	Rock, Schnabel (1973)

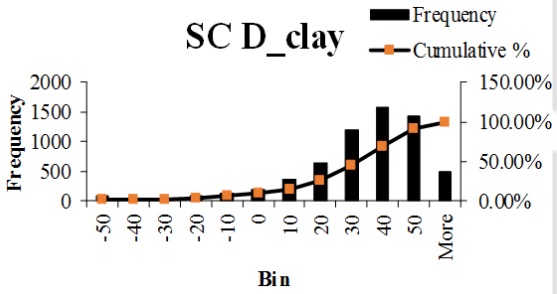

Figure 6.5, Histogram SC D_clay

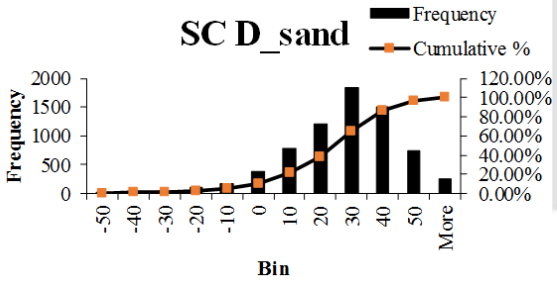

Figure 6.6, Histogram SC D_sand

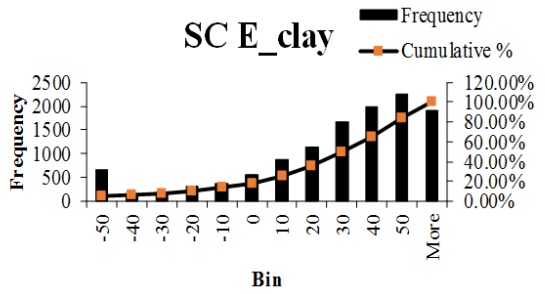

Figure 6.7, Histogram SC E_clay

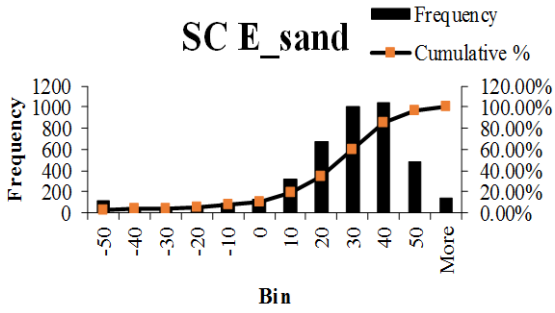

Figure 6.8, Histogram SC E_sand

Table 6.8, SC D_clay Histogram

Bin	*Frequency*	*Cumulative %*
-50	90	1.42%
-40	41	2.07%
-30	50	2.86%
-20	88	4.25%
-10	136	6.40%
0	207	9.67%
10	360	15.36%
20	650	25.62%
30	1202	44.61%
40	1586	69.67%
50	1431	92.27%
More	489	100.00%

Table 6.9, SC D_sand Histogram

Bin	*Frequency*	*Cumulative %*
-50	32	0.45%
-40	19	0.72%
-30	45	1.36%
-20	105	2.84%
-10	172	5.27%
0	373	10.54%
10	785	21.62%
20	1200	38.57%
30	1847	64.66%
40	1512	86.02%
50	733	96.37%
More	257	100.00%

Table 6.10, SC E_clay Histogram

Bin	*Frequency*	*Cumulative %*
-50	673	5.59%
-40	124	6.63%
-30	186	8.17%
-20	324	10.86%
-10	359	13.85%
0	558	18.49%
10	876	25.77%
20	1134	35.20%
30	1672	49.09%
40	1974	65.50%
50	2254	84.24%
More	1896	100.00%

Table 6.11, SC E_sand Histogram

Bin	*Frequency*	*Cumulative %*
-50	116	2.84%
-40	25	3.46%
-30	26	4.09%
-20	56	5.47%
-10	88	7.62%
0	129	10.78%
10	316	18.53%
20	668	34.90%
30	999	59.39%
40	1040	84.88%
50	482	96.69%
More	135	100.00%

a Another important observation, which can be made from Figures 6.5 to 6.9 and Tables 6.8 to 6.11 is that within the percentage error band of -50% to +50%, the cumulative frequency of percentage error values are 90%, 96%, 78% and, 93%, respectively for subgroups SC D_clay, SC D_sand, SC E_clay and, SC E_sand respectively. Above observations clearly highlight that the correlations developed in this chapter are able to predict LSE_{NL} very well. These correlations can be further used to determine PGA_{EL} values based on LGRA for any borehole that consists of sandy and clayey type of soils and for SC D or SC E.

6.7 Conclusions

Though DSPCs are one of the most important input parameters that control the outcome of a GRA study, use of different DSPCs for same site can assess LSE differently. Secondly, performing site-specific GRA for project specific locations will be needing input motions as well as DSPCs of the soil, which many a times are not available. In the light of above challenges, an attempt is made in this chapter to propose empirical correlations which can assess LSE directly. For this purpose, ELGRA are carried out considering 108 boreholes and 30 globally recorded ground motions. Further, the same set of boreholes and ground motions are utilized to perform LGRA. Based on the PGA_{LN} and PGA_{EL} values obtained from LGRA and ELGRA, respectively, four correlations that can estimate LSE_{NL}values based on PGA_{LN} and *h* are proposed for four subgroups SC D_clay, SC D_sand, SC E_clay and, SC E_sand respectively. These correlations can be used along with PGA_{LN} values obtained from LGRA to estimate PGA_{EL} values. Further, the correlations are validated using 51 boreholes which were not used for the development of correlations. Both ELGRA and LGRA are performed on these 51 boreholes using the earlier mentioned set of 30 ground motions. It has to be noted here that for performing ELGRA, a different set of DSPCs is used. Further, based on the proposed correlations and PGA_{LN} values obtained from LGRA, LSE_{NL} values and subsequently PGA_{EL} values are estimated. It is found that the error percentages in estimating PGA_{EL} values are mostly limited from -50% to 50%. Since a different set of DSPCs is employed for the validation, it can be said that the correlations are able to predict PGA_{EL} values accurately irrespective of DSPCs used.

Proposed correlations in this chapter will help to estimate PGA values for different SCs and soil types for Guwahati city based on LGRA, even without using any DSPCs and complete input motion.

CHAPTER 7: CONCLUSIONS AND FUTURE SCOPE

In this thesis, three sets of new frequency domain based methodologies are developed which can be utilized to back-compute DSPCs from downhole array records. Further, proposed IGRA methodologies are first applied to determine DSPCs for the surficial layer. Later, a uniform IGRA methodology is proposed which can be applied to determine DSPCs for multiple soil layer system. Proposed methodologies are validated using EQ records obtained from Lotung downhole array and IWTH27 downhole array. Additional validation is done by utilizing EQ data obtained from a previously conducted GRA study for a typical site in Delhi.

In case, for a site, DSPCs are not available based on laboratory work as well as downhole array based EQ records, an alternative approach is presented in this thesis that can be utilized to determine LSE even without using DSPCs. For the purpose, correlations are proposed for different SCs and soil types that can determine LSE from results obtained based on LGRA study. Collectively, important conclusions which have come out from this thesis are summarized below.

- DSPCs for Lotung site are determined for the surficial layer based on proposed frequency domain IGRA methodology. The G/G_{max} values and β values back-calculated based on the proposed IGRA methodology are consistent with the previously published literature.
- β values are also determined for the surficial layer at the Lotung site. It is to be noted that an exact solution to determine β values in frequency domain is proposed in the present thesis was absent in any existing literature.
- DSPCs for IWTH27 site are back-computed based on available EQ records at the ground surface and at 100m depth. It is to noted that previous IGRA methodologies could determine DSPCs for soil layers perched between two consecutive accelerometers. It has

to be highlighted that such soil layers located between two consecutive accelerometers can consists of different soil types. Earlier methodologies failed to identify DSPCs for such individual soil types. Proposed methodology however determines DSPCs for the surficial fill layer only in spite of presence of 25 different layers located between two consecutive accelerometers at the IWTH27 site.

- Proposed DSPCs for the IWTH27 site are validated by performing ELGRA considering additional ground motions that are not used for IGRA. It is observed that the proposed DSPCs for the IWTH27 site is better suited than standard DSPCs in reproducing the recorded ground motions at the ground surface. Above observation also highlights the importance of considering site specific DSPCs for performing GRA.
- A uniform frequency domain IGRA methodology is proposed that can be utilized to determine DSPCs for multiple number of soil layers. The proposed methodology is applied to determine DSPCs for top three soil layers located between top four accelerometers at Lotung. Later, the methodology is applied to EQ records obtained from a previously conducted GRA study for Delhi region to determine DSPCs for top five soil layers. In both the cases, the proposed IGRA methodology yielded DSPCs that are consistent with earlier published literature. Above observation highlights that the proposed methodology can be applied to any site and for any number of soil layers.
- DSPCs proposed for the Lotung site in this thesis are validated by conducting ELGRA using ground motions that are not used for IGRA study. It is observed that soil responses obtained based on ELGRA study are consistent with actual soil responses based on recorded ground motions.

- Four correlations which can estimate LSE_N values based on PGA_{LN} and H are proposed for four subgroups SC D_clay, SC D_sand, SC E_clay and, SC E_sand respectively based on detailed ELGRA study conducted on 108 boreholes from Guwahati, India. These correlations can be used along with PGA_{LN} values obtained from LGRA to estimate PGA_{EL} values.
- The correlations are validated using 51 boreholes that were not used for the development of correlations. It is found that the error percentages in estimating PGA_{EL} values are mostly within ±50%.
- Such findings will help to estimate PGA values for different SCs and soil types for Guwahati city based on LGRA, even without using any DSPCs.

7.1 Major contributions of the present thesis

Summarizing, the present thesis provides a thorough investigation of frequency domain IGRA methodologies. The major contributions from the thesis are following

- Determination of β values for the surficial layer based on frequency domain IGRA.
- Determination of DSPCs for the surficial layer when EQ records are available at the ground surface and at a great depth.
- Determination of DSPCs for multi-layered soil system based on frequency domain IGRA.
- Estimation of LSE based on LGRA when site specific DSPCs are not available.

7.2 Limitation of the present study

- The proposed frequency domain IGRA methodology is based on the assumption of vertically propagating 1D SH wave. Thus, in case of 2D/ 3D wave propagation the proposed methodology is inadequate.

- The proposed IGRA methodology is based on total stress analysis and thus it doesn't take into account nonlinear soil properties due to generation and dissipation of excess pore water pressure
- The proposed IGRA methodology for multiple layered system is based on the assumption that soil density is uniform in all the soil layers involved.
- The correlations proposed for determination of LSE based on LGRA results provide a wider range of error values (-50% to 50%)

7.3 Future scope of the study

- The proposed IGRA methodology can be modified in future to determine DSPCs for different soil types located between consecutive accelerometers.
- Proposed IGRA framework can be applied to multiple layered system where soil density is not uniform in different layers. For the purpose, study by Vijayendra et al. (2010) can be referred to.

7.4 Practical significance of the work

In this thesis, various IGRA methodologies that were carried out on global downhole arrays are discussed. However, downhole arrays are limited in numbers. Further, EQ data from such downhole arrays are not always accessible. Thus, the practical application of the work conducted in this thesis may seem hindered.

It has to be noted that a few of IGRA methodologies discussed above were subsequently utilized for the determination of DSPC based on dynamic centrifuge testing (DCT). Such DCT facilities were first introduced at the Rensselaer Polytechnic Institute in New York and the University of California at Davis. Later, other DCT facilities were incorporated into University

of Cambridge, French Institute of Science and Technology for Transport Development and Networks, University of Dundee (Scotland), and many more places in Japan, Istanbul, China, etc. A brief overview of various IGRA studies based on DCT is given below.

Brennan et al. (2005) modeled a dry sand layer, a saturated sand layer, soft clay layer, and a model waste layer separately in the DCT facility at University of Cambridge. Based on DCT, DSPCs were back-computed individually for all the above mentioned soil layers. In another IGRA study, Afacan et al. (2014) modeled a NC clay layer resting over a OC clay layer in the DCT at University of California at Davis. In this study also, DSPCs were back computed for both OC clay and NC clay. Based on the test results, the β values were found to be scattered. Afacan et al. (2014) advocated for the use of hinge plate containers over flexible shear beam containers in case of DCT. According to Afacan et al. (2014), hinge plate containers could represent the 1D wave propagation more precisely than flexible shear beam containers. In a separate IGRA study, Li et al. (2013) modeled a sand layer made of Fontainebleau sand in the DCT facility at the French Institute of Science and Technology for Transport Development and Networks. Based on the analysis, Li et al. (2013) back computed DSPCs at different depths for Fontainebleau sand. In another IGRA study, Wang and Brennan (2019) modeled fibre-reinforced sand in the DCT facility at the University of Dundee, Scotland. Based on their study, DSPCs were back computed for several depths in the fiber-reinforced sand layer. It is to be noted here that the above IGRA studies adopted time domain IGRA methodology given by Zeghal et al. (1995) and implemented in DCT in their studies. On the other hand, a different study performed by Conti and Viggiani (2012) utilized a frequency domain least square optimization technique to back compute DSPCs for a sand layer modeled in the DCT facility at the University of Cambridge. It has to be highlighted here that the frequency domain methodology adopted by

Conti and Viggiani (2012) was originally proposed by Carvajal-Uribe et al. (2001). In that study, DSPCs were back computed for different depths in the sand layer. However, the back computed β values were scattered in that study as admitted by Conti and Viggiani (2012).

Above discussion highlights that most of the IGRA methodologies that were performed using DCT, were restricted to be used for single soil type. Further, the IGRA study by Conti and Viggiani (2012) could not back compute β values consistently based on frequency domain IGRA methodology. Thus, two research gaps are identified based on the literature on IGRA methodology following DCT discussed above,

1. Modeling of multiple soil layers in DCT and subsequent application of IGRA methodology
2. Determination β values in frequency domain that are consistent with published literature

IGRA methodologies based on seismic downhole array records have shown reasonable accuracy in estimating DSPCs and representing actual site conditions. However, such downhole arrays are very few in number worldwide. Installing downhole arrays and keeping them in active condition requires expertise and a lot of funding as well. Further, there may be significant time gaps between the occurrences of EQ. Thus, data acquisition in downhole arrays is a slow procedure. Therefore, there is an ambiguity at present in applying IGRA methodologies directly on downhole array records. However, if the circumstances of a downhole array during an EQ shaking can be modeled in laboratory experiments, invaluable information can be collected. Several attempts toward above mentioned objective have already been taken (as highlighted in the last section) based on DCT modeling. Although, installation of DCT facility itself is a costly procedure, input-output data sets for IGRA can be generated from DCT without any hindrance. Previous DCT based IGRA methodologies were restricted to be used for single soil type/ soil

layer. However, a number of DCT based forward GRA studies (Ghosh and Madabhushi 2004; Krstelj and Prevost 1992; Rayhani and El Naggar 2007) have modeled layered soil deposits for analysis as well. Therefore, it is possible to model a multi layered soil deposit in DCT for IGRA purpose. On the other hand, if a frequency domain IGRA methodology can be developed for multi-layered soil profile, that can eliminate both the research gaps highlighted above.

LIST OF PUBLICATIONS

Conferences

- Halder, S., J. K. Mondal, and A. Kumar. "Empirical correlations for strain dependent linear 1D ground response analysis for Guwahati, India based on detailed analyses." *Earthquake Geotechnical Engineering for Protection and Development of Environment and Constructions*. CRC Press, 2019. 2779-2786.

- Harinarayan, N. H., Joy Kumar Mondal, and Abhishek Kumar. "Establishing Seismic Site Class for 4 Recording Stations in Uttarakhand Based on Generalized Inversion and 1-D Equivalent Linear Site-Specific Response Analysis." *Proceedings of the Indian Geotechnical Conference 2019*. Springer, Singapore, 2021.

- Mondal, J. K., N. H. Harinarayan, and A. Kumar. 2020. "Correlation between soil amplification and recorded ground motions for typical locations in Uttarakhand" *Proceeding 17th World Conf. Earthq. Eng.*, 1–12. Sendai.

- *Borah, N., Mondal JK & Kumar, A. (2021) Determination of Site Specific Response Spectra for Site Class D and E for Guwahati city, NE India Region. IGC 2021, NIT Trichy.*

Journals

- Mondal, Joy Kumar, and Abhishek Kumar. "A Systematic Review on Inverse GRA Methodologies Developed for the Determination of Dynamic Soil Properties Using Downhole Seismic Array Records." *Indian Geotechnical Journal* (2021): 1-16.

- Mondal, Joy K., and Abhishek Kumar. "New Frequency Domain–Based Inverse Ground Response Analysis Framework for the Determination of Dynamic Soil Properties." *International Journal of Geomechanics* (**ASCE**) 21.5 (2021): 04021058.

- Mondal, Joy K., and Abhishek Kumar . "A new framework of inverse ground response analysis for the determination of dynamic soil properties of two-layered system." *International Journal of Geomechanics* (**ASCE**, **accepted)**

- Mondal, Joy K., and Abhishek Kumar. "A new framework of inverse ground response analysis for the determination of dynamic soil properties of multi-layered system." (**under review**), Indian Geotechnical Journal

- Mondal, Joy K., and Abhishek Kumar. "Quantification of local site effects due to nonlinear soil behavior" (**under preparation**)

REFERENCES

1. (EPRI), E. P. R. I. 1993. *Guidelines for Site specific ground motions.* Palo Alto, California:
2. Abdel-Ghaffar, A. M., and R. F. Scott. 1979. “Shear moduli and damping factors of earth dam.” *J. Geotech. Eng. Div.*, 105 (12): 1405–1426. American Society of Civil Engineers.
3. Abdirad, H., and C. S. Dossick. 2016. “BIM curriculum design in architecture, engineering, and construction education: A systematic review.” *J. Inf. Technol. Constr.*, 21 (May): 250–271.
4. Afacan, K. B., S. J. Brandenberg, and J. P. Stewart. 2014. “Centrifuge Modeling Studies of Site Response in Soft Clay over Wide Strain Range.” *J. Geotech. Geoenvironmental Eng.*, 140 (2). https://doi.org/10.1061/(asce)gt.1943-5606.0001014.
5. Ameri, G., A. Oth, M. Pilz, D. Bindi, S. Parolai, L. Luzi, and G. Cultrera. 2011. “Separation of source and site effects by generalized inversiontechnique using the aftershock recordings of the 2009 L’Aquila earthquake.” *Bull. Earthq. Eng.*, 9 (3): 717–739.
6. Anbazhagan, P., A. Prabhakaran, H. Madhura, S. S. R. Moustafa, and N. S. N. Al-Arifi. 2017. “Selection of representative shear modulus reduction and damping curves for rock, gravel and sand sites from the KiK-Net downhole array.” *Nat. Hazards*, 88 (3): 1741–1768. Springer Netherlands. https://doi.org/10.1007/s11069-017-2944-x.
7. Anbazhagan, P., T. G. Sitharam, and C. Divya. 2007. “Site response analysis based on site specific soil properties using geotechnical and geophysicla tests: Correlation between Gmax and N60.” *4 Int. Conf. Earthq. Geo. Eng.*, (1286): 12.
8. Anderson, D. G., and Y. K. Tang. 1989. *Summary of soil character- ization program for the Lotung large-scale seismic experiment*. Vol. 2, Rep. No. NP-6I54, Electric Power Research Institute, Palo Alto, Calif.
9. Archuleta, B. Y. R. J., H. Seale, P. V Sangas, L. M. Baker, S. T. Swain, S. D. Glaser, L. G. Baise, S. D. Glaser, T. Sugano, I. A. Beresnev, Kuo-Liang Wen, C. H. Chen, L. Y. Chen, H. C. Chiu, T. Katayama, F. Yamazaki, S. Nagata, L. Lu, T. Turker, I. Oweis, A. Urzua, R. Dobry, S. D. Glaser, V. R. Gunturi, A. W. M. Elgamal, H. T. Tang, A. . Fallis, H. KAWASE, T. SATOH, K. FUKUTAKE, K. IRIKURA, M. Zeghal, A. W. M. Elgamal, R. J. Archuleta, J. H. Steidl, and L. F. Bonilla. 2000a. “Consistency of ground-

motion estimates made using system identification." *J. Struct. Constr. Eng. (Transactions AIJ)*, 61 (4): 993–1009. https://doi.org/10.1017/CBO9781107415324.004.

10. Archuleta, R. J., and S. H. Hartzell. 1981. "Effects of fault finiteness on near-source ground motion." *Bull. Seismol. Soc. Am.*, 71 (4): 939–957. The Seismological Society of America.
11. Archuleta, R. J., J. H. Steidl, and L. F. Bonilla. 2000b. "Engineering insights from data recorded on vertical arrays." *Proc. 12th World Conf. Earthq. Eng.*, 1–7.
12. Baise, L. G., and S. D. Glaser. 2000. "Consistency of ground-motion estimates made using system identification." *Bull. Seismol. Soc. Am.*, 90 (4): 993–1009. https://doi.org/10.1785/0119980169.
13. Bajaj, K., and P. Anbazhagan. 2019. "Identification of Shear Modulus Reduction and Damping Curve for Deep and Shallow Sites: Kik-Net Data." *J. Earthq. Eng.*, 0 (0): 1–29. Taylor & Francis. https://doi.org/10.1080/13632469.2019.1643807.
14. Banerjee, S., and A. Kumar. 2018. "Determination of seismic wave attenuation in Delhi , India , towards quantification of regional seismic hazard American Standard Code for Information Interchange." *Nat. Hazards*, 92 (2): 1039–1064. Springer Netherlands. https://doi.org/10.1007/s11069-018-3238-7.
15. Baro, O., A. Kumar, and A. Ismail-zadeh. 2018. "Seismic hazard assessment of the Shillong Plateau , India." *Geomatics, Nat. Hazards Risk*, 9 (1): 841–861. Taylor & Francis. https://doi.org/10.1080/19475705.2018.1494043.
16. Basu, D., M. Boga, and A. Dey. 2019. "A time-domain nonlinear effective-stress non-Masing approach of ground response analysis of Guwahati city , India" *Earthquake Engineering and Engineering Vibration* 18 (2019): 61-75.
17. Basu, D., and A. Dey. 2017. "1D NONLINEAR GROUND RESPONSE ANALYSIS OF SOILS IN IIT." *16th World Conference on Earthquake, 16WCEE*. 2017.
18. Bayat, M., and A. Ghalandarzadeh. 2020. "Modified Models for Predicting Dynamic Properties of Granular Soil under Anisotropic Consolidation." *Int. J. Geomech.*, 20 (3): 1–15. https://doi.org/10.1061/(ASCE)GM.1943-5622.0001607.
19. Bazzurro, P., C. A. Cornell, N. Shome, and J. E. Carballo. 1998. "Three proposal for characterizing MDOF nonlinear seismic response." *J Struct Eng*, 124 (11): 1281–1289.
20. Beresnev, I. A., and K.-L. Wen. 1996. "Nonlinear soil response—A reality?" *Bull.*

Seismol. Soc. Am., 86 (6): 1964–1978. The Seismological Society of America.

21. Besrat, E. A., W. Asrat, and T. Getnet, M. Wassie Habtesellasie Genet. 2018. "Ground Response Analysis of Representative Sites of Hawassa City." *Geotech. Earthq. Eng. Soil Dyn. V Seism. Hazard Anal. Earthq. Gr. Motions, Reg. Assess.*, M. Brandenberg SC, and Manzari, ed., 422–434.
22. Bindi, D., F. Pacor, L. Luzi, M. Massa, and G. Ameri. 2009. "The M w 6.3, 2009 L'Aquila earthquake: source, path and site effects from spectral analysis of strong motion data." *Geophys. J. Int.*, 179 (3): 1573–1579.
23. BIS, I. S. 1970. "1498 Classification and identification of soils for general engineering purposes." *Methods test soils*.
24. Bonilla, L. F., R. J. Archuleta, and D. Lavallée. 2005. "Hysteretic and dilatant behavior of cohesionless soils and their effects on nonlinear site response: Field data observations and modeling." *Bull. Seismol. Soc. Am.*, 95 (6): 2373–2395. Seismological Society of America.
25. Bonilla, L. F., F. Cotton, and R. J. Archuleta. 2003. "Quelques renseignements sur les effets de site non-lin{é}aires en utilisant des donn{é}es de forage: la base de mouvements forts Kik-net au Japon." *VIe Colloq. Natl. AFPS, Ec. Polytech., Palaiseau, Fr.*
26. Boore, D. M. 2007. *Some thoughts on relating density to velocity. available http//www.ce.memphis.edu/7137/PDFs/Boore/daves_notes_on_relating_density_to_velocity_v1.2.pdf (last accessed Sept. 2019)*. available at http://www.ce.memphis.edu/7137/PDFs/Boore/daves_notes_on_relating_density_to_velocity_v1.2.pdf (last accessed September 2019).
27. Boore, D. M., and J. J. Bommer. 2005. "Processing of strong-motion accelerograms: Needs, options and consequences." *Soil Dyn. Earthq. Eng.*, 25 (2): 93–115. https://doi.org/10.1016/j.soildyn.2004.10.007.
28. Brennan, A. J., N. I. Thusyanthan, and S. P. Madabhushi. 2005. "Evaluation of Shear Modulus and Damping in Dynamic Centrifuge Tests." *J. Geotech. Geoenvironmental Eng.*, 131 (12): 1488–1497. https://doi.org/10.1061/(asce)1090-0241(2005)131:12(1488).
29. BSSC. 2009. *NEHRP recommended seismic provisions for new buildings and other structures (fema p-750)*. Washington, DC.

30. Carlton, B., and K. Tokimatsu. 2015. “Comparison of equivalent linear and nonlinear site response analysis results and model to estimate maximum shear strain.” *Earthq. Spectra*, 32 (3): 1867–1887.
31. Carvajal-Uribe, J. C., V. M. Taboada-Urtuzuastegui, and M. P. Romo. 2001. “Identification of dynamic properties of Mexico City clay in the frequency domain using downhole records.” *Int. Conf. soil Mech. Geotech. Eng.*, 381–384.
32. Chandra, J., P. Guéguen, J. H. Steidl, and L. F. Bonilla. 2015. “In situ assessment of the g–γ curve for characterizing the nonlinear response of soil: Application to the garner valley downhole array and the wildlife liquefaction array.” *Bull. Seismol. Soc. Am.*, 105 (2): 993–1010. https://doi.org/10.1785/0120140209.
33. Chang, C.-Y., M. S. Power, Y. K. Tang, and C. M. Mok. 1989. “Evidence of nonlinear soil response during a moderate earthquake.” *Congr{è}s intrnational m{é}canique des sols des Trav. Fond. 12*, 1927–1930.
34. Chang, C., Y. K. Tang, C. M. Mok, H. T. Tang, and M. S. Power. 1991a. “Development of Shear Modulus Reduction Curves Based on Lotung Downhole Ground Motion Data.” *1991 - Second Int. Conf. Recent Adv. Geotech. Earthq. Eng. Soil Dyn.*, 16 (1): 44.
35. Chang, C. Y., C. M. Mok, A. Memebers, and H. T. Tang. 1996. “Inference of Dynamic Shear Modulus From Lotung downhole data.” *J. Geotech. Eng.*, 122 (8): 657–665.
36. Chang, C. Y., C. M. Mok, and M. S. Power. 1991b. *Analysis of ground response data at Lotung large-scale soil- structure interaction experiment site. Final report*. *No. EPRI-NP-7306-M. Electric Power Research Inst., Palo Alto, CA (United States); Geomatrix Consultants, Inc., San Francisco, CA (United States), 1991*.
37. CNDM. 2002. *Scenario of Seismic Hazard in Assam*. report by Centre for Natural Disaster Management, Assam Administrative Staff Office.
38. Conti, R., and G. M. B. Viggiani. 2012. “Evaluation of soil dynamic properties in centrifuge tests.” *J. Geotech. Geoenvironmental Eng.*, 138 (7): 850–859. https://doi.org/10.1061/(ASCE)GT.1943-5606.0000659.
39. Darendeli, M. B. 2001. “Development of a new family of normalized modulus reduction and material damping curves.” University of Texas at Austin, Austin, Texas.
40. Denyer, D., and D. Tranfield. 2009. “Producing a Systematic Review.” *Sage Handb. Organ. Res. Methods*. London: Sage Publications.

41. Deodatis, D. 1996. “Non-stationary stochastic vector processes: seismic ground motion applications.” *probabilistic Eng. Mech.*, 11: 145–168.
42. Elgamal, A.-W. 1992. “Analysis of wildlife site liquefaction during the 1987 Superstition Hills Earthquake.” *Proc. 4th US-Japan Work. Earthq. Resist. Des. Lifeline Facil. Countermeas. against S*, 87–96.
43. Elgamal, A.-W., M. Zeghal, E. Parra, R. Gunturi, H. T. Tang, and J. C. Stepp. 1996. “Identification and modeling of earthquake ground response﷼I. Site amplification.” *Soil Dyn. Earthq. Eng.*, 15 (8): 499–522. Elsevier.
44. Elgamal, A., T. Lai, Z. Yang, L. He, and S. Ed. Prakash. 2001. “Dynamic soil properties, seismic downhole arrays and applications in practice (CD-ROM).” *Proc. Forth Int. Conf. Recent Adv. Geotech. Earthq. Eng. Soil Dyn.*, 26–31.
45. Elgamal, A. W., M. Zeghal, H. T. Tang, and J. C. Stepp. 1995. “Lotung downhole array. I: Evaluation of site dynamic properties.” *J. Geotech. Eng.*, 121 (4): 350–362. https://doi.org/10.1061/(ASCE)0733-9410(1995)121:4(350).
46. Eseller-Bayat, E. E., and M. Ada. 2019. “A methodology for estimation of site-specific nonlinear dynamic soil behaviour using vertical downhole arrays.” *Eur. J. Environ. Civ. Eng.*, 0 (0): 1–23. Taylor & Francis. https://doi.org/10.1080/19648189.2019.1603122.
47. Field, E. H., P. A. Johnson, I. A. Beresnev, and Y. Zeng. 1997. “Nonlinear ground-motion amplification by sediments during the 1994 Northridge earthquake.” *Nature*, 390 (6660): 599–602. Nature Publishing Group.
48. Frankel, A. D., D. L. Carver, and R. A. Williams. 2002. “Nonlinear and linear site response and basin effects in Seattle for the M 6.8 Nisqually, Washington, earthquake.” *Bull. Seismol. Soc. Am.*, 92 (6): 2090–2109. Seismological Society of America.
49. Gazetas, G., K. Fan, T. Tazoh, M. Kavadas, and N. Makris. 1992. *Seismic pile-group-structure interaction, Piles under dynamic loads*. (S. P. Ed., ed.). ASCE.
50. Gazetas, G., K. Fan, T. Tazoh, and K. Shimizu. 1973. “Seismic Response of the Pile Foundation of Ohba-Ohashi Bridge.” *3rd Int. Conf. case Hist. Geotech. Eng.*, 1803–1809. St. Louis.
51. Ghayamghamian, M. 2001. “Identification of Dynamic Soil Properties Using Vertical Array Recordings.”
52. Ghayamghamian, M. R. 1997. “Nonlinear and linear response of the site with evaluation

of actual dynamic soil properties using vertical array accelerograms and microtremors." *PhD Diss.* Saitama University Japan.

53. Ghayamghamian, M. R., and H. Kawakami. 1996. "On the characteristics of non-linear soil response and dynamic soil properties using vertical array data in Japan." *Earthq. Eng. Struct. Dyn.*, 25 (8): 857–870. https://doi.org/10.1002/(SICI)1096-9845(199608)25:8<857::AID-EQE592>3.0.CO;2-R.
54. Ghayamghamian, M. R., and H. Kawakami. 2000. "On site nonlinear hysteretic curves and dynamic soil properties." *J. Geotech. Geoenvironmental Eng.*, 2 (JUNE): 543–555.
55. Ghayamghamian, M. R., and M. Matosaka. 2001. "Identification of Dynamic Soil Properties Using Vertical Array Recordings." *Proc. int. Conf. Recent Adv. Geotech. Earthq. Eng. Soil Dyn.*
56. Ghayoomi, M., G. Suprunenko, and M. Mirshekari. 2017. "Cyclic triaxial test to measure strain-dependent shear modulus of unsaturated sand." *Int. J. Geomech.*, 17 (9): 1–11. https://doi.org/10.1061/(ASCE)GM.1943-5622.0000917.
57. Ghodrati, A., and A. A. Araei. 2017. "Artificial Neural Networks for Modeling Shear Modulus and Damping Behavior of Gravelly Materials." *Int. J. Geomech.*, 17 (2). https://doi.org/10.1061/(ASCE)GM.1943-5622.0000660.
58. Ghosh, B., and S. P. G. Madabhushi. 2004. "Dynamic soil structure interaction for layered and inhomogeneous ground: a comparitive study." *13th World Conf. Earthq. Eng.*, (440).
59. Glaser, S. D., and L. G. Baise. 2000. "System identification estimation of soil properties at the Lotung site." *Soil Dyn. Earthq. Eng.*, 19 (7): 521–531. https://doi.org/10.1016/S0267-7261(00)00026-9.
60. Glaser, S. D., and A. L. Leeds. 1996. *Estimation of system damping at the Lotung site by application of system identification*. Rep no. NIST GCR 96-700, Colorado School of Mines.
61. GSI. 2000. *Seismotectonic atlas of India and its environs*. Geological Survey of India.
62. Gunturi, V. R., A. W. M. Elgamal, and H. T. Tang. 1998. "Hualien seismic downhole data analysis." *Eng. Geol.*, 50 (1–2): 9–29. https://doi.org/10.1016/S0013-7952(97)00084-7.
63. Hadjian, A. H. 2002. "Fundamental period and mode shape of layered soil profiles." *Soil*

Dyn. Earthq. Eng., 22 (9–12): 885–891. https://doi.org/10.1016/S0267-7261(02)00111-2.

64. Halder, S., J. K. Mondal, and K. A. 2019. "Empirical correlations for strain dependent linear 1D ground response analysis for Guwahati, India based on detailed analyses." *7ICEGE*. Roma.
65. Hanumantharao, C., and G. V. Ramana. 2008. "Dynamic soil properties for microzonation of Delhi, India." *J Earth Syst Sci*, 117 (S2): 719–730.
66. Hardin, B. O., and V. P. Drnevich. 1972. "Shear modulus and damping in soils: Design equation and curves." *J. Soil Mech. Found. Eng. Div.*, 98: 667–691.
67. Harinarayan, N. H. 2020. "Ground Motion Prediction Equation for parts of North India. PhD. Thesis, Indian Institute of Technology Guwahati, India." IIT Guwahati.
68. Hashash, Y. M. A., M. I. Musgrove, J. A. Harmon, I. Okan, D. R. Groholski, C. A. Phillips, and D. Park. 2017. "DEEPSOIL 7.0, User Manual."
69. Honjo, Y., S. Iwamoto, M. Sugimoto, S. Onimaru, and M. Yoshizawa. 1998. "Inverse analysis of dynamic soil properties based on seismometer array records using the Extended Bayesian method." *Soil Sci. Soc. Am. J.*, 38 (1): 131–143.
70. Huang, H. C., C. S. Shieh, and H. C. Chiu. 2001. "Linear and nonlinear behaviors of soft soil layers using Lotung downhole array in Taiwan." *Terr. Atmos. Ocean. Sci.*, 12 (3): 503–524. https://doi.org/10.3319/TAO.2001.12.3.503(T).
71. Ishibashi, I., and X. Zhang. 1993. "Unified dynamic shear moduli and damping ratios of sand and clay." *Soils Found.*, 33 (1): 182–191. The Japanese Geotechnical Society.
72. Iwasaki, T., K. Tokida, S. Yoshida, and F. Tatsuoka. 1979. "Experimental studies on dynamic properties of clay." *Proc 14th Annu. Meet. JSSMFE*, 629–632.
73. Iwasaki, Y. 1995. "Geological and geotechnical characteristics of Kobe area and strong ground motion records by 1995 Kobe earthquake." *Tsuchi to kiso*, 43 (6): 15–20.
74. Iwasaki, Y., and M. Tai. 1996. "Geotechnical aspects of the January 17, 1995 Hyogoken-Nambu earthquake: strong motion record at Kobe Port Island." *Soil Foundn Spcl issue*, 1: 29–40.
75. Kaklamanos, J., L. G. Baise, E. M. Thompson, and L. Dorfmann. 2015. "Comparison of 1D linear, equivalent-linear, and nonlinear site response models at six KiK-net validation sites." *Soil Dyn. Earthq. Eng.*, 69: 207–219. Elsevier. https://doi.org/10.1016/j.soildyn.2014.10.016.

76. Kaklamanos, J., B. A. Bradley, E. M. Thompson, and L. G. Baise. 2013. "Critical parameters affecting bias and variability in site-response analyses using KiK-net downhole array data." *Bull. Seismol. Soc. Am.*, 103 (3): 1733–1749. https://doi.org/10.1785/0120120166.
77. Katayama, T., F. Yamazaki, S. Nagata, L. Lu, and T. Turker. 1990. "A strong motion database for the chiba seismometer array and its engineering analysis." *Earthq. Eng. Struct. Dyn.*, 19 (8): 1089–1106. https://doi.org/10.1002/eqe.4290190802.
78. Kayal, J. R., S. S. Arefiev, S. Barua, D. Hazarika, N. Gogoi, A. Kumar, S. N. Chowdhury, and S. Kalita. 2006. "Shillong plateau earthquakes in northeast India region: complex tectonic model." *Curr. Sci.*, 91: 109–114.
79. Kazama, M., E. Yanagisawa, T. Inatomi, T. Sugano, and H. Inagaki. 1996. "Stress strain relationship in the ground at Kobe Port Island during 1995 Hyogo-ken Nanbu earthquake inferred from strong motion array records." *Doboku Gakkai Ronbunshu*, 1996 (547): 171–182. Japan Society of Civil Engineers.
80. Kennedy, R., S. Short, K. Merz, F. Tokarz, I. Idriss, M. Power, and K. Sadigh. 1984. "*Engineering characterization of ground motion—Task I: effects of characteristics of free field motion on structural response*." No. NUREG/CR-3805. Structural Mechanics Associates, Inc., Newport Beach, CA (USA); Woodward-Clyde Consultants, Walnut Creek, CA (USA), 1984.
81. Khattri, K. N. 1987. "Great earthquakes, seismicity gaps and potential for earthquake disaster along the Himalaya plate boundary." *Tectonophysics*, 138 (1): 79–92. Elsevier. https://doi.org/10.1016/0040-1951(87)90067-9.
82. Khattri, K., and M. Wyss. 1978. "Precursory variation of seismicity rate in the Assam area, India." *Geology*, 6 (11): 685. https://doi.org/10.1130/0091-7613(1978)6685:PVOSRI2.0.CO;2.
83. Khattri, K., M. Wyss, V. K. Gaur, S. N. Saha, and B. K. Bansal. 1983. "Local seismic activity in the region of the Assam gap, northeast India." *Bull. Seismol. Soc. Am.*, 73: 459–469.
84. Kim, B., and Y. M. A. Hashash. 2013. "Site response analysis using downhole array recordings during the March 2011 Tohoku-Oki earthquake and the effect of long-duration ground motions." *Earthq. Spectra*, 29 (SUPPL.1): 37–54.

https://doi.org/10.1193/1.4000114.

85. Kim, B., Y. M. Hashash, J. P. Stewart, E. M. Rathje, J. A. Harmon, M. I. Musgrove, and W. J. Silva. 2016. “Relative differences between nonlinear and equivalent-linear 1-D site response analyses.” *Earthq. Spectra*, 32 (3): 1845–1865.
86. Koga, Y., and O. Matsuo. 1990. “Shaking table test of embankments resting on liquefiable sandy ground.” *Soil Found Engg*, 30: 162–174.
87. Kokusho, T. 1980. “Cyclic Triaxial Test of Dynamic Soil Properties for Wide Strain Range.”
88. Kokusho, T. 1994. “Dynamic properties of gravel layers investigated by in-situ freezing sampling.” *Gr. Fail. under Seism. Cond.*, 121–140.
89. Kokusho, T., T. Aoyagi, and A. Wakunami. 2005. “In situ soil-specific nonlinear properties back-calculated from vertical array records during 1995 Kobe earthquake.” *J. Geotech. Geoenvironmental Eng.*, 131 (12): 1509–1521. https://doi.org/10.1061/(ASCE)1090-0241(2005)131:12(1509).
90. Kokusho, T., and M. Matsumoto. 1998. “Nonlinearity in Site Amplification and Soil Properties During the 1995 Hyogoken-Nambu Earthquake.” *Soils Found.*, 38 (Special): 1–9. https://doi.org/10.3208/sandf.38.special_1.
91. Kokusho, T., K. Sato, and M. Matsumoto. 1996. “Nonlinear dynamic soil properties back-calculated from strong seismic motions during Hyogoken-Nanbu earthquake.” *Proc. 11WCEE.*, Paper no 2080. Acapulco, Mexico.
92. Kramer, S. L. 1996. *Geotechnical Earthquake Engineering*. (H. W.J., ed.).
93. Krstelj, I., and J. H. Prevost. 1992. “Dynamic effects in a saturated layered soil deposit: centrifuge modeling.” *Soil Dyn. Earthq. Eng.*, 11 (8): 485–496. Elsevier.
94. Kumar, A., O. Baro, and N. H. Harinarayan. 2016. “Obtaining the surface PGA from site response analyses based on globally recorded ground motions and matching with the codal values.” *Nat. Hazards*, 81 (1): 543–572. Springer Netherlands. https://doi.org/10.1007/s11069-015-2095-x.
95. Kumar, A., S. Halder, and O. Baro. 2018a. “Approximation of Equivalent Linear Ground Response Analysis at Low Strain by Strain Dependent Linear Ground Response Analysis for Typical Site at Delhi, India.” *Geotech. Earthq. Eng. Soil Dyn. V*. Austin, Texas.
96. Kumar, A., N. H. Harinarayan, and O. Baro. 2017. “Nonlinear soil response to ground

motions during different earthquakes in Nepal, to arrive at surface response spectra." *Nat. Hazards*, 87 (1): 13–33. Springer Netherlands. https://doi.org/10.1007/s11069-017-2751-4.

97. Kumar, A., N. H. Harinarayan, and V. Verma. 2018b. "Seismic Site Classification and Empirical Correlation between Standard Penetration Test N Value and Shear Wave Velocity for Guwahati Based on Thorough Subsoil Investigation." *Pure Appl. Geophys*, 175 (8): 2721–2738.
98. Kumar, A., and J. K. Mondal. 2017. "Newly Developed MATLAB Based Code for Equivalent Linear Site Response Analysis." *Geotech. Geol. Eng.*, 35 (5): 2303–2325. Springer International Publishing. https://doi.org/10.1007/s10706-017-0246-4.
99. Kumar, A., A. Panjamani, and S. Thallak. 2011. "Amplification factor from intensity map and site response analysis for the soil sites during 1999 Chamoli earthquake." *Proceedings of the 3rd Indian young geotechnical engineers conference, New Delhi. 2011*.
100. Kumar, S. S., A. Dey, and A. M. Krishna. 2014a. "Equivalent Linear and Nonlinear Ground Response Analysis of Two TYPICAL SITES AT GUWAHATI CITY." *Indian Geotech. Conf.*, (December): 1–10.
101. Kumar, S. S., and A. M. Krishna. 2013. "Seismic Ground Response Analysis of Some Typical Sites of Guwahati City." 4 (June): 83–101. https://doi.org/10.4018/jgee.2013010106.
102. Kumar, S. S., A. M. Krishna, and A. Dey. 2014b. "NONLINEAR SITE-SPECIFIC GROUND RESPONSE ANALYSIS : CASE STUDY OF AMINGAON , GUWAHATI." *15th symposium on earthquake engineering, IIT Roorke. Vol. 308. 2014.*
103. Lazan, B. J. 1968. *Damping of material and members in structural mechanics*. Pergamon press Ltd. Oxford. U.K.
104. Lee, C. J., and S. F. Sheu. 2007. "The stiffness degradation and damping ratio evolution of Taipei silty clay under cyclic straining." *Soil Dyn Earthq Eng*, 27: 730–740.
105. Li, Z., S. Escoffier, and P. Kotronis. 2013. "Using centrifuge tests data to identify the dynamic soil properties: Application to Fontainebleau sand." *Soil Dyn. Earthq. Eng.*, 52: 77–87. https://doi.org/10.1016/j.soildyn.2013.05.004.
106. Madera, G. A. 1970. *Fundamental Period and Amplification of Peak Acceleration*

in Layered Systems. Dept. of Civil Engineering, M.I.T., Cambridge, Massachusetts.

107. Mai, P. M., and R. Meyers. 2009. "Ground Motion: Complexity and Scaling in the Near Field of Earthquake Ruptures." Citeseer.

108. Mar, M., C. K. Shen, Z. Wang, X. S. Li, and Z. Wang. 1991. "Pore Pressure Response During 1986 Lotung Earthquakes."

109. Midorikawa, S., and H. Miura. 2008. "Nonlinear Behavior Of Soil Response Observed In Strong-Motion Records From Recent Japanese Earthquakes." *World Conf. Earthq. Eng.*, 3.

110. Mondal, J. K., and A. Kumar. 2017. "Impact of Higher Frequency Content of Input Motion Upon Equivalent Linear Site Response Analysis for the Study Area of Delhi." *Geotech. Geol. Eng.*, 35 (3): 959–981. Springer International Publishing. https://doi.org/10.1007/s10706-016-0153-0.

111. Mondal, J. K., and A. Kumar. 2021. "A new frequency domain based inverse ground response analysis framework for the determination of dynamic soil properties." *Int. J. Geomech.*, 21 (5): 1–23. https://doi.org/10.1061/(ASCE)GM.1943-5622.0001973.

112. Motazedian, D., and G. M. Atkinson. 2005. "Stochastic finite-fault modeling based on a dynamic corner frequency." *Bull. Seismol. Soc. Am.*, 95 (3): 995–1010.

113. Nath, S. K., and K. K. S. Thingbaijam. 2011. "Peak ground motion predictions in India : an appraisal for rock sites." *J. Seismol.*, 15: 295–315. https://doi.org/10.1007/s10950-010-9224-5.

114. Ntritsos, N., M. Cubrinovski, and B. A. Bradley. 2021. "Challenges in the definition of input motions for forensic ground-response analysis in the near-source region." *Earthq. Spectra*, 37 (4): 2562–2595. https://doi.org/10.1177/87552930211001376.

115. Ohta, H. 1975. "Application of optimization method to earthquake engineering (part I)- estimation of underground structure of SMAC observation site in Hachinohe Harbour." *Journ Japan Soc. Archit. Engg*.

116. Okur, D. V., and A. Ansal. 2007. "Stiffness degradation of natural fine grained soils during cyclic loading." *Soil Dyn Earthq Eng*, 27: 843–854.

117. Oldham, R. D. 1899. "Report on the Great Earthquake of 12 June 1897." *Mem. Geol. Soc. India*, (29): 379.

118. Oskay, C., and M. Zeghal. 2011. “A survey of geotechnical system identification techniques.” *Soil Dyn. Earthq. Eng.*, 31 (4): 568–582. Elsevier. https://doi.org/10.1016/j.soildyn.2010.11.011.

119. Phanikanth, V. S., D. Choudhury, and G. R. Reddy. 2011. “Equivalent-Linear Seismic Ground Response Analysis of Some Typical Sites in Mumbai.” *Geotech. Geol. Eng.*, 29 (6): 1109–1126. https://doi.org/10.1007/s10706-011-9443-8.

120. Pyke, R. 1979. “Nonlinear soil models for irregular cyclic loadings.” *Journ. Geotech. Engg. Div. ASCE*, 105: 715–725.

121. Raghu Kanth, S. T. G., and S. K. Dash. 2010. “Deterministic seismic scenarios for North East India.” *J. Seismol.*, 14 (2): 143–167. Springer.

122. Raghukanth, S., J. Dixit, and S. Dash. 2011a. “Ground motion for scenario earthquakes at Guwahati city.” *Acta Geod. Geophys. Hungarica*, 46 (3): 326–346. https://doi.org/10.1556/AGeod.46.2011.3.5.

123. Raghukanth, S. T. G., S. K. Dash, and J. Dixit. 2011b. “Ground Motion for Scenario Earthquakes at Guwahati City.” *Acta Geod. Geoph. Hung*, 46 (3): 326–346.

124. Rajendran, C. P., K. Rajendran, B. P. Duarah, S. Baruah, and A. Earnest. 2004. “Interpreting the style of faulting and paleoseismicity associated with the 1897 Shillong, northeast India, earthquake: Implications for regional tectonism.” *Tectonics*, 23 (4): 1–12. https://doi.org/10.1029/2003TC001605.

125. Ramberg, W., and W. R. Osgood. 1943. *Description of stress strain curves by three parameters.* Tech note 902, Washington D.C.

126. Ranjan, R. 2005. “Seismic Response Analysis of Dehradun.” International Institute for Geo-Information Science and Earth Observations -Enschede, Netherlands, P-86.

127. Rayhani, M. H. T., and M. H. El Naggar. 2007. “Centrifuge modeling of seismic response of layered soft clay.” *Bull. Earthq. Eng.*, 5: 571–589. Springer.

128. Régnier, J., H. Cadet, L. F. Bonilla, E. Bertrand, and J.-F. Semblat. 2013. “Assessing nonlinear behavior of soils in seismic site response: Statistical analysis on KiK-net strong-motion data.” *Bull. Seismol. Soc. Am.*, 103 (3): 1750–1770. Seismological Society of America.

129. Ren, Y., R. Wen, X. Yao, and K. Ji. 2017. “Five parameters for the evaluation of

the soil nonlinearity during the Ms8. 0 Wenchuan Earthquake using the HVSR method." *Earth, Planets Sp.*, 69 (1): 1–17. SpringerOpen.

130. Ripperger, J., P. M. Mai, and J.-P. Ampuero. 2008. "Variability of near-field ground motion from dynamic earthquake rupture simulations." *Bull. Seismol. Soc. Am.*, 98 (3): 1207–1228. Seismological Society of America.

131. Romo, M. P. 1995. "Clay behavior, ground response and soil-structure interaction studies in Mexico City." *Proc. 3rd. Conf. Recent Adv. Geotech. Earthq. Engng. Soil Dyn.*, 1039–1051.

132. Sato, K., T. Kokusho, M. Matsumoto, and E. Yamada. 1996. "Nonlinear seismic response and soil property during strong motion." *Soils Found.*, (Special): 41–52. https://doi.org/10.3208/sandf.36.special_41.

133. Schnabel, P. B. 1973. "Effects of Local Geology and Distance from Source on Earthquake Ground Motions." University of California, Berkeley.

134. Schnabel, P. B., J. Lysmer, and H. B. Seed. 1972. *SHAKE- a computer program for earthquake response analysis of horizontally layered sites*. Report no. EERC 72-12.

135. Seed, H. ., and I. . Idriss. 1970a. *Soil moduli and damping factors for dynamic response analysis*. University of California, Berkeley.

136. Seed, H. B., and I. M. Idriss. 1970b. "Analyses of ground motion at Union Bay, Seattle during earthquakes and distant nuclear blasts." *Bull Seism. Soci Am.*, 60 (1): 125–136.

137. Seed, H. B., I. M. Idriss, and K. Tokimatsu. 1986. "Moduli and damping factors for dynamic analyses of cohesionless soils." *J. Geotech. Eng. ASCE*, 112 (11): 1016–1032.

138. Seismosoft. 2020. "SeismoSignal - A computer program for signal processing of time-histories."

139. Sharma, B., A. F. Siddique, and B. J. Medhi. 2018. "One Dimensional Ground Response Analysis and Identification of Liquefiable Strata of Guwahati City." *Civ. Infrastructures Confronting Sev. Weather. Clim. Chang. Conf.*, 145–162.

140. Shima, E. 1962. "Modification of seismic waves in superficial layers as verified by comparative observation on and beneath the syrface." *Bull Earthq Resrc Inst. Tokyo*, 40: 187–259.

141. Siddique, A. F., and B. Sharma. 2020. “Liquefaction Potential Assessment of Guwahati City Using One Dimensional Ground Response Analysis.” *J. Geosci. Environ. Prot.*, 8 (5): 176–194. https://doi.org/10.4236/gep.2020.85011.

142. Singh, S. K., and M. Ordaz. 1993. “On the origin of long coda observed in the lake-bed strong-motion records of Mexico City.” *Bull. Seismol. Soc. Am.*, 83 (4): 1298–1306. The Seismological Society of America.

143. Stanko, D., Z. Gülerce, S. Markušić, and R. Šalić. 2019. “Evaluation of the site amplification factors estimated by equivalent linear site response analysis using time series and random vibration theory based approaches.” *Soil Dyn. Earthq. Eng.*, 117 (October 2018): 16–29. Elsevier Ltd. https://doi.org/10.1016/j.soildyn.2018.11.007.

144. Stanko, D., S. Markušić, S. Strelec, and M. Gazdek. 2017. “Equivalent-linear site response analysis on the site of the historical Trakošćan Castle, Croatia, using HVSR method.” *Environ. Earth Sci.*, 76 (18). https://doi.org/10.1007/s12665-017-6971-4.

145. Street, R., Z. Wang, E. Woolery, J. Hunt, and J. Harris. 1997. “Site effects at a vertical accelerometer array near Paducah, Kentucky.” *Eng. Geol.*, 46 (3–4): 349–367. https://doi.org/10.1016/s0013-7952(97)00011-2.

146. Sun, J. I., R. Golesorkhi, and H. B. Seed. 1988a. *Dynamic moduli and damping ratios for cohesive soils*. Report no EERC 88-15. University of California Berkeley.

147. Sun, J. I., R. Golesorkhi, and H. B. Seed. 1988b. *Dynamic moduli and damping ratios for cohesive soils*. Report no EERC 88-15.

148. Taboada-Urtuzuastegui, V., H. Martinez, M. Romo, and C. Ardila. 2000. “Identification of Mexico City Clay Dynamic Properties.” *Proc. 12th World Conf. Earthq. Eng. Auckland, New Zeal.*, Paper No.: 1–8.

149. Taboada-Urtuzuástegui, V., H. Martínez, and M. P. Romo. 1999. “Evaluation of dynamic soil properties in mexico city using downhole array records.” *Soils Found.*, 39 (5): 81–92. https://doi.org/10.3208/sandf.39.5_81.

150. Taboada, V. M. 1989. “Degradacion de la Arcilla de la Ciudad de Mexico por Carga Dinamica.” *Tesis Maest. DEPFI*. UNAM.

151. Tang, H. T., Y. K. Tang, J. C. Stepp, I. B. Wall, E. Lin, S. C. Cheng, and S. K. Lee. 1989. “A large-scale soil-structure interaction experiment: Design and construction.” *Nucl. Eng. Des.*, 111 (3): 371–379. https://doi.org/10.1016/0029-5493(89)90248-3.

152. Thompson, E. M., L. G. Baise, Y. Tanaka, and R. E. Kayen. 2012. "A taxonomy of site response complexity." *Soil Dyn. Earthq. Eng.*, 41: 32–43. Elsevier. https://doi.org/10.1016/j.soildyn.2012.04.005.

153. Tokimatsu, K., and S. Midorikawa. 1981. "Nonlinear Soil Properties Estimated from Strong Motion Accelerograms." *Proceeding 1st Int Conf Recent Adv. Geotec Earthq Engg Sol Dyn 1st Int Conf Recent Adv. Geotec Earthq Engg Sol Dyn*, 117–122.

154. Tokimatsu, K., S. Midorikawa, and Y. Yoshimi. 1989. "Dynamic soil properties obtained from strong motion records." *12th Int. Conf. soil Mech. Found. Eng.*, 2015–2018.

155. Tokimatsu, K., T. Sekiguchi, H. Miura, and S. Midorikawa. 2006. "Nonlinear dynamic properties of surface soils estimated from strong motion accelerograms at K-NET and JMA stations in Ojiya." *Jour Struct Constr. Engg AIJ*, 600: 43–59.

156. Tsai, C. C., and Y. M. A. Hashash. 2009. "Learning of dynamic soil behavior from downhole arrays." *J. Geotech. Geoenvironmental Eng.*, 135 (6): 745–757. https://doi.org/10.1061/(ASCE)GT.1943-5606.0000050.

157. Tsai, C., and Y. M. A. Hashash. 2007. "an Inverse Analysis Approach To Extract Dynamic Nonlinear Soil Behavior From Downhole Array Data." *Proc 4th Int Conf Earthq Geotech Engg*.

158. Tsuda, K., and J. Steidl. 2006. "Nonlinear site response from the 2003 and 2005 Miyagi-Oki earthquakes." *Earth, planets Sp.*, 58 (12): 1593–1597. SpringerOpen.

159. Uthayakumar, U. M., and E. Naesgaard. 2004. "GROUND RESPONSE ANALYSIS FOR SEISMIC DESIGN IN FRASER RIVER DELTA , BRITISH COLUMBIA." *13 th World Conf. Earthq. Eng.*

160. Vijayendra, K., S. Prasad, and S. Nayak. 2010. "Computation of Fundamental Period of Soil Deposit : A Comparative Study." *Indian Geotech. Conf.*, (1).

161. Vucetic, M. 1994. "Cyclic threshold shear strains in soils." *J. Geotech. Eng.*, 120 (12): 2208–2228.

162. Vucetic, M., and R. Dobry. 1991. "Effect of soil plasticity on cyclic response." *J. Geotech. Eng.*, 117 (1): 89–107.

163. Wang, G. X., and J. Kuwano. 1999. "Modeling of strain dependency of shear modulus and damping of clayey sand." *Soil Dyn Earthq Eng*, 18 (6): 463–471.

164. Wang, H. Y., W. P. Jiang, S. Y. Wang, and Y. Miao. 2019. “In situ assessment of soil dynamic parameters for characterizing nonlinear seismic site response using KiK-net vertical array data.” *Bull. Earthq. Eng.*, 17 (5): 2331–2360. Springer Netherlands. https://doi.org/10.1007/s10518-018-00539-3.

165. Wang, K., and A. Brennan. 2019. “Behaviour of saturated fibre-reinforced sand in centrifuge model tests.” *Soil Dyn. Earthq. Eng.*, 125 (July): 105749. Elsevier Ltd. https://doi.org/10.1016/j.soildyn.2019.105749.

166. Wen, K. -L. 1994. “Non-linear soil response in ground motions.” *Earthq. Eng. Struct. Dyn.*, 23 (6): 599–608. https://doi.org/10.1002/eqe.4290230603.

167. Wen, Y. K. 1976. “Method for random vibration of hysteretic system.” *J. engg. Mech. Div.s*, 102 (2): 249–263.

168. Wolf, J. ., and P. C. Obernhuber. 1982. “Free-field response from inclined SH-waves and Love-waves.” *Earthq. Engg Struct Dyn*, 10: 823–845.

169. Wu, C., Z. Peng, and D. Assimaki. 2009. “Temporal changes in site response associated with the strong ground motion of the 2004 M w 6.6 Mid-Niigata earthquake sequences in Japan.” *Bull. Seismol. Soc. Am.*, 99 (6): 3487–3495. Seismological Society of America.

170. Xu, J., C. Costantino, C. Hofmayer, A. Murphy, N. Chokshi, and Y. Kitada. 2003. *Identification of free-field soil properties using NUPEC recorded ground motions*. Brookhaven National Laboratory (BNL); BNL-NUREG 68192.

171. Xu, J., and H. L. Graves. 1993. “Integrated software system for seismic evaluation of nuclear power plant structures.” *Comput. Struct.*, 46 (4): 717–723. Elsevier.

172. Yamada, S., M. Hyodo, R. Orense, S. V. Dinesh, and T. Hyodo. 2008. “Strain-dependent dynamic properties of remoulded sand-clay mixtures.” *J Geotech Geoenviron Eng*, 134 (7): 972–981.

173. Yangisawa, E., and M. Kazama. 1996. “Nonlinear dynamic behavior of the ground inferred from strong motion array records at Kobe Port Island during the 1995 Hygo-Ken Nanbu earthquake.” *Procee Earthq Engg 11th World Conf Earthq Engg*.

174. Zeghal, M. 1993. “Lotung site: downhole seismic data analysis.” *Rep. Electr. Power Res. Inst.*

175. Zeghal, M., and A. W. Elgamal. 1994. “Analysis of site liquefaction using

earthquake records." *J. Geotech. Eng.*, 120 (6): 996–1017. https://doi.org/10.1061/(ASCE)0733-9410(1994)120:6(996).

176. Zeghal, M., H. T. Tang, and J. C. Stepp. 1995. "Soil Nonlinear Properties." *J. Geotech. Eng.*, 121 (4): 363–378.

177. Zhang, J., R. Andrus, and C. Juang. 2005. "Normalized shear modulus and material damping ratio relationships." *Geotech. Geoenvironmental Eng.*, 131 (4): 453–464. https://doi.org/10.1061/(ASCE)1090-0241(2005)131.

Document Information

Analyzed document	Final PhD Thesis for defense (latest).pdf (D172412023)
Submitted	7/27/2023 7:00:00 PM
Submitted by	Joy Kumar Mondal
Submitter email	joy.mondal@iitg.ac.in
Similarity	1%
Analysis address	joy.mondal.iitg@analysis.urkund.com

Sources included in the report

SA	**SB Plagiarism Check (6%).pdf** Document SB Plagiarism Check (6%).pdf (D21198595)	3
SA	**Shear Modulus and Damping Ratio for sand.docx** Document Shear Modulus and Damping Ratio for sand.docx (D64491842)	1
SA	**Indian Institute of Technology Guwahati / For Plagarism.docx** Document For Plagarism.docx (D110878650) Submitted by: NIRAN521152@iitg.ac.in Receiver: niran521152.iitg@analysis.urkund.com	4
SA	**Paper_final_EB.docx** Document Paper_final_EB.docx (D21236609)	1
SA	**Pakbaz.pdf** Document Pakbaz.pdf (D5069751)	3
SA	**Chapter 2 - LITERATURE REVIEW (15 %).pdf** Document Chapter 2 - LITERATURE REVIEW (15 %).pdf (D21198277)	2
W	URL: http://soilquake.net/Downholearray/Lotung/ Fetched: 7/27/2023 7:00:00 PM	1
SA	**PAPERS63_GEO_2016_03.pdf** Document PAPERS63_GEO_2016_03.pdf (D165486312)	1
SA	**12.docx** Document 12.docx (D22551995)	1

Entire Document

A FREQUENCY DOMAIN BASED
INVERSE GROUND RESPONSE ANALYSIS FRAMEWORK FOR THE DETERMINATION OF DYNAMIC SOIL PROPERTIES
Submitted for the degree of DOCTOR OF PHILOSOPHY By Joy Kumar Mondal DEPARTMENT OF CIVIL ENGINEERING
INDIAN INSTITUTE OF TECHNOLOGY GUWAHATI
GUWAHATI – 781039 December 2022
ii
iii DEDICATED TO MY BELOVED PARENTS, MY BEAUTIFUL WIFE AND MY TEACHER PRANAB KUMAR MAJUMDER
iv Statement I do hereby declare that the matter contained in this thesis is the outcome of investigations carried out by me at the Department of Civil Engineering, Indian Institute of Technology Guwahati, Guwahati, Assam, India. In keeping with the general practice of reporting scientific observations, due acknowledgements have been made whenever the work described is based on findings of other investigators. Place: IIT Guwahati Joy Kumar Mondal Date: 1 st December-2022
v Certificate This is to certify that the thesis entitled "
A Frequency Domain based Inverse Ground Response Analysis Framework for the Determination of Dynamic Soil Properties"
being submitted by Mr. Joy Kumar Mondal, (Enrollment number 176104112) to the Indian Institute of Technology Guwahati for the award of the degree of Doctor of Philosophy is a record of bonafide research work carried out by him. The thesis work in my opinion has reached the requisite standard for the degree of Doctor of Philosophy. The results embodied in this thesis have not been submitted in any other University/ Institute for the award of any Degree or Diploma. Date: Dr. Abhishek Kumar Place: Associate Professor Indian Institute of Technology Guwahati, Assam, India-781039
vi Acknowledgement My PhD research has been accomplished thanks to the kind and unrestrained assistance of many people. I would want to use this occasion to express my heartfelt appreciation to everyone for their unwavering support. I want to start by expressing my gratitude to my mentor and supervisor, Dr. Abhishek Kumar for his unconditional support, priceless technical advice and patience. Working with him during my PhD studies has been a privilege and a wonderful joy that has improved me not only as a researcher but a better person too. He has been like a family member to me who has always inspired me to improve as a researcher, because of his enthusiasm and commitment to his work. I am incredibly appreciative of his personal kindness, compassion, and commitment to my welfare. For my PhD, I could not have asked for a better supervisor. I would also like to thank the rest of my Doctoral committee: Dr. Anil Kumar Mishra, Dr. Rishikesh Bharti and Dr. Sachin S. Gautam for their guidance, constructive comments and creative suggestions at every stage of my PhD research. I am very grateful to my lab mates and dear friends Dr. Harinarayan N.H, Mr. Niranjan Borah, Mr. Surender Singh, Mr. Prem Kumar, Mr. Rahul Raoniar for their delightful presence and personal support. Without them, the lab would have been a monotonous place. I would like to thank the Indian Institute of Technology Guwahati (IITG) for providing me opportunity and financial support to carry out my PhD work.
vii I express my thanks to all my teachers who have laid the cornerstones for this journey in my life. Furthermore, I want to thank my parents immensely for their consistent support and encouragement of me in pursuing my dream. Last but not the least, I want to convey my gratefulness to my wife Ranu for tolerating me and supporting me through the darkest hours of my life. Joy Kumar Mondal
viii ABSTRACT: Effect of local soil in amplifying bedrock motion during earthquakes (EQs) is an important phenomenon, and is observed globally. As a result, the bedrock motion at times increases manifold while reaching the surface. Such amplification in ground motions due to local soil is termed as